Time and thermo-mechanical coupling effects in polymers

Pankaj Yadav

THÈSE POUR OBTENIR LE GRADE DE DOCTEUR
DE L'UNIVERSITÉ DE MONTPELLIER

Mécanique et Génie Civil

École doctorale : Information, Structures et Systèmes

Laboratoire de Mécanique et Génie Civil

Effets du temps et effets de couplage thermomécanique dans les polymères

Time and thermo-mechanical coupling effects in polymers

Présentée par PANKAJ YADAV

Date de la soutenance – 17 Octobre 2019

Devant le jury composé de

Mme Noëlle BILLON	PR	Mines ParisTech	Rapporteur
M Florian LACROIX	PR	Université de Tours	Rapporteur
Mme Sylvie CASTAGNET	DR, CNRS	Institut P'	Présidente
M Gilles ROBERT	IR	Solvay	Examinateur
M Olivier ARNOULD	MCF	Université de Montpellier	Co-encadrant
Mme Sandrine BARDET	MCF	Université de Montpellier	Co-encadrante
M André CHRYSOCHOOS	PR	Université de Montpellier	Directeur de thèse

UNIVERSITÉ DE MONTPELLIER

In memory of my dear grand father.
I cannot express my sorrow in your absence.
I wish you were by my side this day.
May this work be a prayer for the rest of your soul in peace.

Acknowledgement

The work presented in this thesis was carried out within the Thermomechanics of Materials (ThM2) and Wood teams of the Laboratory of Mechanics and Civil Engineering (LMGC-UMR 5508 CNRS-UM) at the University of Montpellier.

First of all, I would like to thank Pr. André CHRYSOCHOOS for directing this thesis work, also for his judicious scientific advice, his legendary humour as well as his patient follow-up of my work from beginning to end. André has been able to devote a lot of attention despite a busy schedule, especially during the modeling and writing part of this thesis. He was the good director who was able to immerse me in thermodynamics of the materials, and the true teacher recognized by his clear, relevant ideas and encouraging that made me an ambitious young researcher. A big thanks to Olivier ARNOULD who was always in charge of guiding me throughout my experiments and suggesting the best to get the desired results. At last, I would like to thank Sandrine BARDET as well, with whom I learned a lot about experimental techniques and to identify the errors during the same. Through several discussions, a way to achieve the desired goal, was developed together. I was simply contented to have people like you as researchers and human beings, which has helped me enormously. You guided me in the moments of doubt and, above all, you have transmitted to me the love to learn and to teach.

I would like to thank Bertrand WATTRISSE and Joseph GRIL for welcoming me in their respective teams. I would also like to show gratitude towards Bertrand WATTRISSE for all the important discussions that we had for improving the infrared experimental techniques. I would like to give a special thanks to Gille CAMP also, who was always available to help me getting ready with my samples and especially for the fabrication of the Infrared door.

In LMGC, I would be very thankful to Chantal ROMANO who supported me morally during my hard time. I would be thankful to all the other researchers who made this scientific experience an expe-human experience: thanks in particular to Yann MONERIE, Hervé LOUCHE, Vincent HUON, Jean Michel MURACCIOLE, Delphine JULLIEN, Joseph GRILL, Patrick CAÑADAS, Cédric MONTERO, Bruno CLAIR, Tancrède ALMERAS.

During these wonderful three years of my lifetime scientific experience, I have met quite a lot of wonderful people in and outside the LMGC. Thank you Sonja ROHMER (for all your moral support and beautiful conversations that we had), Vincent SERANTONI (for all our outings and especially to motivate me for Rock n Roll classes), Luiza OROZCO (for being supportive in different ways), Brice NKOMBOU (to make us laugh by your funny actions especially sleeping in weekly seminars just to concentrate), Kajetan WOJTACKI (for all those motivating speeches to have fun in life including your favourite question always for the last weekend and especially our sport sessions and WAIT!!! How can I forget ZUBROWKA?), Joffrey LHONNEUR (for all those wonderful recipes for exotic food and 44, calva etc. and discotheque plans with loads of

**** and especially sport sessions), Nicolas FALGAYRETTES (for all your adventurous plans of sailing, pyrenees hiking etc.), Anna WOLNIK, Celine MATAR, Aida NSR, Crystal CHEUNG, Sara NA (for all moral support and laughter that we have shared). I especially want to thank Claire MAUDET as well, for being the wonderful person in my life. I will never forget the walk that I shared with you during the peak winter in pyrénées.

I equally would like to be thankful to Tarik MADANI, David CANTOR, Lo VU, Jonaz VASQUEZ VILLEGAS, Fabien ROZAR, Gilles DUSFOUR, Anna DUPLEIX, Ahmad ALKADRI, Capucine CARLIER, Riccardo FERRARA, Piergiorgio CANCI, Thanh Trung VO, Xavier METZ, Noemie PETITJEAN, Thierry SATOH, Adrien SOCIE, Felix LABOUP, Manuel CARDENAS, Julien BONNET and many more that I can't mention their names ;-).

Please forgive me if I have forgotten any of you.

I feel very lucky to have met you. I have enjoyed my three years of stay in Montpellier and elsewhere. Thank you for so many memories.

I would like to thank many people in India as well starting from Dhruv RUIA and Mihir MODI (for all those beautiful memories and time we shared together, especially the things that will stay as secret forever between three of us), Nikita VERMA (for being the most disturbing person during college days), Bhupi SALVI (I still can't forget the prank of "KNOCK KNOCK" in GOKUL hostel), Yogita SONI (for your unconditional support) and Rupanjali AGARWAL (for all those college days that we spent together).

Finally, but certainly the most important, thanks to my family. Especially my dad, mom, and elder brother (Vivek KUMAR) who always believed and supported me in every situation. Thank you for your support, your patience, your dedication, and your infinite generosity. I can not find words to describe everything I thank you for. They are the most important thing I can have in my entire life. I want to thank to my one and only young brother (Pokhraj YADAV) who always have showed affection and love towards me throughout my life.

Thank you dad, thank you mom.

Pankaj Yadav
À Montpellier, le 17/10/2019.

Résumé

L'une des principales classes de matériaux, les polymères, qui peuvent être synthétiques ou d'origine naturelle (bois, fibres végétales, os, cartilage, etc.), représentent le domaine des matériaux le plus vaste et qui a connu la plus forte croissance au siècle dernier. Grâce à leur combinaison unique de propriétés, telles que la légèreté ou la facilité de mise en œuvre, les polymères ont façonné le monde moderne et transformé la qualité de notre vie quotidienne. Ces matériaux polymères sont connus pour présenter un comportement mécanique complexe en fonction du temps (ou de la fréquence des contraintes appliquées), de la température et parfois de l'humidité. Ces matériaux polymériques jouent un rôle important dans le monde, du tissu à la structure, du transport aux moyens de communication, du divertissement aux soins de santé. Par conséquent, pour bon nombre de ces applications, une connaissance précise du comportement mécanique et thermique de cette classe de matériaux est primordiale. En même temps, l'étude de ces matériaux est nécessaire pour optimiser les procédés de fabrication, le dimensionnement, la durée de vie et pour permettre un recyclage efficace des produits en polymère plastique, notamment dans le contexte environnemental actuel. Les études du comportement des matériaux polymériques sont maintenant basées sur un dialogue entre travaux expérimentaux et modélisation rhéologique afin de réduire le nombre et la durée des travaux nécessaires à sa maîtrise.

Les matériaux polymères sont largement connus pour leur comportement thermo-viscoélastique. Cela signifie que les propriétés mécaniques des polymères dépendent du temps ou de la fréquence de la déformation appliquée et de la température. C'est pourquoi un procédé de caractérisation expérimentale du comportement viscoélastique des matériaux polymères en fonction du temps et de la température, appelé DMTA, a été développé. Cette technique de caractérisation permet de recueillir les propriétés viscoélastiques à des fréquences et des températures qui peuvent être atteintes dans les laboratoires de recherche. Mais cette plage de températures et de fréquences ne permet de caractériser le comportement viscoélastique que sur une échelle de temps très courte par rapport aux durée de service des polymères. On a observé que les propriétés viscoélastiques évoluent avec la fréquence au fur et à mesure que la température change, mais semblent se déplacer vers la gauche ou la droite ??? . Par conséquent, le désir de prédire ces propriétés viscoélastiques à de très grande échelle dans le temps à conduit à la formulation d'un principe empirique appelé par les Anglo-saxons "principe de superposition temps-température" et plus explicetement en français "principe d'équivalence temps-température". En utilisant ce principe empirique, il a été possible de déduire un comportement sur une large gamme de temps ou de fréquence équivalente à partir des expériences menées à différentes températures en laboratoire. Ce principe est censé fonctionner pour la classe spéciale de matériaux appelés "matériaux thermorhéologiques simples". En d'autres termes, ce principe empirique suppose que la température affecte de façon équivalente chaque temps caractéristique associé aux mécanismes de relaxation du matériau.

Les travaux de cette thèse se concentrent sur l'étude du principe d'équivalence temps-température (TTSP) et sur les couplages temps-température. Les effets du temps ou de la fréquence sont assez unanimement associés aux effets visqueux. Or sur un plan thermomécanique, il a été observé que les effets dissipatifs associés aux effets visqueux restent souvent très faibles devant les sources de couplage traduisant une forte sensibilité des matériaux polymères aux variations de température. L'objectif de la thèse est donc de revisiter ces concepts afin d'établir le rôle exact des effets de couplage qui, eux aussi, induisent un effet du temps. En utilisant les moyens expérimentaux traditionnels de la visco-analyse (DMTA) et via un analyse énergétique du comportement, l'objectif principal de la thèse est d'analyser la règle d'équivalence temps-température dans le cadre de la Thermodynamique des Processus Irréversibles, en tenant compte des effets dissipatifs et de couplage induits par le processus de déformation.

Ce manuscrit est composé de quatre chapitres. Le chapitre 1 est une revue bibliographique sur les propriétés des polymères, leur comportement viscoélastique, l'équivalence temps-température et les techniques de visco-analyse de type DMTA. Le chapitre 2 présente le cadre théorique de la Thermodynamique des Processus Irreversibles et le formalisme des Matériaux Standards Généralisés (MSG) qui permettent d'exprimer les lois de comportement et les principes thermodynamiques. Les chapitre 3 et 4 concernent les résultats expérimentaux et la modélisation rhéologique. Leur contenu est résumé ci-dessous.

Etude expérimentale:

La sélection des polymères étudiés a été faite en fonction des critères suivants : ils ne doivent pas présenter de mécanismes micromécaniques complexes c'est à dire qu'ils correspondent aux propriétés suivantes: amorphes sans cristallisation sous charge, hydrophobes ou hydrophiles limités, T_g et T_β bien séparés. Selon ces critères, le polystyrène atactique (PS), qui est l'un des thermoplastiques amorphes les plus "simples", le poly(méthacrylate de méthyle) (PMMA), bien connu pour sa compatibilité avec le TTSP et le polyamide (PA-6.6 aussi appelé nylon) qui est un polymère largement utilisé avec une dissipation élevée lors des charges cycliques, ont été choisis. Les paramètres variables dans cette étude sont limités à la température, allant de la température ambiante à quelques degrés en dessous de Tg et à la fréquence de chargement, allant de 0,01 à 10 Hz (trois décades). Cette gamme de fréquence a été choisie en fonction de la gamme la plus appropriée pour les différentes machines d'essais DMTA. Au cours de cette étude, une attention particulière a été portée à la définition du domaine expérimental (température, amplitude de déformation, rapport de charge, etc.) afin de mettre en évidence les changements dans le comportement rhéologique du matériau sans toutefois le dégrader significativement (i.e. dommages limités par un nombre limité de cycles et utilisation d'un échantillon par température).

Par conséquent, la technique de caractérisation mécanique DMTA a été utilisée pour caractériser les propriétés viscoélastiques linéaires des trois polymères choisis (PS, PMMA et PA-6.6). Ces mesures ont été effectuées en mode de déformation contrôlée avec une amplitude de 0,1 %. Cette amplitude a été choisie pour rester dans la région viscoélastique linéaire des polymères, cette limite a été estimée sur le PS par un essai en balayage de déformation à 1Hz et 10Hz à température ambiante et à la température d'essai la plus élevée. Dans un 1er temps, les mesures de DMTA sur PS ont été effectuées dans différents laboratoires (P', ICGM, C2MA, FEMTO-ST et LMGC) en utilisant des échantillons de deux épaisseurs différentes (1.2mm et 4mm) et de deux poids moléculaires différents. Le mode d'essai de flexion en 3 points a été

utilisé en P' avec un seul échantillon pour toutes les températures. Alors que dans d'autres laboratoires, les mesures cycliques ont été effectuées en mode tension-compression en conservant le rapport de charge, $R = -1$. Ces nombreuses mesures dans différents laboratoires ont été effectuées pour valider la mise au point et la procédure d'étalonnage et de correction de la machine dans notre laboratoire (LMGC). Des différences entre les protocoles d'étalonnage et de correction de la rigidité machine ont été observées entre les laboratoires. Dans un 2ème temps, des séries d'essais ont été réalisées au LMGC sur les 3 polymères en affinant le protocole expérimental. On a supposé que tous les composants de la machine DMTA, en particulier les capteurs de contrainte, les mors et les rallonges du four, induisaient un déplacement non négligeable qui était à l'origine d'un biais important dans la mesure du module de rigidité de l'échantillon. On a également supposé que l'électronique de la chaîne d'acquisition de la DMTA avait un effet sur le déphasage entre les signaux imposés (ε) et mesurés (σ). Par conséquent, les résultats bruts obtenus à partir des mesures DMTA effectuées en LMGC ont été corrigés en tenant compte de la rigidité de la machine et du déphasage électronique.

La comparaison de toutes les mesures effectuées dans les différents laboratoires a été effectuée pour les deux échantillons d'épaisseur différente (1,2 mm et 4 mm) (figure 1 and 2). Les valeurs du module E' obtenues au laboratoire P' étaient les plus élevées, ce qui était associé au fait que, pour les essais de flexion en 3 points, les contraintes de traction maximales se situent sur les surfaces supérieures et inférieures tandis que, dans les essais en mode traction, la contrainte est homogène. Pour le reste des mesures au C2MA, FEMTO-ST et LMGC, les résultats étaient tout à fait comparables en termes de E' et on a supposé que la différence pouvait venir de la rigidité de la machine par rapport à celle de l'échantillon. On a également observé que l'énergie d'activation calculée à l'aide de la loi d'Arrhenius après construction des courbes maîtresses de E' était différente pour chaque cas (chaque épaisseur d'échantillon et chaque machine DMTA). Un décalage vertical (b_T) pour construire les courbes maîtresses pour le coefficient de perte a également été observé pour chaque cas et il a été constaté que dans le cas d'échantillons minces (1,2 mm), la variation de (b_T) en fonction de la température était similaire pour C2MA, FEMTO-ST et LMGC, c'est-à-dire décroissant avec la température croissante, et dans le cas des échantillons épais (4 mm) la variation (b_T) était similaire dans tous les laboratoires (FEMTO-ST et LMGC). Les mesures quasi-statiques ont également été effectuées sur les deux échantillons (épaisseur 1.2mm au C2MA et 4mm au FEMTO-ST). On a constaté que les résultats obtenus à partir de mesures quasi-statiques et les résultats par DMTA au LMGC étaient cohérents. Cette cohérence a donc validé l'ensemble de la procédure de réglage et de correction de la rigidité et du déphasage de la machine au LMGC.

Dans le prolongement des mesures DMTA sur PS, des mesures complémentaires sur PMMA et PA-6.6 ont également été réalisées pour caractériser leurs propriétés viscoélastiques en utilisant uniquement la machine DMTA de LMGC, Montpellier. La même procédure que celle utilisée lors des mesures PS et le même protocole de correction des résultats bruts ont été appliqués en tenant compte de la rigidité de la machine et du déphasage électronique.

La technique DMTA nous a permis de caractériser les trois polymères amorphes. Cependant, ces mesures DMTA classiques ne nous ont pas permis de mesurer la température réelle de l'échantillon pendant le test, qui peut être potentiellement différente de la température imposée dans le four. Cette différence peut provenir des effets d'auto-échauffement du polymère dû à la dissipation visqueuse pendant les essais mécaniques cycliques, mais aussi des effets de couplages thermomécaniques. Par conséquent, un dispositif de thermographie synchronisée

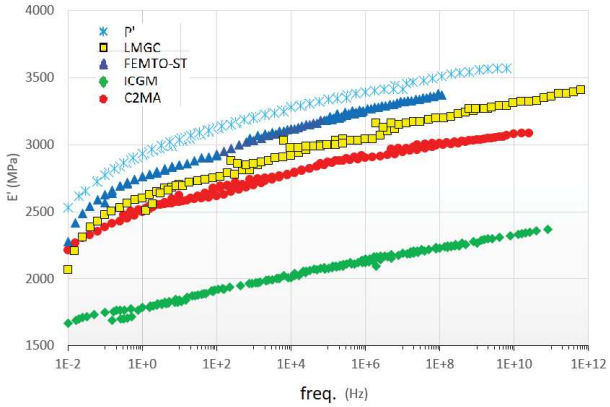

(a) Storage modulus

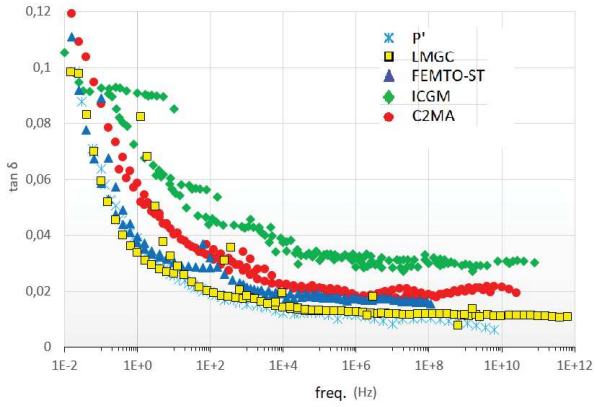

(b) Loss tangent

Figure 1: Comparison of Results for sample with thickness 1.2mm

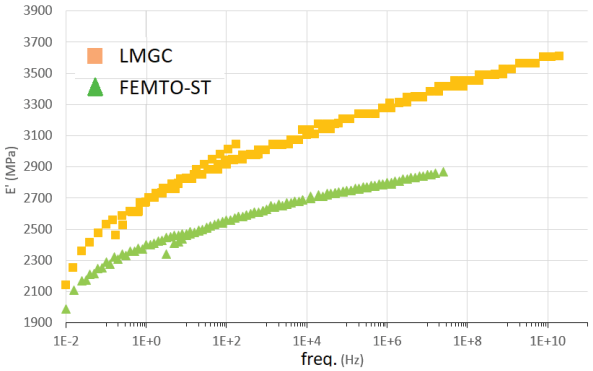

(a) Storage modulus

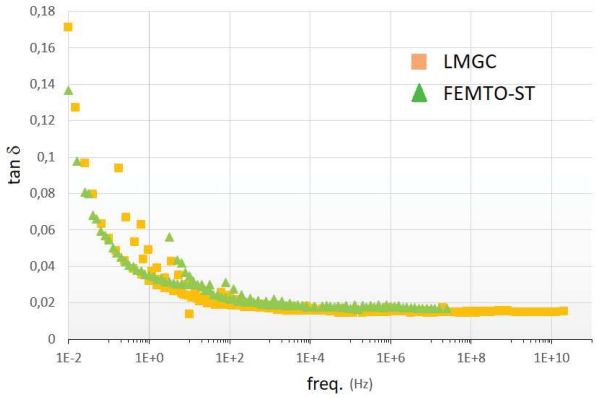

(b) Loss tangent

Figure 2: Comparison of Results for sample with thickness 4mm

spécifique a été mis au point pour observer les variations de température du matériau induites par le chargement mécanique cyclique. Pour les mesures thermographiques, une porte infrarouge spécifique a été fabriquée en LMGC et installée sur le four de la DMTA pour permettre la mesure des radiations infrarouges par la caméra infrarouge. On a supposé que l'auto-échauffement de l'échantillon serait de faible amplitude en raison de la faible vitesse de déformation. Par conséquent, la caméra IR a été calibrée en utilisant la méthode pixel par pixel pour mesurer ces petites variations de température. Cette technique d'étalonnage permet de calibrer les pixels individuellement en fonction de l'ajustement polynomial du niveau numérique s_i délivré par l'élément i_{th} du détecteur, lorsque la caméra est placée devant un corps noir à différentes températures. Les mesures thermographiques ont été effectuées dans la même plage de température que celle utilisée lors des mesures DMTA, mais la plage de fréquence a été réduite entre 0,1 et 10 Hz en raison de la capacité d'enregistrement limitée de la caméra IR. La fréquence d'acquisition de 31Hz a été utilisée pour la caméra IR en fonction de la fréquence des mesures DMTA et du nombre de cycles pour obtenir un nombre suffisant d'images pour le traitement des données. Les échantillons utilisés pour la thermographie ont été peints en noir pour assurer un champ d'émissivité uniforme et proche de celle d'un coirps noir. La précision des mesures thermographiques est dans ce cas de l'ordre ue centième de degré.

Un échantillon différent a été utilisé pour chaque température afin d'éviter la non reproductibilité du chargement mécanique en cas de changement de rigidité d'un échantillon unique. Par la suite, le traitement des données a été effectué sur les données synchronisées enregistrées lors des mesures thermographiques (c.-à-d. les données brutes provenant du DMTA et les images obtenues par caméra IR). Deux échantillons différents ont été utilisés pendant la thermographie, dont un pour observer la régulation de la température du four (échantillon de référence). Le traitement des images a été effectué, via des programmes de traitement développés sous MATLAB, à plusieurs températures et fréquences utilisées pendant les mesures. Au cours de ce traitement d'image, on s'est assuré, à partir des données enregistrées, que le spectre fréquentiel du chargement en déformation utilisé était bien monochromatique tout comme celui de la réponse (viscoélasticité linéaire). Il a également été vérifié que la fréquence des oscillations de température était identique à la fréquence de la déformation imposée (thermoélasticité). Ceci a été effectué en utilisant la technique FFT sur les trois signaux (c.-à-d. déformation imposée, contrainte mesurée et oscillation de température). Ensuite, la température moyenne sur la surface centrale de l'échantillon testé a été calculée et soustraite de la température moyenne sur la surface centrale de l'échantillon de référence afin de minimiser les effets perturbateurs des fluctuations de température du four. Cela a permis de calculer les variations de températures de l'échantillon soumis aux chargements cycliques. Dans le résultat du traitement d'image, l'augmentation monotone de ces variations de température a été associée à l'existence d'une dissipation, tandis que des oscillations de température périodiques ont été attribués aux effets thermoélastiques. A partir de ces données mécaniques et thermiques, on a calculé les aires d'hystérésis associées à la charge mécanique, à E'' et à la dissipation moyenne par cycle. Expérimentalement, dans le cas des PS, malgré la faible amplitude des variations de température, la présence d'oscillations de température a été observée alors qu'aucune augmentation monotone n'a été mise en évidence. Au contraire, dans le cas du PA-6.6 et du PMMA, une augmentation monotone de la température a été observée à des fréquences élevées ainsi que des oscillations de température.

Modélisation rhéologique:

La modélisation rhéologique a été réalisée à partir des résultats obtenus lors de l'étude expérimentale et des mesures thermographiques. Dans cette partie, le modèle rhéologique de Zener a été utilisé pour introduire l'importance de considérer la température comme une variable d'état interne. Par la suite, le modèle généralisé de Maxwell (GMM) a été introduit et placer dans le cadre MSG. L'énergie libre de Helmholtz et un potentiel de dissipation ont été utilisés pour définir les équations de comportement de ce modèle rhéologique. Les différentes sources de chaleur associées au modèle Maxwell généralisé ont également été présentées avec l'équation de la chaleur. Le GMM a également été utilisé pour discuter du TTSP et dériver une expression pour des matériaux thermorhéologiquement simples. Il a été constaté que pour que le GMM soit compatible avec le TTSP, une condition suffisante est que les temps de relaxation soient liés par la même loi dépendant de la température (facteur de décalage a_T pour les matériaux rhéologiquement simples). Cette condition réduit considérablement le nombre de degrés de liberté du modèle puisque l'évolution de la température des modules élastiques et des coefficients de viscosité ne reste plus arbitraire. Par la suite, les résultats obtenus par thermographie lors des essais DMTA, ont été utilisés pour l'identification du modèle rhéologique généralisé, en considérant que la température du matériau restait proche de la température ambiante (température du four) en raison des faibles variations de température observées

expérimentalement. Pour cette identification, un système linéaire d'équations a été résolu. Il est de la forme :

$$\begin{bmatrix} 1 & \frac{\tau_1^2\omega_1^2}{1+\tau_1^2\omega_1^2} & \cdots & \frac{\tau_{n_b}^2\omega_1^2}{1+\tau_1^2\omega_1^2} & 0 \\ \vdots & \vdots & \cdots & \vdots & \vdots \\ 1 & \frac{\tau_1^2\omega_{n_f}^2}{1+\tau_1^2\omega_{n_f}^2} & \cdots & \frac{\tau_{n_b}^2\omega_{n_f}^2}{1+\tau_{n_b}^2\omega_{n_f}^2} & 0 \\ 0 & \frac{\tau_1\omega_1}{1+\tau_1^2\omega_1^2} & \cdots & \frac{\tau_{n_b}\omega_1}{1+\tau_1^2\omega_1^2} & 1 \\ \vdots & \vdots & \cdots & \vdots & \vdots \\ 0 & \frac{\tau_1\omega_{n_f}}{1+\tau_1^2\omega_{n_f}^2} & \cdots & \frac{\tau_{n_b}\omega_{n_f}}{1+\tau_{n_b}^2\omega_{n_f}^2} & 1 \end{bmatrix} \begin{bmatrix} E_0(T_k) \\ \vdots \\ E_i(T_k) \\ E_{i+1}(T_k) \\ \vdots \\ E_{n_b}(T_k) \\ E_{n_b+1}(T_k) \end{bmatrix} = \begin{bmatrix} E'(\omega_1, T_k) \\ \vdots \\ \vdots \\ E'(\omega_{n_f}, T_k) \\ E''(\omega_1, T_k) \\ \vdots \\ \vdots \\ E''(\omega_{n_f}, T_k) \end{bmatrix} \quad (1)$$

Ce système linéaire a été résolu en utilisant la méthode de moindres carrés sous contrainte (il faut que les termes de la solution soient tous positifs). Cette méthode de moindres carrés non négatifs (NNLS) est intégrée dans la boîte à outils d'optimisation de Matlab, sous le nom de fonction *lsqnonneg*. Les résultats obtenus à l'aide de cette méthode nous ont permis d'optimiser le nombre de branches pour le modèle généralisé, c'est-à-dire une branche purement élastique (branche 0), une viscoélastique (branche 1) et une branche purement visqueuse (branche 2). Ensuite, pour les trois différents polymères, les résultats identifiés ont été présentés dans l'ordre suivant : l'évolution des modules élastiques de la branche 0 et 1 par rapport à la température, suivie de l'évolution de la somme $E_0 + E_1$, qui représente approximativement le module tangent du modèle pour les vitesses de chargement élevées. La comparaison des modules de stockage (E') et de perte (E'') identifiés a été faite avec les modules expérimentaux E' et E''. Cette comparaison a été jugée satisfaisante. Afin de donner une image plus quantitative de la pertinence du modèle choisi et de la qualité de son identification, la réponse mécanique du modèle expérimental et identifié a été réalisée pour plusieurs fréquences et températures. Enfin, la branche visqueuse pure et son évolution avec la température et la fréquence de chargement a été présentée.

L'intégration du modèle rhéologique identifié dans le cadre GSM nous a permis de calculer numériquement le bilan énergétique complet. Les différentes sources de chaleur associées aux mécanismes de couplage et aux mécanismes dissipatifs ont donc été calculées. Il est souligné que la prédominance des mécanismes de couplage (en termes d'intensité énergétique) sur les mécanismes dissipatifs a été observée. Il a été rappelé que ces mécanismes de couplage forts peuvent induire des effets de temps (vitesse) sur le comportement mécanique. Heureusement le caractère quasi-adiabatique des transformations étudiées dans ce travail ont limité ces effets du temps. Il a donc été conclu, qu'un modèle de Maxwell généralisé, dont les constantes de temps de relaxation de ses branches viscoélastiques sont toutes reliées par une même loi en température, et dont les variations de température restent faibles sur un cycle de chargement, est compatible avec le principe d'équivalence temps-température.

Contents

List of Figures

List of Tables

Introduction

Polymeric materials, either synthetic or natural (wood, vegetal fibres, bone, cartilage, etc.), exhibit complex mechanical behaviour depending on time (or frequency of applied load), temperature and sometimes humidity. The study of the rheological behaviour of these materials is of prime importance to optimize manufacturing processes, sizing, service life and to allow effective recycling of plastic polymer products, especially in the current environmental context. The studies are now combining experimentation and modelling in order to reduce the number and duration of mechanical tests.

The polymeric materials are widely known for their high viscoelasticity. This signifies the dependence of mechanical properties of polymers on time or frequency of the applied load. This was the reason why a protocol capable of predicting the viscoelastic behaviour of polymeric materials over large time scales and temperatures, named as DMTA, has been developed. This characterization technique allows viscoelastic properties to be collected at frequencies and temperatures that can be adjusted to the constraints of research laboratories. But this limited range of temperatures and frequencies were not enough to characterize the viscoelastic behaviour on a large time scale. However, it was observed that the viscoelastic properties obtained at a given frequency and temperature were similar to the ones obtained at a higher frequency and temperature. Therefore, the desire of extrapolating the viscoelastic properties obtained over a short time to a very large time scale has introduced an empirical principle called *time-temperature superposition principle*. Using this empirical principle, it was possible to infer behaviour over a wide range of equivalent time, or frequency, from the experiments conducted at limited times, or frequencies, range and different temperatures. In other words, this empirical principle implies that time and temperature are generally inversely equivalent in the way they affect the relaxation modulus of polymers [5]. This principle is supposed to apply for the special class of materials called *thermo-rheologically simple materials*.

It was later considered that, during the DMTA characterization, the temperature imposed in the furnace is considered to be the temperature of the specimen. This hypothesis was continued even during the modelling of this viscoelastic behaviour of thermorheologically simple materials. Whereas, the observation made by the researchers that, according to the mechanical point of view, imposing a cyclic loading on the materials induces temperature variations of the specimen called as self-heating phenomenon. In addition, polymer materials are generally the site of thermomechanical couplings (thermodilation, rubber effects, etc.), reflecting strong interactions between mechanical, thermal and microstructural states. Because of the thermal diffusion effects, these couplings make the behaviour sensitive to time (or strain rate) as well as viscosity. So the rate-dependent behaviour of polymers can be, theoretically, partly attributed to this thermo-sensitivity. Using the framework of the thermodynamics of irreversible processes, taking into account the energy mechanisms accompanying material deformation in order to be able to construct a complete energy balance can play an important role in modelling the vis-

coelastic behaviour of polymers.

Therefore, the ability of predicting the so-called dynamic mechanical and thermal behaviour of amorphous polymers for several decades is a strong motivation for the modelling of time-temperature superposition principle under the framework of Thermodynamics of Irreversible Processes, taking into account the dissipative effects and coupling mechanisms induced by deformation.

Based on experimental means of visco analysis (DMTA), phenomenological models have been developed to predict the viscoelastic behaviour of amorphous polymers. While implementing these models, it has been observed that the dissipative effects associated with viscous effects are often very small compared to the coupling of sources indicating a high sensitivity of polymeric materials to temperature variations. This is being ignored since the beginning which can create a difference in the life of a material. To account for these ignored dissipative and coupling effects for the rheological characterisation of amorphous polymers, these concepts are revisited at the base of the "visco-analysis" of amorphous polymers in order to establish the exact role of coupling effects.

The approach taken to achieve the set of objectives is mainly based on different chapters which are summarized as:

• Concerning the synopsis of this doctoral thesis, the first chapter familiarize us with the brief introduction about polymers followed by a brief desciption of their microstructures and mechanical properties. It also includes the brief knowledge about the physical phenomenon in the polymers e.g., the glass transition temperature and relaxation transitions of amorphous polymers. The first chapter also introduces briefly about the DMTA characterization technique followed by the literature survey of previous work carried out by researchers using this characterization technique. Concerning the thermo-mechanical behaviour of amorphous polymers, the attention was put on the viscous analysis of amorphous polymers since it is the main concern of this thesis. A short review was also performed for the experimental work and the parameters used in the manipulations carried out by using DMTA and the implementation of the fundamental concept of time-temperature superposition principle on the outcome of the manipulations. In the end, a brief literature survey was made introducing the thermodynamic interpretation of DMTA measurements.

• The second chapter recalls the notions of thermodynamics of irreversible processes necessary for the local writing of the heat diffusion equation[6] and of the different energy balance terms. The particular framework used is the generalized standard material formalism (GSM) [7] which allows to derive the constitutive equations for the behavior from thermodynamic and dissipation potentials. It also introduces the local expressions of the first and second principle of the thermodynamics, as well as the local formulation of the Clausius-Duhem inequality. These general relations are then applied to cyclic tests to discuss the different mechanisms that can lead to the existence of mechanical hysteresis loops during cyclic measurements. It is then reminded that hysteresis areas may not be due solely to mechanical dissipation. [8].

• The third chapter discusses the experimental setup used in this thesis. The devices used in the experimental setup comprises of several different DMTA i.e., NETZSCH 242e Artemis, BOSE ElectroForce 3200 Series III, METRAVIB DMTA +300 and METRAVIB DMTA 50. A

first set of measurements was performed on PS in several laboratories to check for its monochromatic response to a monochromatic loading and build a reference database for the calibration and validation of different correction procedures (machine stiffness and electronic phase shift) of our DMTA. The DMTA used in LMGC i.e., BOSE Electroforce 3200 Series III was used along with the Infrared focal plane array (IRFPA) camera for synchronized thermography measurements to consider into account the temperature of the sample as well during cyclic loading of the polymer to analyze the energy variations associated with the possible thermo-mechanical couplings and/or dissipative effects induced in the sample during the cyclic measurements. In particular, the chapter discusses the precision experimental setup used in LMGC for the DMTA measurements along with the thermography measurements. Using the corrected data obtained in LMGC, the E' and E" were again computed using least square fitting. These computed E' and E" were compared with the experimental E' and E" followed by the computation of activation energy (E_a) of all the polymers used, using the Arrhenius law. This E_a was later served as a parameter during modelling part in Chapter-4.

• The fourth chapter of this thesis is focused on the identification of the generalized Maxwell model by using the regularization method. This regularization method was used to determine the temperature dependent relaxation spectrum associated to the optimized number of viscoelastic branches for the three different polymers. We then discussed the compatibility of the identified model with the time-temperature superposition principle. The structure of the viscoelastic branches of Maxwell's generalized model then allowed us to find the hypothesis of rheologically simple materials. Indeed we mathematically derive the fact that, for all viscoelastic branch of identified model, the relaxation time constants have to be linked to temperature via a single law (Arrhenius law here). Following the identification of generalized Maxwell model, considering temperature as an internal state variable, the energy balance rate over a cycle were calculated. We observed a predominance, from an energy standpoint of the thermomechanical coupling sources.

This thesis work traditionally ends with the general conclusion based on the experimental results that are obtained in chapter-3 along with the experimental setup. The general conclusion was also based on the rheological modelling was performed in chapter-4, using the experimental results from chapter-3. Some prospects are finally proposed.

Chapter 1

Literature Review

Contents

List of symbols

$H(t-t_0)$ – Heavy side function
Q, Q_0 – Instantaneous force, Initial instantaneous force
q, q_0 – Instantaneous force, Initial instantaneous force
t, t_0 – Time, Initial time
J, j – Creep function, Linear creep function
R, r – Relaxation function, Linear relaxation function
$\varepsilon, \varepsilon_0$ – Deformation, Initial deformation
σ, σ_0 – Stress, Initial stress
ω – Angular frequency
f – Frequency
f_r – Reduced frequency
E' – Storage modulus
E" – Loss modulus
ε^* – Complex deformation
σ^* – Complex stress
E^* – Complex modulus
$tan\delta$ – Loss tangent
δ – Phase angle
T_g – Glass transition temperature
T_0 – Reference temperature
T_s – Softening temperature
G' – Shear storage modulus
ρ, ρ_0 – Density, Density at ref. temperature
η, η_0 – Viscosity, Viscosity at ref. temperature
a_T – Shift factor
E_a – Activation energy
R – Universal gas constant
τ – Relaxation time
τ_n – Chain relaxation
τ_s – Segmental relaxation
f_v – Fraction of free volume
f_g – Fraction of free volume at T_g
V_f – Free volume
V_0 – Occupied volume
α_f – Linear expansion coefficient
M_n – Number average molecular weight
E – Vibration energy
ΔE – Vibration energy loss per cycle

In the first part, we shall recall the fundamental notions concerning polymeric materials and the vitreous state. We shall then examine the main characteristics of the mechanical behavior of the amorphous polymers shown experimentally. Finally, we will review the various modelling approaches to describe the thermomechanical behavior and the implementation of the corresponding superposition principle. Concerning the mechanical properties, the emphasis was put on the viscoelastic behaviour of amorphous polymers specifically Polystyrene (PS) and Poly(methyl methacrylate) (PMMA).

1.1 Polymers

In our everyday life, lots of things are made out of polymers such as plastic and rubber materials, cosmetics, paints etc., but the term polymer covers a very large group of molecules including substances from natural proteins to high-strength Kevlar fibres. Morphologically speaking, the word polymer is derived from the Greek "*poly*" meaning "*many*" and from "*mer*" meaning "*parts*"; thus polymers are substances made of "*many parts*". More precisely, polymers are macromolecules consisting of structural repeating units generally linked together through chemical bonds.

A key feature that distinguishes polymers from other large molecules is the repetition of chemical units in their molecular structure. These repeating units called monomers are typically small molecules of low molecular weight. The process of converting monomers into a polymer is called polymerization and the resulting polymer is often named after the chemical name of the monomer units. The monomers can be identical, or they can have one or more substituted chemical groups. These differences between monomers can affect physical and mechanical properties such as solubility, flexibility or strength. Many polymers are made from combinations of carbon, hydrogen, nitrogen, chlorine or fluorine atoms, to name a few. Although, most polymers are organic (based on carbon chains), there are also some inorganic polymers, mainly based on silicon backbone.

The polymer chains within a substance are often not of equal length. This distribution of chain lengths occur because polymer chains terminate during polymerization after random intervals of chain propagation. This is how the term polymer also describes a distribution of polymer chains of different lengths and not only a single macromolecule.

As another remark, the polymers used for the fabrication of plastics are frequently classified into two categories: the thermoplastics and the thermosetting plastics. Thermoplastics are those, which once shaped or formed, can be softened by the application of heat and can be reshaped repeatedly, until their properties are degraded. Thermosetting plastics are those, which once shaped or formed, cannot be softened by the application of heat. Excess heat will char the material.

1.1.1 Polymer Structure

Polymer molecules may be long straight chains, or they may be branched with small chains extending out from the molecular backbone. The branches also may grow until they join with other branches to form a huge three-dimensional matrix. Thermoplastics are predominantly

linear or branced polymers while thermosetting plastics usually forma three-dimensional network of polymer chains [9].

1.1.1.1 Branching

In radical polymerization, branching can occur during the propagation of polymer chains when a chain curls back and bonds to an earlier part of the chain. But the chain curl will break starting the growth of small chains from the main polymer chain. Branched chains cannot line up as close to each other as unbranched chains can (figure 1.1). This causes less contact between the atoms of different chains, and fewer opportunities for induced or permanent dipoles to occur. A low density results from the chains being further apart. Lower melting points and tensile strengths are evident, because the inter-molecular bonds are weaker and requires less energy to break.

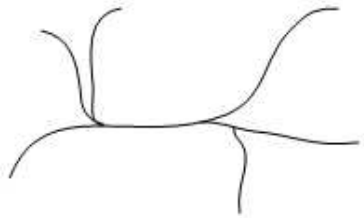

Figure 1.1: Schematic representation of a branched polymer
[9]

1.1.1.2 Crosslinking

Crosslinking is the process of chemically joining two or more molecules by a covalent bond. Chemical crosslinks are the characteristic property of thermosetting plastic materials (figure 1.2).

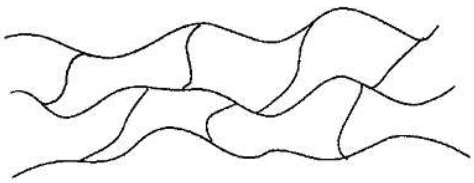

Figure 1.2: Schematic representation of a crosslinked polymer
[9]

They are formed by chemical reactions that are initiated by heat or/and pressure, or by the mixing of an unpolymerized or partially polymerized resin with various chemicals. Crosslinking can also be induced in materials that are normally thermoplastic through exposure to radiation. In most cases, crosslinking is irreversible, and the resulting thermosetting material will degrade

or burn if heated, without melting.

In addition to primary valence bonds and if the polymer chains are long enough, it is also possible to keep the chains together by secondary valencies such as the van der Waals forces (intermolecular forces).

1.1.1.3 Stereoregularity

Stereoregularity or tacticity describes the isomeric arrangement of functional groups on the backbone of carbon chains. As shown in figure 1.3, isotactic chains are defined as having side-groups aligned in one directions. Syndiotactic chains are defined as having side-groups alternated regularly in opposite directions. Because of this regularity, both isotactic and syndiotactic chains can position themselves close to each other, creating crystalline areas. This results in highly rigid polymers with high tensile strength. In contrast, atactic chains have randomly aligned side-groups. The chains do not fit together well and the intermolecular forces are low. This leads to polymers with low density and low tensile strength.

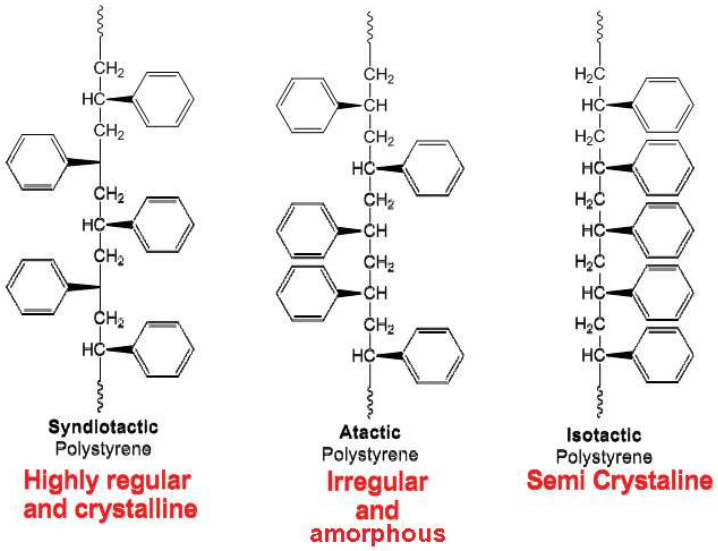

Figure 1.3: The three stereoregularity forms of PS
[10]

1.1.1.4 Amorphous and semi-crystalline thermoplastic polymers

Depending on the degree of chain ordering and alignment, thermoplastic polymers can range from amorphous to crystalline. A semi-crystalline polymer contains crystalline and amorphous regions. It is neither all crystalline in nature, nor is it all amorphous. A few examples of amorphous and semi-crystalline polymers is given in table 1.1.

As shown in figure 1.4, amorphous refers to the random alignment of the polymer chains showing no structural order while crystalline refers to a structured alignment of the polymer

Amorphous polymers	Semi-crystalline polymers
Polystyrene	High density polyethylene
Poly(vinyl chloride)	Low density polyethylene
Poly(methyl methacrylate)	Polypropylene
Polycarbonate	Polyamide 11

Table 1.1: Some amorphous and semi-crystalline polymers

chains in a polymer matrix.

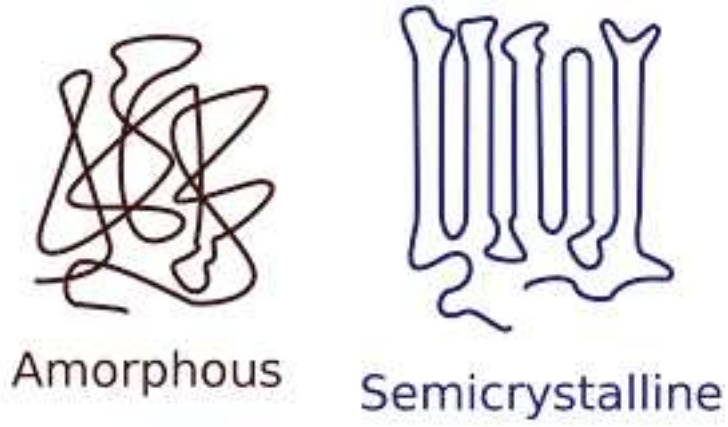

Figure 1.4: Schematic representation of amorphous and semi-crystalline structure of a polymer [11]

1.1.2 Mechanical properties of polymers

Polymer class of materials is so diverse that they differ from liquid to solid and soft to rigid rubbers. Their different properties buckled with their light weight make them an alternative option in place of metallic and composite materials. An attentive deliberation must be given to the mechanical properties of the polymers while their selection. Few properties of the amorphous polymers such as PMMA and PS is shown in the table 1.2.

Properties	PMMA	PS
Density (g/cm^3)	1.17-1.20	1.03-1.06
Young's modulus (MPa)	3200-3700	3100-3500
Tensile strength (MPa)	62-90	30-100
Hardness (Rockwell)	92-100	60-90

Table 1.2: Some properties of amorphous polymers PMMA and PS (Goodfellow)

This attentive deliberation is important not only in the applications where mechanical properties of the chosen polymers are of elementary role but also in the applications where other

aspects of the polymers are also of decisive importance. The polymer's microstructure or the morphology is the main the responsible reason for its mechanical behaviour. The mechanical properties of polymers show a much stronger time and temperature dependency in comparison to the other materials like metals and ceramics. This strong dependence of mechanical properties of polymers on time and temperature is the result of viscoelastic nature of the polymers i.e., the polymers shows combined viscous and elastic behaviour.

The polymers are also well known for excessive elastic deformation due to deficient rigidity or stiffness, for which, elastic modulus is the primary controlling mechanical material property. Therefore, to establish the successful performance of the polymers, it is an obligation to study their mechanical behaviour applicable for different stress conditions such as creep and stress relaxation experiments.

1.1.2.1 Creep experiments

Creep is the tendency of a material after being subjected to high levels of stress, e.g. high temperatures, to change its form in relation to time. It is also known as the retardation phenomenon.

Let us suppose that, an instantaneous force Q is applied at the initial value of Q_0 at time t_0 and displacement q, which was zero up to t_0, is recorded as a function of time t for $t \geq t_0$. The creep test exhibits the creep faculty of the viscoelastic material, i.e., the ability to flow when subjected to a constant force. An illustration of the creep test is shown in the figure 1.5.

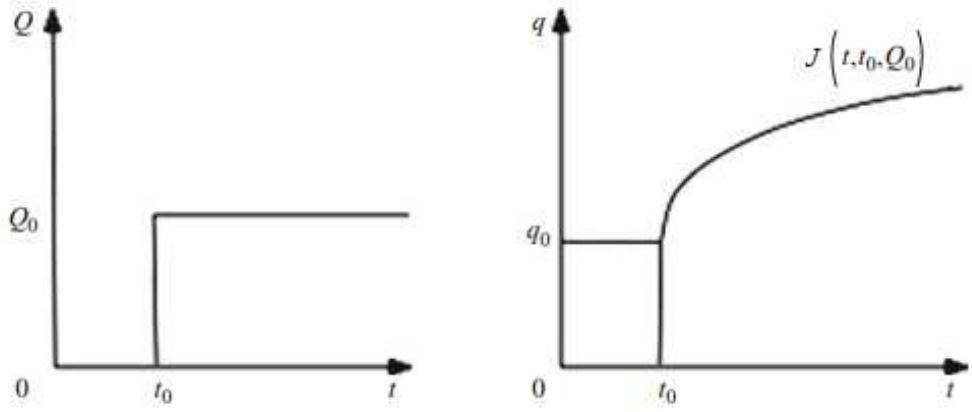

Figure 1.5: Creep test
[12]

This test can be written in mathematical form as follows:

$$Q(t,t_0) = Q_0 H(t,t_0) \Rightarrow q(t,t_0) = J(t,t_0,Q_0) \tag{1.1}$$

where $H(t - t_0)$ is a Heaviside unit step function at time t_0 and $J(t, t_0, Q_0)$ is the general form of the creep function.

1.1.2.2 Stress relaxation experiments

The aspect of Q and q are reverted with respect to the creep test; an instantaneous displacement q is applied with a initial value of q_0 at time t_0 and force Q, which is recorded as a function of time t for t$\geq t_0$. In the end, Q might tend towards the constant Q_∞. An illustration of the stress relaxation test is shown in the figure 1.6.

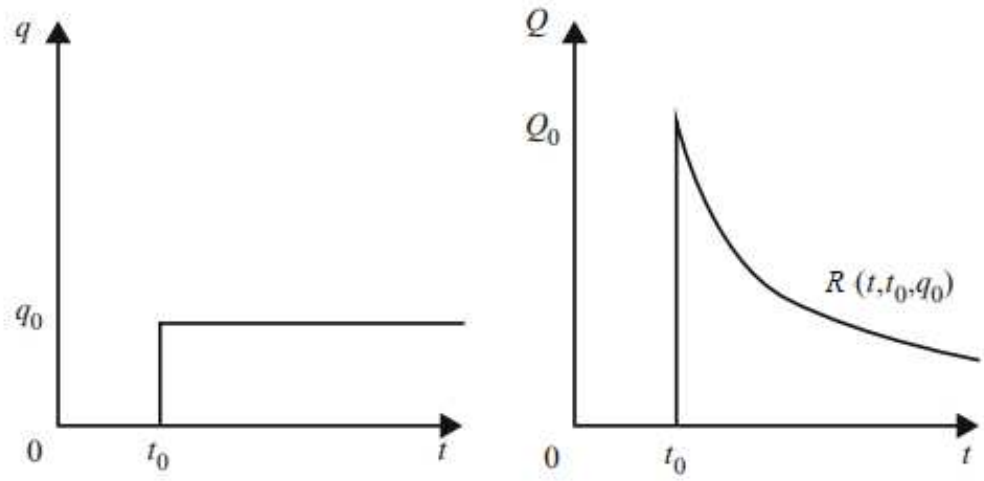

Figure 1.6: Stress relaxation test
[12]

This test can be written in mathematical form as follows:

$$q(t, t_0) = q_0 H(t, t_0) \Rightarrow Q(t, t_0) = R(t, t_0, q_0) \tag{1.2}$$

where $H(t - t_0)$ is a Heaviside unit step function at time t_0 as in creep test and $R(t, t_0, q_0)$ is the general form of the relaxation function.

1.1.3 Linear viscoelasticity

1.1.3.1 Linear creep and relaxation function

Linearity signifies that in a creep test, when the instantaneous force Q_0 is multiplied by λ, the response in terms of displacement is given by equation 1.1 as $q(t, t_0) = R(t, t_0, Q_0)$ must also be multiplied by λ. Therefore, the general form of the creep function $R(t, t_0, Q_0)$ can be written

as

$$J(t, t_0, Q_0) = Q_0 j(t, t_0) \tag{1.3}$$

where $j(t, t_0)$ is a linear creep function. Similarly, for a relaxation test,

$$R(t, t_0, q_0) = q_0 r(t, t_0) \tag{1.4}$$

where $r(t, t_0)$ is the linear relaxation function.

1.1.3.2 Boltzmann Superposition Principle

A linear material obeys the superposition principle of BOLTZMANN, which makes it possible to write the response to any loading and no longer necessarily constant, from the functions of creep or relaxation. The formulation of BOLTZMANN principle presented here is based on the response of the history of displacement, a modification of Q and q makes it possible to find the formulas for a response to the history of Q. Therfore, for a linear viscoelastic system defined by the variables (Q,q), the BOLTZMANN principle reads for two Q-histories Q^1 and Q^2,

$$(Q^1 \Rightarrow q^1, Q^2 \Rightarrow q^2) \Rightarrow (\lambda_1 Q^1 + \lambda_2 Q^2 \Rightarrow \lambda_1 q^1 + \lambda_2 q^2) \tag{1.5}$$

which is similar for the case of two q-histories.

Any Q-history starting from $t = t_0$ (figure 1.7) can be considered as the superposition of the incremental steps,

$$dQ(\tau) = \frac{dQ}{d\tau} d\tau H(t - \tau) \tag{1.6}$$

Since, the response according to the figure 1.7 is $\frac{dQ}{d\tau} d\tau j(t, \tau)$, the entire response should be

$$q(t) = Q(t) j(t, t) - \int_0^t Q(\tau) \frac{\partial j(t, \tau)}{\partial \tau} d\tau \tag{1.7}$$

where the instantaneous and the delayed responses have been clearly separated.

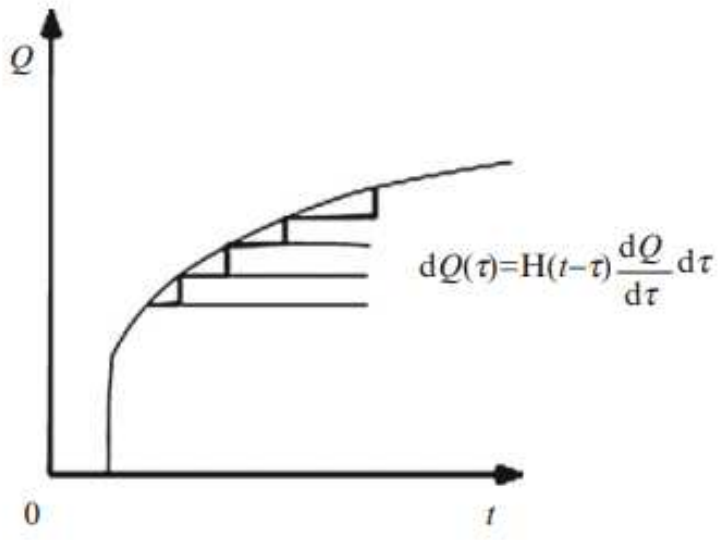

Figure 1.7: Decomposition of a Q-history into incremental steps
[12]

1.1.3.3 Harmonic experiments

Harmonic tests are the tests which consist of imposing a stress or a deformation which varies sinusoidally with time according to the frequency f. For a linear viscoelastic material, the response to a sinusoidal stress is also sinusoidal, of the same frequency but out of phase by an angle δ.

In the case of harmonic tests where deformation ε is imposed,

$$\varepsilon(t) = \varepsilon_0 cos(\omega t) \tag{1.8}$$

where ε_0 is the initial deformation and ω is the angular frequency ($\omega = 2\pi f$).
The response in form of stress is given as,

$$\sigma(t) = \sigma_0 cos(\omega t + \delta) \tag{1.9}$$

The use of complex numbers facilitates the writing of equations, therefore, we introduce the complex quantities σ^* and ε^* given as,

$$\varepsilon^*(t) = \varepsilon_0 e^{i\omega t} \quad and \quad \sigma^*(t) = \sigma_0 e^{i(\omega t+\delta)} \tag{1.10}$$

Therefore, we can introduce the complex modulus (E^*) which can be written as,

$$E^* = \frac{\sigma^*(t)}{\varepsilon^*(t)} \tag{1.11}$$

The real part of the complex modulus is called as storage modulus (E') and the imaginary part is known as the loss modulus (E"). Using these real and imaginary parts of the complex modulus, we can write the loss tangent (also called damping coefficient) as:

$$tan\delta = \frac{E"}{E'} \tag{1.12}$$

where, $E'(\omega) = E(\omega)cos(\delta)$ which represents the elastic part of the stress response and $E"(\omega) = E(\omega)sin(\delta)$ which represents the viscous part of the stress response.

1.2 Relaxation Transitions of Amorphous Polymers

Transition is a process or a phenomenon or a period of changing from one state/condition to another. A classical illustration of transition in polymers is shown in the figure 1.8 [13] cited by [14].

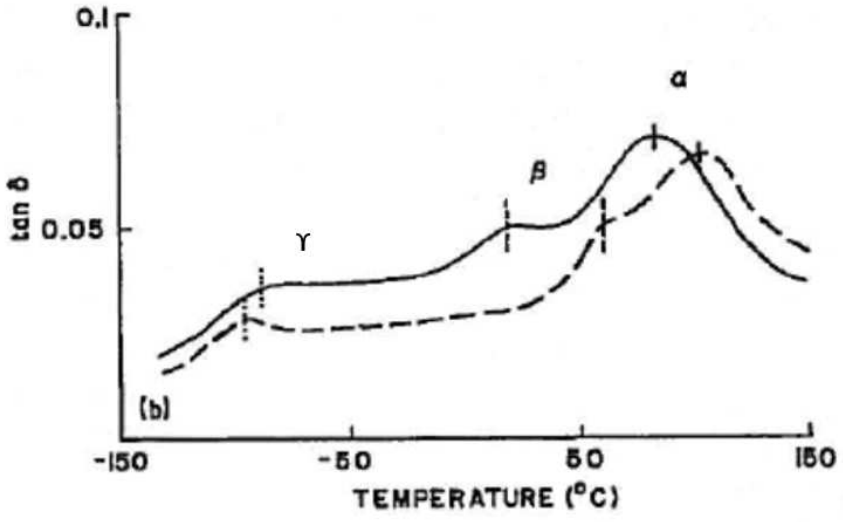

Figure 1.8: A classical illustration of transition regions in polymers

Amorphous polymers show more than one transition region. These different transitions must be labelled with the symbols α, β and γ to identify and to compare these different regions for several polymers. A dramatic change in the modulus occurs in the region of the glass transition

temperature. This can be thought of as being due to the available thermal energy falling below the required for chain segments to have the energy needed to overcome the potential barriers to move which locks the system in glassy state and this transition is called as α transition or α relaxation. 'α' relates to the transition at higher temperatures and is considered as the first transition region in any polymer. The 'β' and 'γ' relates to the other transition regions in order of the decreasing temperatures. Each transition region is associated with analogous activation energy change in storage modulus and mainly in the dissipation.

Figure 1.9 illustrates how the storage modulus and damping of an amourphous polymers depends on the temperature which results in the occurance of relaxation peaks in damping followed by the transitions in the storage modulus of the amorphous polymers. In the glass transition T_g, the modulus drops by a factor of thousand; in the same transition region the material changes from glassy to rubbery. This transition corresponds to a high loss peak in damping which is called as α relaxation or α peak [15].

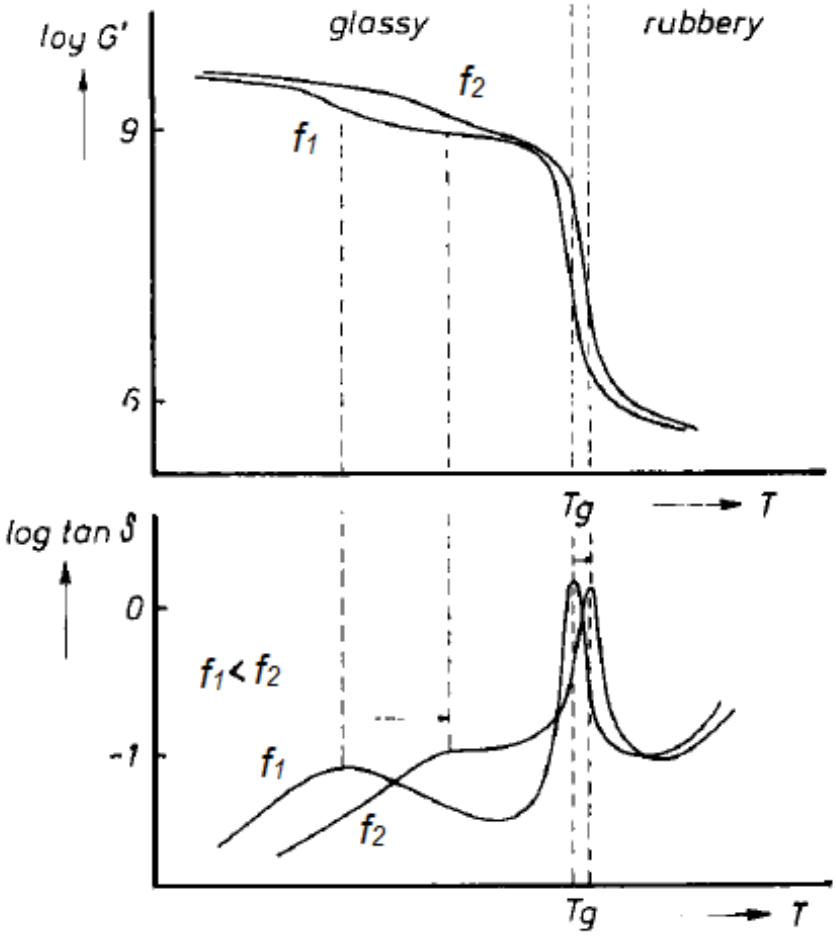

Figure 1.9: Storage modulus G' and damping tan δ as a function of temperature T at two frequencies f_1 and f_2 for an amorphous polymer
[15]

Except for this main transition, nearly there are always minor transitions in the glassy region which results in the decrease of modulus by a factor of e.g. not more than two which

is almost negligible in comparison to the decrease of modulus in main transition. Though these secondary or minor transitions might have a sound effect on the mechanical properties of amorphous polymers. From the figure 1.9, secondary transition seems to be very clear in the damping curves than in the modulus curves; the modulus curve hardly shows a steeper decrease whereas the different maximum is shown by the loss tangent curves. If these secondary transitions are more in number, they are generally named as β, γ and so on from higher to lower temperatures using successive greek letters.

1.2.1 Glass transition

1.2.1.1 Definition

The glass transition is a kinetic transition which results of molecular dynamic rearrangement of polymer chains between the glassy state (localized molecular movement) and a rubber-like state (high amplitude movement). The glass transition temperature is denoted as Tg and is known to be widely influenced by the chemical structure of the polymer. The introduction of side chains and relatively stiff chemical groups like benzene ring usually increases Tg. An illustration to show the glass transition temperature of an amorphous polymer (polystyrene) is shown in the figure 1.10.

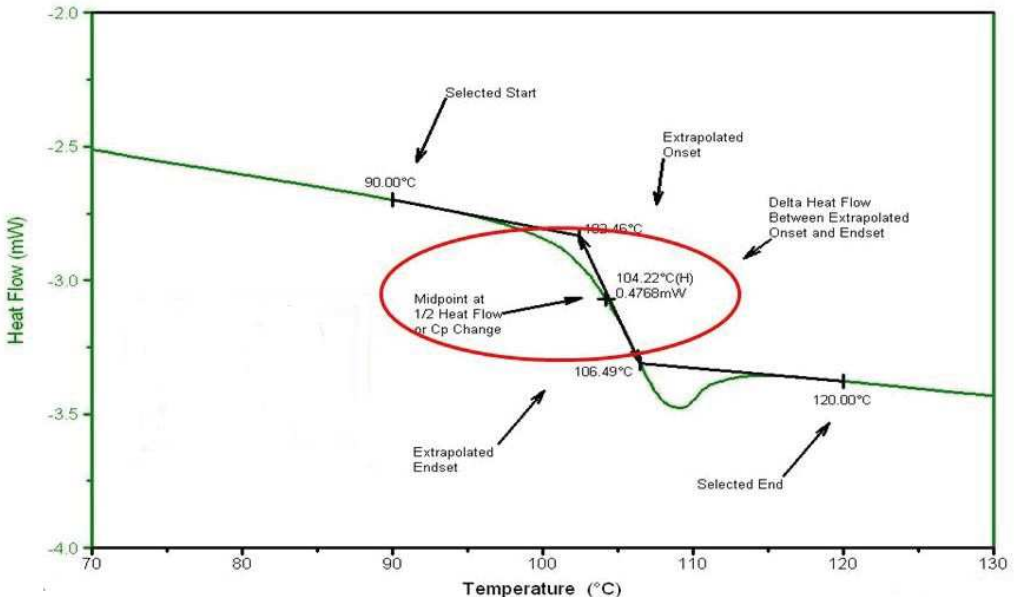

Figure 1.10: An illustration to show glass transition temperature of polystyrene [16]

In this figure 1.10, the Differential Scanning Calorimetry (DSC) technique was used to determine the glass transition temperature of polystyrene. This technique uses the step change in the heat capacity of the material to detect the glass transition temperature by peak in derivative method.

1.2.1.2 Glass transition from a thermal point of view

The glass transition is frequently characterized by a step change of calorific capacity of the polymer, like it is the case for second order thermodynamic transitions. However, there is no thermodynamic equilibrium between the glassy state and rubber-like state, but a meta-stable equilibrium. The glass transition is not isothermal, since it occurs on a range of a determination by Differential Scanning Calorimetry. Other factors such as heat treatment may have an effect on Tg ranging from very subtle to dramatic.

1.2.1.3 Glass transition from a mechanical point of view

Tg is the temperature at which a solid amorphous polymer softens into a flexible viscous rubber. As a very simple explanation, below Tg, the polymer chains cannot move the polymer is frozen into a rigid glassy state. Upon heating to Tg, complete segments of the polymer chain become free to move as local entities and the polymer behaves like a soft rubber.

1.2.2 Secondary relaxations of amorphous polymers - A brief review

According to J. Heijboer [15], the second type of motion is the local main-chain motion which is the only possible molecular mechanism causing a secondary loss peak in a polymer possessing no side groups that can move independently of the main chain. This kind of motion generally found in polycarbonates (PC). The third type of motion is a side group motion with some cooperation of main chain, e.g., a partial rotation of the side group about the bond linking it to the main chain and this type of motion was found by J. Heijboer [15] to be regarded in β maximum of poly (methyl methacrylate) (PMMA) which is contrary to the molecular motion found by Havriliak and Roman [17] which suppose that the β maximum of PMMA is due to the main chain motion. Fourth type of motion is an internal motion within a side group without interference by the main chain. Hoff et al. [18] found that the internal motions within R of the –COOR group of poly-methacrylate (PMA) are without interference by the main chain. A fifth type of motion is the motion of a small molecule dissolved in the polymer.

The β relaxation in PMMA has been assigned to the hindered rotation of the side group. The hindrance to this rotation mainly arises from interaction with the main chain methyl groups of the adjacent units [19] where J. Heijboer [15] argues that the alkoxy groups cannot be responsible for the β maximum of PMMA even if the calculated value of the barrier to the rotation of alkoxy group is not so far from the activation energy observed experimentally.

F. Krum and F.H. Muller [20] (Cited by [21]) found that PC (Poly-carbonate) is one of the best example in which both primary and secondary transitions are observed through motions of –O-CO-O group in the main chain. The basic requirement according to most of the researchers who have studied the relaxations, for the secondary transition would be the provision for enough local motion among the segments of the main chain in the glassy state. S. Matsuoka and Y. Ishida [21] also found that polymer like PC would be a great choice who would dissipate strain energy effectively during deformation.

1.2.3 Temperature dependence of relaxation mechanisms in amorphous polymers

Polymers exhibit peculiar viscoelastic behaviour due to chain relaxation that controls their viscosity and mechanical propeties. The traditional assumption is that the friction coefficient is the same for various chain (β, γ) and segmental (α) modes. The apparent friction coefficient is the ratio of the tangential force to the normal load applied to a moving tip in contact with the surface of a material [22]. The various relaxation processes in a polymer are expected to have the same temperature dependence and it leads to the *time-temperature superposition* [23], whereas JD Ferry in 1980 [24] mentioned that in an amorphous polymer, above its glass transition temperature, a single empirical function can describe the temperature dependence of all mechanical relaxation processes. The ratio a_T of any mechanical relaxation time at temperature T to its value at a reference temperature T_0, appear to be identical over wide ranges of time scale. An example is shown from literature in figure 1.11, showing the dependence of shift factor for two different amorphous polymers on the temperature.

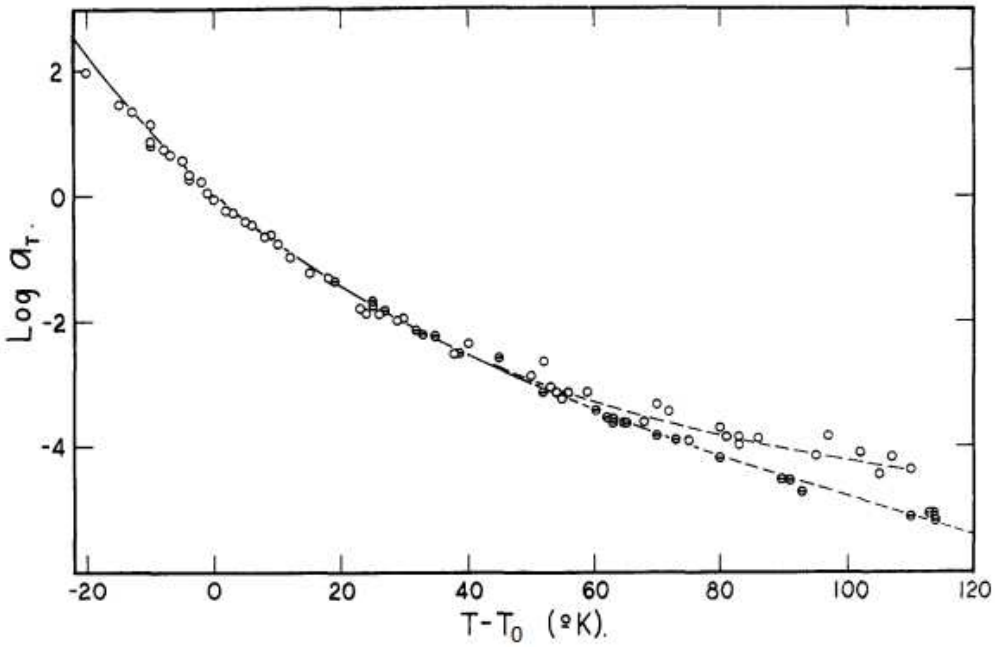

Figure 1.11: Log a_T plotted against T-T_0 for polystyrene (open circles) and polyisobutylene (slotted circles).

[25]

In this figure 1.11, a divergence between the $a_T = \dfrac{\eta T_0 \rho_0}{\eta_0 T \rho}$ curves of two different polymers was observed by William, Landel and Ferry in 1955 [25] where ρ and η are the density and viscosity at temperature T and ρ_0 and η_0 are the corresponding quantities at reference temperature T_0.

Since near T_g, viscosity and other mechanical measurements are more difficult and data in this region is often lacking, therefore, T_s (softening temperature usually considered as $T_g + 50^oK$ for amorphous polymers) can always be considered as the reference temperature even if it is based on the value of original arbitrary choice. It was also found by William-Landel-Ferry in

1955 [25] that temperature dependence of viscosity and mechanical relaxations in amorphous polymers arises from the fact that these processes depend on temperature primarily through their dependence on free volume (explained further in the section 1.3.4).

1.3 DMTA (Dynamic Mechanical and Thermal Analysis)

1.3.1 Introduction

Dynamic mechanical and thermal analysis (DMTA) is a great complement to stress-strain experiments by both measuring elastic and viscous properties. The technique consists in the application of an oscillatory strain to a polymer sample. The resulting sinusoidal stress is measured and correlated against the input strain. The strain is oscillated at a constant amplitude, ε_0, and at a constant harmonic frequency, ω. The strain input is given by,

$$\varepsilon(t) = \varepsilon_0 \sin(\omega t) \tag{1.13}$$

The associated stress, $\sigma(t)$, will respond with the same frequency but with a phase difference as shown in figure 1.12:

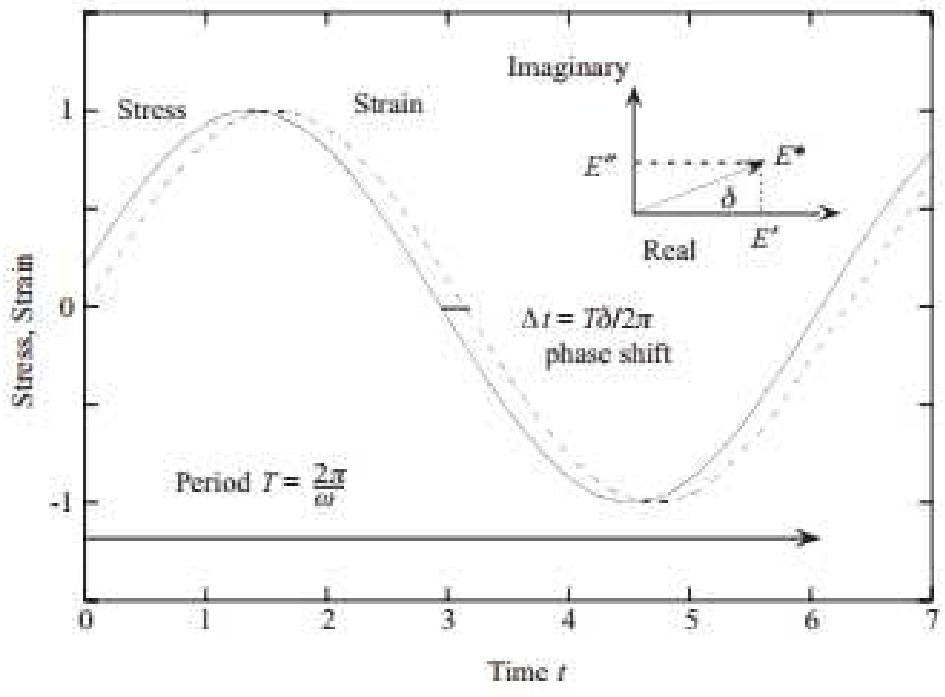

Figure 1.12: Stress and strain vs time, with a phase shift. Arbitrary units of stress and time. [26]

$$\sigma(t) = \sigma_0 \sin(\omega t + \delta) = E(\omega)\varepsilon_0 \sin(\omega t + \delta) \tag{1.14}$$

where δ is the phase angle and E(ω) is the dynamic modulus defined by the ratio of stress to strain ($E(\omega) = \frac{\sigma_0}{\varepsilon_0}$). The phase angle, δ, describes the viscous character of the material. For viscoelastic materials, δ is between 0 and $\frac{\pi}{2}$. If δ=0, the stress is in phase with the strain and the material is totally elastic. If $\delta = \frac{\pi}{2}$, the stress is completely out of phase and the material is completely viscous [27].

1.3.1.1 Storage and Loss moduli

The DMTA data are frequently described with an alternative representation. The stress function is expanded and rewritten as,

$$\sigma(t) = E^{'}(\omega)\varepsilon_0 \sin(\omega t) + E^{"}(\omega)\varepsilon_0 \cos(\omega t) \tag{1.15}$$

where,

$$E^{'}(\omega) = E(\omega)\cos(\delta) \tag{1.16a}$$
$$E^{"}(\omega) = E(\omega)\sin(\delta) \tag{1.16b}$$

$E^{'}(\omega)$ is the storage modulus which describes the elastic part of the stress response. In other words, storage modulus $E^{'}(\omega)$ is a measure of energy stored and recovered per cycle, when different systems are compared at the same strain amplitude. An example of storage modulus vs frequency plot is shown in figure 1.13a and 1.13b (experimental results). These tests conducted on the sample of dimension 85 x 12 x 4 (length x breadth x thickness) of PMMA and PS at ambient temperature (25^{o}C). The cyclic deformation of 0.1% was used for this dynamic mechanical test and the viscoelastic behaviour was recorded in the form of storage modulus and loss modulus.

$E^{"}(\omega)$ is the loss modulus which describes the viscous part of the stress response. In other words, loss modulus $E^{"}(\omega)$ is a measure of the energy dissipated or lost as heat per cycle of sinusoidal deformation, when different systems are compared at the same strain amplitude. An example of loss modulus vs frequency plot is shown in figure 1.14a and 1.14b (experimental results).

Inverse relations of the previous results can be derived as,

$$E(\omega) = \sqrt{E'(\omega)^2 + E^{"}(\omega)^2} \tag{1.17a}$$
$$\tan\delta = \frac{E^{"}(\omega)}{E'(\omega)} \tag{1.17b}$$

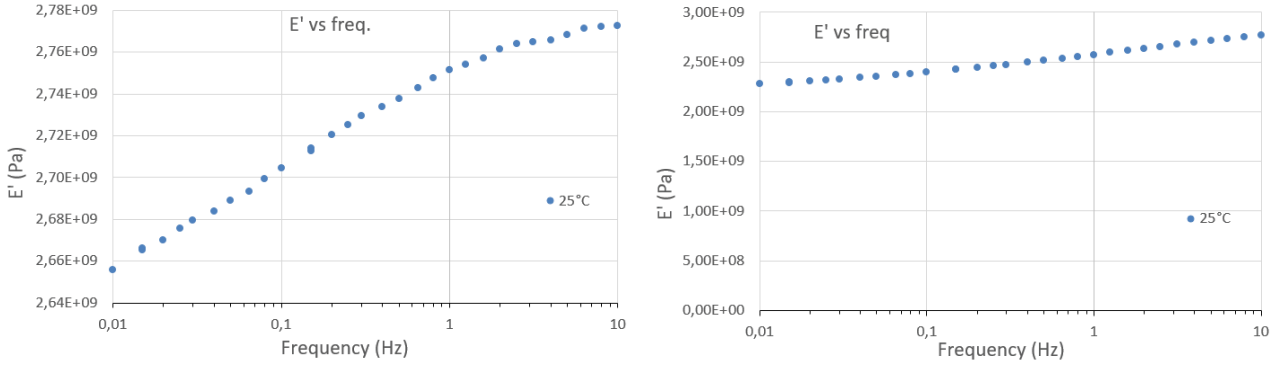

(a) PS (b) PMMA

Figure 1.13: Storage modulus vs frequency plots of (a)PS and (b)PMMA

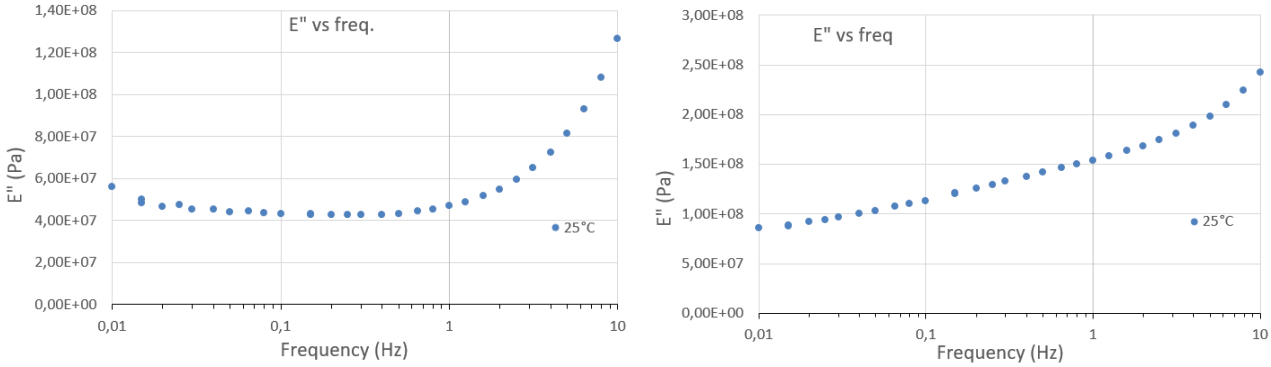

(a) PS (b) PMMA

Figure 1.14: Loss modulus vs frequency plots of (a)PS and (b)PMMA

A common practice for the presentation of DMTA results is to give the data simply for $E^{'}(\omega)$ and $\tan\delta$, since among the four previous dynamic quantities, only two are independent. We note that the temperature dependence of the storage modulus is frequently assimilated to the temperature dependence of the Young's modulus [27].

Where, $\tan\delta$ is a useful parameter, which is dimensionless and conveys no physical magnitude but is a measure of the ratio of energy lost or dissipated to the energy stored in a cyclic deformation is known as loss tangent, $\tan\delta = E^{"}/E^{'}$ [24].

1.3.2 Viscoelastic behaviour

A body which is not quite solid does not maintain a constant deformation under constant stress but goes on slowly deforming with time, or creeps. When such a body is constrained at constant deformation, the stress required to hold it diminishes gradually, or relaxes. On the other hand, a body which is not quite liquid may, while flowing under constant stress, store some of the energy input, instead of dissipating it all as heat. When such bodies are subjected to sinusoidally oscillating stress, the strain is neither exactly in phase with the stress (as it would

be for a perfectly elastic solid) nor 90^o out of phase (as it would be for a perfectly viscous liquid) but is somewhere in between. Some of the energy input is stored and recovered in each cycle, and some is dissipated as heat. Materials whose behaviour exhibits such characteristics are widely known as viscoelastic materials. If, in a given experiment the ratio of stress to strain is a function of time (or frequency) alone, and not of stress magnitude, then the behaviour is supposed to be linear viscoelastic behaviour [24].

The technique DMTA mentioned above in section 1.3 is one of the most efficient technique to characterize the linear viscoelastic behaviour of the special class of materials called polymers.

1.3.3 Typical DMTA data for amorphous polymers

Some typical DMTA data for an amorphous polymer as a function of temperature at a given frequency is plotted in figure 1.15:

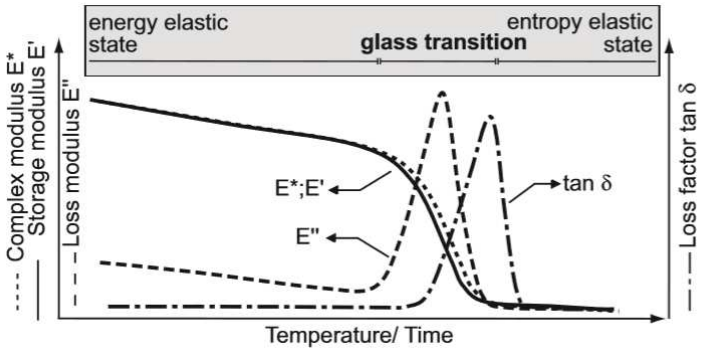

Figure 1.15: Typical DMTA data for an amorphous polymer
[28]

The temperature dependence of the loss factor, tan δ, is a convenient method to determine the relaxations of a polymer, such as the glass transition and the sub-T_g transitions. At the glass transition, a predominant mechanical loss peak is usually detected. The observation of the smaller peaks remains one of the best methods for the study of secondary relaxations.

Concerning the storage modulus, within a rough estimate, it can be considered constant in the glassy region ($T < T_g$). When the loss factor is small, the loss modulus is also small and the storage modulus is close to the young's modulus of the polymer that would be measured in a static test. Above T_g, the storage modulus drops dramatically, before reaching a plateau value in the rubbery zone. However, we have to mention that the modulus of a polymer is also sensitive to the sub-T_g transitions.

1.3.4 Time-temperature superposition principle

For a special class of materials called as polymers, it is possible to infer behaviour over a wide range of equivalent time or frequency from experiments conducted at different temperatures.

For a class of materials called *thermorheologically simple materials*, a change in temperature is equivalent to a shift of the behaviour on the log time or log frequency axis which is termed as *time-temperature superposition principle* (TTSP) or *time-temperature equivalence*. In other words, time-temperature superposition implies that time and temperature are generally equivalent in affecting the relaxation modulus of polymers [29].

Time-temperature equivalence was introduced by Leaderman [30] cited by [19] for creep compliance experiments (stress was held constant while strain is measured as a function of time; $J(t) = \varepsilon(t)/\sigma_0$) and it holds that time is equivalent to temperature for viscoelastic materials. It is experimentally observed that the creep at very long times and at a reference temperature can be expected to be equivalent to the creep at shorter times and at some higher temperatures. Conversely, the creep at shorter times at the reference temperature can be expected to be equivalent to the creep at longer times at some lower temperatures. An illustration for the amorphous polymers PMMA and PS from the literature is shown by the figure 1.16 [31] and figure 1.19 [32] in the section 1.3.6.

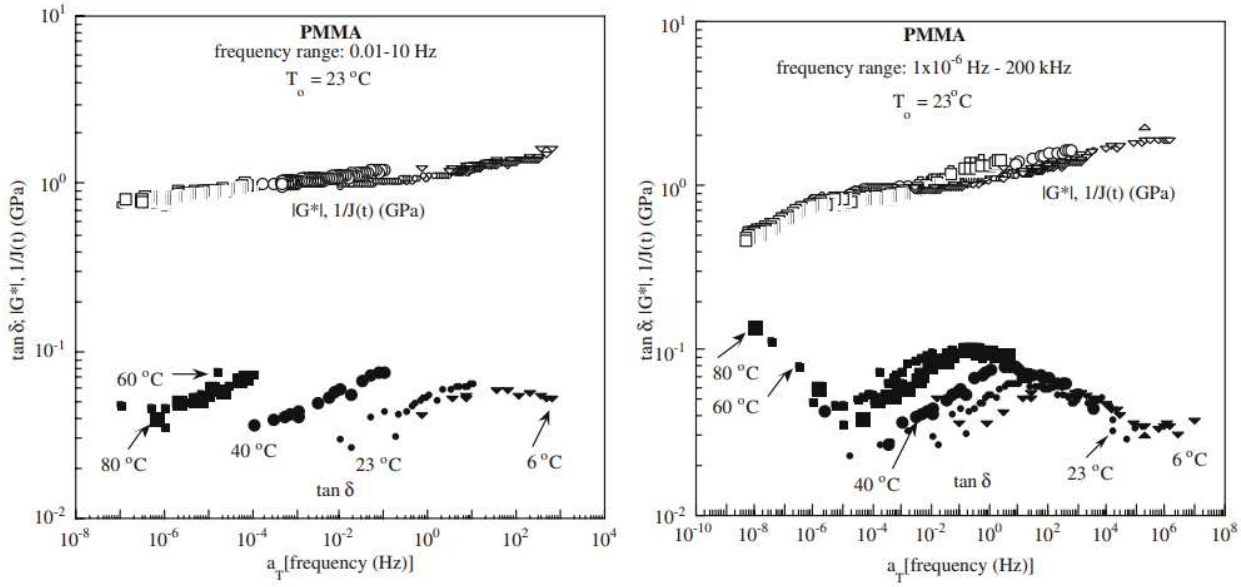

Figure 1.16: Illustration of master curve reduced to 23^oC at two different frequency ranges where solid symbols are for tanδ and open symbols are for complex dynamic shear modulus. [31]

For the results shown in figure 1.16, the tests were conducted on the PMMA rods of diameter 3.33mm and length 1.8m with density of 1.15 g/cm^3. These tests were conducted for two different frequency range but at the same temperature i.e., 23^{o}C. The frequency range was 0.01-10 Hz and 1x10^6-200kHz. For the latter frequency range, Resonant Ultrasound Spectroscopy (RUS) was used, in which, the specimen was held by its edges between two shear ultrasonic transducers and frequency was varied through the fundamental natural frequency at room temperature.

It was shown by John D Ferry [24] that the time-temperature superposition can be applied to DMTA data effectively where the frequency of the dynamic testing substitutes to the role of time in the superposition principle. Figure 1.17, illustrates the validity of the time-temperature

superposition principle on the shear storage modulus of a statistical copolymer.

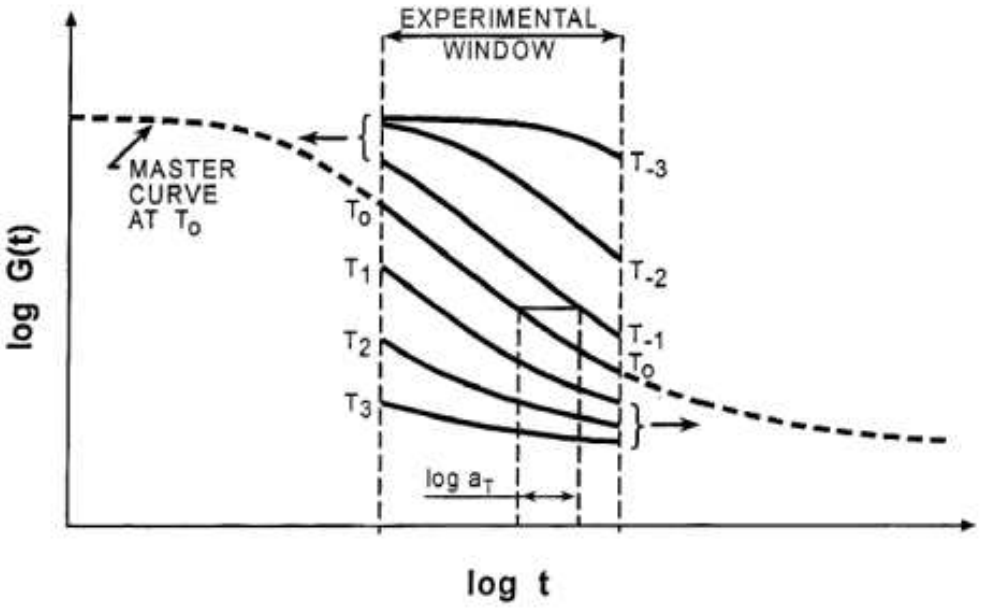

Figure 1.17: Illustration of Time-temperature superposition principle [33]

The master curve was built for a lone temperature T_0. The entire curve was obtained from the raw data by shifting curves horizontally until they achieve the maximum overlap with data at the reference temperature T_0. The horizontal shift, log a_T, relates the real frequency, f, with the reduced frequency, f_r. The expression of log a_T is given by,

$$loga_T = logf - logf_r \tag{1.18}$$

Consequently, to move the curve at a give temperature to the master curve, the curve has to be moved or shifted horizontally by the amount -log a_T. The curve is shifted to the right if log $a_T < 0$ and to the left if log $a_T > 0$. The term log a_T is thus known as the shift factor. Because for $T > T_0$, the curves are shifted to the right according to the WLF (William-Landel-Ferry) law as log a_T is less than zero. At T_0, log a_T is equal to zero and for $T < T_0$, log a_T is greater than zero as follows the Arrhenius law to construct a master curve.

The time-temperature superposition principle works on the two different law based on the temperature region and are known as WLF law and Arrhenius law which are explained further in detail.

The WLF law is an empirical law discovered by William, Landel and Ferry which is associated with time-temperature superposition principle. This law is shown below in the form of an equation,

$$log(a_T) = \frac{-C_1(T - T_0)}{C_2 + (T - T_0)} \tag{1.19}$$

where, T is the temperature, T_0 is the reference temperature chosen to construct the master curve and C_1 and C_2 are the empirical constants adjusted to fit the values of the superposition parameter a_T. This is the law which comes into play when the temperature is above the glass transition temperature(T_g).

The Arrhenius law gives the dependence of the rate constant of a chemical reaction on the absolute temperature, a pre-exponential factor and other constants of the reactions. Mathematically,

$$log(a_T) = \frac{E_a}{RT}[\frac{1}{T} - \frac{1}{T_0}] \tag{1.20}$$

where, R represents the universal gas constant.

This equation has a vast and important application in determining the calculation of energy of activation (E_a). This law comes into play when the temperature used is the temperature below the glass transition temperature.

1.3.4.1 When the time-temperature superposition principle is suppose to exist?

There are various concepts that has been published till date by several researchers explaining the criteria/conditions for existence of time temperature superposition principle.

The fundamental assumption for existence of TTSP is that the polymer shouldn't change in structure as a function of time [34]. As referred, TTSP holds when the exact matching of shapes of adjacent (time or frequency dependent) curves is obtained, a_T has the same value for all viscoelastic functions, and the temperature dependence of a_T has a reasonable form such as the Arrhenius and WLF models [35, 36, 37]. Where William-Landel-Ferry [25] found that TTSP holds when all the retardation times in the distribution are displaced (take over the place) along the "$ln\tau$" axis by "lna_T" when temperature is changed from T_0 to T. Later, JD Ferry, in 1980, mentioned in his book [24] that TTSP exists when $\frac{\tau_n}{\tau_\alpha}$ remains constant with variation of temperature or relaxation time, which was confirmed by AP Sokolov and Y Hayashi in 2007 from experiment to the coupling model [38], where, τ_n is chain relaxation and τ_s is segmental relaxation.

1.3.4.2 Breakdown cases of time-temperature superposition principle

According to the time-temperature superposition (TTSP) principle, the ratio $\frac{\tau_n}{\tau_\alpha}$ should remain constant with the variation of temperature and relaxation time [24]. But DJ Plazek [23], was the first who identified that TTSP principle breaks down for many polymers when the temperature approaches the glass transition temperature. According to Y Ding and AP Sokolov [39], τ_n and τ_α seem to decouple (start to have a different temperature dependence) at a similar range of $\tau_\alpha \sim 10^{-5}to10^{-7}$ seconds for most of the polymers. It was also found that dependence of τ_n

on $\frac{T_g}{T}$ was also similar on all the polymers studied whereas they differ strongly in behaviour of τ_α (fragility) for example, *polycarbonate* (PC) and *Polystyrene* (PS) [39],

where fragility parameter (m) was defined as,

$$m = \frac{d(log\tau_\alpha)}{d(\frac{T_g}{T})} \tag{1.21}$$

Y Ding and AP Sokolov [39] speculated that the transition might happen at the dynamic crossover temperatures of polymers which is known to appear around the same relaxation time $\tau_\alpha \sim 10^{-5} to 10^{-7}$ seconds.

These results [39] supported the earlier speculations [40] that TTSP breakdown might be related to the dynamic crossover temperature.

1.3.5 Free volume theory

By building a master curve from the raw DMTA data, the temperature dependence of the shift factor, log a_T, is found to follow an empirical equation: the so called WLF equations [25]. If the reference temperature is glass transition temperature, T_g, the expression of the WLF equation is given by,

$$loga_T = \frac{-c_1^g(T - T_g)}{c_2^g + (T - T_g)} \tag{1.22}$$

where c_1^g and c_2^g are two constants referring to the reference temperature [24]. The use of the WLF equation finds some justification in the theory of free volume. Aklonis and Macknight [41] have mentioned that the total volume of a polymer sample can be considered to be the sum of an occupied volume and of a free volume. The occupied volume corresponds to the whole volume occupied by the polymer chains whereas the free volume can be perceived as being the unoccupied free regions accessible to chain motions. As the temperature changes, occupied volume and free volume, both will change in specific volume. The occupied volume expands at the same rate below and above T_g, while the free volume increases considerably above T_g. The expansion of the different volumes is shown schematically in figure 1.18.

At any given temperature, the fraction of free volume, f_v, is given by,

$$f_v(T) = \frac{V_f}{V_f + V_0} \approx \frac{V_f}{V_0} \tag{1.23}$$

where V_f is the free volume and V_0 is the occupied volume. The approximation is based on the fact that the fraction of free volume is weak (about 2-3%). Around and above T_g, the fraction of free volume can be expressed as

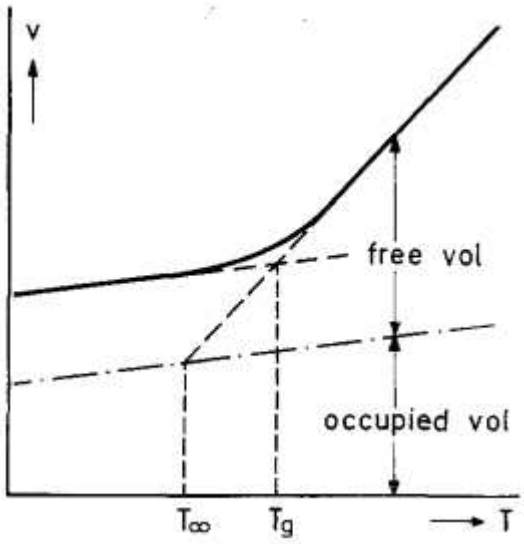

Figure 1.18: Schematic representation of the free volume theory
[42]

$$f(T) = f_g + \alpha_f \cdot (T - T_g) \tag{1.24}$$

where f_g is the fraction of free volume at T_g and α_f is the expansion coefficient of the fraction of free volume. To retrieve WLF equation, two intermediate equations have now to be introduced.

The first one is the Doolittle's viscosity equation [43], which relates the viscosity to the free volume:

$$ln\eta(T) = A + \frac{B}{f(T)} \tag{1.25}$$

where $\eta(T)$ is the viscosity, A and B are constants. The second equation is the expression of the shift factor in terms of viscosity:

$$lna_T = ln\frac{\eta(T)}{\eta(T_g)} \tag{1.26}$$

where $T > T_g$ and T_g is the reference temperature. Combining equations 1.25 and 1.26, the shift factor is given by,

$$lna_T = ln\frac{\eta(T)}{\eta(T_g)} = B \cdot (\frac{1}{f(T)} - \frac{1}{f_g}) \tag{1.27}$$

Finally, by using equation 1.24, equation 1.27 can be arranged to get:

$$loga_T = \frac{\frac{-B}{ln10 \cdot f} \cdot (T - T_g)}{\frac{f_g}{\alpha_f} + (T - T_g)} \tag{1.28}$$

which is the WLF equation. In the previous derivation, there was nothing special about the choice of T_g. In fact, any reference temperature could be used as long as the fraction of free volume can be expressed by the equation given earlier. In general, this requirement limits temperatures to near T_g. That is why the WLF equation can only be expected to be quantitative near and above T_g [41]. Moreover by choosing T_g as the reference temperature, it has been observed that the WLF constants, c_1^g and c_2^g, appear to be universal for several polymers. For a wide variety of polymers the WLF parameters given by,

$$c_1^g \approx -17.44 \tag{1.29a}$$

$$c_2^g \approx 51.6 \tag{1.29b}$$

However, in practice, it is recommended to use only in last resort the WLF universal constants. It is better to determine shift factors experimentally or to find WLF constants specific to the polymer of interest.

1.3.6 Previous experimental work on time-temperature superposition principle and the used parameters

As it was mentioned in the introduction, it is interesting to review the many efforts in experimental work and the confined parameters, which have been directed towards the fundamental understanding of the time-temperature superposition principle of amorphous polymers since the early work of Leaderman. A variety of different rheological equipments were used in the previous investigations. Since the parameters used for experimental work influences the after results, therefore, the parameters were also reviewed along with the techniques used for experimentation of extrapolating the viscoelastic data over a wide span of time or frequency. This short review is mainly focused on the amorphous polymers with an extra importance given to Poly(methyl methacrylate)(PMMA) and Polystyrene (PS) as are the main concern of this thesis. Before starting the short review about the time-temperature superposition principle and the parameter used, an illustration is shown in figure 1.19 showing the validity of time-temperature superposition principle for shear storage modulus in case of Polystyrene (PS). The samples of polystyrene (M_n = 98000, Number average molecular weight) of dimension 2 x 5 x 35 mm were selected for validity tests of TTSP. These tests were made in the temperature range from 359.7^{o}K to 373.9^{o}K and frequency range of 0.001-10 Hz.

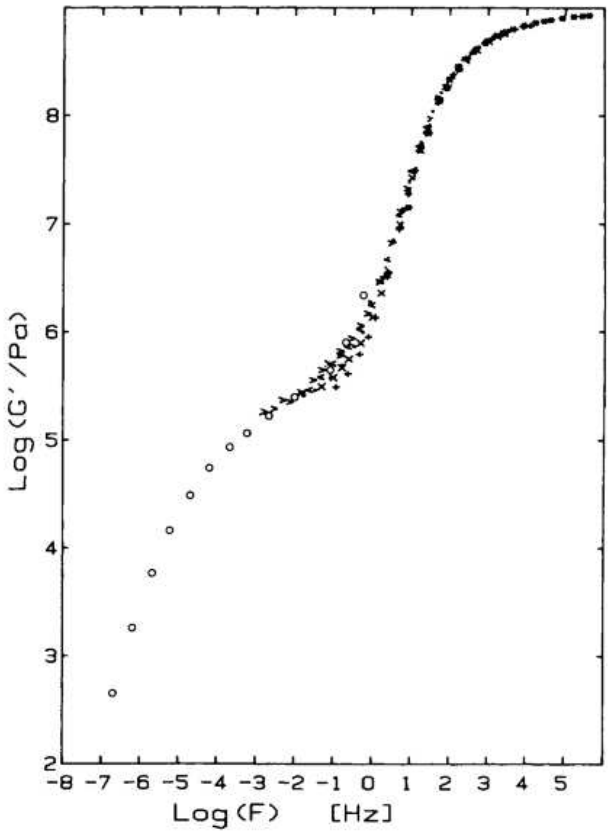

Figure 1.19: The time-temperature superposition of G' curves for polystyrene. [32]

Despite presenting monomer units very similar in volume and molecular weight and exhibiting the glass transition in the same temperature range, PS and conventional PMMA are known to behave differently in many respects in solution and in the melt. In the same year when Leaderman observed about the time-temperature superposition principle, Alfrey et al. [44] mentioned in his published work about the effect of cooling rate on the transition region of PS. He also added that the complex time effects can be observed in the intermediate temperature range (say 40^{o}C to 80^{o}C). He focused his entire work in the intermediate temperature range, where according to him, time effects are very important for PS. Later in 1960's, Plazek has shown in his work [23] that for PS, an attempt of superimposing the creep compliance curves in the temperature range of 95^{o}C - 160^{o}C by reducing the data at 100^{o}C got failed, where it was possible to make a master curve for recoverable compliance by reducing it to 100^o. It was shown in the figure 1.20 and 1.21 [23].

After a semi decade in 1970, Onogi et al. [45] tried to build master curves in the temperature range 120^{o}C - 280^{o}C and 0.004 Hz to 0.5 Hz frequency range from the dynamic viscoelastic parameters (storage modulus and loss modulus) of PS with several molecular weight distribution. He found that storage modulus curves superimpose in transition zone for high molecular weight but contrary for low molecular weight samples. It was concluded later in the same work that molecular weight can play an important role in implementation of time-temperature superposition principle on the viscoelastic behaviour of the polymers. In 1980, Schwarzl and Zahradnik [42] also found the application of time-temperature superposition with reasonable accuracy to the measurements of shear compliance for PS over a wide frequency range of 5

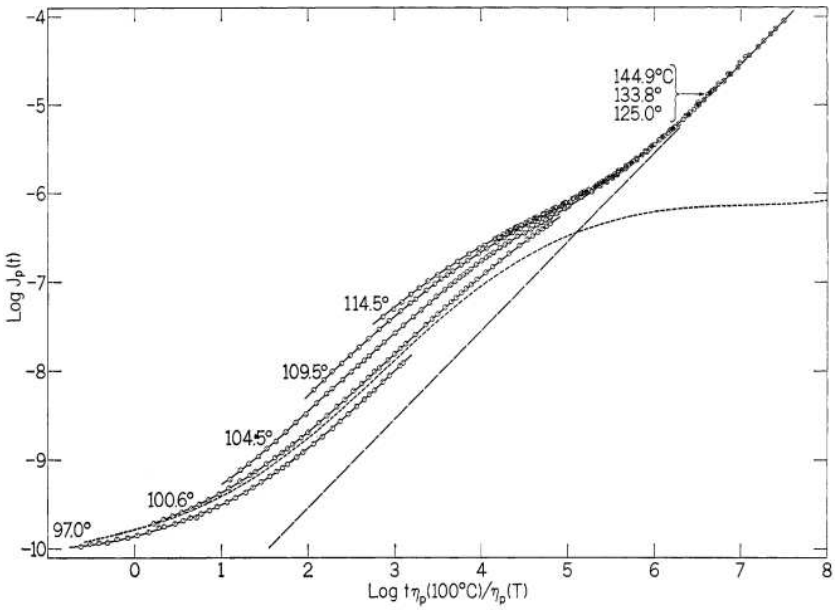

Figure 1.20: Log plot of creep compliance for PS, $\frac{t}{a_T}$ is reduced time. Failure of temperature reduction indicated.

[23]

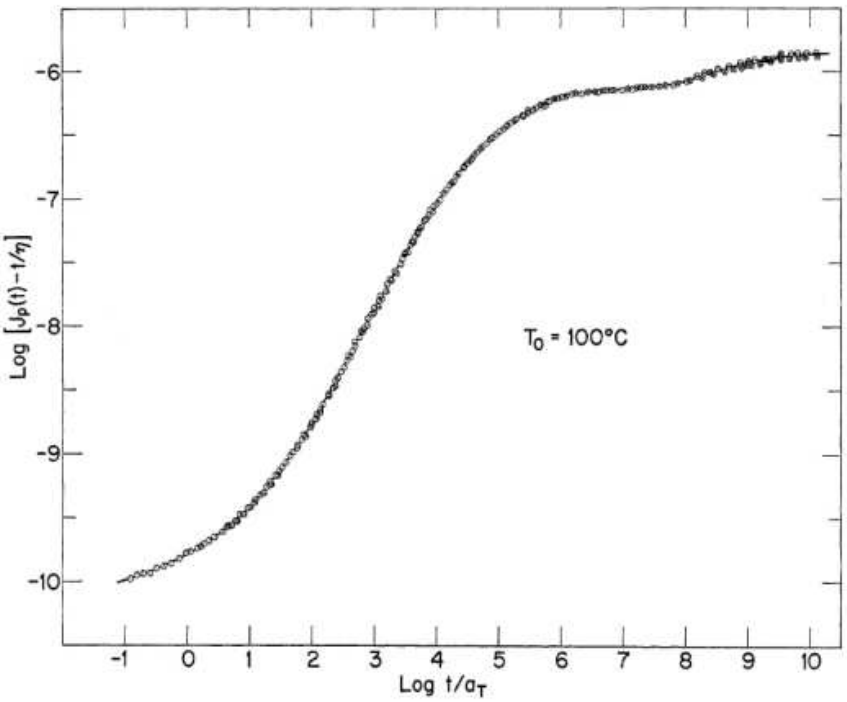

Figure 1.21: Log plot of recoverable compliance for PS, $\frac{t}{a_T}$ is reduced time.

[23]

decades (0.001-1000 Hz) with temperature ranging from 70^{o}C to 135^{o}C. It was also seen that at lowest temperatures and longest creep times, increase in creep curves is less steep than would be expected from the shift. The time-temperature shift was found to be described accurately

by the WLF equation in the temperature region above the glass transition temperature. While working on atactic PS, in 1987, Cavaille et al [32] found that a superposition by a displacement along the frequency scale alone cannot yield a master curve for the loss tangent spectrum. Although Cavaille et al. found a satisfactory superposition of shear loss modulus and storage modulus, they mentioned that it could be the possible artifact of the logarithmic plots and hence, they suggested to analyze the results in terms of their ratio (loss tangent) before making a conclusion on reliable master curve. According to them, the deviations in loss tangent master curves becomes more pronounced because of relatively larger change in shear storage modulus than loss modulus. Following the research work related to the time-temperature superposition principle, in 1992, Lomellini tried to validate previous published work in reference [46]. He performed dynamic measurements on narrow-distribution PS samples over a frequency range of 0.1 to 100 rad/sec and a temperature range of 150^{o}C to 290^{o}C with a steps of 10^{o}C for each temperature. He focused on using a new sample for each temperature because using same sample for each temperature has intrinsically a larger experimental error (perhaps due to the non-reproducibility of loading the sample). The maximum strain amplitude used was 10%, which was within the linear viscoelastic limit of the material. It was concluded by Lomellini that WLF free volume model is better than the Arrhenius one for the interpretation of viscoelastic behaviour upto around T_g + 185^{o}C.

After a brief description about the experimental work along with parameters used for application of time-temperature superposition in case of PS, another short review was discussed about PMMA.

After almost a decade, when Leaderman observed the existence of time-temperature superposition, McLoughlin and Tobolsky [47] found the effect of molecular weight distribution on the viscoelastic properties of PMMA. According to them, lower molecular weight material bears a greater superposition to build a master curve than the higher molecular weight material which deviates slightly in the temperature range from 125^{o}C - 155^{o}C. This was later confirmed by Onogi et al. for PS.

1.4 Thermo-mechanical interpretation of DMTA measurements

DMTA measurements are one of the best known technique in the present era to characterize the viscoelastic properties of a material (especially polymers). This technique of characterising the viscoelastic properties allows us to measure the response in terms of stress as a result of a imposed signal in terms of strain which gives rise to a hysteresis area while plotting stress against strain. This hysteresis area is supposed to be interpreted as the amount of energy dissipated by the material which sometime also show the effect of loading history on the deformation response of the materials (metals). Whereas, in the late 1930's, an observation was made by a researcher named C. Zener that the hysteresis loop could be the result of a thermoelastic internal fricion [48], which is explained in detail in the following discussion.

Thermoelastic internal friction:

Thermoelastic internal friction, which is also known as thermoelastic damping is a source of

internal material damping due to the thermoelasticity of the materials. It defines the coupling field between the elastic field in the material caused by the deformation and the temperature field.

In the vibrating structures, a change in the internal energy is caused by the strain field such that the rise in temperature occurs (taking into consideration a positive thermal expansion coefficient) during compression and during the tension in the given vibrating structure, the temperature diminishes and hence making the extended part cooler. The resulting lack of thermal equilibrium between the vibrating structure parts give rise to this mechanism responsible for thermoelastic internal friction or thermoelastic damping. And the occurance of the temperature gradient driven by the irreversible heat flow results in the dissipation of energy in the vibrating structures.

In other words, the local heat currents are caused by the fluctuations in temperature which are the obvious cause of stress inhomogeneities in a vibrating structure. Since, these heat currents are responsible for the increase in the entropy of the vibrating structure, therefore are called as the source of internal friction [48]. He also found that the flow of heat back and forth through the reed also responsible for the occurance of part of internal friction. He also proved that the internal friction is of large magnitude in the molecules due to this thermoelastic effect over a wide range of frequencies [49].

This internal friction can be predicted/interpreted theoretically in two different ways:

• If the elastic modulus is replaced by the complex modulus i.e., $E^* = E' + iE"$ in case of viscoelastic materials, then the ratio of loss modulus to storage modulus i.e., loss tangent could be the dimensionless measure of the physical phenomenon called internal friction.
• Again, if the energy of vibration is denoted by E and loss per cycle of energy of vibration by $\triangle E$, then the ratio $\frac{\triangle E}{E}$ can also be interpreted in the terms of internal friction.

These theoretical measures are almost related to each other, and to the experimental measures by the equation,

$$Q^{-1} = \frac{1}{2\pi}.\frac{\Delta E}{E} = \frac{E"}{E'} \tag{1.30}$$

The terms in the expression for the internal friction i.e., given in equation 1.30 can be defined separately, such as, ΔE can be defined as the mechanical work needed per cycle to maintain the steady vibration of the solid.

1.5 Conclusion

Concerning the synopsis of this first chapter, this chapter consist of four different sections where first section explains about the polymers, their structure, mechanical properties and linear viscoelasticity of the polymers which are actually used during this thesis. Second section of this chapter states about the facts of relaxation transition and their temperature dependence and

especially the existence of secondary relaxations in amorphous polymers. Concerning the thermodynamical behaviour of amorphous polymers, the attention was given to the visco-analysis (DMTA technique) of the amorphous polymers in the third section. The visco-analysis was used to introduce the empirical principle of TTSP along with the brief explanation about its advancements in the field of amorphous polymers. The conditions were also discussed where the application of TTSP is not supposed to work i.e., the cases where the failure of TTSP could take place. The final section of this chapter focuses on the literature of the thermodynamic analysis of cyclic tests, where, the origin of generation of hysteresis loop has been discussed.

Chapter 2

Theoretical Framework for Thermomechanical Analysis

Contents

List of symbols

Ω – System
Ω_s – Sub-system
$\overrightarrow{f_v}$ – Volumic forces
r_e – External heat sources
σ – Cauchy's stress tensor
$\overrightarrow{n}$ – Unit normal
$\overrightarrow{q}$ – Instantaneous heat flow
σ – Cauchy's stress tensor
ρ – Density of material
$\overrightarrow{v}$ – Velocity vector
E – Internal energy
C – Kinectic energy
P_e – Power of external forces
Q – Heat rate received
e – Specific internal energy
D – Eulerian strain rate tensor
$\dot{\varepsilon}$ – Strain rate tensor for small deformations
T – Absolute temperature
S – Entropy
s – Specific entropy
k – Conduction tensor
ψ – Helmholtz free energy potential
σ^r – Reversible stress
σ^{ir} – Irreversible stress
ϕ – Dissipation potential
ϕ – Dissipation potential
D_1 – Intrinsic volumic dissipation
D_2 – Volumic heat dissipation
W'_{an} – Anelastic deformation energy rate
W_{def} – Deformation energy
W_e – Elastic energy
W_{an} – Anelastic energy
W_d – Dissipated anelastic energy
W_s – Stored anelastic energy
s_{ctm} – Thermomechanical coupling sources
C_x – Specific heat, where x = p, ε, α
s_{ch} – Global heat source
θ – Temperature variations
ε_e – Elastic strain
ε_v – Viscous strain
σ^e – Elastic stress
σ^v – Viscous stress

s_{ther} – Thermoelastic sources
K_e – Thermoelastic coefficient

This chapter presents some essential points of thermodynamics of irreversible processes (TIP) with internal variables that will serve as a framework for interpreting the DMA tests of the following chapters. The local expressions of the first and second principle of thermodynamics are first recalled. Their combination makes it possible to achieve Clausius-Duhem Inequality, which is fundamental to describe irreversibilities accompanying the deformation process. We will use the specific framework of generalized standard materials (GSM) to write the constitutive behavioral equations derived from a thermodynamic potential and a dissipation potential. This part is naturally inspired by many books and PhD manuscripts dealing with continum thermomechanics [Halphen and Son Nguyen, 1975, Callen, 1960, Coirier and Nadot-Martin, 2007, Lemaître and Chaboche, 2004, Suquet, 2003, Germain, 1986a, Germain, 1986b].

Following the description of irreversibility accompanying the deformation process, this chapter deals with the introduction of GSM formalism to describe the local equilibrium states (Helmholtz free energy potential) and the irreversible processes (dissipation potential) [7]. Using this GSM formalism, consititutive equations are derived from these two thermodynamic potentials, constructed from state and evolution laws for the state variables. The GSM formalism part has been encouraged by many books and articles [7, 50, 51, 6]. The GSM formalism is followed by the introduction of heat diffusion equation obtained by combining the two laws of thermodynamics and then detailing the energy balance during the deformation process at small strains (application to DMTA techniques). Later, the GSM formalism, local heat diffusion equation and energy balance was used for the application to rheological modelling while detailing the thermomechanical couplings separately.

2.1 Thermomechanical formalism used

In this section, we recall the notions underlying the formalism of the thermodynamics of irreversible processes with internal variables. This formalism is based on the axiom of the local state, which states that "*if a system is out of equilibrium, the material points that constitute it can be considered as a meeting of the thermodynamic subsystem homogeneous in a state of equilibrium.*" This means that the time of return to the equilibrium of each material point remains infinitely small in front of the characteristic time of the global system. This local axiom makes it possible in particular to introduce the concept of quasi-static (in the thermodynamic sense) process that is made of a continuous series of equilibrium states and makes it possible to characterize a system via a finite number of fields of state variables.

Consider a sub system Ω_s of a system Ω subjected to the volumic forces $\overrightarrow{f_v}$ and a source density of external heat r_e (figure 2.1).

The contour of the subsystem $\partial\Omega_s$ develops a stress vector $\overrightarrow{t} = \sigma.\overrightarrow{n}$ (σ is Cauchy's stress tensor and $\overrightarrow{n}$ is the unit normal of the contour $\partial\Omega_s$) translating the mechanical actions of Ω on Ω_s. This boundary also exchanges an instantaneous heat flow $\overrightarrow{q}$.

2.1.1 Conservation law

Classical physics, macroscopically, is based on a number of key principles of conservation. As far as we are concerned here we will take into account the mass balance, the momentum balance and that of the energy balance. The energy balance corresponds to the first principle

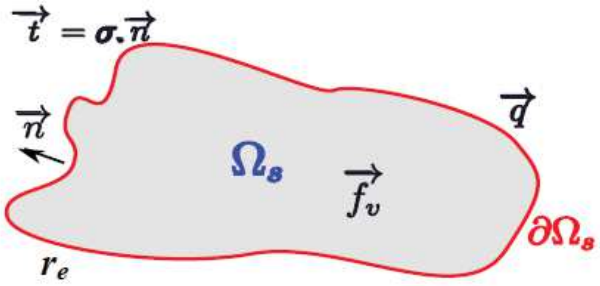

Figure 2.1: Body subjected to volumic forces exchanging an instantaneous heat flux via its contour with an external heat source

[52]

of Thermodynamics. Noting by ρ, the density of the material, $\overrightarrow{v}$ the velocity vector of the material points which constitute it, the expressions of these conservation laws can be defined by :

- Mass balance:

$$\frac{d}{dt}\int_{\Omega_s} \rho d\Omega_s = 0 \tag{2.1}$$

- Momentum balance:

$$\frac{d}{dt}\int_{\Omega_s} \rho \overrightarrow{v}\, d\Omega_s = \int_{\partial\Omega_s} \overrightarrow{t}\, d(\partial\Omega_s) + \int_{\Omega_s} \overrightarrow{f_v} d\Omega_s \tag{2.2}$$

- Energy balance (or first principle of thermodynamics) which states that at each instant, the variation of internal energy E and kinetic C (measured relative to a Galilean reference) is equal to the sum of the heat rate received and the power of external forces applied to the system (measured against a Galilean reference)

$$\frac{dE}{dt} + \frac{dC}{dt} = P_e + Q \tag{2.3}$$

The different terms involved in equation 2.3 can be obtained as follows:

- The variation of the internal energy E is expressed as a function of the specific internal energy e (by unit of mass) by the following relation:

$$\frac{dE}{dt} = \frac{d}{dt}\int_{\Omega_s} \rho e d\Omega_s \tag{2.4}$$

• The variation of the kinetic energy C can be expressed by using the law of mass balance and defining the acceleration vector $\overrightarrow{\gamma}$ of material points relative to a Galilean referential, by the following relation :

$$\frac{dC}{dt} = \frac{d}{dt}\int_{\Omega_s} \frac{1}{2}\rho \overrightarrow{v} \cdot \overrightarrow{v}\, d\Omega_s = \int_{\Omega_s} \rho \overrightarrow{\gamma} \cdot \overrightarrow{v}\, d\Omega_s \tag{2.5}$$

• The power of external efforts P_e can express itself by using momentum balance, the mass balance and the divergence theorem, by the following relation :

$$P_e = \int_{\partial\Omega_s} \overrightarrow{t} \cdot \overrightarrow{v}\, d(\partial\Omega_s) + \int_{\Omega_s} \overrightarrow{f_v} \cdot \overrightarrow{v}\, d\Omega_s = \int_{\Omega_s} \rho \overrightarrow{\gamma} \cdot \overrightarrow{v}\, d\Omega_s + \int_{\Omega_s} \sigma : D d\Omega_s \tag{2.6}$$

where D is the Eulerian strain rate tensor.

• Finally, the expression of the heat rate received by the system can be obtained by using the divergence theorem, by the relation :

$$Q = \int_{\partial\Omega_s} -\overrightarrow{q} \cdot \overrightarrow{n}\, d(\partial\Omega_s) + \int_{\Omega_s} r_e d\Omega_s = \int_{\Omega_s} [r_e - div\, \overrightarrow{q}] d\Omega_s \tag{2.7}$$

Taking into account the previous expressions, the energy balance equation (equation 2.3) becomes :

$$\frac{d}{dt}\int_{\Omega_s} \rho e d\Omega_s = \int_{\Omega_s} \sigma : D d\Omega_s + \int_{\Omega_s} [r_e - div\, \overrightarrow{q}] d\Omega_s \tag{2.8}$$

Given the continuity of the integrand, the local Eulerian form of this first principle leads to:

$$\rho \dot{e} = \sigma : D + r_e - div\, \overrightarrow{q} \tag{2.9}$$

In the context of small strain and displacements, this equation becomes :

$$\rho \dot{e} = \sigma : \dot{\varepsilon} + r_e - div\, \overrightarrow{q} \tag{2.10}$$

where $\dot{\varepsilon}$ represents the strain rate tensor of small deformations.

2.1.2 Second principle of thermodynamics

The second principle of thermodynamics involves two important notions: absolute temperature T and entropy S. The absolute temperature is the partial derivative of the internal energy of the system with respect to the entropy. The internal energy being supposed a monotonous function of the entropy, the absolute temperature is always a positive quantity [53]. The specific entropy s could be defined and related to the entropy of the system by:

$$S = \int_{\Omega_s} \rho s d\Omega_s \tag{2.11}$$

The second principle postulates that the entropy rate of the system is always greater than or equal to the entropy variation induced by the heat exchanged with the surroundings. In other words, there can be "creation" of internal entropy but never "disappearance / consumption". It is said that the source of irreversible entropy may only be positive or, at best, null, during reversible transformations. It will be admitted that this result is general: of any transformation of any system, the term internal production entropy is always positive or zero. This results in the following relationship :

$$\frac{dS^{ir}}{dt} = \frac{dS}{dt} - \int_{\Omega_s} \frac{r_e}{T} d\Omega_s + \int_{\partial\Omega_s} \frac{\overrightarrow{q} \cdot \overrightarrow{n}}{T} (d\partial\Omega_s) \geq 0 \tag{2.12}$$

The divergence theorem allows, by using the specific entropy of the material s, to write locally this in equation expressing the irreversible production rate of entropy :

$$\int_{\Omega_s} [\rho \frac{ds}{dt} + div(\frac{\overrightarrow{q}}{T}) - \frac{r_e}{T}] d\Omega_s \geq 0 \tag{2.13}$$

By expressing r_e using the relation derived from the first principle (equation 2.10) written for small strain, noticing that:

$$div(\frac{\overrightarrow{q}}{T}) = \frac{div(\overrightarrow{q})}{T} - \frac{\overrightarrow{q} \cdot \overrightarrow{grad}(T)}{T^2} \tag{2.14}$$

and by introducing the notion of specific free energy to the material (Legendre transform of the internal energy e with respect to the couple $(T, s) : \psi = e - Ts$), first and second principles of thermodynamics are summarized by the classical inequality of Clausius-Duhem next in which the positivity of the term $-\frac{\overrightarrow{q}}{T} \cdot \overrightarrow{grad}(T)$ is ensured by the data of the Fourier conduction law $\overrightarrow{q} = -k\overrightarrow{grad}(T)$ with k the conduction tensor, symmetrically defined, positive:

$$\sigma : \dot{\varepsilon} - \rho(\dot{\psi} + s\dot{T}) - \frac{\overrightarrow{q}}{T} \cdot \overrightarrow{grad}(T) \geq 0 \tag{2.15}$$

2.1.3 Thermodynamic potential and State variables

2.1.3.1 State variables

A thermodynamic process is therefore considered here as a continuous succession of equilibrium states to describe the evolution of the material system. And a system out of equilibrium can be considered as a set of sub-systems in equilibrium (local state axiom). The local thermodynamic state is then fully described by a finite set of variables $(\alpha_0, \alpha_1, \alpha_2, \cdots, \alpha_m)$ scalar or tensorial, called state variables. These variables translate the geometric, physico-chemical and mechanical characteristics of the material under consideration. Their choice depends mainly on the phenomena occurring during the process and their variation over time does not intervene in the definition of the state. Note that this is no longer true in other thermodynamic formalisms like extended thermodynamics of irreversible processes [54]. In our applications, we will distinguish two types of variables: so-called observable variables such as the absolute temperature $T = \alpha_0$ and the strain tensor $\varepsilon = \alpha_1$, other variables complementing the description of equilibrium thermodynamics of the material, called complementary or internal state variables. These variables are represented in the following by the set of variables $[\alpha_k]_{k=2,3,...,m}$. Their number is to be defined in each situation and their choice depends on the phenomena we want to describe (elastic coupling, phase transition, viscous dissipation etc.). This choice is both a great asset of the thermomechanical approach but it is also a commitment which condition for the rest of the modelling process because it assumes that the set of state variables used is sufficient to describe the set of mechanisms that are claimed to describe on a fixed observation scale.

2.1.3.2 Thermodynamic potential and state laws

The second challenge of the thermodynamic approach is to assume that all (mechanical, thermal, electric, magnetic, microstructural, ...) properties of the equilibrium states can be summarized in a thermodynamic potential. The partial derivative w.r.t. all state variables introduces the series of conjugate variables whose equations defining them represent the system state equations. In this work, we chose the Helmholtz free energy potential which depends primarily on temperature and strain. The time derivative of $\psi\ (T, \varepsilon, \{\alpha_k\}_{k=2,3,...,m})$ is given by :

$$\dot{\psi}(T, \varepsilon, \alpha_k) = \frac{\partial \psi}{\partial T}\dot{T} + \frac{\partial \psi}{\partial \varepsilon} : \dot{\varepsilon} + \frac{\partial \psi}{\partial \alpha_k}\dot{\alpha_k}, \quad k = \{2, 3, ..., m\} \tag{2.16}$$

This writing thus makes it possible to define the state laws:

- The specific entropy s is defined by

$$s = -\frac{\partial \psi}{\partial T}, \quad k = \{2, 3, ..., m\} \tag{2.17}$$

• The reversible part of the stress σ^r is defined by

$$\sigma^r = \frac{\partial \psi}{\partial \varepsilon}; \quad k = \{2, 3, ..., m\} \tag{2.18}$$

• The conjugate variable J_k sometimes called by certain affinity [55] or chemical potential when the variable of state α_k represents a quantity of constituent [50]:

$$J_k = \frac{\partial \psi}{\partial \alpha_k}; \quad k = \{2, 3, ..., m\} \tag{2.19}$$

2.1.4 Dissipation potential and complementary laws

If the equations of state describe the properties of the equilibrium states of the system, its evolution will be given by the complementary laws. These laws of evolution are, in the framework of the GSM, deduced from another potential ϕ called dissipation potential dependent on the flow of state variables $(\dot{\varepsilon}, \{\dot{\alpha}_k\}_{k=2,3,...,m}, \overrightarrow{q})$. As it has been done for the state variables and their conjugate variables, the dissipation potential relates the thermodynamic forces to the state variable flows using the so-called dissipation potential.

We then define the set of thermodynamic forces :

$$\chi = (\sigma^{ir}, \{X_k\}_{k=2,3,...,m}, -\overrightarrow{grad}(T)/T) \tag{2.20}$$

where,

• The irreversible part of the stress is given by:

$$X_{\dot{\varepsilon}} = \frac{\partial \phi}{\partial \dot{\varepsilon}} = \sigma^{ir} \tag{2.21}$$

• The thermodynamic force associated with $\dot{\alpha}_k$ is given by:

$$X_{\dot{\alpha}_k} = \frac{\partial \phi}{\partial \dot{\alpha_k}} \tag{2.22}$$

• The thermodynamic force associated with $\overrightarrow{q}$ is given by:

$$X_{\overrightarrow{q}} = \frac{\partial \phi}{\partial \overrightarrow{q}} = -\overrightarrow{grad} T/T \tag{2.23}$$

The GSM formalism [7] is based on the following hypothesis: for any "generalized flux vector" $\wp = (\dot{\varepsilon}, \{\dot{\alpha}_k\}_{k=2,3,...,m}, \overrightarrow{q})$, there is a continuous function $\phi = \phi(\wp)$, convex and positive minimum and zero in $(0, \{0_k\}_{k=2,3,...,m}, \overrightarrow{0})$, as:

$$\chi = \overrightarrow{grad}\phi(\wp) \tag{2.24}$$

This function is called dissipation potential. The mathematical hypotheses imposed on the dissipation potential allow the behaviour models derived from this kind of potential to automatically check the Clausius-Duhem inequality, whatever the evolution of the system.

With the retained state variables, the Clausius-Duhem inequality becomes:

$$D = \underbrace{\frac{\partial \phi}{\partial \dot{\varepsilon}} : \dot{\varepsilon} \ + \frac{\partial \phi}{\partial \dot{\alpha_k}} \dot{\alpha_k}}_{D_1} \ \underbrace{- \frac{\partial \phi}{\partial \overrightarrow{q}} \cdot \overrightarrow{q}}_{D_2} \geq 0 \tag{2.25}$$

It can be seen that the dissipation can be written as the sum of product made of thermodynamic forces and fluxes. The left-hand side of the inequality represents the total dissipation which usually breaks down into an intrinsic volume dissipation D_1 and a volume heat dissipation D_2. Classically, it is assumed that there is a decoupling of the thermal and mechanical dissipations (the two dissipations are then separately positive or zero [6]). Regarding, D_2, it is worth noting that its positivity is ensured by the Fourier's law, the conduction tensor k being a symmetric definite positive tensor.

2.2 Local heat diffusion equation and energy balance

By combining the local expressions of the two principles of thermodynamics (equation 2.10 and 2.15), we obtain classically the local heat diffusion equation. This equation plays an important role here because it allows to link the quantities of heat involved to thermally accessible data. It consists of a part of a partial derivative operator applied to temperature and on the other hand to different heat sources. By setting $C = -T\dfrac{\partial^2 \psi}{\partial T^2}$, the specific heat at ε and α_k constants, the local equation of heat diffusion is given by:

$$\rho C_{\varepsilon,\alpha} \dot{T} + div(\underbrace{-k grad T}_{q}) = \underbrace{(\sigma - \rho \frac{\partial \psi}{\partial \varepsilon}) : \dot{\varepsilon} - \rho \frac{\partial \psi}{\partial \alpha_k} \dot{\alpha_k}}_{D_1} + \underbrace{\rho T \frac{\partial^2 \psi}{\partial T \partial \varepsilon} : \dot{\varepsilon} + \rho T \frac{\partial^2 \psi}{\partial T \partial \alpha_k} \dot{\alpha_k}}_{s_{ctm}} + r_e \quad k = 1, 2, ..., m. \tag{2.26}$$

Starting from left to right, we explain each of the terms of this equation as following:

• The two terms on the left are classic in the heat diffusion equation:

◇ The term $\rho C_{\varepsilon,\alpha}\dot{T}$ is related to thermal inertia; it represents the heat rate lost or absorbed by the material.

◇ The term $div(\underbrace{-kgradT}_{q})$ represents the local heat losses by conduction in the medium, where k represents the thermal conductivity tensor.

• The terms on the right represents the various heat sources:

◇ The term intrinsic dissipation D_1. This term is responsible for the degradation of the materials and may have as origin several phenomena of irreversible nature such as viscosity, damage etc. The dissipation is the part of the anelastic deformation energy rate W'_{an} partially converted to heat. In many works, the fraction of dissipated energy rate is introduced at this level $\beta_{diff} = \dfrac{D_1}{W'_{an}}$ [56] to show in the models the thermal effects induced by the dissipation, without necessarily resorting to a complete thermodynamic framework. This consideration is even simpler to realize if we consider that the fraction β_{diff} remains constant throughout the mechanical transformation. The notation $(.)'$ used here indicates that the energies considered are not a priority state functions and their derivative with respect to time depend on the thermodynamic path followed.

◇ The term s_{ctm} characterizes the sources induced by the thermomechanical couplings. This term accounts for interactions between temperature and state variables characterizing the mechanical and/or microstructural state. For example, the thermoelastic effects are the coupling mechanisms between the temperature and the elastic strain which comes from the thermo-dilatibility of the material. The thermoelastic source will have tendency to cool the material in tension and to heat it in compression. But in a dual way, the material will expand during a warm-up and will shrink on cooling.

◇ The term r_e represents the heat sources symbolizing any volume heat exchange of external origin (radiation, joule effect etc.)

Heat sources therefore have several origins: dissipative sources induced by the presence of irreversible deformation mechanisms and so called coupling sources translating a strong interaction between thermal, mechanical and microstructural states. The temperature variations accompanying the deformation depend on nature of the sources involved, their respective intensity and their distribution. But these temperature variations still depend on the thermo-physical properties of the material (mass density, specific heat, conduction) and naturally the thermal boundary conditions.

The local heat diffusion equation presented (equation 2.26) may be simplified in some situations. Unless otherwise stated, in this work it will be assumed that:

• The material diffuses the heat isotropically and its conductivity is constant, so:

$$k_{ij} = k\delta_{ij} \Rightarrow div \underbrace{(-kgradT)}_{q} = -k\Delta_3 T \tag{2.27}$$

where Δ_3 is the laplacian operator. The index 3 here indicate that the conduction mechanism is considered in 3 orthogonal directions of space.

• The density ρ and the specific heat $C_{\varepsilon,\alpha}$ are material constants independent of the thermodynamic state.

• The term external heat source due to radiation heat exchange is time independent. This implies that the temperature T_o field balance checks:

$$-k\Delta_3 T_o = r_e \tag{2.28}$$

• The tests are slow enough (quasi-static tests) and the temperature gradients are sufficiently small so that we can neglect as a first approximation, convective terms in the expression of the particular time derivative of temperature:

$$\frac{dT}{dt} = \overrightarrow{v} \cdot \overrightarrow{grad}(T) + \frac{\partial T}{\partial t} \Rightarrow \frac{dT}{dt} \approx \frac{\partial T}{\partial t} \tag{2.29}$$

Under all these assumptions, we can adopt the simplified writing of the following heat-diffusion equation:

$$\rho C_{\varepsilon,\alpha}\frac{\partial \theta}{\partial t} - k\Delta_3\theta = \overbrace{\underbrace{D_1}_{\beta_{diff}W'_{an}} + s_{ctm}}^{s_{ch}} \tag{2.30}$$

where $\theta = T - T_o$ represents the temperature variation and s_{ch} is the global heat source. In what follows, we will define the densities of the different energies in play during a quasi-static deformation process (negligible kinetic energy variations and acceleration).

2.2.1 Estimated stored energy rate

Deformation energy W_{def} is the energy developed by the material during its deformation. During a quasi-static loading this energy will be equal to the work of the external forces applied to the material to deform it. This deformation energy can be expressed between two moments t_o and t_f and per unit of volume, using the stress tensor σ and the strain rate $\dot{\varepsilon}$:

$$W_{def} = \int_{t_o}^{t_f} \sigma : \dot{\varepsilon} dt \tag{2.31}$$

For 1D cyclic loadings, this strain energy represents the hysteresis area observed in the stress strain diagram. It can be broken down into an elastic energy W_e, representing the reversible part and therefore recoverable by the material, and anelastic energy W_{an}, representing the non-recoverable part (mechanically). This anelastic energy can in turn be decomposed into a dissipated part W_d and a stored part W_s by/in the material. The dissipated power density is the intrinsic dissipation D_1 introduced into the diffusion equation (equation 2.26 or 2.30).

The dissipated energy can be determined by analyzing the temperature variations observed when the material is stressed. As for energy stored, it represents the internal energy variations induced by the micro-structural transformations produced during the deformation process. In general, the value of this stored energy is not directly accessible and requires the establishment of a complete energy balance. For example, during the fatigue tests, we estimate the energy stored in the cycle n as the difference between the deformation energy and the sum of dissipated energy and the elastic energy. We then write:

$$W_s^{(n)} = W_{def}^{(n)} - (W_e^{(n)} + W_d^{(n)}) \tag{2.32}$$

where, $W_s^{(n)}$, ($W_e^{(n)}$ and $W_d^{(n)}$) represents the stored energy, elastic energy and dissipated energy over a cycle n. As the elastic energy averaged over the cycle remains close to zero, we can consider that the deformation energy averaged per cycle is equal to that of the anelastic energy $(W_{def})^{(n)} \approx (W_{an})^{(n)}$. The evaluation of stored energy can be derived from two approaches which are completely separate. In the literature[57], we often define at this level, the stored energy rate by the following relationship:

$$F_{w_s} = \frac{W_s}{W_{an}} = \frac{W_{def} - W_e - W_d}{W_{def} - W_e} = \frac{W_s}{W_s + W_d} \tag{2.33}$$

where the difference $W_{def} - W_e$ represents the anelastic work W_{an}. In case the elastic energy is weak in front of the deformation energy, it comes that:

$$F_{w_s} = \frac{W_s}{W_{an}} \approx 1 - \frac{W_d}{W_{def}} \tag{2.34}$$

In the case where the strain energy is assumed to be constant (as in the first work of Taylor and Quinney), the rate of the fraction of strain energy is also constant and is equal to the fraction of the stored energy. It should be written as:

$$\dot{F_{w_s}} = \frac{d}{dt}(\frac{W_s}{W_{an}}) = \frac{W_{an}W_s^{'} - W_{an}^{'}W_s}{W_{an}^2} \approx 0 \Rightarrow \beta_s = \frac{W_s^{'}}{W_{an}^{'}} = F_{w_s}^{'} = 1 - \beta_{diff} \tag{2.35}$$

where $\beta_{diff} = \dfrac{W_d^{'}}{W_{def}^{'}}$ termed as DTQC (differential Taylor-Quinney Coefficient), introduced by Rittel [58].

2.2.2 Energy analysis of the mechanical hysteresis area

The cyclic tests envisaged in the following represent a series of loading-unloading cycles. It is therefore proposed to analyze the particular form of the energy balance during loading-unloading cycle. We note by $A = (T_A, \varepsilon_A, \alpha_A)$ and $B = (T_B, \varepsilon_B, \alpha_B)$ the thermodynamic states

of a point material at the beginning and at the end of the cycle. We can then distinguish three interesting cases of energy balance sheets whose schematization is given in the figure 2.2.

• The general case corresponds to the situation where the two thermodynamic states are separate: $A \neq B$.

• The particular case where the load-unload cycle is a mechanical cycle in the sense that the stresses but also the strains are the same in A and B. In this case, two thermodynamic states are always assumed to be distinct $A \neq B$ but we have $\varepsilon_A = \varepsilon_B$.

• Finally, the special case where the mechanical cycle becomes a thermodynamic cycle, the two thermodynamic states A and B are then equal i.e., A=B.

By setting $t_B - t_A$ the duration of the cycle, and by combining the local expressions of the two principles of thermodynamics, we obtain, for a load-unload cycle, the following expression of the strain energy:

$$W_{def} = \int_{t_A}^{t_B} D_1 dt + \int_{t_A}^{t_B} (\rho \dot{e} - \rho C_{\varepsilon,\alpha} \dot{T} + s_{ctm}) dt \tag{2.36}$$

This equation shows that:

• In the general case, the deformation energy involved can be partly dissipated, correspond to variations in internal energy, or be converted into heat associated with thermo-mechanical coupling mechanisms.

• When the load-unload cycle is a mechanical cycle, and if the loading is uniaxial, the strain energy is equal to the area of mechanical hysteresis $W_{def} = A_h$ (in grey in the figure 2.2). The possible transformations of this energy are the same as those mentioned in the general case.

• In the case where the mechanical cycle becomes a thermodynamic cycle, the possible transformations of the strain energy are induced by the dissipative and thermomechanical coupling effects.

Remarks:

• It is common in the literature to estimate the energy dissipated in a cycle by calculating the area of the hysteresis loop of the stress-strain diagram (this area actually corresponds to the strain energy). This type of estimation therefore implies that the stored energy is negligible over a complete cycle just like the energies induced by the thermo-mechanical couplings.

• The estimation of the strain energy from a hysteresis loop is valid only in the uniaxial case. If the state of stress is (or becomes) multiaxial, it should be taken into account in the calculation of the deformation energy[60].

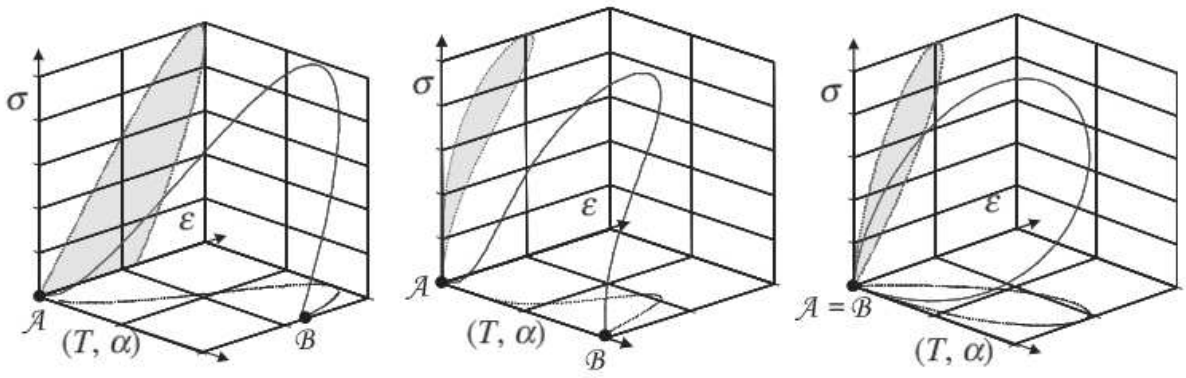

Figure 2.2: Schematic stress–strain diagrams for a load–unload test; t_B–t_A is the cycle duration, from left to right (i)$A \neq B$, (ii)$\varepsilon_A = \varepsilon_B$ and (iii)A=B
[59]

2.3 Application to rheological examples

During the cyclic loading of the materials, the mechanisms of thermomechanical coupling were observed: the thermo-elasticity which is related to the thermodilatability of the material, the entropic elasticity which is related to the thermal effects accompanying the orientation of the material's macromolecular chains under stress and the material dissipative effects which leads to a degradation of the deformation energy into heat and a heat transfer to the surrounding. These mechanisms are well known and can co-exist giving rise to the famous "thermo-elastic inversion" effect [61] and "visco-thermo-elasticity". In this following section, we briefly recall the behaviour models associated with these thermomechanical phenomenons along with explaining the importance of these effects w.r.t. the application of DMTA.

2.3.1 Viscoelasticity

Viscoelasticity is the property of the material which shows both viscous as well as the elastic behaviour while subjected to the deformation. The viscoelasticity can be divided into two different parts i.e., linear and non-linear, depending upon the change of strain rate versus stress inside the material. A viscoelastic material is also known to show a hysteresis loop in the stress-strain diagram during a load-unload cycle. This hysteresis is supposed to have the dissipation as the origin, which is related to the viscous part of the material. This complex behaviour of viscoelastic material is usually shown by the combination of spring and dashpot rheological elements. It has been shown that any model is a particular case of Biot's general model according to the linear theory of viscoelasticity [62]. And therefore, any series model(Poynting-Thomson) having N relaxation times is mechanically equivalent to a parallel model(Zener)[24, 63, 64]. Not only they are mechanically equivalent but,it can be also shown that both of these equivalent models also dissipate and stored at each time the same amount of mechanical energy. Therefore, a simple parallel rheological model (Zener model) (figure 2.3) is considered in the following to gradually accustom the reader to the thermomechancial interactions.

The weakly coupled thermomechanical behaviour of this model is shown mathematically for the strain controlled cyclic tests, where elastic(^{e}) and viscous(^{v}) strains are considered as the

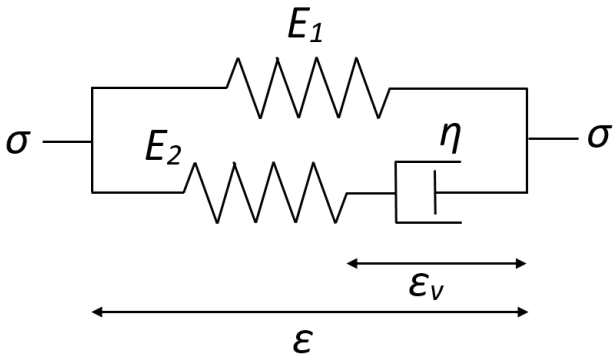

Figure 2.3: Zener model

state variables and temperature is considered to be the controlled parameter.

$$\varepsilon = \varepsilon_0 sin\omega t \tag{2.37}$$

$$\sigma^e = E_1\varepsilon \tag{2.38a}$$

$$\sigma^v = \eta\dot{\varepsilon_v} = E_2\varepsilon_e \tag{2.38b}$$

Using equation 2.37, 2.38a and 2.38b and $\varepsilon = \varepsilon_e + \varepsilon_v$, the mechanical behaviour of zener model can be written as:

$$\sigma = E_1\varepsilon - \frac{\eta}{E_2}\dot{\sigma} + \dot{\varepsilon}\eta(1 + \frac{E_1}{E_2}) \tag{2.39}$$

and heat diffusion equation can be modified by considering viscous dissipation as the heat sources on the right side of the equation as:

$$\rho C_p(\dot{\theta} + \frac{\theta}{\tau_{th}}) = \eta\dot{\varepsilon_v}^2 \tag{2.40}$$

This heat equation gives a link between the viscous strain rate (kinematic variable) and the temperature variation of the material. Strictly speaking, the deformation process should have been considered in this situation as an non-isothermal process. However,it can be seen from equation 2.39 and 2.40 that the Zener model has the same mechanical response in both cases (isothermal and non-isothermal viscoelastic framework) as the temperature variations are considered to have no influence on the mechanical response. To depict this situation, the expression "weak thermomechanical coupling" will be used in the following. That's the reason why the mechanical behaviour of the Zener model is often used without taking the self heating phenomenon of the specimen into account. The temperature is then more or less explicitly

considered as a controlled (constant) parameter but, at the same time, from a thermodynamic standpoint, it must be remember that the self heating phenomenon during the cyclic loading and the low thermal diffusivity of polymer materials can make the deformation process non-isothermal.

Another attitude would have been to consider temperature as a state variable. This point of view is discussed later in the upcoming sections as it leads to the concept of "strong thermo-mechancial couplings" as the so-called thermoelastic or entropic effects. In this situation, the thermal and mechanical states of the material are strongly linked.

2.3.2 Thermoelasticity

The effects of thermoelastic coupling were observed for the first time by Weber in 1830 [65] and modeled by William Thomson (Lord Kelvin) between 1853 and 1878 cited by [52] and James Prescott Joule in 1859. These effects are induced by the thermodilatability of the material. For cyclic tests, these couplings result in oscillations of the temperature variations in opposition with the signal of the stress illustrated in figure 2.2 for the case of polystyrene stressed in cyclic tension, where the oscillation of the temperature is in opposition of phase with the stress. Of course, other effects (e.g. dissipative) can be superimposed on the thermoelastic response.

2.3.2.1 Brief bibliographic analysis

A linear relation was derived by Thomson between the temperature variations of an isotropic solid and the first invariant of the stress tensor. Compton and Webster confirm this theory experimentally in 1915 [66]. Later, in his research, Zener published a series of patents on internal friction in solids and takes up the theoretical bases developed by Thomson [49, 48, 48] . Rocca and Bever [67] measure the thermoelastic response of iron and nickel to Curie temperature by modelling the non-linear effects of thermoelasticity. During the 1950s, Biot uses the thermodynamics of irreversible processes to extend this isotropic linear thermoelastic theory to other aspects such as anisotropy, visco(thermo)elasticity and (thermo)elastoplasticity of materials [62, 68, 69, 70]. Subsequently, this phenomenon has been studied experimentally by a large number of authors. Belgen was the first to use an infrared radiometer to relate the stresses to the small variations in temperature measured in a cantilever vibrating beam. Subsequently, studies on the subject continue to progress and lead to several commercial applications. As an example, we can mention the work of Mountain and Webber [71] who developed in 1978 the first prototype of the commercial system SPATE (Stress Pattern Analysis by Thermal Emission) for the British Ministry of Defense. Since 1982, several works, whose subject is mainly dedicated to thermoelastic analysis, are mainly based on data acquired by the SPATE system [72]. A large bibliography in thermoelastic analysis was proposed by Harwood and Cummings [73].

2.3.2.2 Brief reminders on the equations of linearized thermoelasticity

For a material with linearized thermoelastic behaviour, the temperature and tensor of (small) deformations are sufficient to describe its thermomechanical state. It is further considered

that, for such a material, the intrinsic dissipation remains zero whatever the load is. The elastic materials have, morover, a particular memory. Their state of stress depends only on the "distance" from the current state to the reference state. For adiabatic processes (in practice: fast loading and of short duration), the process of thermoelastic deformation becomes reversible (isentropic). In this context, for example, Potter and Greaves proposed the following form of thermoelastic response for anisotropic materials [74] :

$$\rho C_\varepsilon \frac{\Delta T}{T} = [\frac{\partial C_{ijkl}}{\partial T}(\varepsilon_{kl} - \alpha_{kl}\Delta T) - C_{ijkl}(\alpha_{kl} + \Delta T\frac{\partial \alpha_{kl}}{\partial T})]d\varepsilon_{ij} \tag{2.41}$$

where C_{ijkl} is the elasticity tensor, α_{kl} is the thermal dilatation cofficient tensor and ε_{kl} is the deformation tensor. Specific versions have been extracted from this general equation to include other aspects such as the effects of average stress, cyclic plasticity, residual stresses or dependence of the properties of materials in temperature [75, 76, 77]. In the case of an elastic, linear, homogeneous and isotropic material and under the assumption that the tests are adiabatic and that one is close to the thermal equilibrium (small variations of temperature), this relation of thermoelasticity can be reduced at:

$$\rho C_\varepsilon \frac{\Delta \theta}{T_o} = -\alpha_{th}\Delta\sigma_{ii} \tag{2.42}$$

where $\Delta\sigma_{ii} = \Delta(\sigma_{11} + \sigma_{22} + \sigma_{33})$ represents the extent of the trace of the main constraints and α_{th} the isotropic dilatation coefficient. This relationship reflects the fact that the extent of temperature variations varies linearly depending on the extent of the trace of the stress. Under the assumption of plane stresses, during adiabatic transformations, s_{ther}, thermoelastic sources are determined by:

$$s_{ther} = K_e(\Delta\sigma_{11} + \Delta\sigma_{22}) \tag{2.43}$$

where K_e is the thermoelastic coefficient, and σ_{11} and σ_{22} are the principle stresses. This equation suggests that the shear stresses can not generate temperature variations, the thermoelastic sources then remains systematically zero. The majority of these theories differ according to the assumptions taken into account during their formulation. If one places oneself in the case of an isotropic elastic material subjected to a uniaxial cyclic solicitation ($\sigma_{11} = \sigma_{kk} = \sigma_m + \Delta\sigma sin(\omega t), \sigma_{22} = \sigma_{33} = \sigma_{12} = \sigma_{12} = \sigma_{23} = 0$ with σ_{kk}, the first invariant of the stress tensor and σ_m, $\Delta\sigma$ and ω are respectively the mean, the amplitude and the pulsation of the stress signal), where it is assumed that there is no source of heat other than that due to the effects of thermomechanical couplings, and if we assume that the effects of conduction are neglected (the deformation rates remain sufficiently large), the thermoelastic relation can take the following form:

$$\rho C_\varepsilon \frac{\Delta \theta}{T_o} = -(\alpha_{th} - \frac{1}{E^2}\frac{\partial E}{\partial T}\sigma_m)\Delta\sigma sin(\omega t) - \frac{1}{4E^2}\frac{\partial E}{\partial T}(\Delta\sigma)^2 cos(2\omega t) \tag{2.44}$$

where E is the Young's modulus assumed to be non-linearly varied with temperature as indicated by equation 2.45 and α_{th} is the isotropic expansion coefficient. It should also be noted that the formulation of this equation takes into account the hypothesis of small temperature variations $\theta = T - T_o \ll T_o$ as well as verifying that $\frac{\partial \alpha_{th}}{\partial T}\Delta T \ll \alpha_{th}$.

Note that the equation above shows that the temperature variation $\Delta\theta$ is decomposed into a synchronous term at the pulsation bias ω plus another pulse variation 2ω proportional to the square of the amplitude $\Delta\sigma$. The difference between this equation and the one introduced by Thomson's theory (Lord Kelvin) can be seen neglecting the term dependent on temperature in equation 2.46

$$\rho C_\varepsilon \frac{\Delta\theta}{T_o} = -\alpha_{th}\Delta\sigma sin(\omega t) \tag{2.45}$$

These temperature variations can be acquired experimentally using infrared thermography techniques, which allows us to go back to uniaxial stress variations. As a simplification of equation 2.44, the coefficient $\frac{1}{4E^2}\frac{\partial E}{\partial T}(\Delta\sigma)^2$ is assumed to be weak when the stress applied amplitudes are small. Since we can only have the harmonic part of the temperature signal, equation 2.46 can be reduced to

$$\rho C_\varepsilon \frac{\Delta\theta}{T_o} = -(\alpha_{th} - \frac{1}{E^2}\frac{\partial E}{\partial T}\sigma_m)\Delta\sigma sin(\omega t) \tag{2.46}$$

By analogy with equation 2.45, this equation (equation 2.48) leads to the formulation of an effective thermoelastic parameter depending on the average stress, given by the following relation

$$K_e = \frac{1}{\rho C_\varepsilon}(\alpha_{th} - \frac{1}{E^2}\frac{\partial E}{\partial T}\sigma_m) \tag{2.47}$$

From this equation, we can extract the expression of the conventional thermoelastic constant $K_o = \frac{\alpha_{th}}{\rho C_\varepsilon}$ by deriving the effective thermoelastic parameter from the mean stress σ_m, is:

$$\frac{1}{K_o}\frac{\partial K_e}{\partial \sigma_m} = -\frac{1}{\alpha_{th}E^2}\frac{\partial E}{\partial T} \tag{2.48}$$

The adiabaticity hypothesis introduced in the majority of the theories mentioned above remains a very good approximation in the case of short tests carried out at high stress frequencies or for materials having a very low thermal conductivity such as polymers. In the case of cyclic

fatigue, the tests are long compared to the characteristic time of return to thermal equilibrium. However, we will see that on a cycle, thermal losses have very little effect on the thermoelastic response as soon as the period of a cycle is weak compared to the characteristic time of the losses.

This linear thermoelasticity can also be presented by the combination of an hookean spring with thermo-dilatation element (figure 2.4).

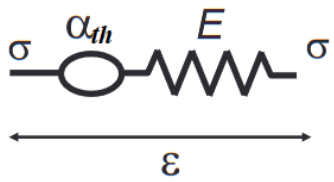

Figure 2.4: Linear thermoelasticity representation
[78]

Linear thermoelasticity can be represented in the GSM framework as well by considering temperature and strain as the state variables ($\theta = T - T_0$, ε). In the linear thermoelastic framework, the mechanical and thermal energy is stored by the material and at the same time, thermal energy is dissipated as well to an extent. The linear thermoelasticity can be represented in terms of free energy potential and dissipation potentials. Since, $\sigma^{ir} = 0$ in this case of linear thermoelasticity, the mechanical dissipation becomes zero i.e., $d_1 = 0$ and the thermal dissipation can be represented by $d_2 = -\dfrac{gradT}{T}q$.

$$\psi(\theta, \varepsilon) = \frac{1}{2}E(\varepsilon - \alpha_{th}\theta)^2 - s_0\theta - \frac{\rho_0 C_0}{2T_0}(1 + \frac{E\alpha_{th}^2 T_0}{\rho_0 C_0})\theta^2 \tag{2.49}$$

Using equation 2.49, the reversible stress can be written as:

$$\sigma^r = \frac{\partial \psi}{\partial \varepsilon} = E(\varepsilon - \alpha_{th}\theta) \tag{2.50a}$$

$$s = -\frac{\partial \psi}{\partial \theta} = s_0 + \frac{\rho_0 C_0}{T_0}(1 + \frac{E\alpha_{th}^2 T_0}{\rho_0 C_0})\theta \tag{2.50b}$$

where s represents the specific volumic entropy. In this case of linear thermoelasticity, the heat equation can be transformed as:

$$\rho C_p(\dot{\theta} + \frac{\theta}{\tau_{th}}) = -E\alpha_{th}T_0\dot{\varepsilon} \tag{2.51}$$

2.3.3 Rubber elasticity of entropic origin

2.3.3.1 Statistical and molecular theory

Since Mooney in 1940 [79] and Treloar in 1944 [80], many behavioral models have been proposed to describe the hyperelastic behaviour (elasticity in large transformations) of materials. Other models have been developed to predict mechanical behaviour in the quasi-static and/or dynamic regime [81, 82]. These models combine different concepts ranging from the principles of thermodynamics, from molecular structure to the hypothesis of relative deformation. Other rather phenomenological models based on the existence of a hyperelastic potential within the framework of the continuous mechanics have also been developed [83, 84].

It should be noted that the majority of forms of deformation energy existing in the literature do not have the domains of validity. It must therefore be verified that the domain of validity of the constitutive law considered is compatible with the conditions of solicitation.

The entropic character often encountered in cases of hyperelastic stress was first demonstrated by John Gough. He describes his experiences on a rubber as follows cited by [52]:

•First experience : "*Hold one end of the slip, thus prepared, between the thumb and forefinger of each hand, bring the middle of the piece into slight contact with the edges of the lips, taking care to keep it straight at the time, but not to stretch it much beyond its natural length : after taking these preparatory steps, extend the slip suddenly, and you will immediately perceive a sensation of warm in the part of the mouth which touches it, arising from an augmentation of temperature in the rubber; for this, resin evidently grows warmer the further it is extended, and the edges of the lips possess a high degree of sensibility, which enables them to discover these changes with greater facility*".

•Second experience : "*If one end of a slip of rubber be fastened to a rod of metal or wood, and a weight be fixed to the other extremity, in order to keep it in a vertical position, the thong will be found to become shorter with heat and longer with cold*".

Gough did not provide at this time any explaination as to whether the material shrinks with increasing temperature or dual, that the material heats up when stretched. It will take 50 years before a presentation of entropy elasticity in a thermodynamic framework is formulated.

In the following, it is proposed to give the main elements of the thermodynamic theory reflecting the entropic effect of rubber elasticity. The aim of the presentation is to show how the literature accesses a relation between stress, temperature and strain starting from a description of the mechanisms of deformationat the scale of a flexible macromolecular chain. That is, a macromolecular chain subjected to a uniaxial force f which produces an extension. The force exerted on this chain meets a "resistance of entropic origin" called retraction force, which favors the return to the initial form of equilibrium. In the case where the quasi-static transformation follows a reversible process, the energy balance (or the first principle of thermodynamics) results in a variation of the internal energy that is written:

$$dE = TdS + dW \tag{2.52}$$

where W represents the work provided. Taking into account, the variations of free energy $d\psi = dE - TdS - SdT$, under isothermal conditions ($dT = 0$):

$$d\psi = dE - TdS \tag{2.53}$$

This allows us to write:

$$d\psi = dW \tag{2.54}$$

From this equation and under the hypotheses previously introduced (reversible and isothermal phenomenon), it follows that the work provided is equal to the free energy variation of Helmholtz. For uniaxial elongation, the work provided is defined by;

$$dW = fdl \tag{2.55}$$

this leads us to write:

$$f = (\frac{\partial \psi}{\partial l})_T = (\frac{\partial E}{\partial l})_T - T(\frac{\partial S}{\partial l})_T \tag{2.56}$$

In this equation, the terms on the right shows two contributions, one comes from variations in internal energy and the other is associated with variations of entropic origin. The term internal energy is predominant in the case of small elongations, while the term entropy is predominant at low temperature and/or in large elongations. To clearly explain the effect coming from the internal energy and the entropy, let us take again the expression giving the variation of free energy of Helmholtz :

$$d\psi = dE - TdS - SdT \tag{2.57}$$

This variation of free energy is written by taking into account equation 2.53:

$$d\psi = fdl - SdT \tag{2.58}$$

$d\psi$ being an exact total differential (if we have a temperature variation T, the volume V remains constant), we deduce from this equation that

$$f = (\frac{\partial \psi}{\partial l})_T \quad and \quad S = -(\frac{\partial \psi}{\partial T})_l \tag{2.59}$$

By swapping the order of the derivations, it comes:

$$\frac{\partial}{\partial l}(\frac{\partial \psi}{\partial T})_l = \frac{\partial}{\partial T}(\frac{\partial \psi}{\partial l})_T \tag{2.60}$$

We then deduce from equation 2.59

$$(\frac{\partial S}{\partial l})_T = -(\frac{\partial f}{\partial T})_l \tag{2.61}$$

This simple relation is known as Maxwell's relation in tension. It shows that, if experimentally the temperature increases with the force, the elongation of the chain is accompanied by a decrease of entropy. This mechanism is consistent with Gough's observations mentioned above.

Therefore, by combining this last result with equation 2.56, it comes that:

$$f = (\frac{\partial E}{\partial l})_T + T(\frac{\partial f}{\partial T})_l \tag{2.62}$$

This equation represents in another way the contribution of energy origin and the contribution of entropic origin. Several experiments have highlighted these two contributions by measuring the force required to maintain a predefined elongation (see for example [85]).

The GSM framework is again introduced to describe the entropic elasticity mathematically. As this entropic elasticity belongs to the rubbery state, it refers to the huge molecular mobility during the cyclic loading, which can be considered as the perfect gas analogy. Therefore, it can be written as:

$$e_c(s, \varepsilon) = \breve{e}(T) \tag{2.63}$$

where ε is the logarithmic strain. As it is known that there is no irreversible stress σ^{ir} in entropic elasticity case, therefore, the σ can be written as:

$$\sigma = \sigma^r = \frac{\partial e_c}{\partial \varepsilon} \tag{2.64}$$

where,

$$\dot{e_c} = T\dot{s} + \sigma : \dot{\varepsilon} = \overset{\frown}{e}'\dot{T} \tag{2.65}$$

but the entropy can still be written as:

$$s = -\frac{\partial \psi_c(T,\varepsilon)}{\partial T} \tag{2.66a}$$

$$\dot{s} = -\frac{\partial^2 \psi_c(T,\varepsilon)}{\partial T^2}\dot{T} - \frac{\partial^2 \psi_c(T,\varepsilon)}{\partial \varepsilon \partial T} : \dot{\varepsilon} \tag{2.66b}$$

Using equation 2.66b, equation 2.65 becomes,

$$\dot{e}_r = -T\frac{\partial^2 \psi_c}{\partial T^2}\dot{T} + (-T\frac{\partial \sigma}{\partial T} + \sigma) : \dot{\varepsilon} = \overset{\frown}{e}'\dot{T} \tag{2.67}$$

Therefore, the potential free energy for entropic elasticity can be written as:

$$\psi_c(T,\varepsilon) = TK_1(\varepsilon) + K_2(T) \tag{2.68a}$$

$$\phi(q,\dot{\varepsilon}) = \frac{q^2}{kT} \tag{2.68b}$$

Since, $\sigma^{ir} = 0$, the state laws can then be written as:

$$\sigma^r = \frac{\partial \psi}{\partial T} = TK_1^{'}(\varepsilon) = \sigma \tag{2.69}$$

and the heat equation by considering the entropic elasticity as a heat source can be represented as:

$$\rho(\dot{\theta} + \frac{\theta}{\tau_{th}}) = K_c T(e^{2\varepsilon} - e^{-\varepsilon})\dot{\varepsilon} \tag{2.70}$$

where K_c represents a physical constant of the material.

2.3.4 Visco-thermo-elasticity

Following the discussion in subsection 2.3.1, the temperature, which may play an important role in modelling the material behaviour is now considered as one (the first in fact) of the state variable, since the Helmholtz free energy is chosen as thermodynamic potential. In accordance with what has often been observed experimentally on polymer materials, significant thermoelastic effects are introduced into the Zener model(figure 2.5).

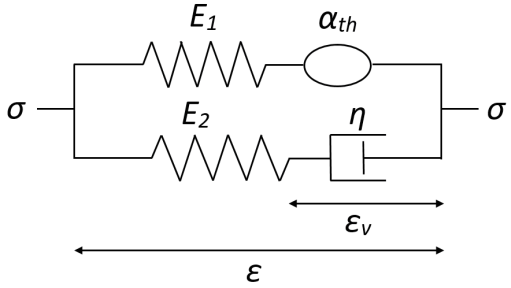

Figure 2.5: Zener visco(thermo)elastic Model

The behaviour of Zener visco-thermoelastic model could be derived in form of equation 2.71 as:

$$\sigma = E_1\varepsilon - \alpha_{th}\theta + \dot{\varepsilon}\eta(1 + \frac{E_1}{E_2}) - \frac{\eta}{E_2}\dot{\sigma} - \frac{\eta}{E_2}\alpha_{th}\dot{\theta} \tag{2.71}$$

and heat diffusion equation can be modified by considering viscous dissipation and thermoelastic source :

$$\rho C_p(\dot{\theta} + \frac{\theta}{\tau_{th}}) = \eta\dot{\varepsilon_v}^2 - E_1\alpha_{th}T_0(\dot{\varepsilon} - \dot{\varepsilon_v}) \tag{2.72}$$

Comparing equation 2.71 with equation 2.39, it can easily be observed that the behaviour shown by the two rheological models is different as the temperature variations are taken into account in the equation 2.71.

This visco-thermo-elastic behaviour can also be written in terms of Helmholtz free energy potential and dissipation potential as:

$$\psi = \frac{1}{2}E_2(\varepsilon - \varepsilon_v)^2 + (-\frac{\rho C_p}{2T_0}(1 + \frac{E_1\alpha_{th}T_0}{\rho C_p})\theta^2 + \frac{E_1}{2}(\varepsilon - \alpha_{th}\theta)^2 - s_0\theta) \tag{2.73a}$$

$$\phi = \frac{1}{2}\eta\dot{\varepsilon_v}^2 + \frac{\overrightarrow{q}\cdot\overrightarrow{q}}{2kT} \tag{2.73b}$$

where k represents the heat conduction coefficient. The state equations can be written as:

$$\sigma^r = \frac{\partial\psi}{\partial\varepsilon} = E_2(\varepsilon - \varepsilon_v) + E_1(\varepsilon - \alpha_{th}\theta) \tag{2.74a}$$

$$\sigma^{ir} = \frac{\partial\phi}{\partial\dot{\varepsilon}} = 0 \tag{2.74b}$$

$$A_v = \frac{\partial\psi}{\partial\varepsilon_v} = -E_2(\varepsilon - \varepsilon_v) \tag{2.74c}$$

and their complementary equations as:

$$X_v = \frac{\partial\phi}{\partial\dot{\varepsilon_v}} = \eta\dot{\varepsilon_v} \tag{2.75a}$$

$$X_q = -k\frac{\overrightarrow{gradT}}{T} \tag{2.75b}$$

2.4 Conclusion of the chapter

In this chapter, we exposed the general thermomechanical framework including the laws of thermodynamics. This framework has led us to write the local heat diffusion on which the source estimation is based. We then presented the general form that the energy balance takes during a load-unload cycle and then during cyclic fatigue tests. A result that we think is important to remember here is that the energy content of a mechanical hysteresis loop can be associated, not only with energy dissipation, but also with thermo-mechanical coupling mechanisms (in non-isothermal and non-adiabatic) or internal energy storage induced by microstructural changes. Following the energy analysis of the mechanical hysteresis area, the different thermomechanical couplings were discussed based on the application to the rheological models along with an example discussing the mechanical behaviour in GSM framework. In the latter case, it was shown, how a rheological model can behave differently considering the temperature as a state variable instead of just a controlled parameter. This thermomechanical formalism explained in this chapter has been used in modelling the viscoelastic behaviour of polymers (Chapter-4) based on the DMTA experimental results (Chapter-3), where, thermography is used to measure

the self-heating of the material under cyclic loading during the DMTA measurements and image processing was performed to observe the thermoelastic couplings.

Chapter 3

Experimental Methodology and Results

Contents

List of symbols

T_g – Glass transition temperature
T_β – Beta transition temperature
R – Load ratio
ρ – Density
m – Mass of the specimen
V – Volume of the specimen
M – Molecular weight
M_w – Weight average molecular weight
M_n – Number average molecular weight
α – Coefficient of thermal expansion
C_p – Specific heat capacity
S_0 – Cross section area
ε – Strain
σ – Stress
δ – Phase shift between stress and strain
f – frequency
E' – Storage modulus
E'' – Loss modulus
$\tan\delta$ – loss tangent
R_u – Universal gas constant
E_a – Activation energy
T_0 – Reference temperature
T – Temperature
a_T – Horizontal shift factor
b_T – Vertical shift factor
δ_{el} – Electronic phase shift
K_m – Apparent sample stiffness
K_1 – Machine stiffness
K_2 – Sample complex stiffness
A_h – Mechanical hysteresis area
A_{HL} – Hysteresis area associated to the loss modulus
A_{hd} – Hysteresis area associated to the dissipation
$\dot{\theta}$ – Temperature variations
τ_{th} – Time constant for heat losses
δ_{th} – Phase shift between temperature and strain

3.1 Introduction and experimental framework

The literature review presented in the first chapter shows the importance of many factors for the viscoelastic properties of polymers along with the cases where the time-temperature superposition principle has been applied successfully and the cases where it has failed to predict the behaviour of polymers on a long time scale. Even the study of the linear viscoelasticity of amorphous polymers becomes complex when one combines different behaviour, e.g., thermomechanical coupling(s) and viscous dissipation, especially in the temperature range near or around the glass transition (T_g) because identifying and understanding the physical mechanisms involved is still an open question. We have therefore chosen to study more particularly the time-temperature superposition principle below the glass transition temperature by considering both thermomechanical couplings and dissipation as well as heat exchanges. We decided to do the study below the glass transition temperature where the behaviour is the simplest and where the dependence of the time shift coefficients with temperature, for the time-temperature superposition principle, follows an Arrhenius law that has a physical background, compared to the WLF law above T_g.

The polymer selection criteria for this study was it shouldn't show complex micro-mechanical mechanisms (e.g., amorphous without crystallization under loading, hydrophobic or limited hydrophilicity, T_g and T_β well separated). For an easier experimental set-up, the glass transition temperature had to be quite low (i.e., between $\approx$ 50 and 100 °C). Finally, this polymer had to be a well-known amorphous polymer that has already been well mechanically characterized previously and for which the application of the time-temperature superposition principle seems to be reasonably applicable. This is why we chose to study mainly atactic polystyrene (PS) that is one of the most "simple" amorphous thermoplastic, which is also used to calibrate DMTA, with a low water absorption ($< 0.4\%/24h$ [86]). This polymer was supplied in the form of plates of two different thicknesses (denoted as "thin" and "thick" below). Two other amorphous polymers were used to complete the study: poly(methyl methacrylate) (PMMA), which is well-known for the applicability of the time-temperature superposition principle and that has a very limited water absorption ($< 0.2\%/24h$ [86]), and one polyamide (PA-6.6 also known as nylon) that has already been study in the laboratory, a widely used polymer with a high dissipation during cyclic loading but a high hygroscopicity (water absorption up to 9% [87]).

The variable parameters involved in the study are limited to temperature, ranging from ambient to a few degrees below T_g, and loading frequency, ranging from 0.01 to 10 Hz (three decades) depending on the frequency range most suitable for the different DMTA testing machines used here. Particular attention is paid to the choice of the experimental domain (temperature, strain amplitude, load ratio, etc.) in order to highlight changes in the rheological behavior of the material without however degrading it significantly (i.e., damage limited by a reduce number of cycles and the use of one sample per temperature). The DMTA cyclic measurements were conducted in the tension-compression mode, with a load ratio of $R = -1$, to ensure an homogeneous and symmetric loading of the sample (i.e., no stress or strain gradient as in bending for example). These measurements were strain controlled with an amplitude of 0.1%. This amplitude was chosen to remain in the linear viscoelastic region (LVR) of the polymer, estimated through a strain sweep at 1 Hz and 10 Hz at room temperature and at the highest test temperature.

The objective of this chapter is to describe the experimental study done on the three different polymers that led us to obtain the parameters required for the final identification of the rheological model and the associated thermodynamic study: physical parameters (density, glass transition temperature, thermal expansion coefficient, specific heat capacity, etc.), viscoelastic "moduli" (storage and loss moduli, loss tangent), time-temperature superposition principle parameters (shift factors and associated activation energy) and heat sources (characteristic time constant for heat losses, mechanical energy dissipated over a cycle, amplitude and phase of the cyclic temperature variation due to thermo-mechanical coupling, etc.). This experimental study is based on the calibration and validation of a whole set-up composed of a DMTA coupled, in a second step, to an infra-red camera.

3.2 Physical Characterization

This section provides the techniques used to measure the physical properties of the three amorphous polymers used in this thesis. Several physical properties are also taken from the literature due to the lack of availability of the required devices. The physical properties that are shown below are density, molecular weight, glass transition temperature, linear expansion coefficient and specific heat capacity.

3.2.1 Density (ρ)

Density is a property of the material that gives the mass of material of an object knowing its volume:

$$\text{Density } \rho = \frac{\text{mass } m \text{ (kg)}}{\text{volume } V \text{ (m}^3\text{)}}. \tag{3.1}$$

To measure the mass of the sample, an analytical balance (METTLER TOLEDO ME204) was used and is shown in figure 3.1. This balance has a maximum capacity of 220 g with an accuracy of 0.1 mg. The volume is assessed by measuring the sample dimensions using a caliper (accuracy of 0.02 mm), with three measurements per dimension along the sample. The result are given in table 3.1 with an estimation of the measurement error. In parallel to these measurements, the obtained values for the three polymers were compared to the literature [87, 88] and found to be very similar.

Polymers	Density (kg/m^3)
Polystyrene (PS) (thick)	1040±7
Polystyrene (PS) (thin)	1080±7
Poly(methyl methacrylate) (PMMA)	1180±8
Polyamide-6.6 (PA-6.6)	1138±8

Table 3.1: Density of the three different polymers used

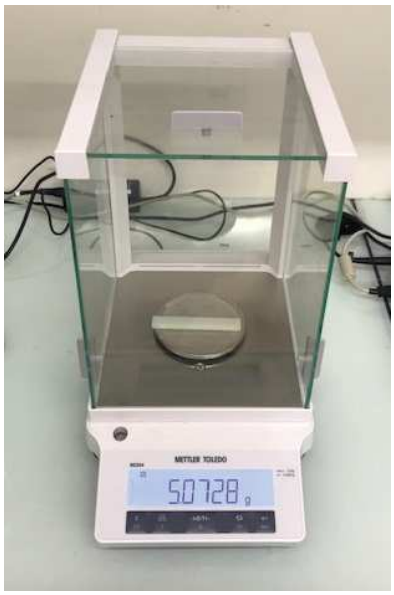

Figure 3.1: Analytical balance

3.2.2 Molecular weight (M)

The molecular weight plays an important role in the physical properties of polymers. For example, increasing the molecular weight increases the glass transition temperature [89]. Together with the glass transition temperature modification, other properties of the polymer are changed like density or moduli. Therefore, in order to be able to compare our results –especially moduli– with the data in the literature, the molecular weight of the three used polymers were estimated by using size-exclusion chromatography (SEC) technique. This is one of the technique to characterize the molar mass distribution of molecules in solution that are separated by their size and, in some cases, molecular weight. This technique has the advantage of allowing to change the conditions to suit the type of sample or the requirements for further purification, analysis or storage without altering the separation [90]. Measurements were done by Dr. Coline Pinese of the Department of Polymers for Health and Biomaterials at IBMM laboratory (UMR 5247) of the University of Montpellier.

SEC is based on resins made of a porous matrix of spherical particles that lack reactivity and adsorptive properties. After the sample has been dissolved in a solvent, its molecules larger than the pores are unable to diffuse into the beads, so they elute first. Molecules, that range in size between the very big and very small ones can penetrate the pores to varying degrees based on their size. If a molecule is smaller than the smallest pores in the resin, it will be able to enter the total pore volume. Molecules that enter the total pore volume are eluted last. Samples are eluted isocratically so there is no need to use different buffers during the separation [91].

The solvent used for SEC analysis of PS was Tetrahydrofuran (THF) along with a calibration done with a reference sample of PS. An example of the outcome of SEC technique is shown in figure 3.2.

The results for the molecular weight for all the three polymers are shown in table 3.2 where M_w and M_n represent the weight average molecular weight and number average molecular

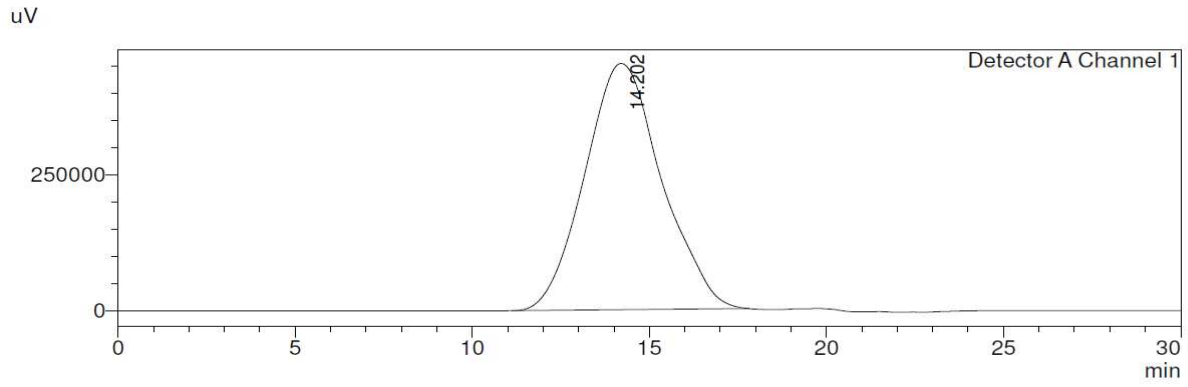

Figure 3.2: Example of a molecular weight measurement by SEC on PS

weight, respectively, and dispersity Đ computed as M_w/M_n. M_w is based on the fact that a bigger molecule contains more of the total mass of the polymer sample than the smaller molecules do whereas M_n is just the total weight of all the polymer molecules in a sample divided by the total number of polymer molecules in a sample [92]. Data for PMMA and PA-6.6 are taken from the literature as they require very strong solvent for the measurement and a specific SEC device, which is not available in Montpellier.

Polymers	M_w (g/mol)	M_n (g/mol)	Đ=M_w/M_n (-)
PS (thick)	$9.52 \cdot 10^4$	$2.74 \cdot 10^4$	3.5
PS (thin)	$11.14 \cdot 10^4$	$3.62 \cdot 10^4$	3
PMMA* [93]	$9.6 \cdot 10^4$	$5.05 \cdot 10^4$	1.9
PA-6.6* [87]	$2.4 - 4 \cdot 10^4$	$1.2 - 2 \cdot 10^4$	2

*Table 3.2: Molecular weight and dispersity of the three different polymers used. * data from the literature.*

3.2.3 Glass transition temperature (T_g)

The glass transition corresponds the gradual and reversible transition in amorphous materials, from a stiff and relatively brittle "glassy" state to a viscous or rubbery state, as the temperature increases. The mean temperature at which this transition occurs is known as glass transition temperature.

There are several ways and experimental conditions to measure this temperature, which do not give exactly the same value. In the present case, as we mainly need this value to do DMTA measurements below it, it was measured using classical Differential Scanning Calorimetry (DSC), using DSC-3 device from METTLER TOLEDO at ICGM laboratory of the University of Montpellier. DSC is a technique in which the difference in the amount of heat required to increase the temperature of a sample and a reference sample is measured as a function of temperature. For the measurement, a sample of $1 - 3$ mg of each polymer was placed in a hermetic aluminium pan. A hole was produced by drilling the lid with a pair of tweezers.

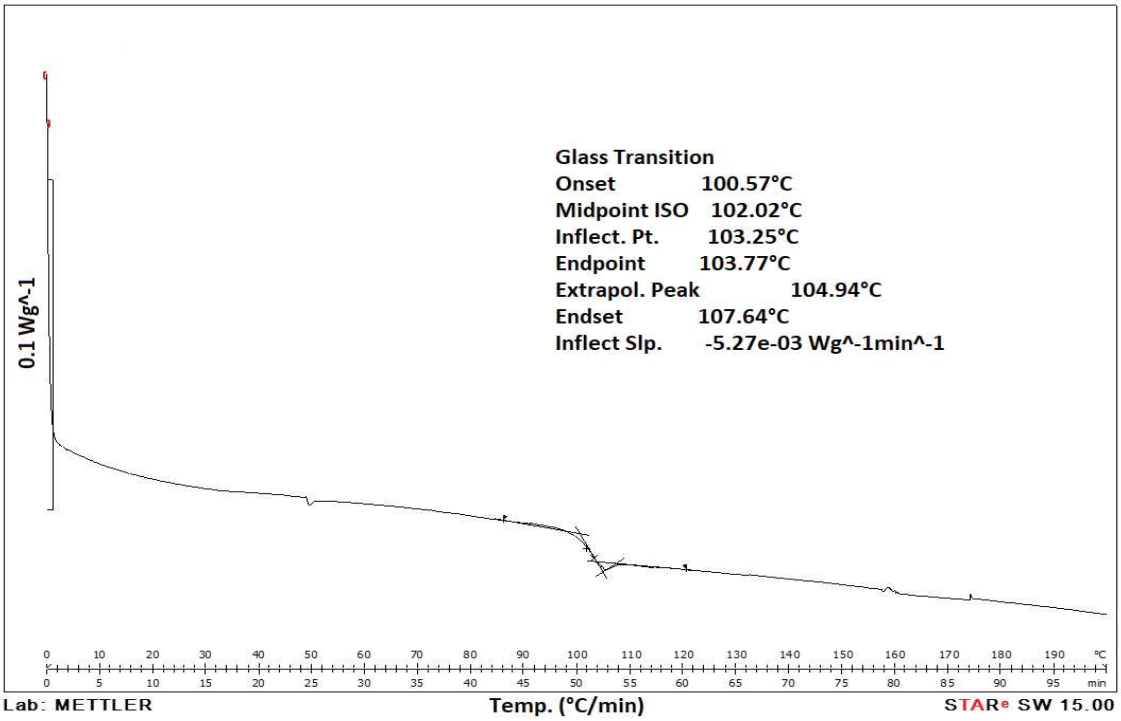

Figure 3.3: Typical DSC curve on PS. The abscissa axis represents the temperature and the elapsed time (in minutes) and the ordinate axis the corresponding heat flow.

The sample was weighed after the lid was drilled. The method used was modulated reversed calorimetry where the temperature was increased by a ramp of 2 °C/min up to 200 °C. The glass transition temperature can be defined in different ways. Here, the onset temperature and the inflection point temperature determine T_g (figure 3.3). The glass transition temperature of all the polymers used are shown in the table 3.3.

Polymers	T_g (°C)
Polystyrene (thick)	103
Polystyrene (thin)	102
PMMA	102
Polyamide-6.6	63

Table 3.3: Glass transition temperatures measured by DSC

The glass transition temperature values of PS, PMMA and PA-6.6 were in accordance with the value range found in the literature except for PMMA, i.e. $85 - 110$ °C for PS, $130 - 148$ °C for PMMA and $60 - 75$ °C for PA-6.6 [88, 94]. It was also observed that the T_g of PMMA is in accordance with the T_g provided by its suppliers [86]. The significant difference in the T_g of PMMA from the literature hereby could be associated to the several manufacturing parameters such as molecular weight distribution, the amount of cross-linking chains etc.

3.2.4 Coefficient of thermal expansion (α)

The coefficient of thermal expansion is a material property that indicates the extent to which a volume of material expands upon an increase of its temperature. An increase of temperature corresponds to an increase of the kinetic energy (or "thermal agitation energy") of each atom of the material that induces an increase of the mean inter-atomic distance. This increase depends on the intensity of the bond between atoms. This dimensional response to a temperature change is expressed by its coefficients of thermal expansion [95].

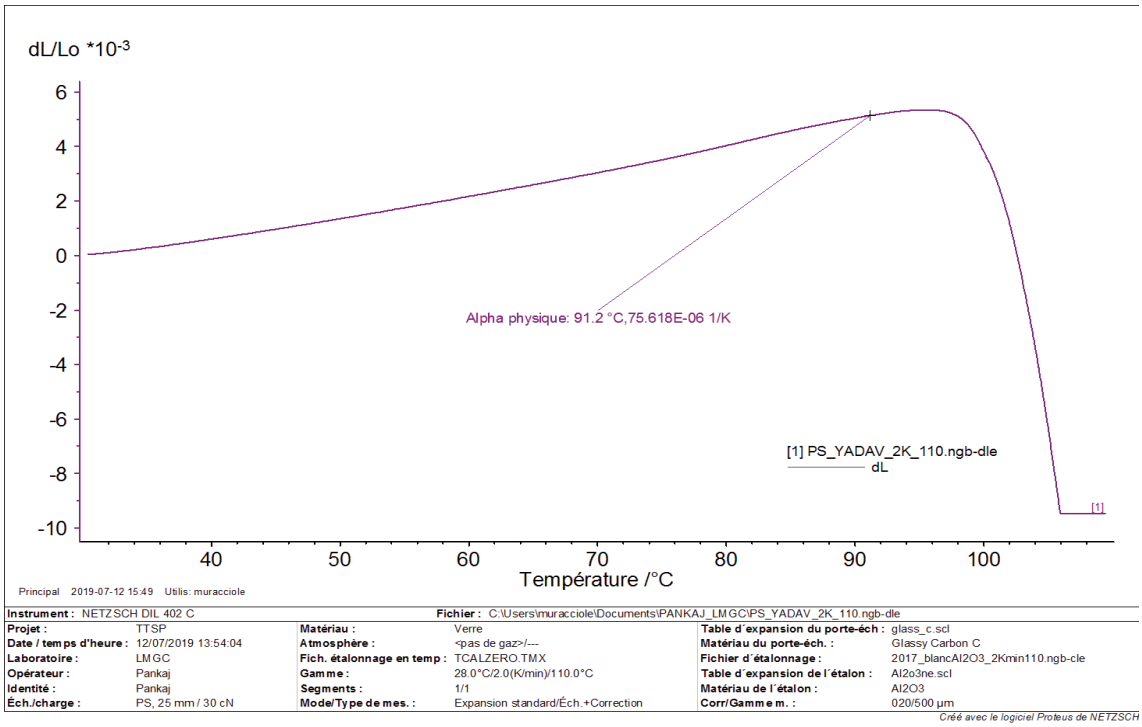

Figure 3.4: Thermal expansion curve for PS

This coefficient can depend on the temperature but, in our case of limited variation of the temperature, we only consider a constant coefficient with a linear response and one coefficient of linear thermal expansion (CLTE), as the polymers used can be considered isotropic. This can be expressed by the following equation:

$$\alpha = \frac{1}{L}\left(\frac{\partial L}{\partial T}\right), \tag{3.2}$$

where L is the length of the sample. This was measured using the dilatometry technique. The dilatometer used for these measurements (NETZSCH DIL 402 Expedis Classic) is shown in figure 3.5a along with a schematic principle view (figure 3.5b). This dilatometer has a temperature accuracy of 0.1 K and a maximum elongation measurement of around 5000 µm. A temperature ramp rate of 2 K/min was used with the temperature variation from 20 to 110 °C.

(a) NETZSCH DIL 402 Expedis Classic

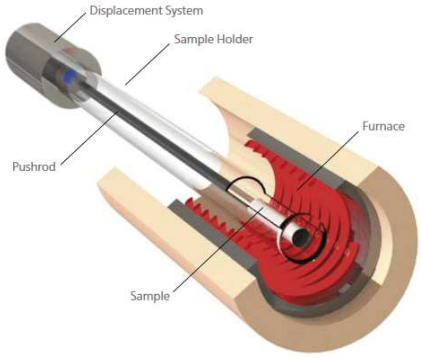

(b) Schematic principle view of a dilatometer

Figure 3.5: Dilatometer for the measurement of thermal expansion coefficient [96]

Polymers	α (1/K)
PS (thick)	$7.5 \cdot 10^{-5}$
PMMA	$8.2 \cdot 10^{-5}$
PA-6.6	$12 \cdot 10^{-5}$

Table 3.4: Coefficient of linear thermal expansion

These measurements were performed with the help of Dr. Jean-Michel Muracciole at the department of Materials Science and Engineering of Polytech'Montpellier engineering school of the University of Montpellier. An example of the obtained curve for PS can be seen in figure 3.4. The results obtained from these measurements are reported in table 3.4. The measured values of CLTE were compared with literature data. It was found that the measured values were in the same order of magnitude, except for PMMA, i.e. $6 - 8 \cdot 10^{-5}$ K^{-1} for PS, $4 - 6 \cdot 10^{-5}$ K^{-1} for PMMA and $10 - 14 \cdot 10^{-5}$ K^{-1} for PA-6.6 [87]. As mentioned in earlier section 3.2.3, this difference in CLTE could again be associated with the several manufacturing parameters such as the amount of cross-linking chains and molecular weight distribution.

3.2.5 Specific heat capacity (C_p)

The specific heat capacity is defined as the amount of energy required to induce a change of 1 °C of the temperature of a unit mass of material. It was measured using the DSC technique as well. To determine the heat capacity of polymers, the DSC heat flow signal from the sample is compared to the DSC signal of a calibration standard of known specific heat capacity. Later, both curves are corrected by a zero line, or base line, correction experiment where an empty reference and empty sample crucible are placed in the furnace and the system signal drift is measured under identical experimental conditions [97]. The results of the DSC measurements of the specific heat capacity of the three polymers are reported in table 3.5

The C_p measurements for PS were carried out in C2MA laboratory (Alès) on a METTLER TOLEDO DSC3. The measured values were compared with literature data and were found in

Polymers	C_p (J/K · kg)
PS (thick)	1400
PMMA* [88]	1450
PA-6.6* [88]	1700

*Table 3.5: Specific heat capacity of the three polymers. * data from the literature.*

the same order of magnitude, i.e. 1400 J/K.kg [88]. Data for PMMA and PA-6.6 are taken from the literature directly as it wasn't possible to carry out the C_p measurements.

3.3 Classical DMTA measurements on PS

To study the time-temperature superposition principle (TTSP), experimental data on the influence of the temperature and mechanical loading frequency on the linear viscoelastic response of a polymer are required. This kind of measurements is usually done using Dynamical Mechanical and Thermal Analysis (DMTA) device that can be more or less "automatic", with different kind of loading (e.g., tension-compression, bending, shear by rotation, etc.) and load capacity (e.g., from a few tenths to several tens or hundreds of N). In our case, we focused on a tensile-compression loading in order to have a homogeneous stress and strain field in the sample that, contrary to bending for example, avoids amplifying possible surface effect (e.g., water adsorption) or the effect of any gradient in the material properties through the thickness (e.g., due to the moulding process of the polymer plate like injection or extrusion moulding). During these measurements, a sinusoidal one-dimensional deformation (ΔL) is applied to the sample and the resulting load (F) is measured. The mean applied strain (ε) is then computed taken the initial sample length between the machine grips (L_0) and the mean stress (σ) from the ratio of the load to the sample initial cross-section area ($S_0 = t_0 \times h_0$). All these parameters are computed under the infinitesimal strain assumption as the measurements are done in the linear viscoelastic region (LVR) of the material. Note that the length and cross-section area used for the calculations can take into account the thermal expansion of the sample but this only induces a change of $\approx 1\%$ of the length and $\approx 2\%$ of the cross-section area, considering an average coefficient of thermal expansion (table 3.4) and a maximum temperature change from 20 to 100 °C.

As described in the first chapter, the applied strain and the resulting stress can be mathematically written as:

$$\varepsilon(t) = \varepsilon_0 \sin(2\pi f\, t), \tag{3.3}$$

and

$$\sigma(t) = \sigma_0 \sin(2\pi f\, t + \delta), \tag{3.4}$$

where it is assumed that a monochromatic loading in strain (frequency f and amplitude ε_0) results in a monochromatic response in stress (same frequency f and amplitude σ_0) with a phase shift δ, also denoted as the loss tangent $\tan\delta$. Eq. (3.4) can be rewritten as:

$$\sigma(t) = E'\varepsilon_0 \sin(2\pi f\, t) + E''\varepsilon_0 \cos(2\pi f\, t), \tag{3.5}$$

where,

$$E' = \frac{\sigma_0}{\varepsilon_0} \cos \delta, \tag{3.6a}$$

and

$$E'' = \frac{\sigma_0}{\varepsilon_0} \sin \delta, \tag{3.6b}$$

with E' and E'' the so-called storage and loss modulus, respectively, and $E^* = \sigma_0/\varepsilon_0$ the complex modulus.

The objective here is to do a comparative study between different DMTA devices available in three different laboratories in France on a similar set of PS samples, the "simplest" polymer of this study. This will provide a robust database on this polymer to validate our own corrections and calibration procedure made on our DMTA, described in the later section. All the samples were made in the LMGC workshop with different rectangular shape, to fit with the different DMTA capabilities, where length and width were machined with a precision of $\approx \pm 0.1$ mm. The thickness corresponds to that of the plate delivered by Goodfellow with, as a reminder, two kinds of thickness: 1.2 mm±20% and 4 mm±20%.

3.3.1 Institut P', Poitiers

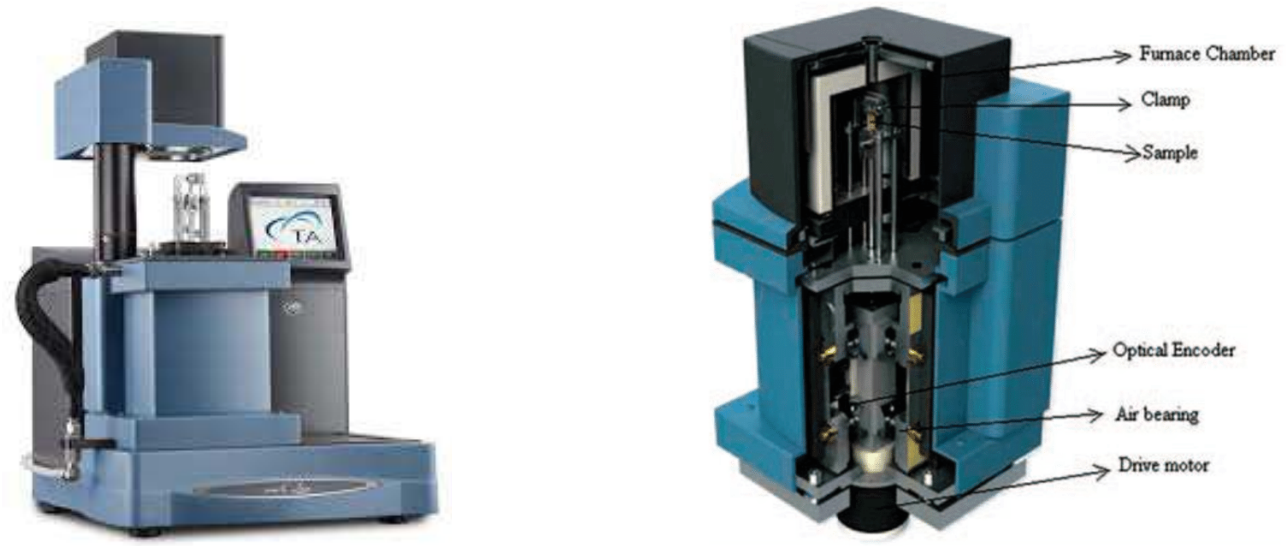

(a) TA instruments Q800

(b) General constitutive scheme of Q800

Figure 3.6: TA instruments, Q800 [1]

3.3.1.1 Material and method

This series of DMTA measurements was done by David Mellier and processed by Pr. Sylvie Castagnet. The DMTA used (TA instruments, Q800) is shown in figure 3.6a with its general constitutive scheme (figure 3.6b). This DMTA device has the best specifications with a force resolution of 10 µN, displacement resolution of 1 nm, a relative modulus precision of ±1%, $\tan \delta$

sensitivity of 0.0001, a temperature stability of ±0.1 °C [98].

The DMTA measurements were performed in the most common way, i.e., 3-point bending mode, on thin rectangular samples of PS of dimensions $80 \times 4 \times 1.2$ mm. Since, the glass or secondary transitions can be seen both during a frequency sweep and a temperature sweep, these measurements were conducted in the multidimensional mode, i.e., combined frequency and temperature sweep. This is the test mode where the temperature sweep is conducted at various frequencies or the frequency sweep is conducted at various temperatures on one sample. This type of measurement of a polymer's viscoelastic response is the fastest, most common and most plug-and-play. During these measurements, the order of frequency used was from 10 Hz to 0.01 Hz. The different parameters used during these measurements are reported in table 3.6.

Parameters	Values
Strain amplitude	0.1%
Frequency range	$0.01 - 10$ Hz (4 points per decade)
Temperatures	30, 50, 60, 70, 75, 80, 85, 90°C

Table 3.6: Controlled parameters used for tests in P', Poitiers

3.3.1.2 Results and application of TTSP

After the completion of combined sweep performed in the mode of 3-point bending, we obtained a consequent set of data for the same sample, as it wasn't possible to change the sample during the combined sweep. Raw results obtained are presented in figures 3.7a and 3.7b, showing the influence of temperature and frequency on the storage modulus and loss tangent of PS. The standard behaviour of polymer below T_g is observed, i.e., the storage modulus is increasing with the frequency and decreasing with the temperature. This evolution of results is in accordance with [2] shown in figure 3.8. It is pointed out that figure 3.8 is shown only to compare the evolution of storage modulus obtained in the results.

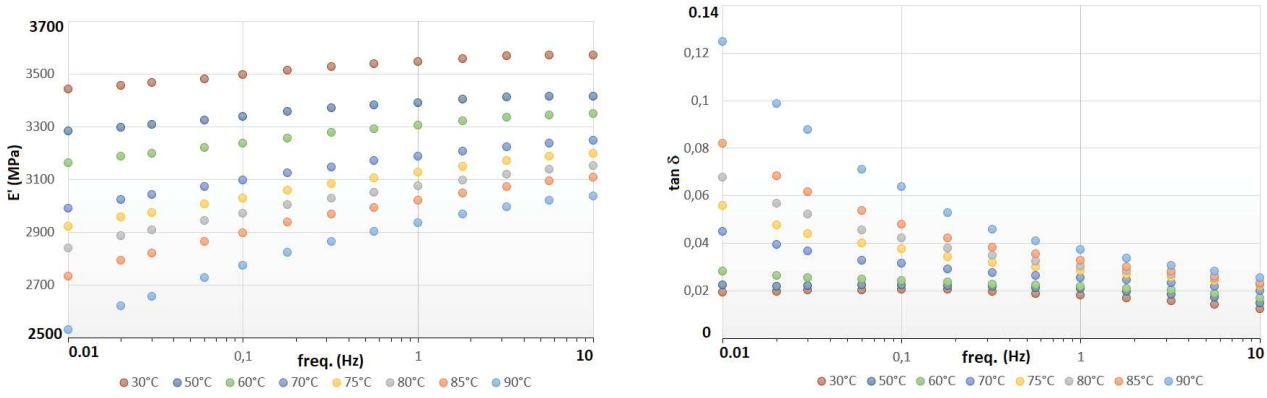

(a) Storage modulus vs frequency

(b) Loss tangent vs frequency

Figure 3.7: Raw results of DMTA measurements on PS (thin) obtained at P', Poitiers

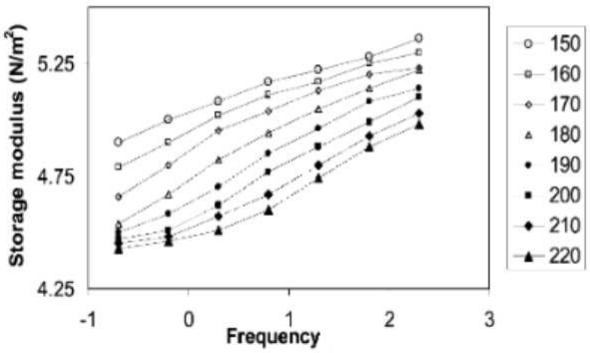

Figure 3.8: Double logarithmic plot of storage modulus against frequency at several different temperatures on Polystyrene with M_w of $35.7 \cdot 10^4 g/mol$. [2]

In the following of the analysis of the raw experimental results, the TTSP was applied manually [29] on E' data, i.e., we chose the highest temperature as the reference one $T_0 = 90\,°C$ and the other isothermal curves are shifted on the frequency axis, following $f(T_0) = f(T)/a_{T_0}(T)$ with a_{T_0} the shift factor, so that all the curves overlap to visually form a single continuous and smooth curve called master curve (figure 3.9a and 3.9b). Following the shifting of curves at T_0, the activation energy was calculated using the slope of a linear regression on the plot of shift factors versus $1/T - 1/T_0$ (figure 3.10) and was found to be $E_a = 313kJ/mol$. Note that the slope is equal to $-E_a/R_u$, where, $R_u = 8.314J/(mol.K)$ represents the universal gas constant.

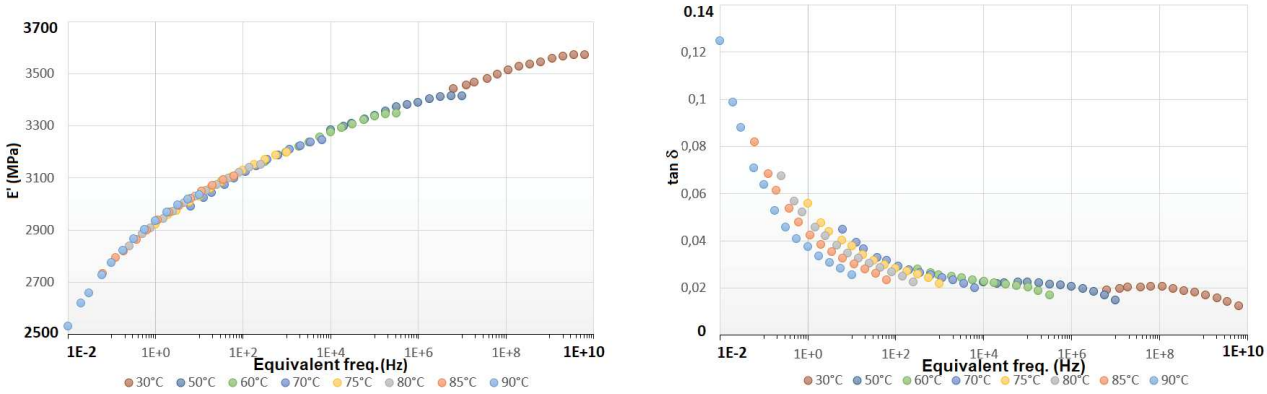

(a) Storage modulus vs frequency

(b) Loss tangent vs frequency

Figure 3.9: Building of the master curves at a reference temperature of 90 °C for data from P', Poitiers

It was observed that, after applying the same horizontal shift as for the isothermal curves of E', the master curve in case of the loss tangent is not continuous, in accordance with the research work of Cavaille et al. [32]. Therefore, we could wonder if different horizontal shift factors should be applied in the case of the loss tangent (and the physical reason for that). Usually in such a case, vertical shifts are added to the horizontal ones based on the effect of the dilation for amorphous polymers (figure 3.11). The added vertical shift variation with the temperature can be seen in figure 3.12. These vertical shift values are very small i.e., between 0.5-1 and are an increasing function of temperature like dilation. This trend of evolution and values of vertical shift were found in accordance with Rouleau et al. [99]. It was observed This added vertical shift can be mathematically represented by equation 3.7:

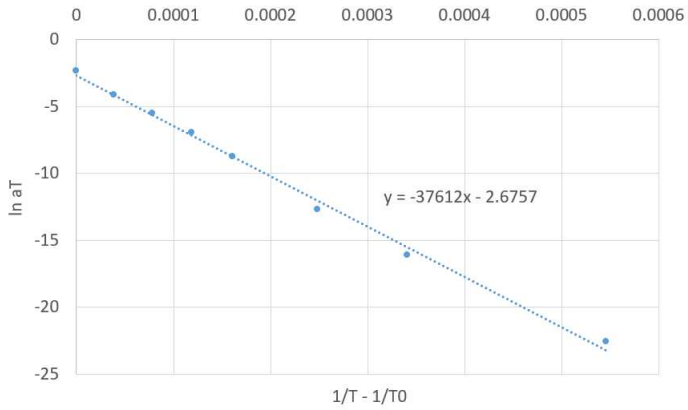

Figure 3.10: Activation energy calculation using Arrhenius plot for data from P', Poitiers

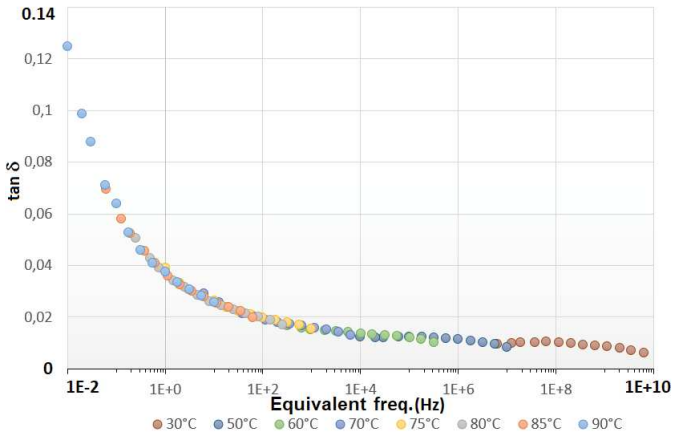

Figure 3.11: Added vertical shift in the case of loss tangent for data from P', Poitiers

$$\tan \delta_f = \tan \delta_i * b_T, \tag{3.7}$$

where tan δ_f and tan δ_i represents the final and initial loss tangent after and before adding the vertical shift.

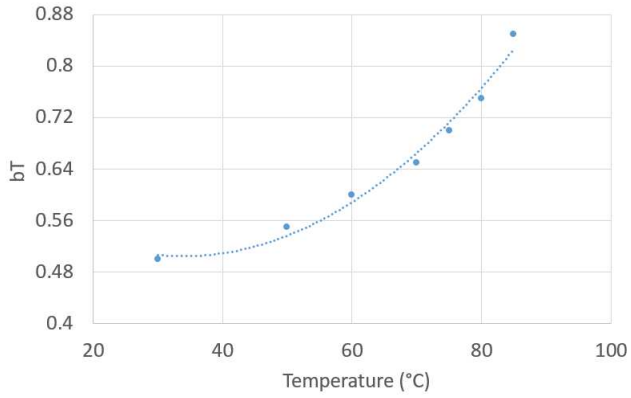

Figure 3.12: Variation of vertical shift versus temperature for data from P', Poitiers

3.3.2 ICGM, Montpellier

3.3.2.1 Material and method

The DMTA used (NETZSCH DMTA 242e Artemis) is shown in figure 3.13a along with a general constitutive scheme in figure 3.13b. It has the same principle of measurement as the previous one, i.e., it doesn't allow to record the imposed cyclic load or displacement neither the response that could include some electronic correction (e.g., machine stiffness). The experimental device allows different mechanical tests (compression, shear, tension, 3-point bending test and torsion) to be carried out at different temperatures from -170 to 600 °C and frequency range from 0.01 to 100 Hz. This machine is capable of maximum controlled displacement amplitude up to $\pm 240\ \mu m$, damping range ($\tan\delta$) from 0.005 to 100. There are two major kind of tests modes which can be used to probe the viscoelastic properties of the sample: temperature sweep and frequency sweep.

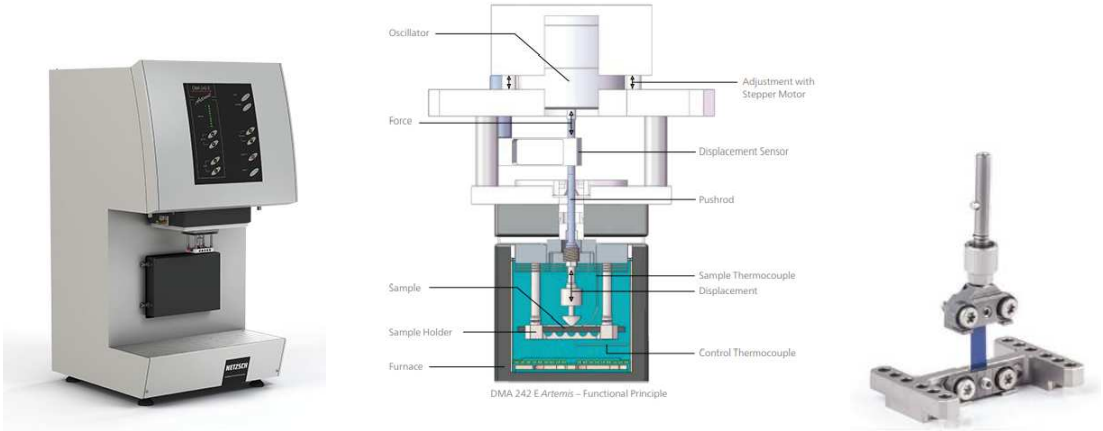

(a) NETZSCH DMTA 242e Artemis

(b) General constitutive scheme

(c) Tension mode clamps

Figure 3.13: NETZSCH DMTA 242e Artemis [3]

The test mode used here was frequency sweep with, this time, tension-compression loading (figure 3.13c), with strain control, on rectangular sample of PS of dimensions $26 \times 4 \times 1.2$ mm with an operating length between the clamps of 14 mm. These dimensions have been chosen to fit with the machine load and displacement capacity. The frequency sweep is done at a given and controlled temperature and a new sample is used at each temperature step. The experimental procedure described in the previous section was not preferred, i.e. using the same sample for all temperatures, to avoid the non-reproducibility of results between each temperature [46]. Temperature were held constant to within 0.5 °C with a stabilisation time of 45 minutes. The linear viscoelastic region was measured using a strain sweep at 1 Hz and 10 Hz at room temperature and 90 °C. The strain sweep was carried out from 0.01 to 0.2%. The strain sweep is the test mode in which the complex modulus is measured at constant frequency and constant temperature while varying the strain amplitude. The results of the strain sweep are shown in figure 3.14. It was observed from the results that the storage modulus stays almost constant throughout the strain sweep but, for safety purposes, the linear viscoelastic region was considered to be until 0.1% of strain and hence the same was used for all the following measurements. No hold time was imposed between two frequencies. The number of cycles were

varied from few cycles (low frequency) to some hundreds of cycles (high frequency). The viscoelastic properties were then calculated within the integral DMTA Analysis software *Proteus*. The different parameters used during these measurements are summarized in table 3.7. During these measurements, the order of frequency used was from 0.01 Hz to 10 Hz.

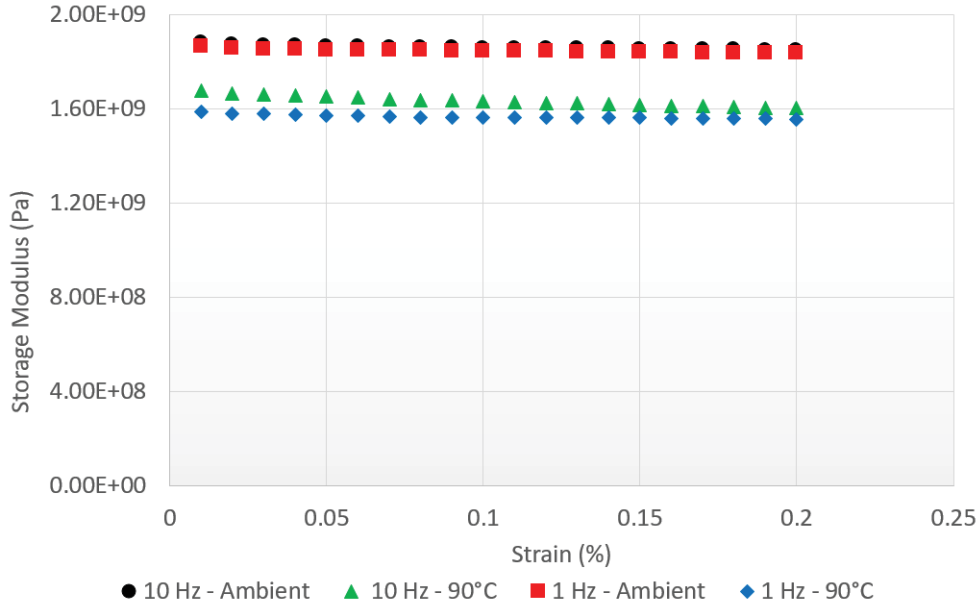

Figure 3.14: Strain sweep measurement

Parameters	Values
Strain amplitude	0.1%
Maximum force	±12 N
Load ratio (R)	-1
Frequency range	$0.01 - 10$ Hz (6 points per decade)
Heating rate	2 K/min
Temperature	50, 60, 70, 75, 80, 85, 87, 90°C

Table 3.7: Parameters used for tests in ICGM, Montpellier

3.3.2.2 Results and application of TTSP

The raw data of a frequency sweep on PS at the room temperature are shown as an example in the figure 3.15, where storage modulus (E') and loss modulus (E'') are plotted against the measurement time for the different loading frequencies. After the completion of these frequency sweep measurements, entire series of results concerning several samples of PS tested in tension-compression mode was obtained (figures 3.16a and 3.16b).

Each different color in the figures 3.16a and 3.16b shows different temperature. It was observed that the storage modulus has an unexpected behaviour as it has increased with temperature at 60 °C. According to T. Alfrey and G. Goldfinger [44], in the intermediate temperature

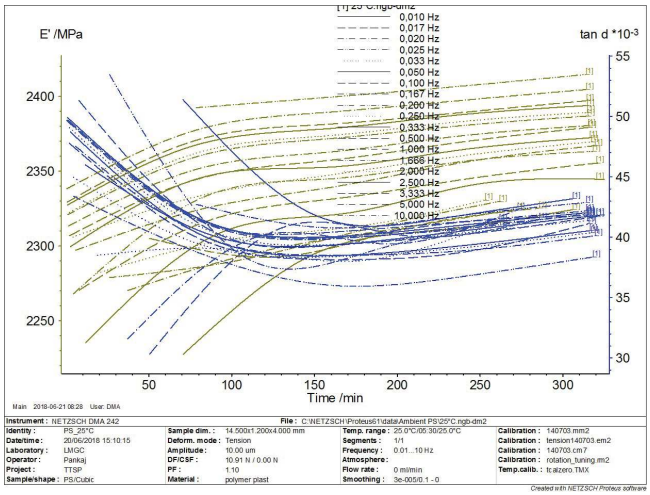

Figure 3.15: Frequency sweep results on PS at room temperature (25 °C) at ICGM, Montpellier

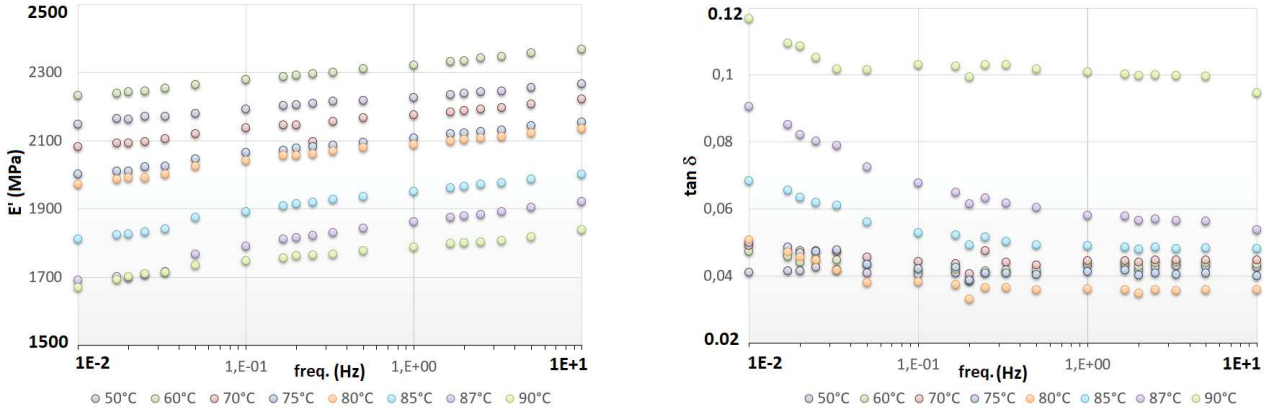

(a) Storage modulus vs frequency

(b) Loss tangent vs frequency

Figure 3.16: Raw results of DMTA measurements on PS (thin) obtained at ICGM, Montpellier

range (say from 40 to 80 °C), complex time effects can be observed. It was assumed that it's not consistent as such a contraction wasn't observed during the thermal expansion measurements. Moreover, it was also assumed that this unexpected behaviour of the storage modulus could come from the problem of temperature stabilisation.

In the following of the analysis of the raw experimental results, the TTSP was applied manually similarly to the previous data from P' with the same reference temperature of 90 °C. The resulting master curves are shown in figures 3.17a and 3.17b. The horizontal shifting found for E' was applied to all the data, loss modulus and loss tangent also. Following the application of horizontal shift, the activation energy was calculated using an Arrhenius plot and was found to be $E_a = 457kJ/mol$. The plot of horizontal shift factor against $1/T - 1/T_0$ can be seen in figure 3.18. Again, after implementing horizontal shift to all the experimental data, it was observed during the construction of master curves that superposition by shifting along the frequency axis alone cannot yield a smooth master curve for the loss tangent ($\tan\delta$). Later, a vertical shift is added in the case of the loss tangent curves to get a smooth master (figure 3.19).

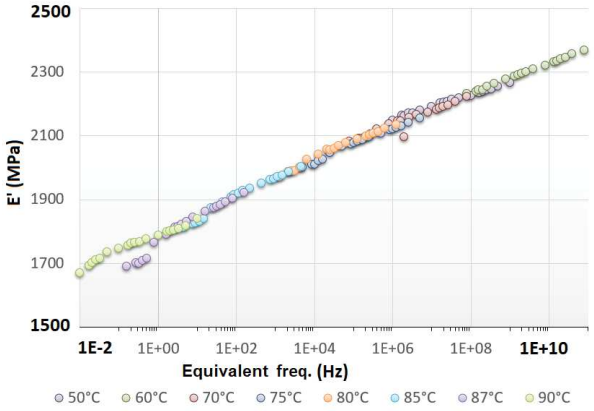

(a) Storage modulus vs frequency

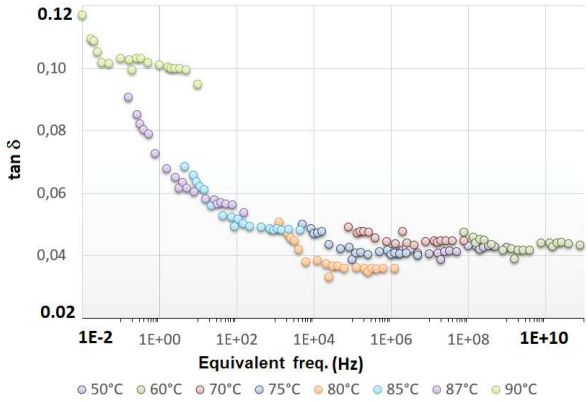

(b) loss tangent vs frequency

Figure 3.17: Building of the master curves at a reference temperature of 90 °C *for data from ICGM, Montpellier*

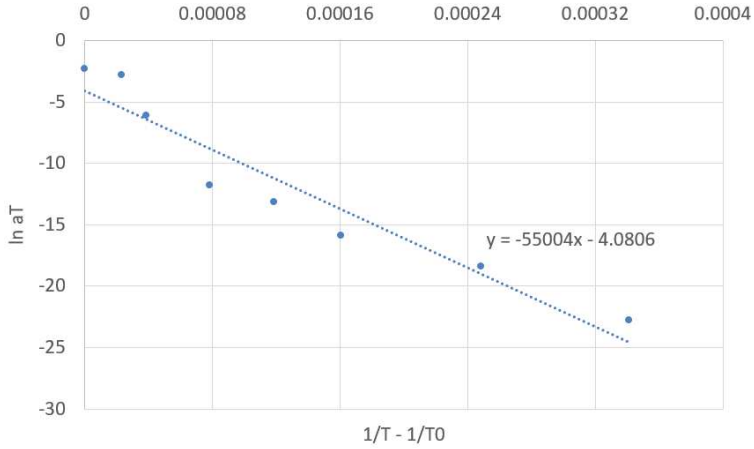

Figure 3.18: Activation energy calculation using Arrhenius law for data from ICGM, Montpellier

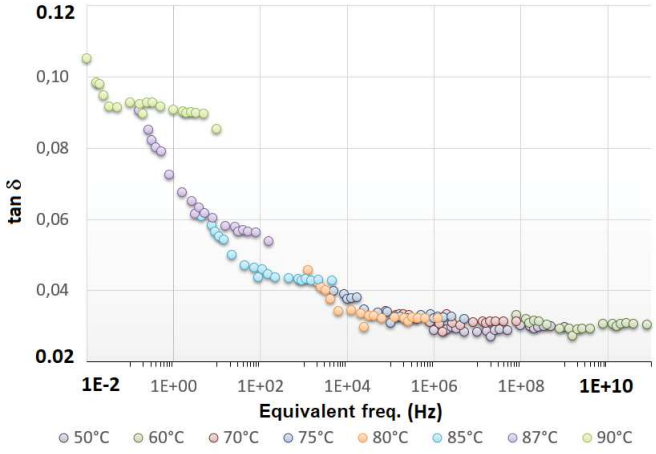

Figure 3.19: Added vertical shift in the case of loss tangent for data from ICGM, Montpellier

The variation of added vertical shift with the temperature can be seen in figure 3.20.

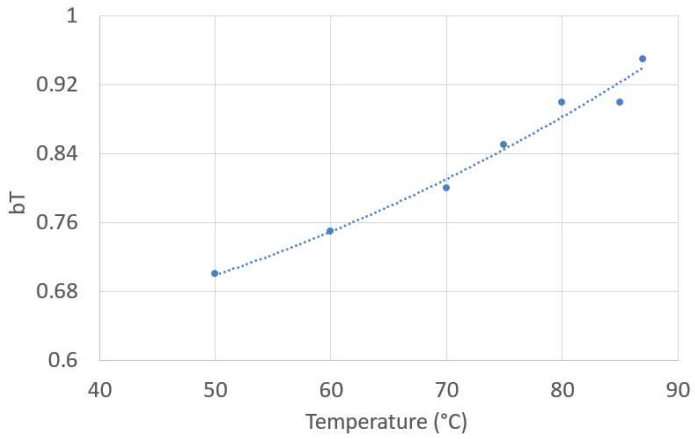

Figure 3.20: Variation of vertical shift versus temperature for data from ICGM, Montpellier

3.3.3 C2MA, Alès

3.3.3.1 Material and Method

The nature of the measurements was the same as followed in the previous measurements at ICGM (Montpellier). The DMTA used for the measurements at C2MA (Metravib DMA 50) is shown in figure 3.21. This DMTA device has the flexible specifications with a displacement accuracy of $\pm 1 \mu m$, frequency range from 0.00001 Hz to 200 Hz, and temperature range from -150°C to 500°C. It also provides extra features like reversible frame, humidity control capability, etc. The PS (thin) sample were rectangular, with the dimensions $60 \times 8 \times 1.2$ mm, and tested in the tension-compression mode and strain controlled. The frequency range and testing temperatures are the same as the other measurements. The order of frequency was the same as was used in ICGM i.e., from 0.01 Hz to 10 Hz. A hold time of 10 minutes was done for the very first frequency to ensure a uniform distribution of the temperature in the sample. The maximum force of ±33 N was measured by the DMTA load sensors at the beginning to get a strain of ±0.1%. The other parameters used are reported in the table 3.8.

Parameters	**Values**
Strain amplitude	0.1%
Maximum force	±33 N
Load ratio (R)	-1
Frequency range	$0.01 - 10$ Hz (5 points per decade)
Heating rate	5 K/min
Temperature	40, 50, 60, 70, 75, 80, 85, 90°C

Table 3.8: Parameters used for tests in C2MA, Alès

Figure 3.21: METRAVIB DMA 50
[100]

3.3.3.2 Results and application of TTSP

Completion of the series of frequency sweeps at different temperatures provided us a series of data concerning several samples, as a new sample was used for each temperature just like in the previous measurements at ICGM. The evolution of the storage modulus (E') and loss tangent ($\tan\delta$) of PS samples is shown in figures 3.22a and 3.22b. Similar trends to previous results of E' and $\tan\delta$ with temperature and frequency are observed.

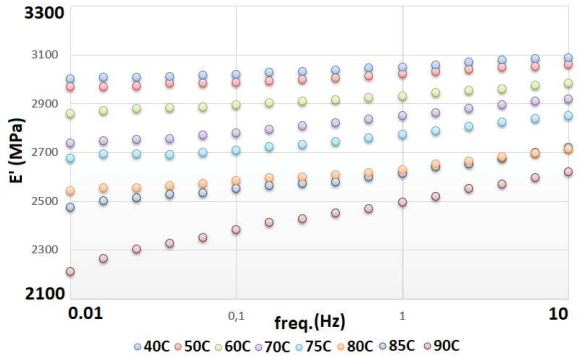

(a) E' vs frequency

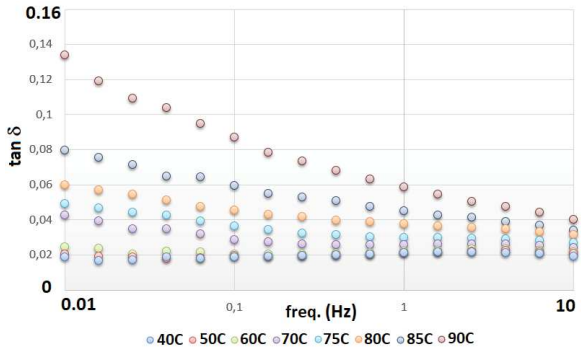

(b) tan δ vs frequency

Figure 3.22: Raw results of DMTA measurements on PS (thin) obtained at C2MA, Alès

In continuation to the analysis of experimental results, the TTSP has been applied to them with the same procedure as the previous results and yields the master curves reported on figures 3.23a and 3.23b. Following the application of horizontal shift, the activation energy was calculated using an Arrhenius plot and was found to be $E_a = 397kJ/mol$. The plot of horizontal shift factor against $1/T - 1/T_0$ can be seen in figure 3.24. Again, this horizontal shift was supplemented by a vertical one in case of the loss tangent to get a smooth master curve (figure 3.25).

The added vertical shift variation with the temperature can be seen in figure 3.26. In this case of addition of vertical shift to get the master curve, it was observed that the vertical shift was decreasing with the temperature unlike in the case of P' and ICGM. Moreover, it was

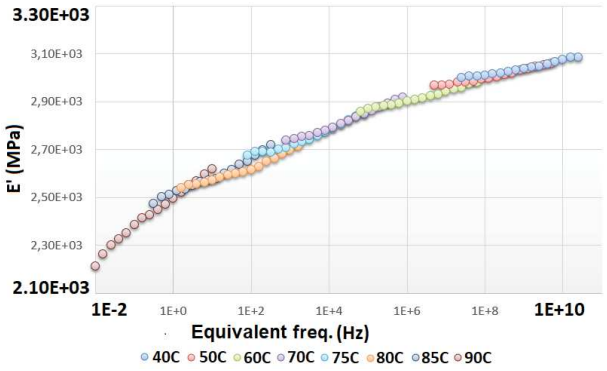

(a) Storage modulus vs frequency

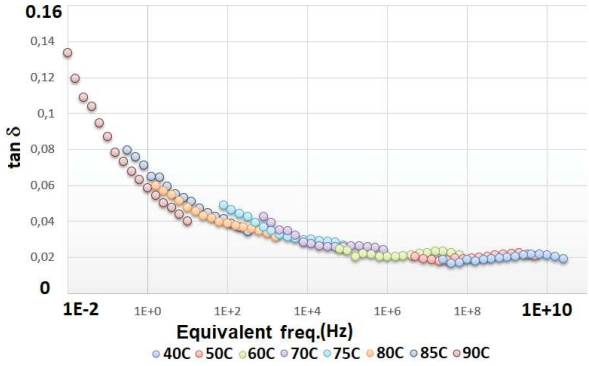

(b) loss tangent vs frequency

Figure 3.23: Building of the master curves at a reference temperature of 90 °C *for data from C2MA, Alès*

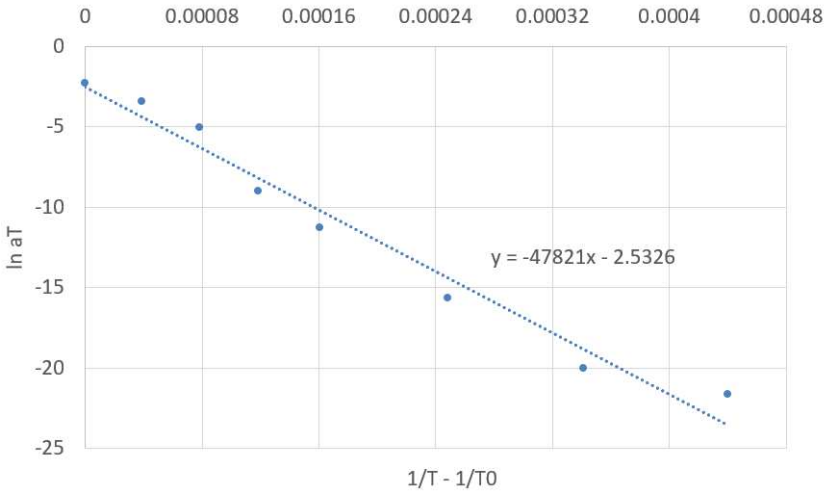

Figure 3.24: Activation energy calculation using Arrhenius law for data from C2MA, Alès

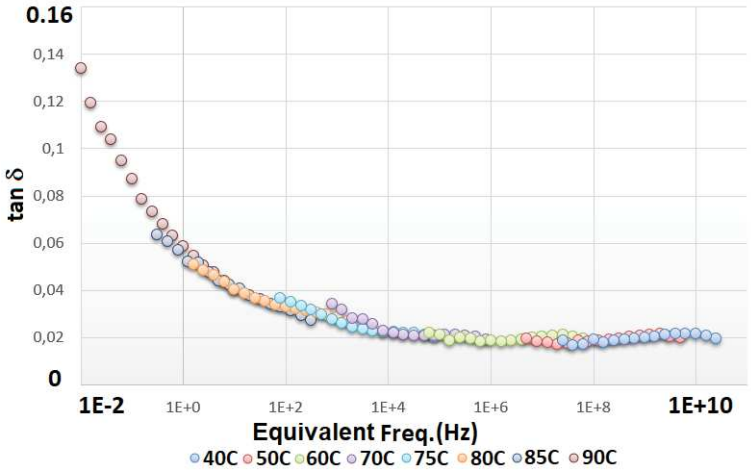

Figure 3.25: Added vertical shift in the case of loss tangent for data from C2MA, Alès

also observed that the vertical shift values are quite high in comparison to P' and ICGM at particular temperatures. Being the higher values of vertical shift in C2MA than in case of P'

and ICGM, these values also stayed in between 0.6-1.

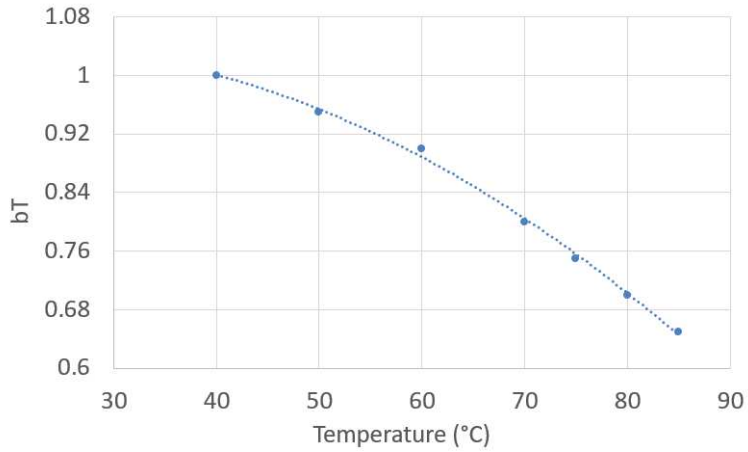

Figure 3.26: Variation of vertical shift versus temperature for data from C2MA, Alès

3.3.4 FEMTO-ST, Besançon

After the completion of the series of the tests at P' (Poitiers), ICGM (Montpellier) and C2MA (Alès), it was observed that the values of the storage modulus and loss tangent (or loss modulus) are not always comparable for these laboratories for samples coming from the same plate. These discrepancies, especially for E' and the values of b_T, lead us to perform some more measurements on an other DMTA, closer to ours in terms of capabilities. Therefore, thanks to the collaboration between LMGC (Montpellier) and FEMTO-ST (Besançon), several tests were performed on the same kind of samples in Besançon. The details of the specimen dimensions, the tests performed in FEMTO-ST and the details of the machines are given in the following sections.

3.3.4.1 Material and Method

The nature of tests carried out in FEMTO-ST are exactly the same as carried out in ICGM and C2MA to make the comparison more convenient. The DMTA used in FEMTO-ST (Metravib DMA +300) is shown in figure 3.27.

The material chosen for the tests was the same as in P', ICGM and C2MA but with the different dimensions to fit with the specifications of the DMTA machine used in FEMTO-ST. This DMTA device has the flexible specifications with a displacement accuracy of $\pm 1 \mu m$, frequency range from 0.00001 Hz to 1000 Hz, and temperature range from -150°C to 500°C. It also provides extra features like reversible frame, optional humidity control capability, etc. Taking the fact that there's two kinds of PS, two different kinds of sample dimensions were made: $60 \times 8 \times 1.2$ mm (from the thin plate) and $60 \times 4 \times 4$ mm (from the thick plate). Tests are done, as previously, in symmetric tension-compression in strain controlled mode with a frequency sweep with one sample per temperature. No hold time was imposed between each frequency in a sweep except for the first frequency in order to obtain an homogeneous distribution of the temperature in the sample. The maximum force, of ± 55 N for the thick samples

Figure 3.27: METRAVIB DMA +300
[101]

and ±33 N for the thin samples, was recorded by the DMTA load sensors to get the strain of 0.1%. The order of frequency was the same as was used in ICGM and C2MA i.e., from 0.01 Hz to 10 Hz. The test parameters used are reported in table 3.9.

Parameters	**Values**
Strain amplitude	0.1%
Maximum force	±55 N (thick samples) / ±33 N (thin samples)
Load ratio (R)	-1
Frequency range	$0.01 - 10$ Hz (5 points per decade)
Heating rate	2 K/min
Temperature	40, 50, 60, 70, 75 (thick only), 80, 85 (thick only), 90°C

Table 3.9: Parameters used for tests in FEMTO-ST, Besançon

3.3.4.2 Results and application of TTSP

Completion of all the tests performed in FEMTO-ST on the thick and thin samples provided us a series of data concerning several samples as a new sample was used for each temperature, just like the other tests performed at ICGM and C2MA to avoid the non-reproducibility of results between each temperature. The influence of the frequency on the storage modulus (E') and loss tangent ($\tan\delta$) for the thick and thin samples is shown in the figure 3.28 and 3.29.

Each different color in the figure 3.28 and 3.29 shows different temperature. As in ICGM (Montpellier) on thin samples but not in C2MA (Alès) nor in P' (Poitiers) on thin samples, it was observed that the storage modulus has an unexpected behaviour in the case of the thick samples, i.e., it shows a slight increase and decrease around a temperature of 50 °C whereas the thin samples shows a monotonic behaviour, i.e., decreasing with increasing temperature. This could be due to the difference in the molecular weight of the samples that induces a different behaviour or we suspect that it is due to a temperature gradient in the sample due to a too

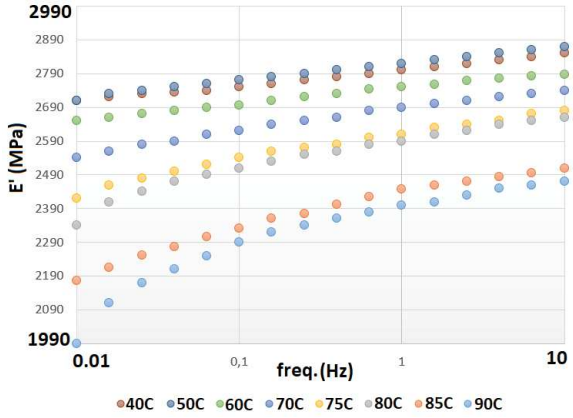

(a) E' vs frequency

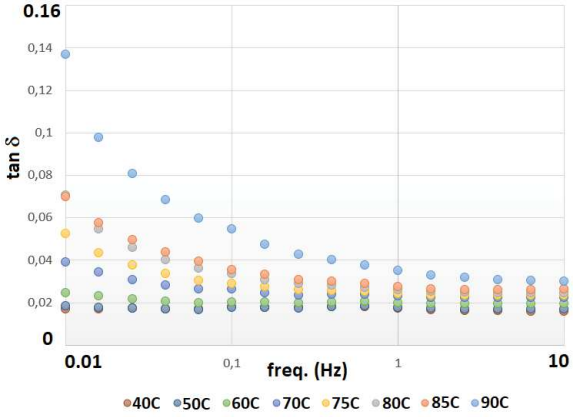

(b) tan δ vs frequency

Figure 3.28: Raw results of DMTA measurements on thick samples of PS obtained at FEMTO-ST, Besançon

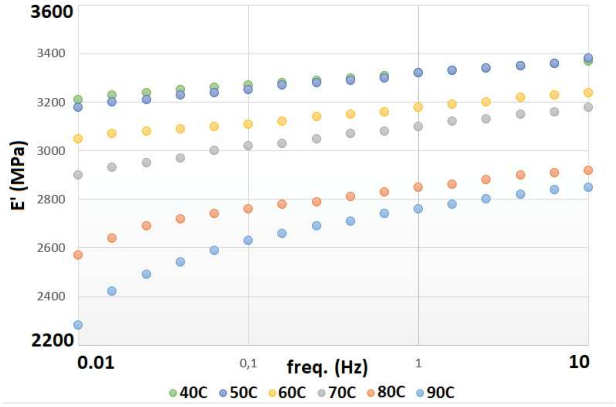

(a) E' vs frequency

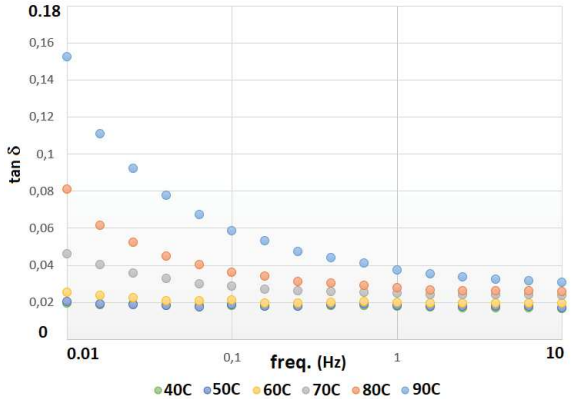

(b) tan δ vs frequency

Figure 3.29: Raw results of DMTA measurements on thin samples of PS obtained at FEMTO-ST, Besançon

short hold time before the starting of the frequency sweep (temperature inhomogeneity).

In continuation to the analysis of experimental results, the TTSP has been applied to the experimental results with the same procedure as the previous ones and yields the master curves reported on figures 3.30 and 3.31. Following the application of horizontal shift, the activation energy was calculated separately for the samples of both thickness using an Arrhenius plot and was found to be $E_a = 335kJ/mol$ for thin samples whereas, $E_a = 284kJ/mol$ for the thick samples. The plot of horizontal shift factor against $1/T - 1/T_0$ can be seen in figure 3.32. Again, this horizontal shift was supplemented by a vertical one in case of the loss tangent to get a smooth master curve (figures 3.33 and 3.34).

The added vertical shift variation with the temperature for both samples (i.e., thick and thin) can be seen in figure 3.35. Here, it was observed that the values of added vertical shifts in thin and thick cases are almost the same and also in accordance with Rouleau et al. [99] as the values of added vertical shift factors are in between 0.5-1. It was also observed that the

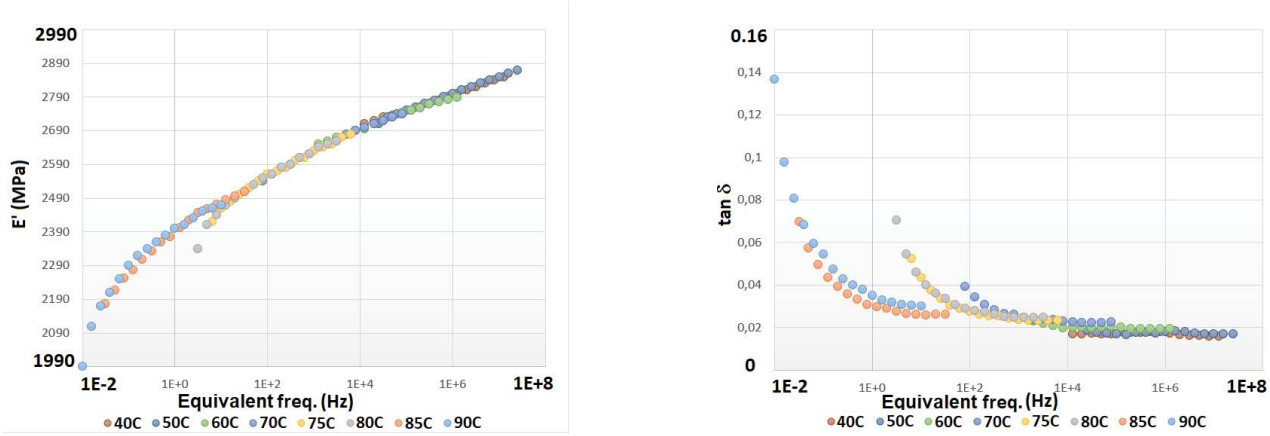

(a) Storage modulus vs frequency

(b) Loss tangent vs frequency

Figure 3.30: Building of the master curves at a reference temperature of 90 °C *for thick samples in FEMTO-ST, Besançon*

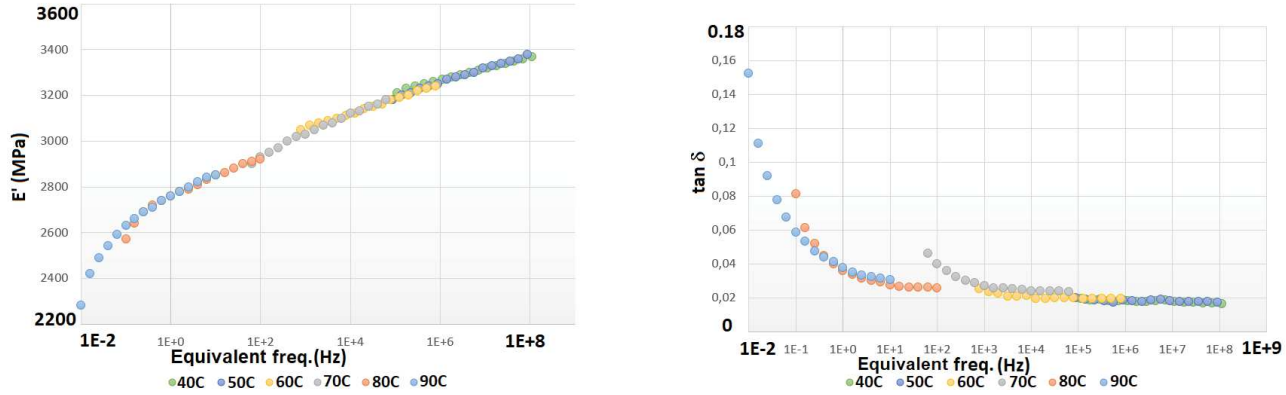

(a) Storage modulus vs frequency

(b) Loss tangent vs frequency

Figure 3.31: Building of the master curves at a reference temperature of 90 °C *for thin samples in FEMTO-ST, Besançon*

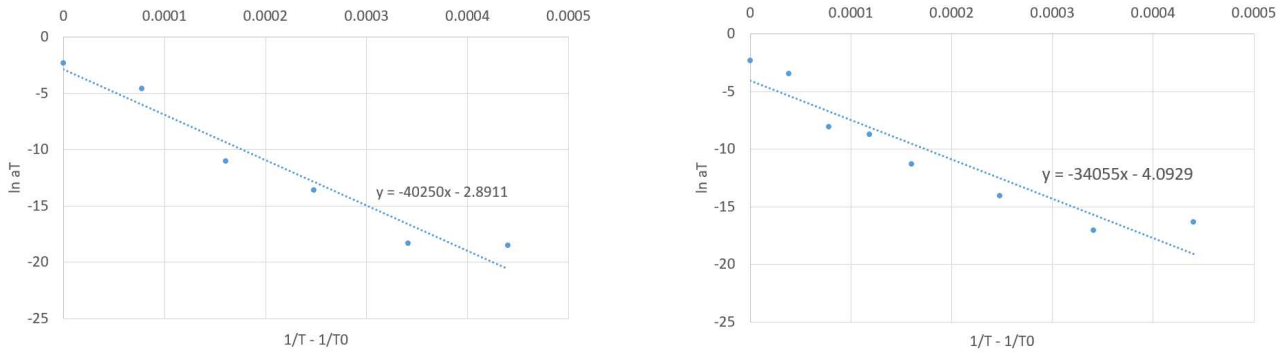

(a) Thin Sample case

(b) Thick sample case

Figure 3.32: Activation energy calculation using Arrhenius law for data from FEMTO-ST, Besançon

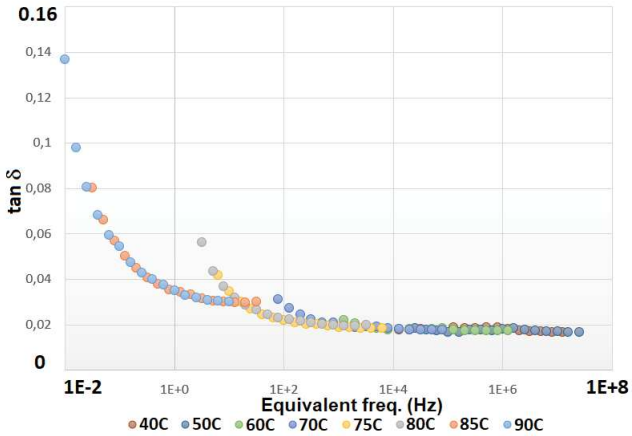

Figure 3.33: Added vertical shift in the case of loss tangent for thick specimens in FEMTO-ST, Besançon

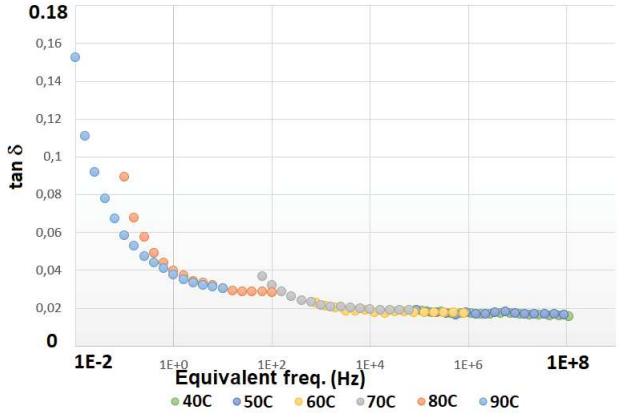

Figure 3.34: Added vertical shift in the case of loss tangent for thin specimens in FEMTO-ST, Besançon

values of b_T used in case of FEMTO-ST are similar to the ones used in case of C2MA but not in case of P' and ICGM.

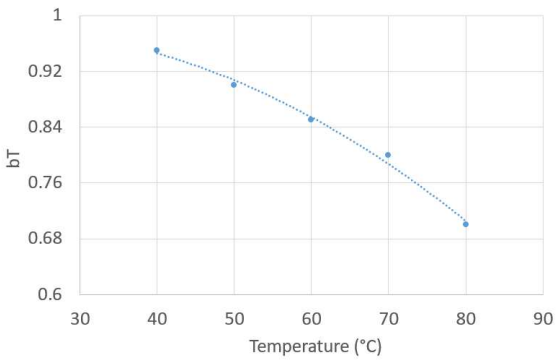

(a) Thin Sample case

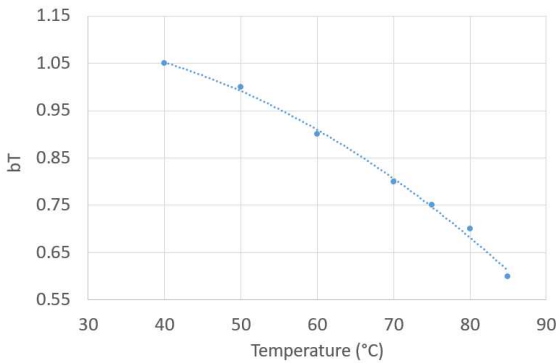

(b) Thick sample case

Figure 3.35: Variation of vertical shift versus temperature for data from FEMTO-ST, Besançon

3.4 Classical DMTA in LMGC, Montpellier and comparisons

After the completion of the first part of the experimental tests in P', ICGM, C2MA and FEMTO-ST, a second part of the experimental tests were performed in LMGC (Montpellier). This part of the tests are performed on a less classical DMTA (BOSE ElectroForce 3200 series III, figure 3.36), which is a more open system as it allows, among other things, to record the raw imposed cyclic load and the response of the sample as well. The recording of the raw signal then allowed us to check if the cyclic load or displacement imposed by the machine is monochromatic and, especially, if the response of the sample is also monochromatic. Moreover, it allows us to control the whole signal processing taking electronic phase shift and machine stiffness (e.g., due to the frame, clamps or load cell stiffness) into account as this will be explained in details in the following section. The comparison with the data obtained in the other laboratories will be used to validate our whole procedure of calibration and correction.

3.4.1 Material and method

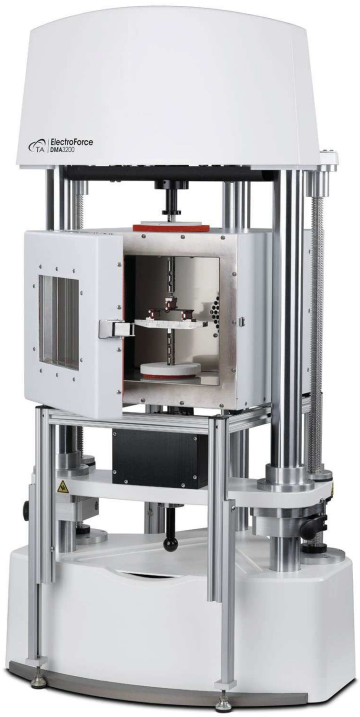

Figure 3.36: BOSE (TA) ElectroForce 3200 Series III
[102]

To compare these experimental results with the previous ones, we used the same amorphous polymer, i.e., polystyrene (PS), coming from the same plates delivered by Goodfellow and ma-

chined to rectangular samples of dimensions 85 × 13 × 4 mm (thick plate) and 80 × 8 × 1.2 mm (thin plate) with, in all cases, an operating length of 60 mm between the clamps.

The Bose-Electroforce 3230 DMTA, controlled by dedicated WinTest 8.0 software, is equipped with a ±450 N (±0.17% maximum error) load cell (Honeywell) and a capacitance-based non-contact displacement transducer (HRDT, Lion Precision) of ±0.5 mm±0.26% maximum error. A home-made stiffener has been designed to increase the lateral stiffness of the mobile upper part of the machine. It is equipped with a hot-cold chamber (Sun corporation), or furnace, of -150 to 315 °C temperature range.

After each sample was mounted and clamps tightened, a quasi-static loading, higher than the maximum load used during the DMTA measurements, was imposed to verify that there will be no slippage of the sample in the clamps during the subsequent loading used for the determination of linear viscoelastic properties. After an automatic adjustement of the feedback control, the WinTest DMTA software is launched and set-up with the parameters reported in table 3.10. The order of frequency was the same as was used in ICGM, C2MA and FEMTO-ST i.e., from 0.01 Hz to 10 Hz. A pre-cycle of 60 seconds is used before the measurement is done at each frequency, followed by a holding time of 20 minutes for the sample temperature homogenization and stabilization. The number of cycles imposed at each frequency was automatically determined by the software to optimise the quantity of data points for subsequent calculations. Viscoelastic properties were first calculated within the integral DMTA software analysis. The software uses Fourier analysis to determine the actual frequency of the test and the phase shift (δ) between ε and σ at this frequency.

Parameters	**Thick Samples**	**Thin Samples**
Strain amplitude	0.1%	
Maximum force	±175 N	±33 N
Load ratio (R)	-1	
Frequency range	0.01-10 Hz (5 points per decade)	
Temperature	40, 50, 60, 70, 75, 80, 85, 90°C	40, 50, 60, 70, 80, 90°C

Table 3.10: Parameters used for tests in LMGC, Montpellier

These results will be used to compare with the results obtained during the first series of measurements on different DMTA in different laboratories.

3.4.2 Electronic phase shift correction

The DMTA electronics, or acquisition chain, has an effect on the phase shift between the imposed (ε) and measured (σ) signals. Therefore, an electronic phase shift correction is done on the raw DMTA results obtained. This electronic phase shift value, δ_{el}, was measured at different frequencies, using a steel sheet whose section area is such that it has a stiffness equivalent to that of PS samples, by considering that there won't be any phase shift due to the material (steel) as of its pure elastic properties.

To accomplish the correction of electronic phase shift, several DMTA measurements were performed on a steel sheet of dimension $85 \times 13 \times 0.1$ mm, with an operating length of 60 mm, at all previously used frequencies in different laboratories and at ambiant temperature (28°C) and 60°C, to be sure that this electronic phase shift doesn't vary much with the temperature. The purpose of using the same operating length as polymer samples but a different cross-section was to stay as close as possible to the stiffness of the polymer samples in order to test the machine under the same conditions of load and displacement. The imposed displacement and measured load signal were recorded to compute the phase angle between these two, using the displacement as a reference, using a MATLAB code. This computed phase shift changes with the frequency is shown in figure 3.37 varying linearly with the frequency.

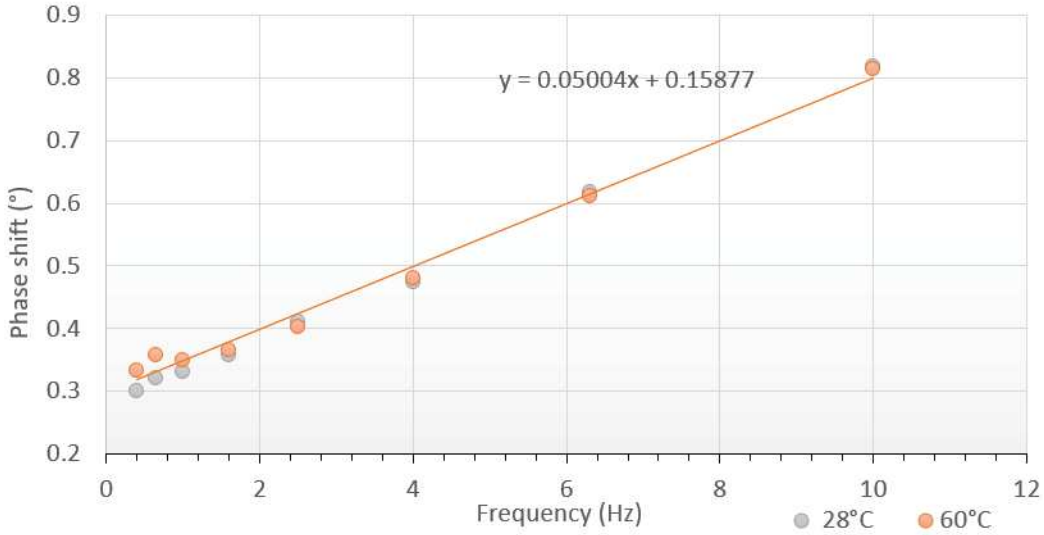

Figure 3.37: Electronic phase shift with frequency

Using a linear regression to the variation of phase angle δ_{el} vs. frequency, we obtained $\delta^{\circ}_{\text{el}} = 0.05004f + 0.15877$ where $\delta^{\circ}_{\text{el}}$ is in degree and f in Hz.

3.4.3 Correction of the effect of the machine stiffness

It was considered that all the components (especially load cell, clamps and extension rods for the hot-cold chamber) of the DMTA machine used induces a non-negligible spurious displacement that induce an important bias in the stiffness of sample, as this latter appears at least softer as illustrated in figures 3.38a and 3.38b. Therefore, the results obtained from the frequency sweep tests at various temperatures were corrected following the demonstration made in the NPL (National Physical Laboratory) report [103].

In the figure 3.38b, the three viscoelastic branches in parallel is a schematization of the rheological behaviour of the sample in 3.38a, whereas the only spring in series with these viscoelastic branches models all the parts of the machine that deform significantly under load and that are assumed to be purely elastic in behaviour (figure 3.38a). Therefore, the apparent measured stiffness of the sample K_m can be written as:

$$\frac{1}{K_m} = \frac{1}{K_1} + \frac{1}{K_2}, \tag{3.8}$$

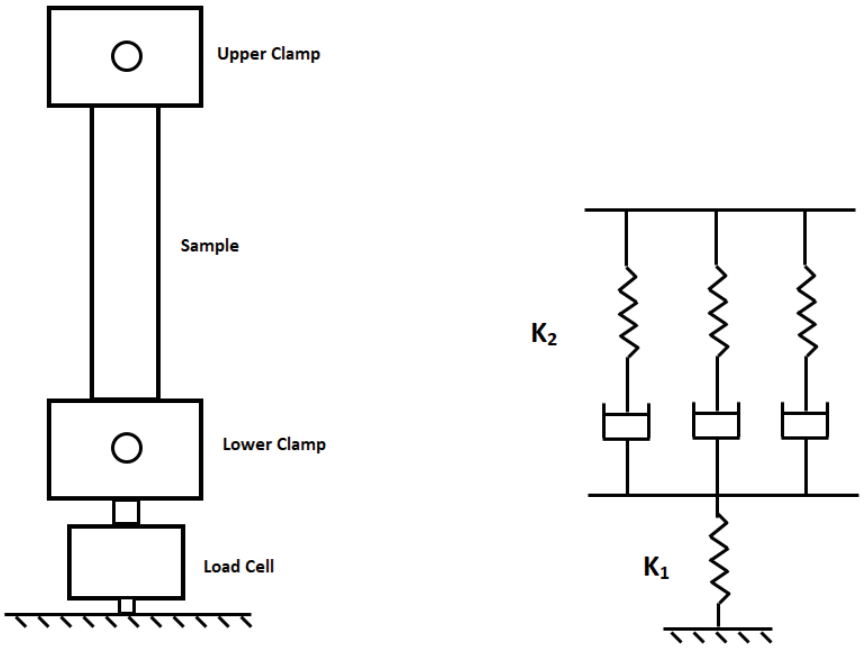

(a) Scheme of the machine and the sample

(b) Rheological modeling of the machine and the sample

Figure 3.38: Illustration of the machine stiffness effect

where K_1 is machine stiffness and K_2 is the sample complex stiffness. Equation 3.8 shows that the stiffness of the machine K_1 must be much larger than K_2 so that its effect on the measured stiffness is negligible, which is not the case in LMGC (i.e., the measured machine stiffness was 3295 N/mm, whereas, the stiffness of a polymer sample is ≈2600 N/mm for E≈3 GPa). Therefore, the effect of stiffness of the machine was corrected by the following procedure.

If the sample stiffness K_2 is replaced by element of infinite stiffness ($K_2 = \infty$), then equation 3.8 can written as:

$$K_m = K_1 = K_\infty, \tag{3.9}$$

where K_∞ refers to the measured stiffness with an infinitely stiff sample and corresponds to the machine stiffness. In our case, the stiffness of the whole setup was determined by measuring the global displacement for different applied load on a stiff sample made of aluminium ($85 \times 7 \times 4$ mm, i.e., $K_2 \approx 37$ kN/mm) as shown in figure 3.39. We deduce a stiffness $K_\infty \approx 3295$ N/mm. As the objective is to extract the sample stiffness from the measured one, one can rewrite Eq. (3.8) as:

$$K_2 = \frac{K_m K_\infty}{K_\infty - K_m}. \tag{3.10}$$

As the material is viscoelastic, its stiffnes is complex, i.e., $K_2 \rightarrow K_2^* = K_2' + iK_2''$. Then $K_m \rightarrow K_m^* = K_m' + iK_m''$ and Eq. 3.10 is rewritten as:

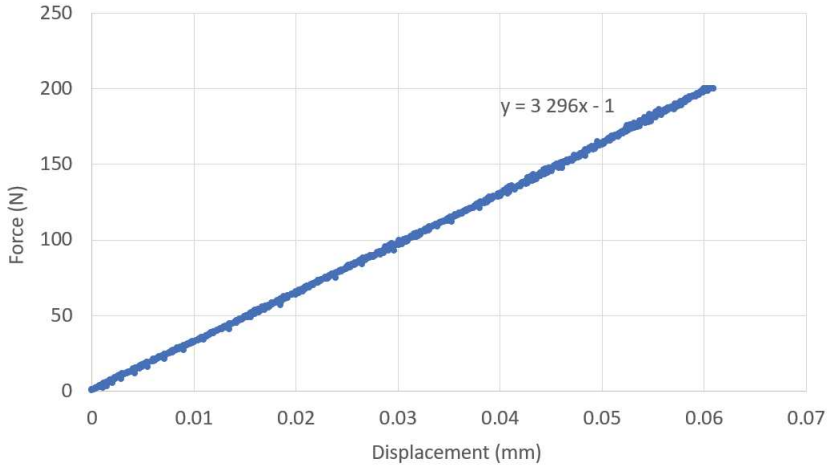

Figure 3.39: Experimentally measured machine stiffness

$$K_2' + iK_2'' = \frac{(K_m' + iK_m'')K_\infty}{K_\infty - K_m' - iK_m''}. \tag{3.11}$$

And thus:

$$K_2' + iK_2'' = \frac{K_\infty\{[K_m'(K_\infty' - K_m') - K_m''^2] + i[K_m''(K_\infty - K_m') + K_m'K_m'']\}}{(K_\infty - K_m')^2 + (K_m'')^2}, \tag{3.12}$$

that leads to identify the real and imaginary parts of the sample stiffness:

$$K_2' = \frac{K_\infty[K_m'(K_\infty - K_m') - K_m''^2]}{(K_\infty - K_m')^2 + K_m''^2} \tag{3.13}$$

$$K_2'' = \frac{K_\infty[K_m''(K_\infty - K_m') + K_m''^2]}{(K_\infty - K_m')^2 + K_m''^2} \tag{3.14}$$

These two equations will be used to correct the measured $E' = K'L/S$, $E'' = K''L/S$ and $\tan\delta = K''/K'$, where L is the operating sample length and S its cross-section area, using the measured machine stiffness K_∞.

3.4.4 Alignment of the clamps

Before starting the DMTA measurements, the alignment of the tension mode clamps has also to be verified and adjusted as it was important to be sure that no torsion or bending of the specimen can occur during the measurements. Therefore, we used four strain gauges (Kyowa Industries, Gauge factor=2, resistance=120 Ω, length=5mm) glued on each kind of polymer sample, two gauges by side, along with a Vishay P3 bridge and amplifier to verify if the strain is (almost) equal for all the four gauges for different applied load in tension or compression.

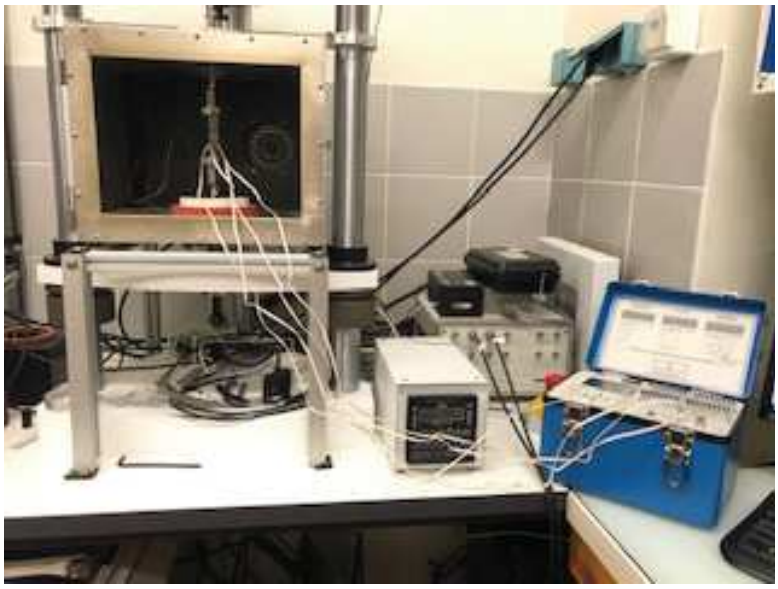

Figure 3.40: Setup for the verification of the alignment

Using the setup shown in figure 3.40, the verification of alignment of tension mode clamps was performed by moving one of the grips back and forth until the strain distribution throughout the sample becomes uniform. The comparison between the strain distribution before and after adjusting the tension mode clamps is shown in figure 3.41.

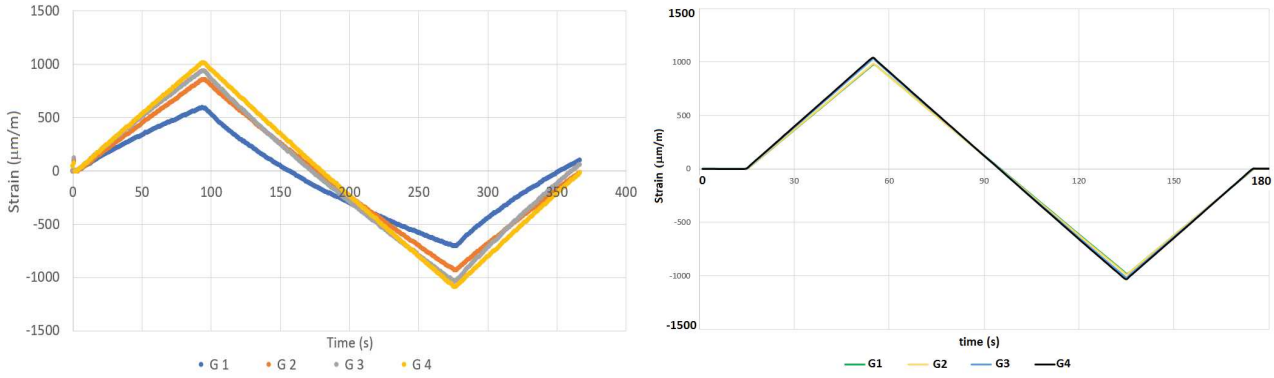

(a) Before (b) After

Figure 3.41: Comparison of the alignment before and after correction with the strain measured by the four strain gauges on PS (thick)

In order to ensure that the alignment performed was good enough to continue the measurements, the stress-strain (mean strain gauges values) data were also plotted to verify their shape followed by the calculation of the Young's modulus. This stress-strain plot is shown in figure 3.42. The alignment of the clamps was again verified in section 3.5 with the help of an infrared camera. In these measurements, a homogeneous field of the amplitude of the thermoelastic coupling over the specimen surface confirmed the good alignment of the clamps.

Following the correction of effect of machine frame stiffness, electronic phase shift and proper alignment of the sample, the verification of monochromatic response of the sample was also per-

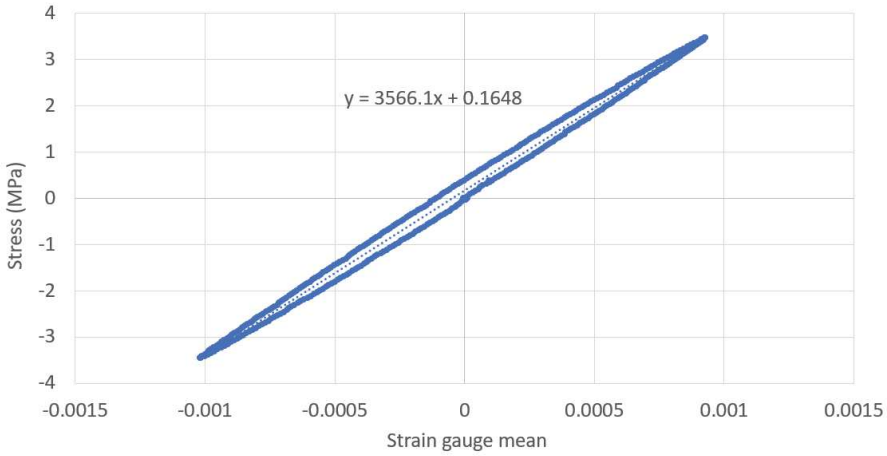

Figure 3.42: Verification of the final alignment of the sample by plotting stress-strain response curve on PS (thick)

formed as detail in the following section.

3.4.5 Verification of the monochromatic response of PS sample

The objective here was twofold. First, we want to check that the applied displacement by the machine is effectively monochromatic and, especially, that the response of the tested polymer is monochromatic too in the linear viscoelastic region as it is the basis for the definition of E' and E'' (Eqs. 3.3 and 3.4). Second, for the synchronized thermal measurements (section 3.5), we need to record the raw output signals of force and displacement from the acquisition box of the DMTA. So we wanted to check that these output signals correspond to the raw ones shown in the machine control software (WinTest) without any change in the frequency or monochromatic nature.

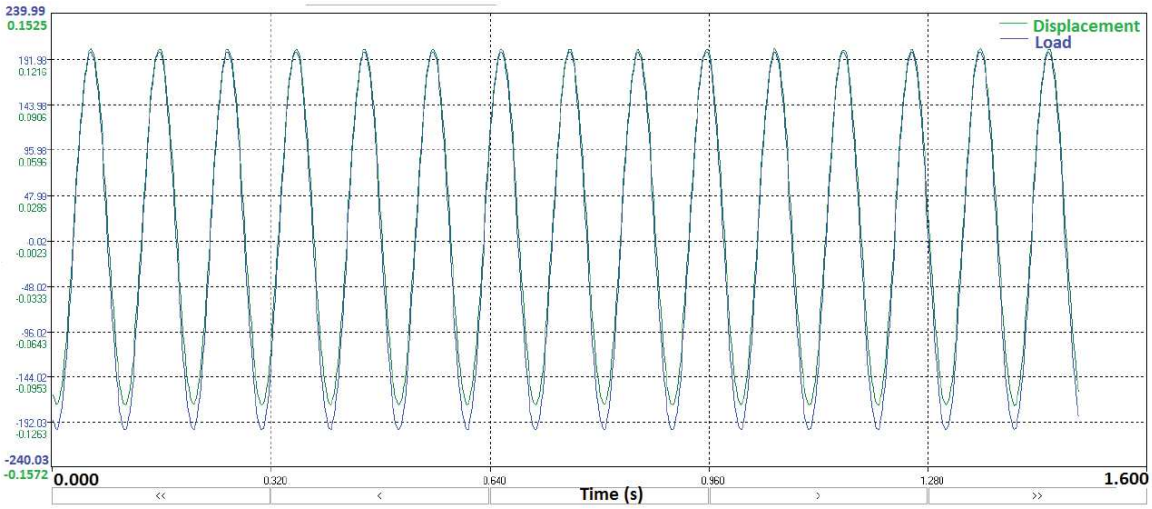

Figure 3.43: Raw force and displacement as a function of time for a PS sample at 1 Hz *(WinTest screenshot)*

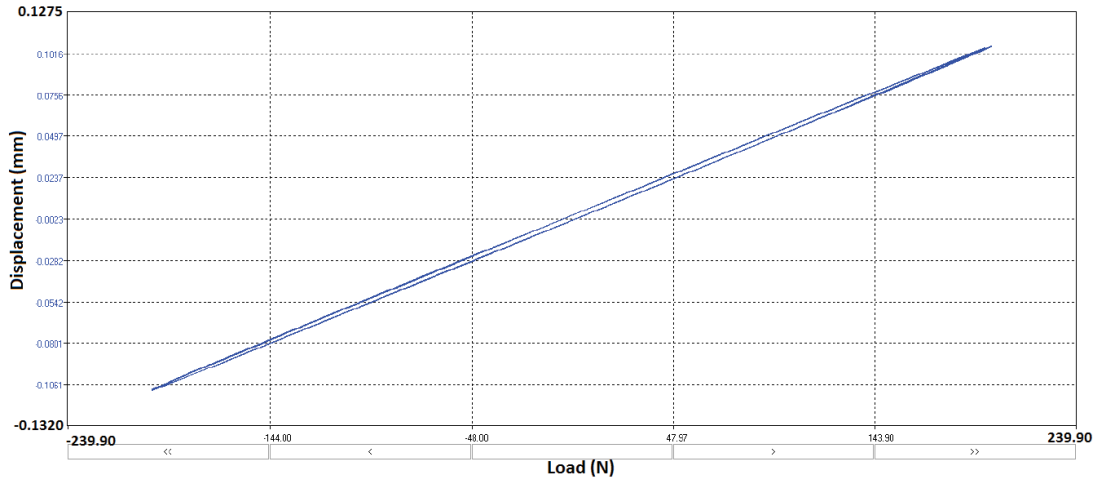

Figure 3.44: Raw displacement as function of the raw resulting force for a PS sample at 1 Hz *(WintTest screenshot)*

Thus, cyclic tests were performed on a PS samples at all the above listed frequencies (see table 3.10). An example of the raw signals of force and displacement, recorded at 1 Hz by the DMTA software, is shown in figure 3.43 together with the raw hysteresis loop which is the result of the phase shift between the displacement and the force (figure 3.44). This series of measurement was then used to study the monochromatic aspect of each signals recorded by the DMTA. In parallel, we have recorded the output raw signals from the acquisition box of the DMTA with an oscilloscope (Picoscope, Pico Technology [104]).

The two pairs of force and displacement signals, one from the WinTest software provided by DMTA and the other corresponding to the raw output signals of the DMTA acquired by the oscilloscope, were analysed using fast-fourier transform (FFT) with MATLAB. Since the number of frequencies used are quite a lot, only the FFT for the signal at 1 Hz is shown in figures 3.45 and 3.46.

It can thus be seen that, for an experimental test at 1 Hz, the raw signals of the WinTest software and the raw output signals are all monochromatic with the fundamental frequency of 1 Hz. It can nevertheless be observed that the peaks of frequencies of the raw signals have a few “imperfections” at their base. This is due to the resolution on frequency and in measured voltage of the oscilloscope. It may also be noted that the amplitude of the signals is also not the same between the two pairs. In fact the values provided by WinTest are directly expressed in force (N) and displacement (mm) whereas the values of the oscilloscope are expressed in volts (V). This allowed us to check the conversion between Volts and Newton or millimeter.

After observation at all frequencies, it was concluded that there was no change in the signal across the WinTest program, the values provided by the DMTA are therefore just as exploitable as the raw values of the output signals. Moreover, the verification of the monochromaticity of the signal imposed by the machine and the response of the polymer allowed us to continue our experimental DMTA measurements on PS to study and compare the viscoelastic response at several temperatures.

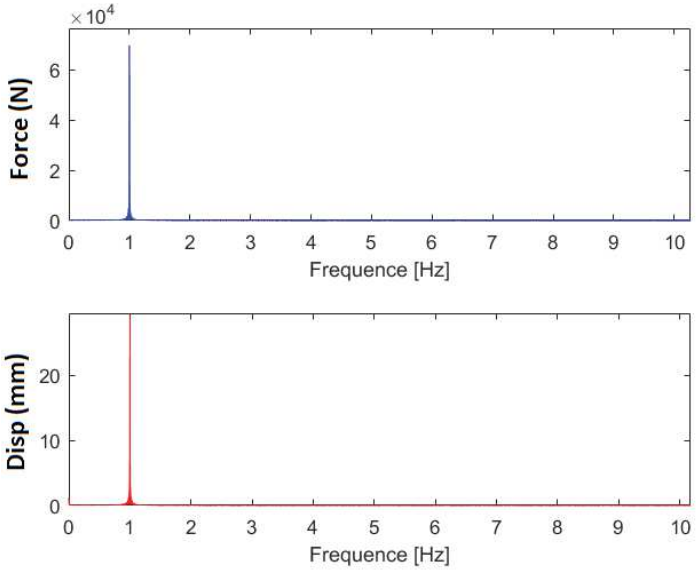

Figure 3.45: FFT of the force and displacement signals acquired from WinTest program

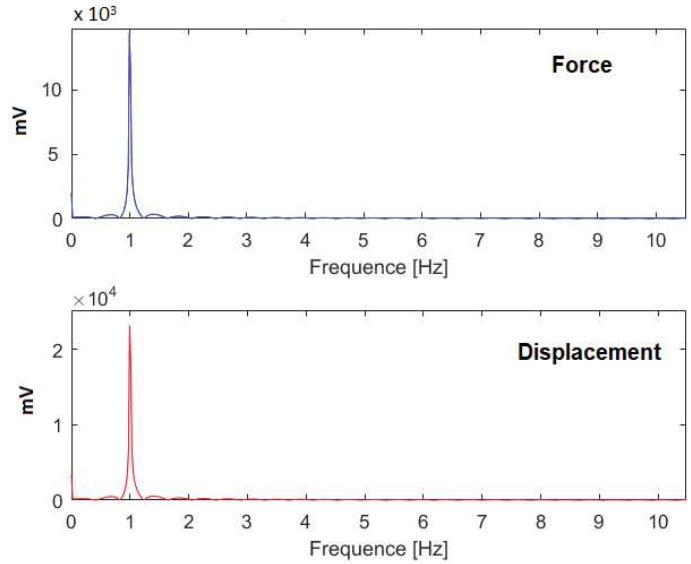

Figure 3.46: FFT of the force and displacement output signals acquired with an oscilloscope

3.4.6 Results and application of TTSP

After the completion of the series of frequency sweeps at various temperatures on PS samples of thickness 1.2 (thin sample) and 4 mm (thick sample), with one sample per temperature, all the procedure detailed above was applied to the raw data. The obtained corrected storage modulus (E') and loss tangent ($\tan\delta$) for both type of samples is shown in the figures 3.47 and 3.48 as a function of the loading frequency (each temperature is shown by different colour in the plots). The unusual behaviour of the storage modulus of the thin samples observed at ICGM (Montpellier) and FEMTO-ST (Besançon) is not observed here, i.e., E' is decreasing with the

increasing temperature in both cases of sample thickness.

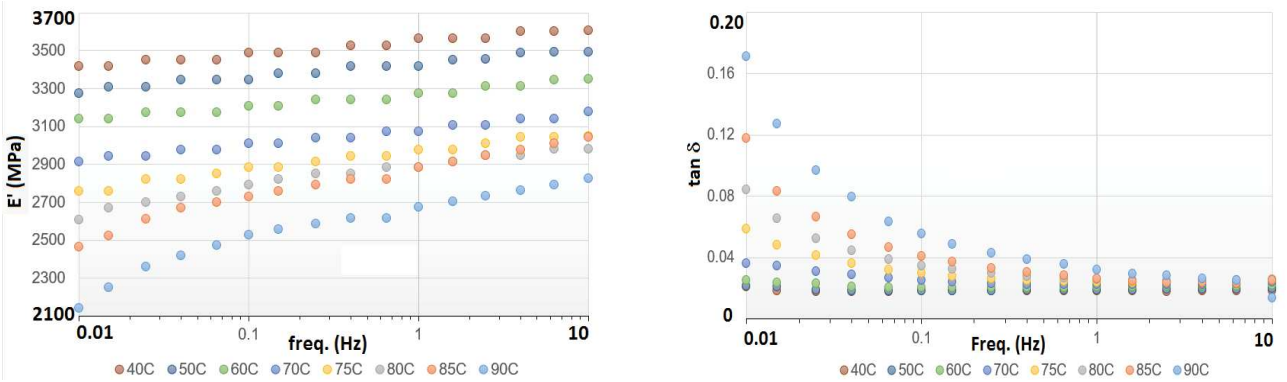

(a) Storage modulus vs frequency

(b) Loss tangent vs frequency

Figure 3.47: Corrected results of DMTA measurements on thick samples of PS obtained at LMGC, Montpellier (thick sample)

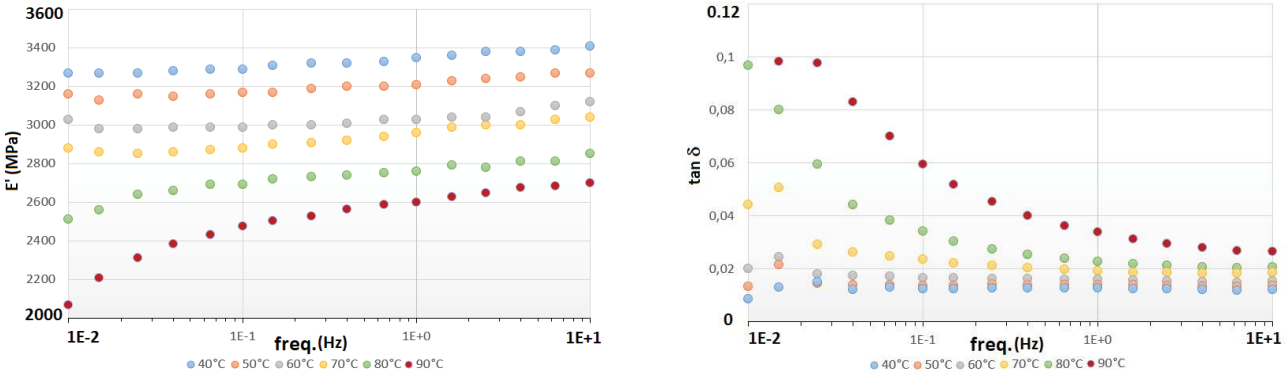

(a) Storage modulus vs frequency

(b) Loss tangent vs frequency

Figure 3.48: Corrected results of DMTA measurements on thin samples of PS obtained at LMGC, Montpellier (thin sample)

In continuation to the analysis of experimental results, the TTSP has been applied to the experimental results with the same procedure as the previous results obtained in the other laboratories, always with a reference temperature of 90 °C, and yields the master curves reported on figures 3.49 and 3.50. Following the application of horizontal shift, the activation energy was calculated like in previous cases, for samples of both thicknesses using an Arrhenius plot and was found to be $E_a = 434kJ/mol$ for thin samples and $E_a = 392kJ/mol$ for thick samples. The plot of horizontal shift factor against $1/T - 1/T_0$ can be seen in figure 3.51. Again, the horizontal shift has been completed by a vertical one in the case of the loss tangent to get a smooth master curve (figures 3.52 and 3.53). The added vertical shift variation with the temperature for both samples (i.e., thick and thin) can be seen in figure 3.54.

As already mentioned, it seems that the results would be better with a different horizontal shift, i.e., different activation energy, for the loss tangent compared to E' as discussed in [99], but it raises questions about the physical meaning or applicability of the TTSP.

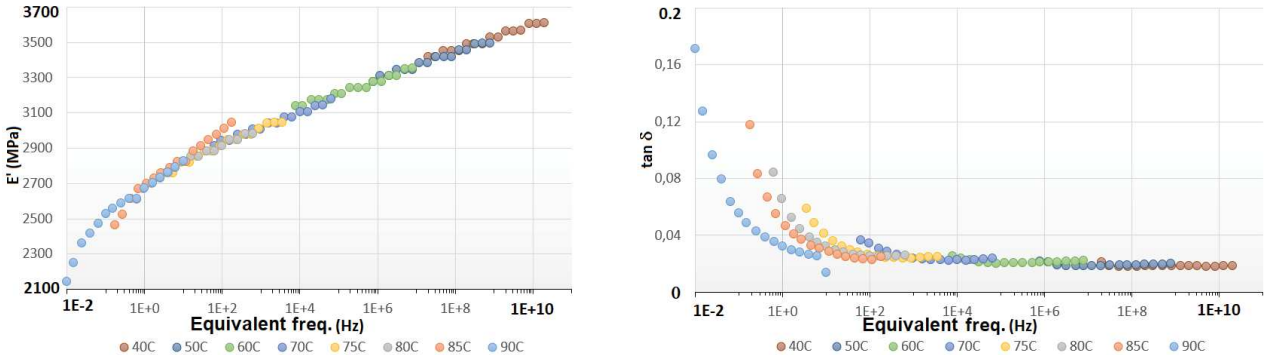

(a) Storage modulus vs frequency (b) Loss tangent vs frequency

Figure 3.49: Building of the master curves at a reference temperature of 90 °C *for thick samples in LMGC, Montpellier*

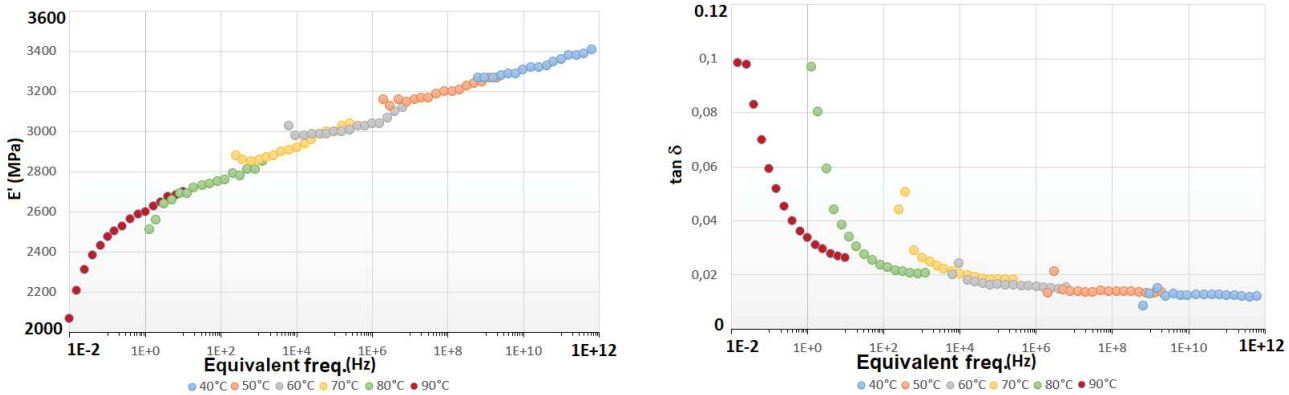

(a) Storage modulus vs frequency (b) Loss tangent vs frequency

Figure 3.50: Building of the master curves at a reference temperature of 90 °C *for thin samples in LMGC, Montpellier*

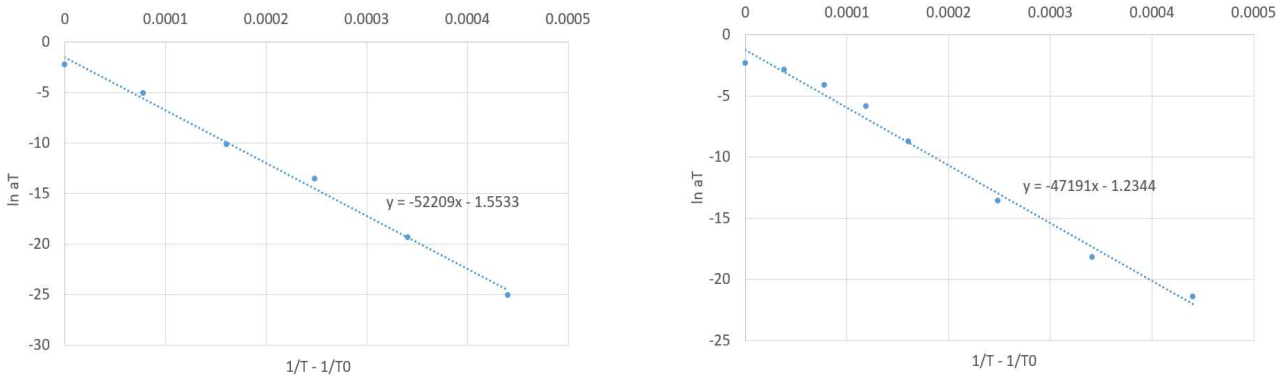

(a) Thin Sample case (b) Thick sample case

Figure 3.51: Activation energy calculation using Arrhenius law for data from LMGC, Montpellier

Again, it was observed that the values of vertical shift added for both the samples were between 0.5-1 as in the case of C2MA and FEMTO-ST. It was also observed that the trend of

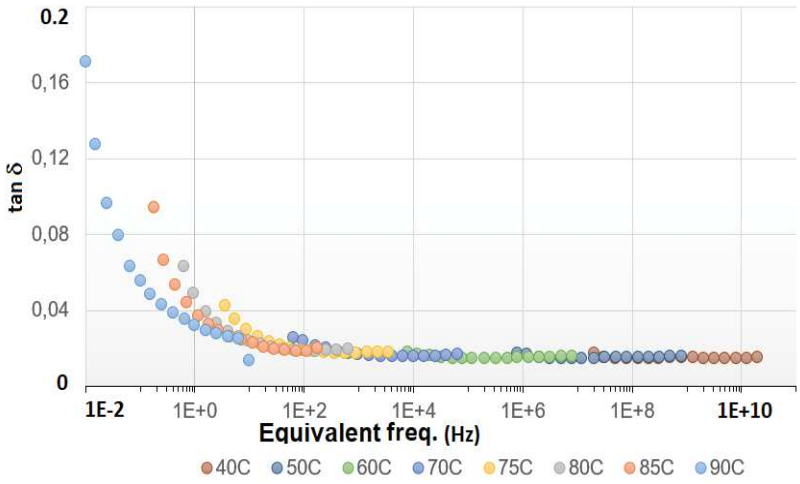

Figure 3.52: Added vertical shift in the case of loss tangent for thick specimens in LMGC, Montpellier

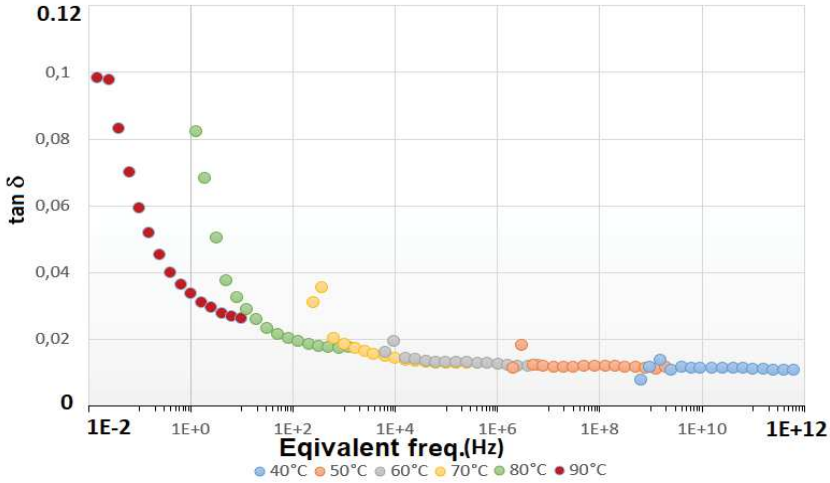

Figure 3.53: Added vertical shift in the case of loss tangent for thin specimens in LMGC, Montpellier

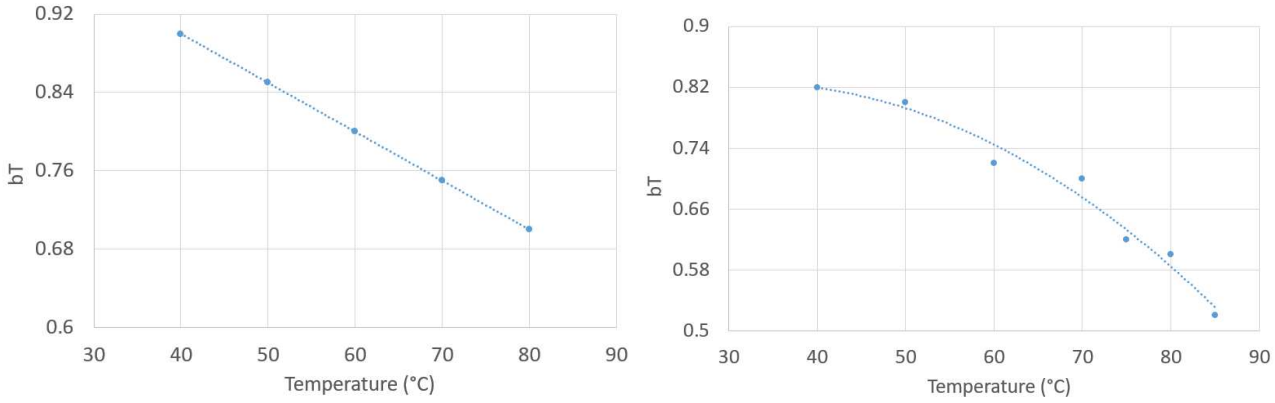

(a) Thin sample case

(b) Thick sample case

Figure 3.54: Variation of vertical shift versus temperature for data from LMGC, Montpellier

added vertical shifts in case of LMGC was similar to the trend observed in the case of C2MA and FEMTO-ST i.e., the value of vertical shift was decreasing with the increasing temperature.

3.4.7 Comparison of the results on PS between all laboratories

The comparison of the computed activation energies from the Arrhenius law for all the measurements performed in different laboratories is shown separately in table 3.11. The overall horizontal shift factors (a_T) used for computation of activation energies are compared in figure 3.55. The comparison of variation of added vertical shift with temperature is also shown in figure 3.56 for all the measurements performed in different labs. The analysis of all the results, obtained from the series of frequency sweeps at different temperature in different laboratories, will be done by considering the difference in the molecular weight between the samples coming from a thin plate (thickness of 1.2 mm) and those coming from a thick plate (thickness of 4 mm). So the comparison will be made between samples coming from the same plate, i.e., having the same molecular weight. Therefore the comparison of the master curves for samples with a thickness of 1.2 mm is shown in figures 3.57 and 3.58.

Laboratory	Activation Energy, E_a (kJ/mol)	
	Thick samples	Thin samples
P'	-	313
ICGM	-	457
C2MA	-	397
FEMTO-ST	284	335
LMGC	392	434

Table 3.11: Activation energy comparison

The comparison of activation energy for the measurements from different labs was performed. It was observed that the computed activation energy was scattered i.e., different in each case. For thin samples, the computed E_a, in case of P', and FEMTO-ST was found to be similar whereas, in case of ICGM, C2MA and LMGC, it was found to be similar. For thick samples, the E_a was again found to be different. An interesting observation was observed in case of LMGC and FEMTO-ST i.e., the E_a for both type of samples are of same order of magnitude.

The comparison of horizontal shift factor used for thin and thick cases was made. It was observed that the evolution of a_T in case of thin specimen is following the same pattern with almost same values except in case of ICGM. Similarly, in case of thick specimen, the pattern and the values of a_T are almost the same. Following the comparison of horizontal shift (a_T), the comparison of variation of added vertical shift (b_T) with temperature, to get the master curve in case of loss tangent was made. It was observed that the vertical shift, in case of P' and ICGM was increasing with the increasing temperature. Whereas, in all the other cases, the vertical shift (b_T) was decreasing with temperature. Despite being the different evolution of b_T, the values of b_T used were always between 0.5-1.

The evolution of the storage modulus (E') and loss tangent ($\tan\delta$) is the same with frequency and temperature in all the five cases (P', FEMTO-ST, C2MA, LMGC and ICGM) for thin samples. During the DMTA measurements in ICGM, a problem of stiffness correction

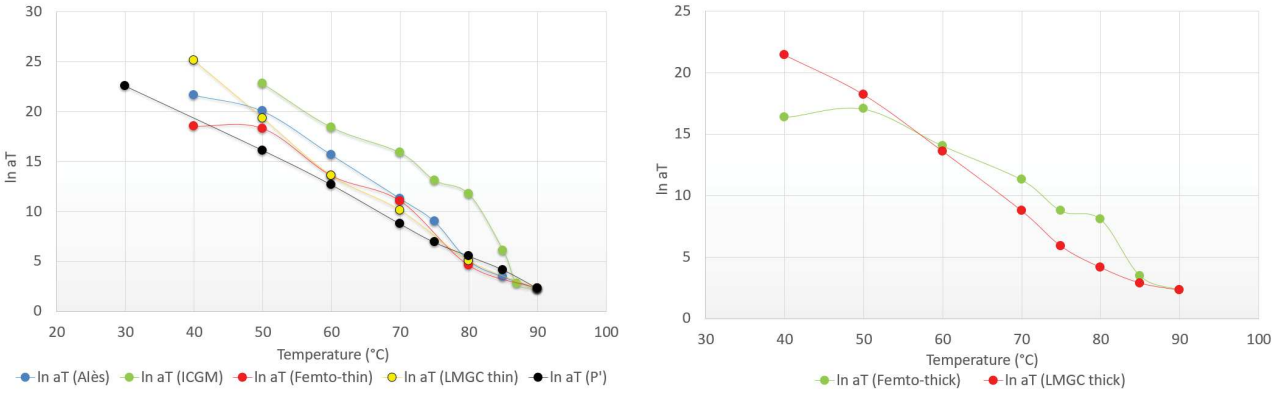

(a) Thin sample case (b) Thick sample case

Figure 3.55: Comparison of variation of horizontal shift versus temperature for data from different laboratories

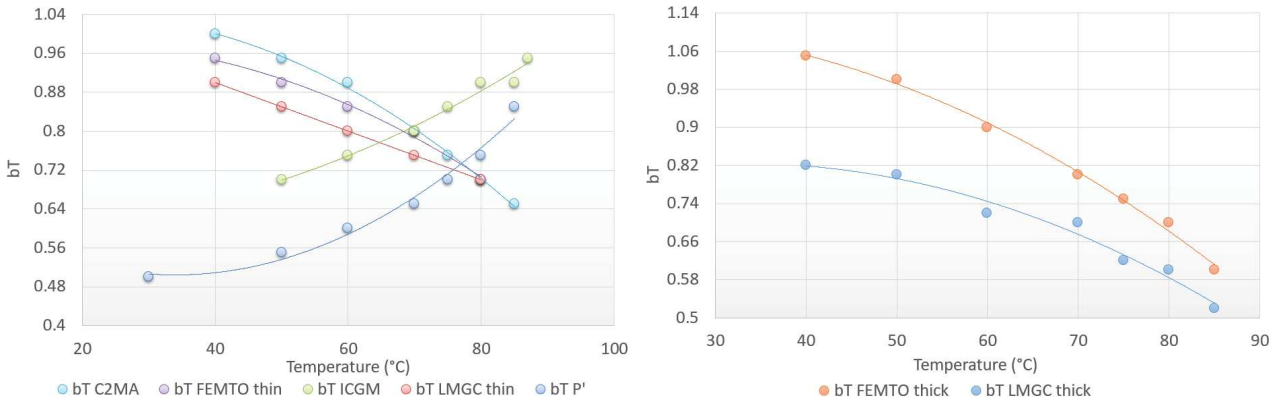

(a) Thin sample case (b) Thick sample case

Figure 3.56: Comparison of variation of vertical shift versus temperature for data from different laboratories

and calibration was observed. It was assumed that a too stiff sample, compared to the machine capabilities, was tested in tension mode. It was also assumed that the sample was not slender enough to perform a good tension mode measurement. For P', only one sample was used for all the measurements, i.e., for all the temperatures and frequencies (combined sweep), whereas, in other cases, one sample per temperature was used. It was observed that, in P', the magnitude of E' is the highest but tests were performed in 3-point bending mode unlike other laboratories. It was assumed that this highest magnitude of E' could be due to surface artifacts as, in bending tests, the maximum tensile stresses are on the top surfaces. Accordingly, for similar sized test specimens, the tensile mode tests sees the maximum stresses throughout its entire gauge length i.e., over a much larger volume than the bending specimen. For rest of the measurements in C2MA, FEMTO-ST and LMGC, the results are quite comparable in terms of E' and it was assumed that the difference could come from the machine stiffness compared to the sample stiffness. As the stiffness of the machine has less effect on loss tangent of the material, it can be seen that the results in terms of loss tangent are more comparable than in the case of storage modulus.

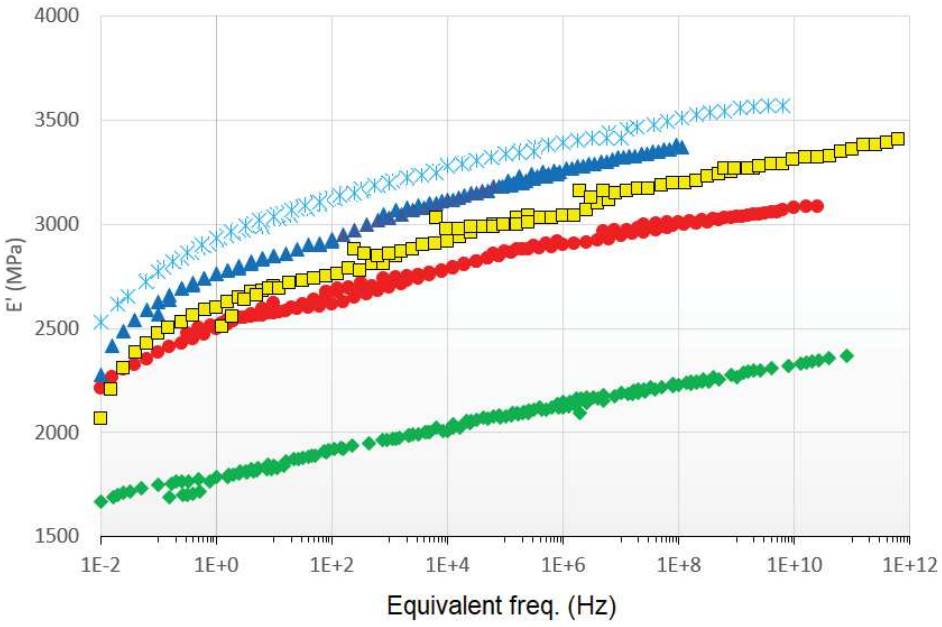

Figure 3.57: Comparison of the Storage modulus of samples with thickness of 1.2*mm*, *where* $*$ *shows P', □ shows LMGC, △ shows FEMTO-ST, ◯ shows C2MA and ⋄ shows ICGM.*

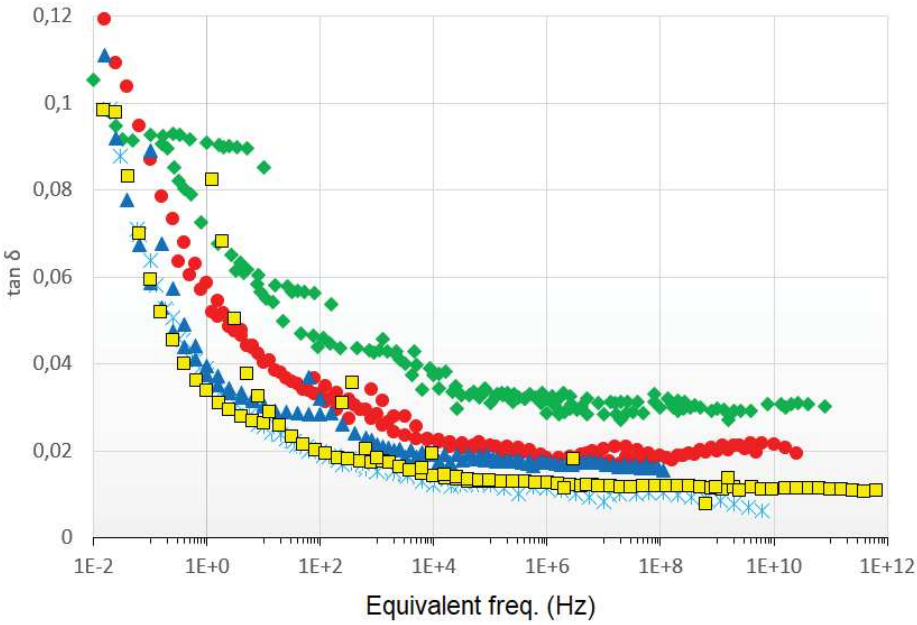

Figure 3.58: Comparison of the loss tangent of samples with thickness of 1.2*mm*, *where* $*$ *shows P', □ shows LMGC, △ shows FEMTO-ST, ◯ shows C2MA and ⋄ shows ICGM.*

The Young's modulus of a thin samples was also measured using a quasi-static testing machine, with a speed of 0.01 MPa/s, along with the use of an extensometer in C2MA (Alès). This allows us to to check the magnitude of the storage or complex modulus (as $\tan\delta$ is small) that we have obtained from the different laboratories. The plot of stress vs strain of this measurement on a thin sample in C2MA (Alès) is shown in figure 3.59 where we obtained a Young's modulus of ≈ 3.4 GPa. It is observed that the magnitude of the storage modulus in all the case, except for ICGM and to a lesser extent P', is more comparable to the Young's modulus

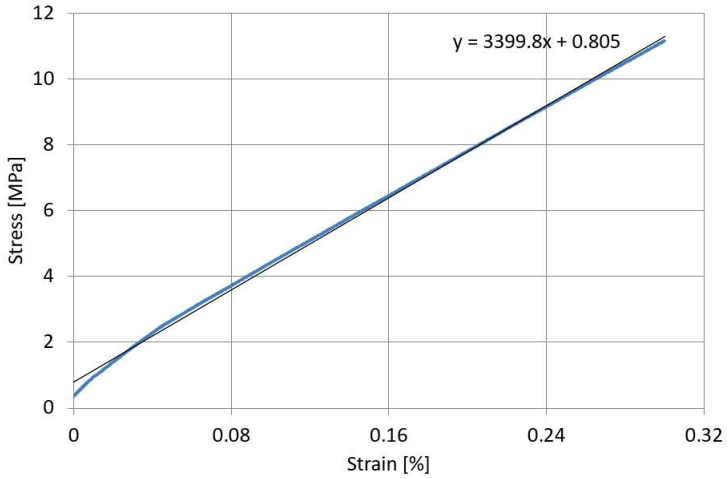

Figure 3.59: Stress-strain plot for thin sample measured in C2MA (Alès) using a quasi-static testing machine with an extensometer

found using quasi-static measurement. Following the comparison of the results obtained for thin samples, the comparison of the master curves for samples with a thickness of 4 mm is shown in figures 3.60 and 3.61.

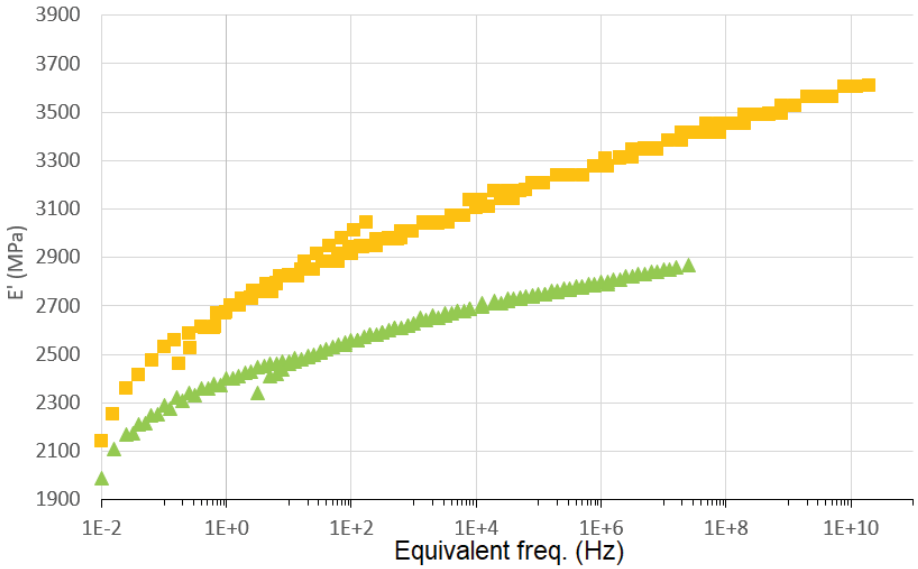

Figure 3.60: Comparison of the Storage modulus of samples with thickness of 4mm, where △ shows $FEMTO-ST$ and □ shows LMGC.

Again, a difference in the order of magnitude of the storage modulus between both measurements is observed and is more pronounced than in the case of the thin samples. This pronounced difference in magnitude of storage modulus could be associated with the stiffness of the machine compared to the stiffness of the sample. In FEMTO-ST, it was observed that the sample stiffness was close to the machine stiffness, considering a chart provided by the manufacturer (METRAVIB), but, to our better knowledge, no machine stiffness correction is done. Using Eq. (3.10), one can see that no correction of the machine stiffness induces an apparent lower sample stiffness. This could explain the fact that FEMTO-ST modulus is lower

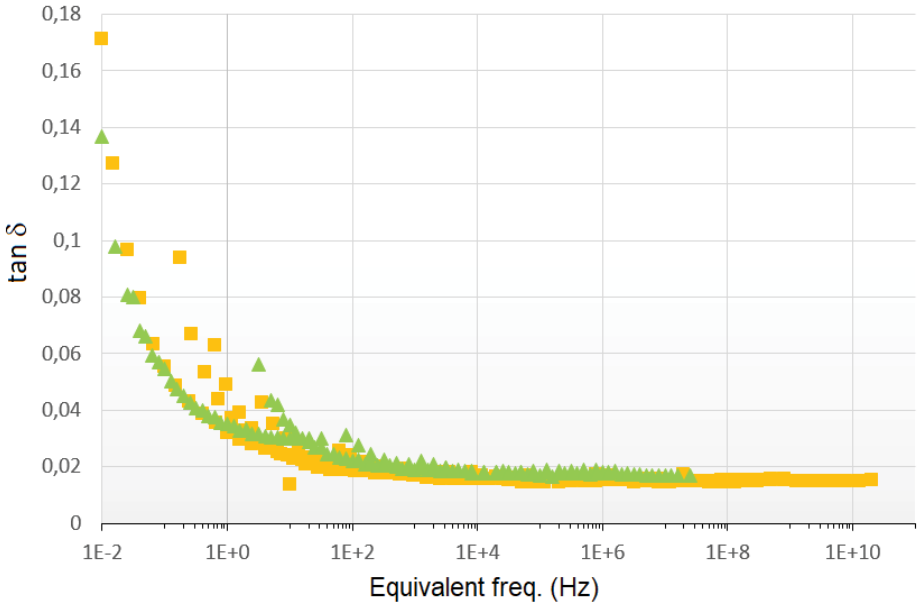

Figure 3.61: Comparison of the loss tangent of samples with thickness of 4mm, where △ shows FEMTO − ST and □ shows LMGC.

Figure 3.62: Experimental setup in FEMTO-ST (Besançon) for the quasi-static measurement of the Young's modulus

than the one measured in LMGC.

In contrast, $\tan\delta$ values are very much comparable in case of thick samples as the stiffness has less effect on this parameter. Finally, the Young's modulus of a thick sample was also measured using quasi-static tests and an extensometer at FEMTO-ST, in order to verify the magnitude of storage modulus that we have obtained from the two laboratories. The machine and the setup used for this quasi-static test are shown in figure 3.62 followed by the plot of

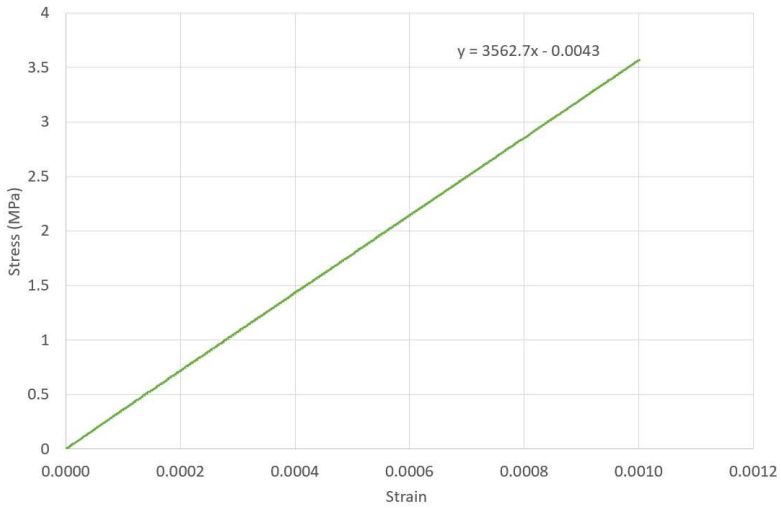

Figure 3.63: Stress-strain plot for thick sample measured in FEMTO-ST (Besançon) using a quasi-static testing machine with an extensometer

stress vs strain in figure 3.63. The value of Young's modulus obtained from this quasi-static measurement was around 3.6 GPa. This value was found to be consistent with the magnitude of the storage modulus obtained through DMTA measurements in LMGC and with the measured Young's modulus obtained with the strain gauges in figure 3.41. This consistency has once again validated our whole procedure of calibration and correction of our machine and setup.

3.4.8 DMTA measurements on PMMA and PA-6.6

Complementary DMTA measurements were performed on PMMA and PA-6.6 to characterize their viscoelastic properties using only the DMTA machine in LMGC, Montpellier. They were followed by the same procedure that was adopted for PS, i.e., the results obtained were later corrected by taking into account the machine stiffness and electronic phase shift.

3.4.8.1 Material and method

The samples of both polymers were machined in a linear rectangular shape. To ensure that the alignment of the clamps remains good, PA-6.6 were machined with the same dimensions, especially the same thickness, as the PS ones, i.e., 85 x 13 x 4 mm. In the cases of the samples of PMMA, they have the same width and length but a different thickness, as sheets purchased from Goodfellow were 5 mm thick. Thus a specific sample of PMMA, with strain gauges, was made for the clamps alignment. The parameters used for the measurements performed on PA-6.6 and PMMA are reported in table 3.12. The order of frequency used in case of PA-6.6 and PMMA was kept the same as was used in earlier cases of LMGC to keep the entire order of frequency in the same way.

The linear viscoelastic region was assumed to be the same as for PS, i.e., until 0.1% strain. All the other parameters used for the measurements on PA-6.6 and PMMA were exactly the same as for PS, except for the temperature range that is adjusted to T_g (Tab. 3.3). The temperature range used for PA-6.6 was from 35 to 60°C with an interval of 5°C. For the same reason, the temperature range used for PMMA was 40-80°C. During these DMTA measurements of

Parameters	PA-6.6	PMMA
Strain amplitude	0.1%	
Load ratio (R)	-1	
Frequency range	0.01-10 Hz (5 points per decade)	
Temperature	35, 40, 45, 50, 55, 60°C	40, 50, 60, 70, 75, 80°C

Table 3.12: Parameters used for DMTA measurements on PA-6.6 and PMMA

PA-6.6, the relative humidity of the sample was not controlled, knowing the fact that they are highly sensitive to this parameter unlike PS and PMMA.

3.4.8.2 Results and application of TTSP

Following the completion of the series of frequency sweeps at various temperatures, with one sample per temperature, corrections were performed on the results as was performed on PS and are shown separately in figures 3.64 and 3.65 for PA-6.6 and PMMA in terms of E' and loss tangent against frequency.

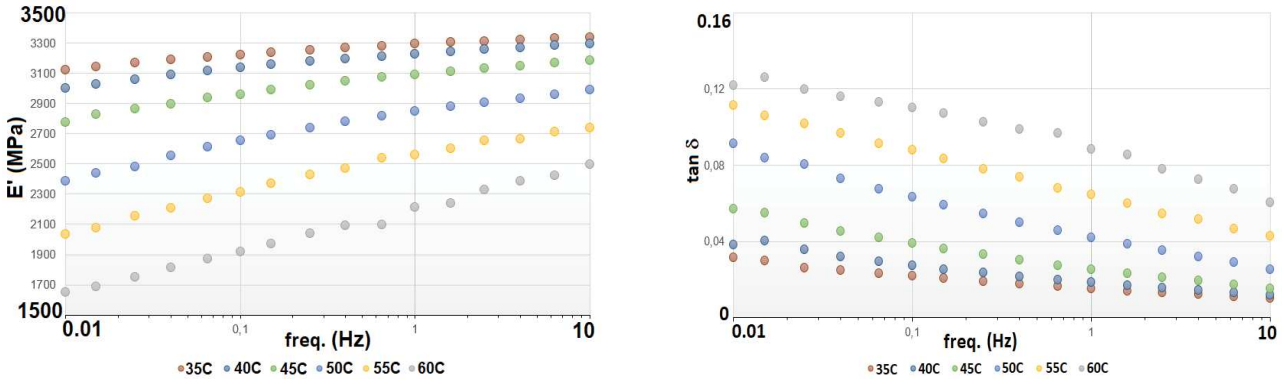

(a) Storage modulus vs frequency

(b) Loss tangent vs frequency

Figure 3.64: Corrected results of DMTA measurements on PA-6.6

The evolution of viscoelastic properties of PA-6.6 is similar to PS, i.e., the evolution of E' is increasing with the frequency and decreasing with the temperature whereas $\tan\delta$ has an opposite behaviour. This is in accordance with the results obtained by Arif [105]. On the other hand, a complex evolution of PMMA was observed in the case of the loss tangent, i.e., decreasing until 0.4 Hz and then increasing. This β damping peak was observed by Roderic and Julie [31] at 10 Hz and reference temperature of 23 °C.

In continuation to the experimental results analysis, the TTSP has been applied to the DMTA results. The horizontal shift was applied to the results as previously for PS. Therefore, shifting of the curves is done manually by considering 60°C as the reference temperature in the case of PA-6.6 and 80°C in the case of PMMA. This procedure requires that the horizontal shifts for E' and $\tan\delta$ are the same and, as previously, shift factors are determined on the basis of E' smooth master curve and then applied to $\tan\delta$. The results after applying horizontal shifts

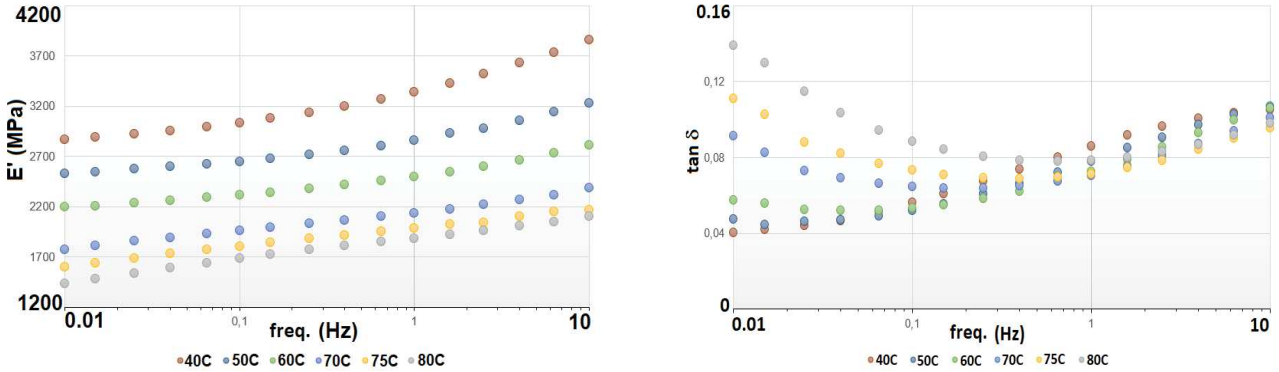

(a) Storage modulus vs frequency (b) Loss tangent vs frequency

Figure 3.65: Corrected results of DMTA measurements on PMMA

are shown in figures 3.66 and 3.67. Following the application of horizontal shift, the activation energy was calculated separately like in previous cases, for the samples of PA-6.6 and PMMA using Arrhenius law and was found $E_a = 574kJ/mol$ for PA-6.6 samples and $E_a = 309kJ/mol$ for PMMA samples. The plot of horizontal shift factor against $1/T - 1/T_0$ can be seen in figure 3.68.

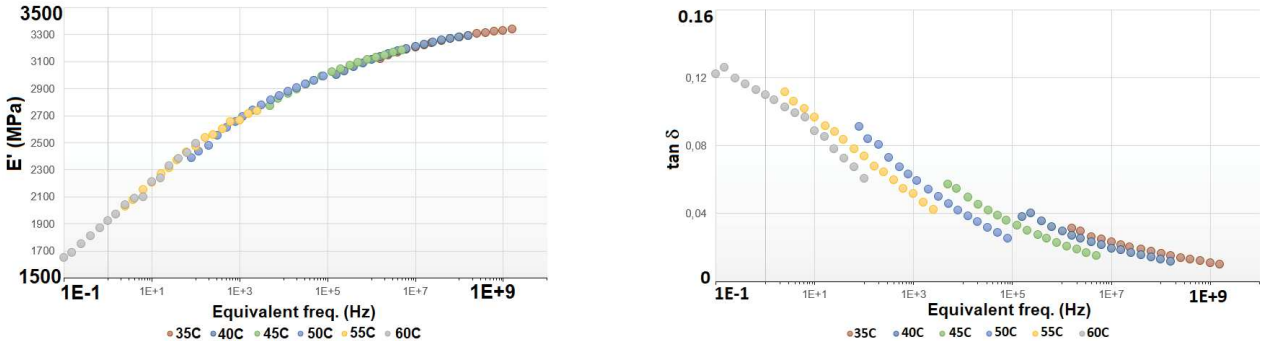

(a) Storage modulus vs frequency (b) Loss tangent vs frequency

Figure 3.66: Building of the master curves at a reference temperature of 60° C for PA-6.6

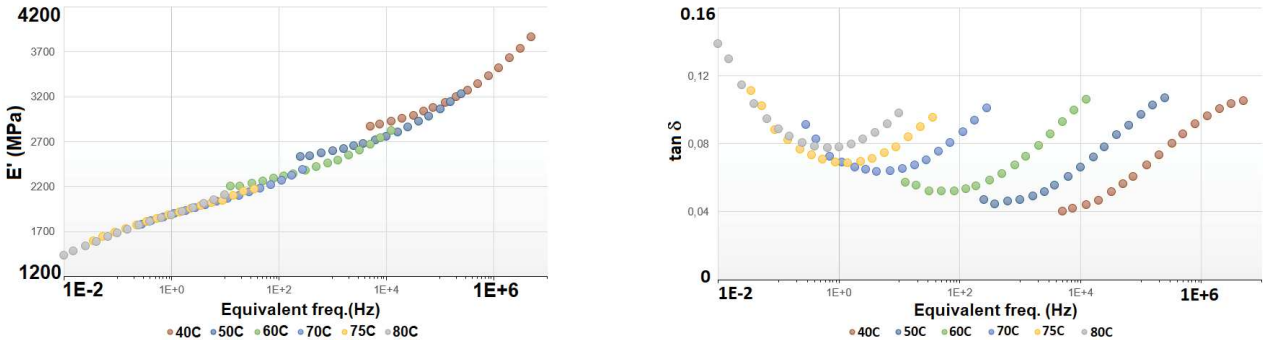

(a) Storage modulus vs frequency (b) Loss tangent vs frequency

Figure 3.67: Building of the master curves at a reference temperature of 80° C for PMMA

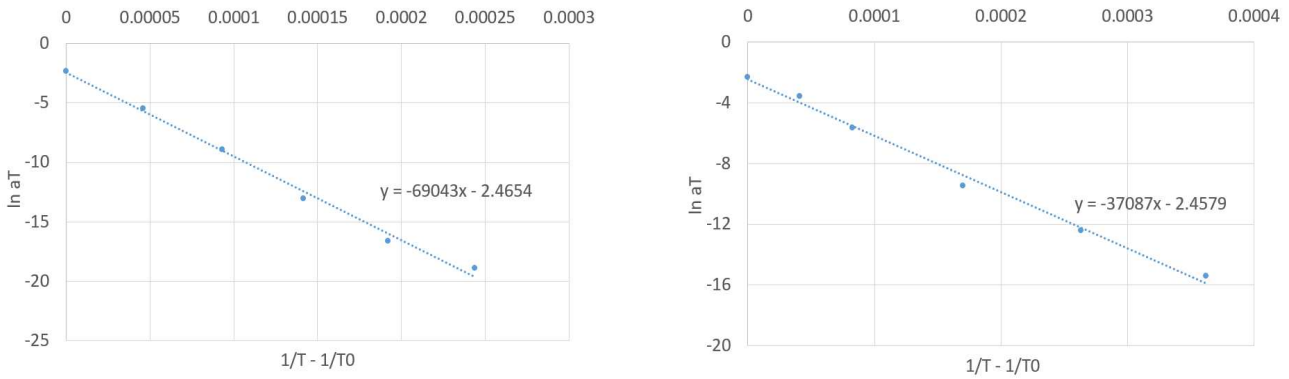

(a) PA-6.6 (b) PMMA

Figure 3.68: Activation energy calculation using Arrhenius law for PA-6.6 and PMMA

Later, the horizontal shift was completed by a vertical shift only in the case of the loss tangent ($\tan\delta$) to get a smoothed master curve (figures 3.69 and 3.70). The master curve in case of loss tangent for PMMA seems to go towards a β transition around 10 Hz and reference temperature of 80 °C. This vertical shift can be related to the effect of dilation of the amorphous polymers. The added vertical shift variation with the temperature for both samples (i.e., PA6.6 and PMMA) can be seen in figure 3.71.

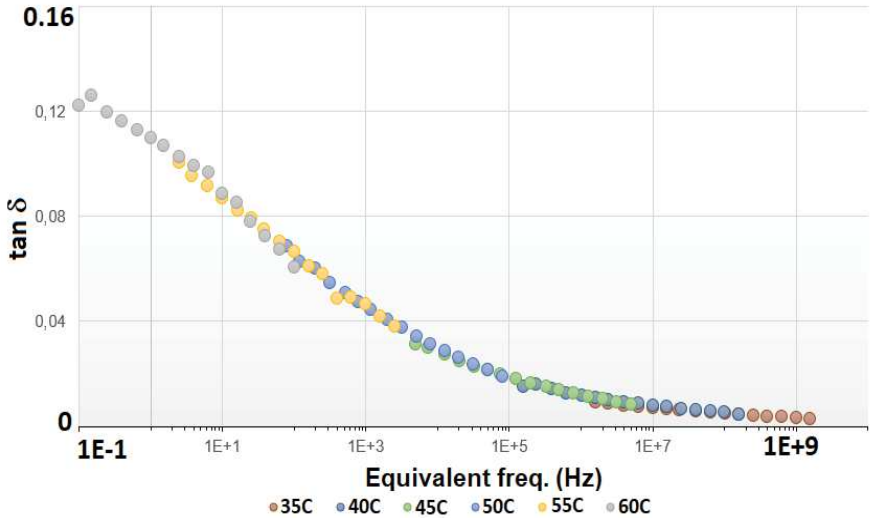

Figure 3.69: Added vertical shift in the case of loss tangent for PA-6.6

It was observed in figure 3.71, that the added vertical shift is increasing with the temperature in case of PA-6.6 and the values are quite small i.e., in between 0.2-1. This trend was found in accordance with PS (P' and ICGM). Whereas, in case of PMMA, the variation of b_T was found to be different i.e., it is keep on increasing with the increasing temperature and the values are quite high i.e., in between 1-7.

Following the analysis of the DMTA results on PMMA, the comparison of master curve in terms of E' was done with literature [4] to verify the performed analysis by application of TTSP. This comparison was performed to verify the trend observed in our case as magnitude

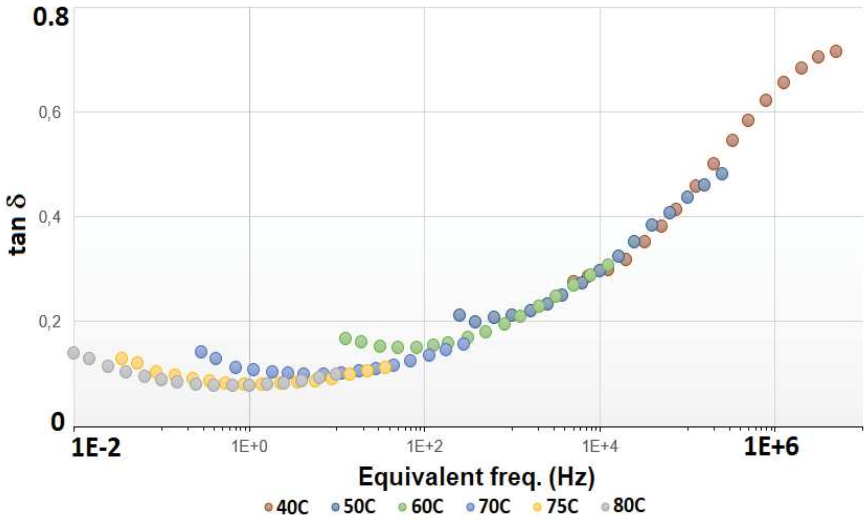

Figure 3.70: Added vertical shift in the case of loss tangent for PMMA

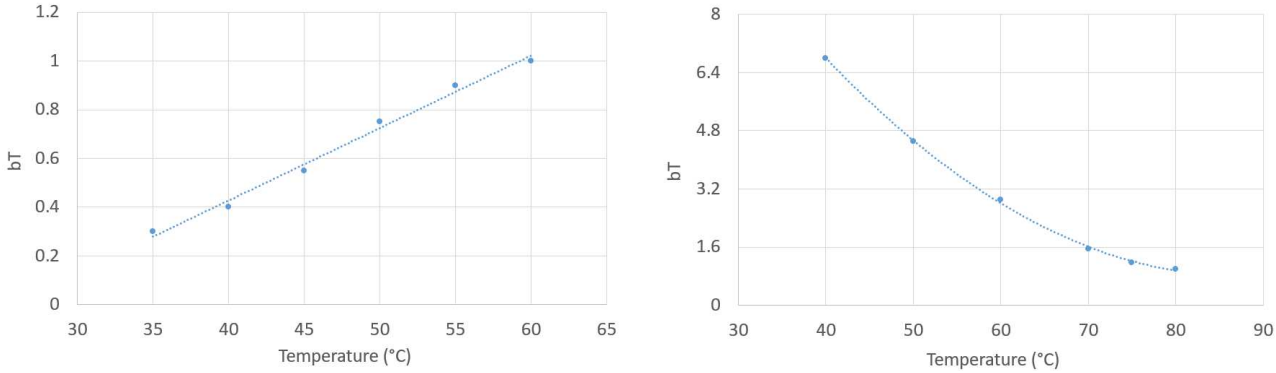

(a) PA-6.6 (b) PMMA

Figure 3.71: Variation of vertical shift versus temperature for PA-6.6 and PMMA

of the E' can vary depending on the manufacturing of the material and several different parameters like frequency and temperature. The comparison of the PMMA is shown in figure 3.72.

3.5 Synchronized thermal measurements

DMTA technique helped us to characterize the viscoelastic behaviour of PS, PMMA and PA-6.6 for 3 decades of time and later, with the help of TTSP, this short time range was extended to almost 8-9 decades. However, these classical DMTA measurements didn't allow us to measure the real temperature of the sample during a test, which is supposed to be different than the temperature imposed in the furnace. This difference could come from the self-heating of the polymer during cyclic measurements that can increase its temperature (e.g., dissipation due to the viscous nature of the material that is linked to the loss tangent). So, we wanted to measure the temperature of the sample during DMTA tests from 0.1 to 10 Hz and, due to the low dynamic and local measurement of thermocouples, we decided to use an infra-red camera.

Therefore, we build a specific setup where DMTA measurements are performed along with

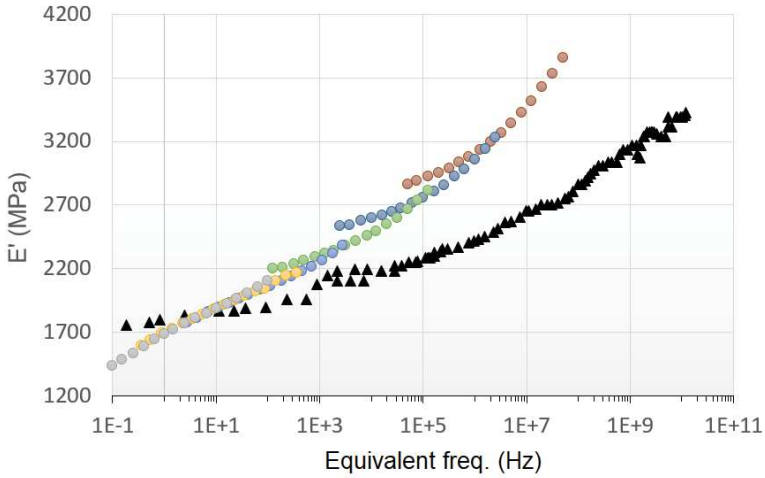

Figure 3.72: Comparison of PMMA master curve with literature [4]

the utilisation of a synchronised infra-red camera during the cyclic tests to observe self-heating phenomenon of the material, which is either due to the energy dissipation (viscosity) and/or to thermo-mechanical couplings [48, 78, 106, 107]. The experimental setup is explained in detail in the following section.

3.5.1 Experimental setup

The infrared camera was used during the DMTA frequency sweeps at different temperatures to observe and analyse the self heating phenomenon of the polymers during the cyclic tests. The infrared camera was being calibrated pixel by pixel for each temperature before starting the cyclic test. The reason behind selecting the pixel by pixel calibration method was the small amplitude of temperature induction due to the self-heating of the material during the cyclic test. The experimental setup used is shown in the figure 3.73.

The infra-red camera used for these extended DMTA measurements is described later along with the pixel-by-pixel calibration method used before starting the cyclic tests. The basic sketch of the thermography workstation is shown in figure 3.74.

The IR influx passing through the lens is converted into an electrical tension signal by the detector. An analog-to-digital converter (ADC) then provides a digital signal coded in digital levels (DL). The next stage takes the non-uniform response of the detector elements when placed in front of a uniform radiative source into account. This is the non-uniformity correction (NUC) operation. At this stage, the so-called "bad pixels" are also tracked and replaced. This is the bad pixel replacement (BPR) operation. These basic operations are part of the standard calibration protocol. The digital video is finally stored in the RAM of the computer. A software package developed by the camera manufacturer then enables calibration, processing and visualization of thermal data.

3.5.1.1 Infrared camera

The infrared camera used here is a Cedip titanium grand format that is specifically designed for academic and industrial R&D applications, with the highest sensitivity, accuracy, spatial

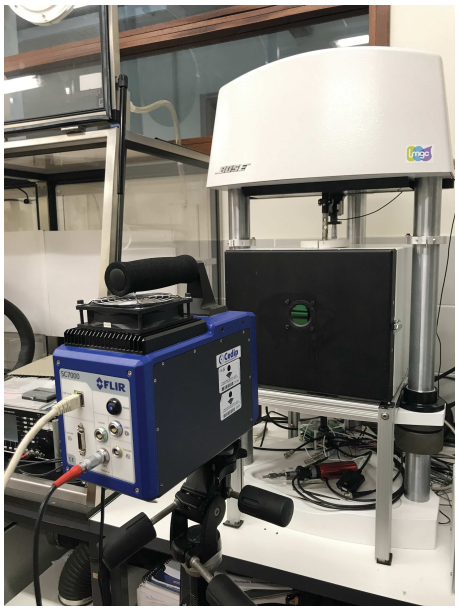

Figure 3.73: Synchronized thermal measurement setup

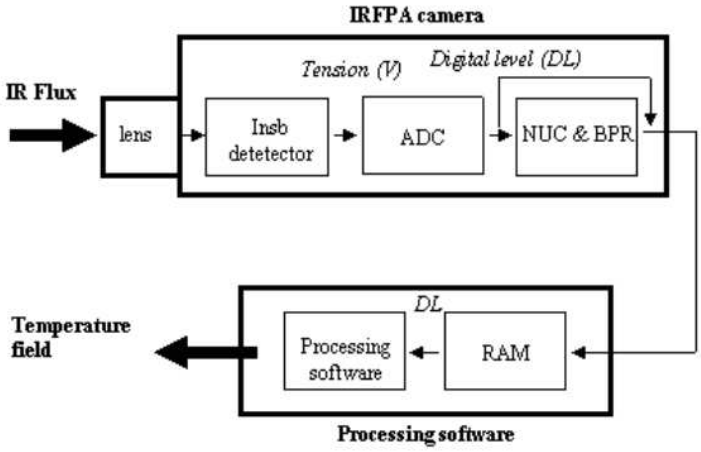

Figure 3.74: Temperature field acquisition chain in an infra-red camera [108]

resolution and acquisition speed. This infrared camera is shown in the figure 3.75.

This infrared camera provides us with many features which are mentioned below [109]:

• Choice of detector: It is available with a wide range of detectors for single and multispectral analysis. It provide researchers with a choice between mid-wave Indium Antimonide (InSb) and Mercury Cadmium Telluride (MCT) detectors.

• 640 x 512 pixels: It provides the crisp thermal images with a resolution of 640 x 512 pixels.

• High sensitivity: 20 mK thermal sensitivity that allows to capture the finest image details and temperature difference information.

Figure 3.75: Infrared Camera Titanium Grand format (CEDIP)

• Ultra high frame rates with windowing: This series of camera can get thermal images up to 62,000/second where windowing allows a subset of total image to be selectively readout with user adjustable window size.

• Adjustable integration time: Adjustable integration time allows us to manage the image capturing most suitable to a particular temperature and is adjustable in nanosecond increment.

3.5.1.2 Material and Method

The PS samples used for thermography were of the same dimensions (85 x 13 x 4 mm) as were used in LMGC, Montpellier for DMTA measurements. The calibration of the camera at every temperature that was used for DMTA measurements, using Pixel-by-pixel calibration method was followed by using the calibrated infrared camera during the DMTA measurements.

3.5.1.3 Pixel-by-Pixel calibration

Pixel-by-pixel calibration is one of the best known calibration technique for the thermography used for measuring the small temperature amplitudes [108]. This calibration technique allowed us to calibrate individual pixel based on the polynomial fitting of the digital level s_i delivered by the i_{th} element of the detector (Eq. (3.15)) when the camera is placed in front of a black body (CI SR 80) at different temperatures T (figure 3.76a and 3.76b).

$$s_i(T) = \sum_{p=0}^{P} a_{ip} T^p \quad for \quad T \in [T_1, T_2] \tag{3.15}$$

The a_{ip} coefficients were derived from a least-squares fit. A polynomial of level 4 is chosen. Once the data was fitted, the system considered a pixel i to be bad pixel based on the temperature difference predicted by the polynomial fitting and the ordered temperature of the black body source. If the difference was greater than the predefined threshold δT, then the pixel

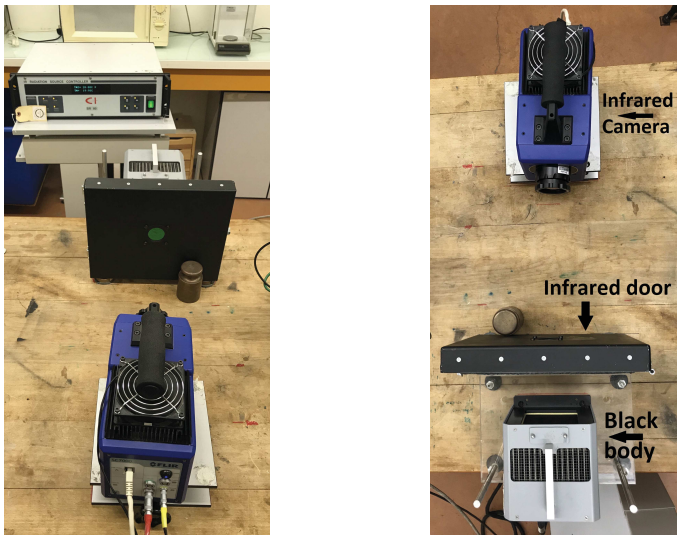

(a) (b)

Figure 3.76: Pixel-by-Pixel calibration setup

was considered as a bad pixel. Generally, this threshold is typically about $\delta T = 50mK$ and is greater than the black body specifications.

The bad pixels could be well distributed over the detector surface. When a pixel is considered as bad, it is no longer taken into account in the continuation of the image processing (filtering, energy estimation over a cycle and heat source computation) as the bad pixel replacement (BPR) procedure substantially distorts the thermal gradient calculations in these regions [108]. An example of bad pixels and pixel temperature differences is shown in figure 3.77 and 3.78.

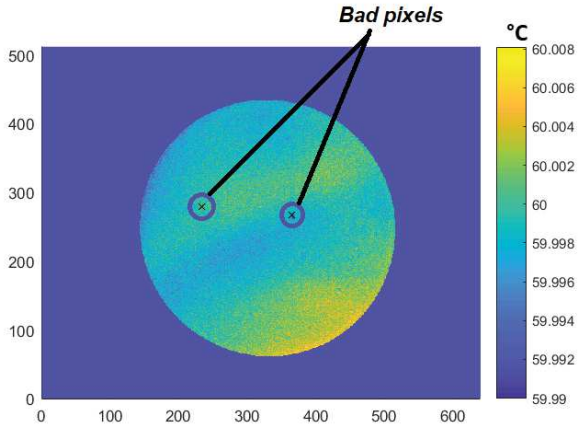

Figure 3.77: Bad pixel detection

The symmetry centre spread was reduced and the change was warranted by the fact that all the distribution function means stay within the interval $[-\delta T_R, +\delta T_R]$ imposed by the black body performance. With this reduced symmetry, a new set of histograms was plotted in fig-

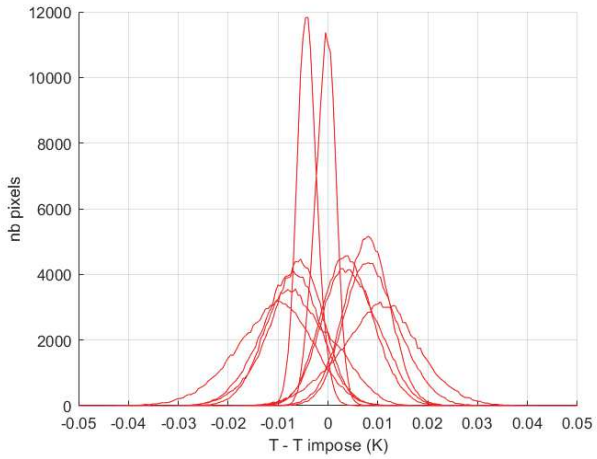

Figure 3.78: Histogram of pixel temperature differences

ure 3.79 [108].

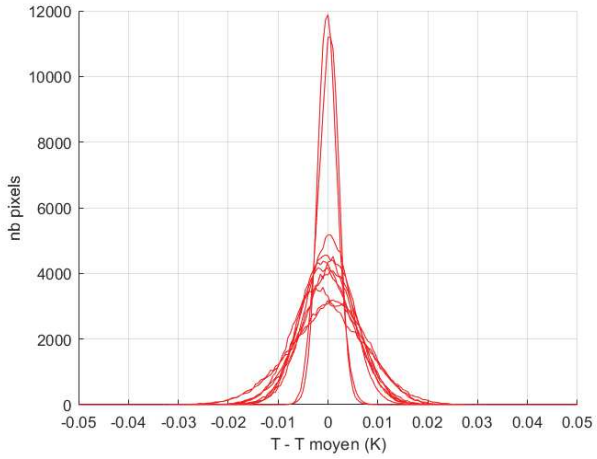

Figure 3.79: Temperature difference histogram computed for all temperatures

The examples shown in the figures 3.77, 3.78 and 3.79 are the tests performed on PS at temperature 60°C with the calibration temperature range of 55°C - 65°C. This calibration procedure was used for each temperature used during the DMTA measurements to ensure that we will be able to measure the very small amplitude of the self-heating effects of the polymers tested. To avoid thermal drift effect of the camera, these calibrations and measurements were performed about 4-5 hours after switching it on. Calibrations were done with a black body and the specific furnace door (see bellow) placed at the same distance and angle to the camera as the polymer samples and door in the DMTA (see figure 3.76).

3.5.1.4 Thermography Measurement Setup

The setup for thermography measurements during the DMTA measurements is shown in the figure 3.80.

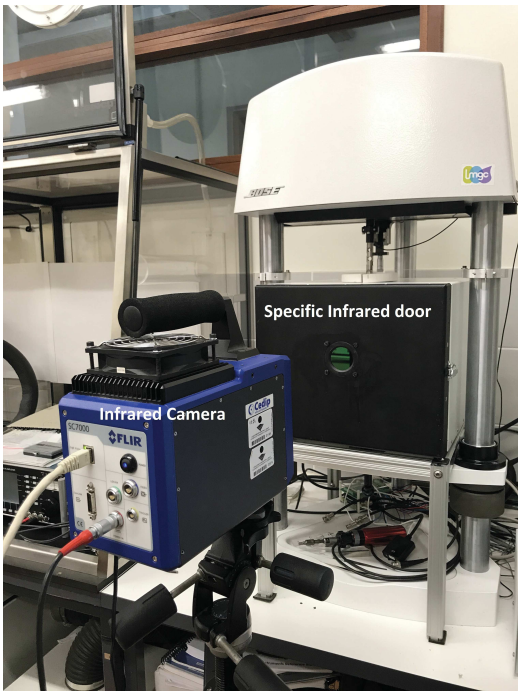

Figure 3.80: Thermography setup

A specific door for the DMTA furnace has been designed and manufactured at LMGC with a transparent window as far as possible to the infrared to allow infrared radiations to be measured by the infrared camera. The infrared window was bought from EDMUND Optics. This door has the following specifications:

- Material : Silicon
- Diameter : 50.00 mm
- Thickness : 1.00 mm
- Thickness tolerance : $\pm$0.1 mm
- Treated surface : 3-5 μm
- Wavelength range : 3000-5000 nm

The thermography was performed in the same temperature range that was used for the previous DMTA measurements but the loading frequency range was reduced to 0.1-10 Hz. This frequency range was selected because of the fact that below this range, the recording limit of the IR camera didn't allow to record the minimum number of loading cycles required to perform the data processing. A final acquisition frequency of 31 Hz was used for all the loading frequencies. This acquisition frequency has been chosen in order to remain within the system's capabilities while ensuring a sufficient sampling at "low" loading frequencies (i.e., below 3 Hz) and a heterodyne effect at higher frequencies, allowing a complete cycle to be reconstructed. The other parameters used for DMTA measurements during thermography is reported in the table 3.13.

Parameters	PS	PA-6.6	PMMA
Strain amplitude	0.1%		
Load ratio (R)	-1		
Freq.	0.1-10 Hz (5 points per decade)		
Temp.	(40 - 90)°C	(35 - 60)°C	(40 - 80)°C

Table 3.13: Parameters used for thermography measurements on PS, PA-6.6 and PMMA

It was then checked whether it was necessary to paint the samples with matt black paint, to ensure good emissivity and thus good measurement, as paintless polymer samples, unlike metals, generally give a good measurement by infrared camera. We thus used a half painted sample of PS (figure 3.81) and did all the image processing on both side to check if the amplitude of thermoelastic coupling is same on unpainted or painted side.

Figure 3.81: Half painted sample of PS

In order to be sure that the data from the infrared camera and the DMTA are well synchronized, a synchronization device, called "synchrocam" (figure 3.82a), was used. It allows for the storage of the data coming from the DMTA outputs (load and displacement in volts) using Labview (figure 3.82b) and it generates an external trigger signal for the infrared camera. This electronic synchronisation box has been designed previously in the laboratory [60].

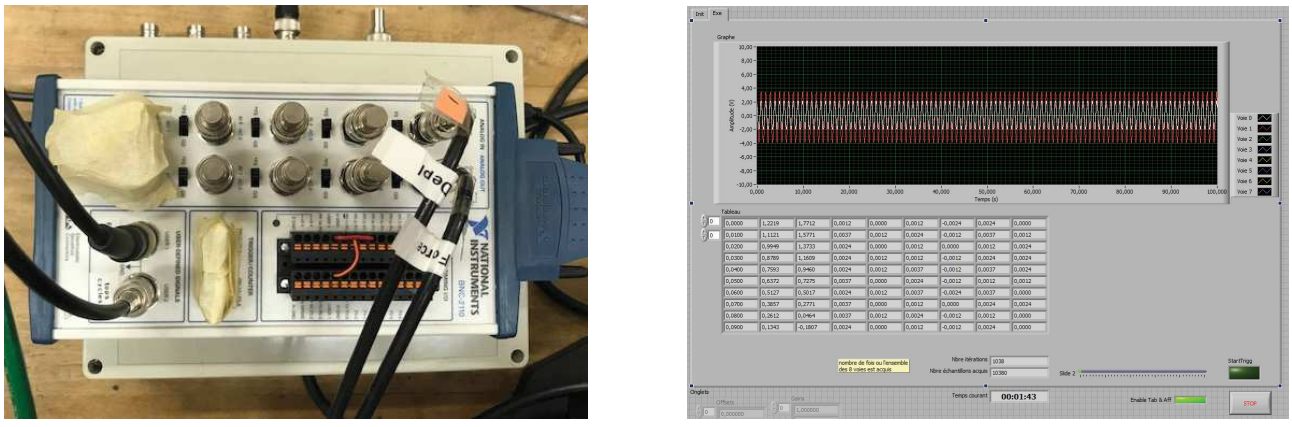

(a) Synchrocam (b) Labview Recordings

Figure 3.82: Synchrocam box integrated with Labview for synchronised data acquisition

This specific electronic box allows to acquire different input signals and send a synchronous pulse to trigger any other acquisition device such as an infrared camera. The principle of the synchrocam box is as follows: it sends 2 rising edges. The first one is dedicated to the acquisition card of the infrared camera (trigger) and the second one is dedicated to the acquisition of

the signals of the sensors coming from the electronic box of the DMTA machine. A frequency generator integrated in the Labview software provides the common time base for acquisitions. This simultaneous acquisition allows for the analog output signals from the DMTA device to be digitized for each image acquisition. As explained in section 3.4.2, the electronic phase shift between load and displacement output signals was check again with the steel sheet sample using the synchrocam measurements.

3.5.2 Data Processing

The realization of the series of measurements by thermography at different temperatures during the DMTA measurements allows us to observe the thermo-mechanical couplings and dissipative effects during cyclic loading, with a new sample per test temperature as in previous DMTA measurements. An additional unloaded sample (dummy specimen) was used in parallel during these measurements in order to measure the actual regulation temperature of the furnace. An example of the thermal image captured by the infrared camera is shown in the figure 3.83a along with figure 3.83b showing the homogeneous amplitude field of thermoelastic coupling throughout in the specimen. This thermoelastic coupling field was calculated for each pixel over the entire bunch of images followed by computation of average thermoelastic coupling amplitude over all the images for every pixel. This average thermoelastic coupling amplitude was plotted over the interest region of area over the sample.

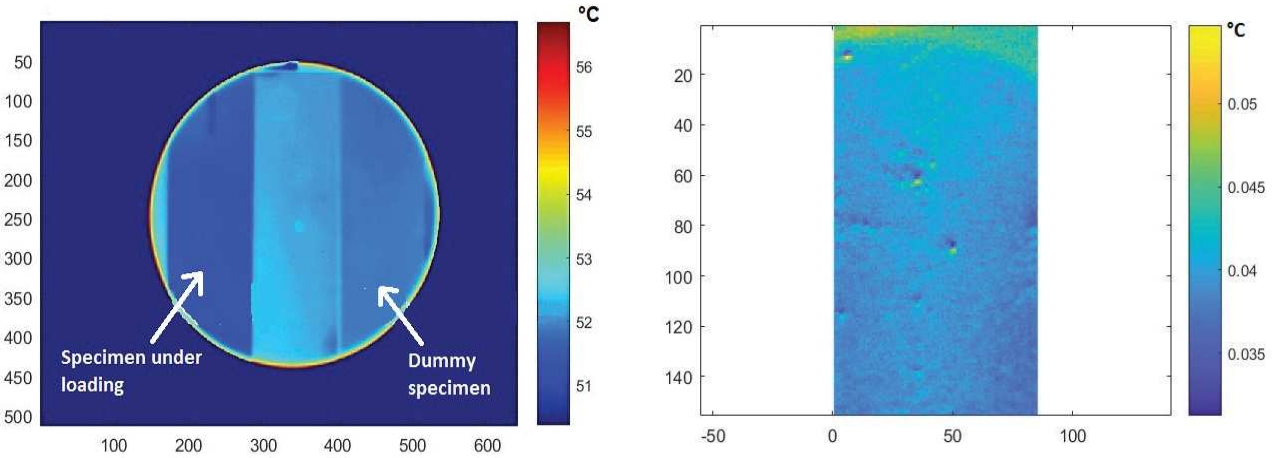

(a) (b)

Figure 3.83: (a) Thermal image captured by the infrared camera and (b) Homogeneous thermoelastic coupling amplitude throughout the specimen

Image processing was performed using a MATLAB code on the images recorded by infrared camera at several temperatures and frequencies. During this part of image processing, despite being using the synchrocam acquisition box, the frequency of the temperature oscillations using the recorded images, for a particular measurement, was checked using the FFT technique. This was done to verify if the corresponding DMTA measurement has the same loading frequency as well. After the verification of the frequency of temperature signals, the area of interest on the sample under loading was selected in such a way, that it covers maximum of the central surface of the specimen (leaving the tensile mode clamps outside the area of interest) under

loading. Similarly, the area of interest was selected on the surface of reference sample as well. Later, the mean temperature of the surface of the reference sample was subtracted to the mean temperature of the loaded sample to minimize the temperature fluctuations of the furnace due to its regulation. The mean of the amplitude of these temperature oscillations for each pixel over the total number of images, was plotted over the area of interest on the surface of the specimen to get the thermoelastic field in the specimen under loading. A virtual sinusoidal signal was created using the parameters used for the experimental measurements. Using the least square fitting methods, the adjustment of the virtual sinusoidal curves was done (for strain, stress and temperature signals) with the experimentally observed curves to be sure about the image processing output.

Using this procedure of image processing, it was verified (on the half painted sample, painted on the right side) if painting the sample black will affect the emissivity of the sample. The thermoelastic field of half painted sample is shown in figure 3.84. The imposed displacement for this measurements was 0.11 mm at 40 °C and 1 Hz. The dimensions in the figures are in pixels whereas, the temperature is in °C. It was observed that painting the sample in black induces a difference of 10% in the amplitude of thermoelastic couplings between the painted and unpainted side of the sample and the results are more noisy on the unpainted side. This helped us to conclude that painting the sample black would provide precision to the thermography measurements and hence the samples of PS and PMMA were painted black.

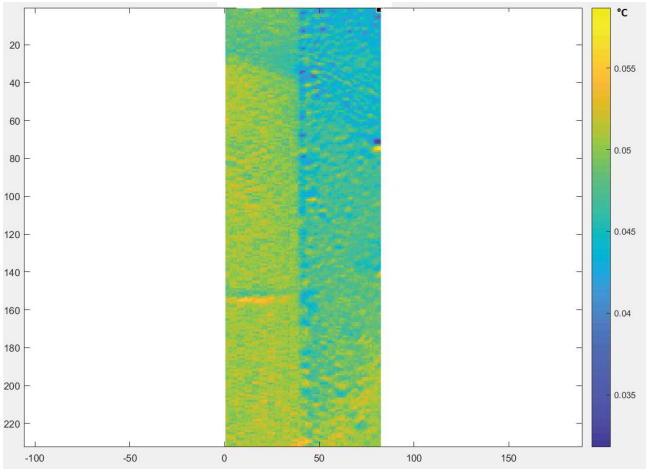

Figure 3.84: Amplitude field of the thermoelastic coupling for the half-painted sample

Later, the entire data was processed one-by-one using MATLAB code to verify if the stress, strain and the temperature signal are well synchronized even after using synchrocam for synchronizing all the signals. During this entire data processing, a problem of phase shift between temperature and strain was observed at high frequencies. This problem is explained in detail in the following subsection 3.5.2.1. The normalized signals on the same graph were also plotted as can be seen in figure 3.85.

It was observed in figure 3.85 that the temperature is in opposite phase with strain, i.e., the sample is cooling while in tension and heating up while in compression. This observation of temperature being in opposite phase with loading was in accordance with [78, 106, 110]. In continuation, the hysteresis plots were observed inducing from the mechanical loading and

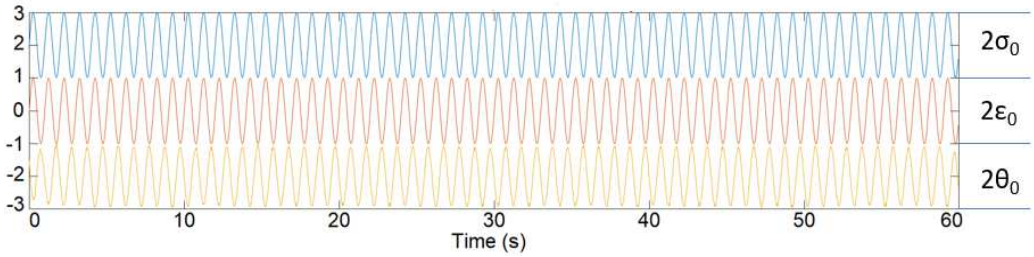

Figure 3.85: Normalized stress, strain and temperature signal for PS at 40 °C *and* 1 Hz

from the phase shift between the strain and the temperature (i.e., strain as a function of temperature). An example for these hysteresis loops are shown in figure 3.86.

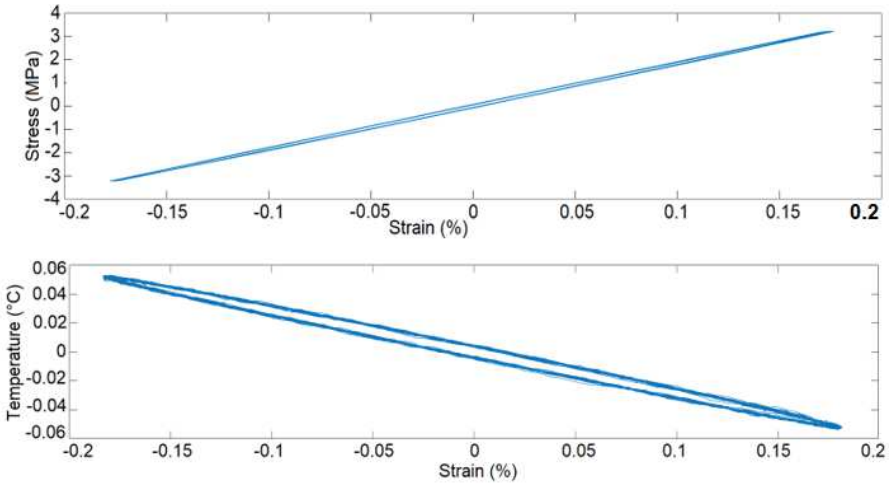

Figure 3.86: Hysteresis loops for mechanical loading and temperature as a function of temperature for PS at 40 °C *and* 1 Hz

3.5.2.1 Temperature-strain phase shift

The amplitude of the temperature oscillations due to the thermoelastic coupling was observed from the thermography measurements. This amplitude is shown in table 3.14. An hysteresis area associated with these thermoelastic couplings (see figure 3.86) can also be computed using:

$$A_{the} = -\oint_{cycle} E'\alpha\theta\dot{\varepsilon}dt, \tag{3.16}$$

Integrating equation 3.16 over a cycle, we can write:

$$A_{the} = -E'\alpha\theta_0\varepsilon_0\omega\int_0^T \sin(\omega t + \delta_{th})\cos\omega t dt, \tag{3.17}$$

where, $\theta = \theta_0 \sin(\omega t + \delta_{th})$ and $\varepsilon = \varepsilon_0 \sin \omega t$. Here, δ_{th} is the phase shift between temperature and strain oscillations. Solving the integral part, we get the analytical solution for a pure viscoelastic material with thermoelastic coupling:

$$A_{the} = -E' \alpha \theta_0 \varepsilon_0 \pi \sin \delta_{th}, \tag{3.18}$$

Polymers	Temperature amplitude θ_0 (°C)
PS	0.055
PA-6.6	0.03
PMMA	0.05

Table 3.14: Temperature amplitude due to thermoelastic couplings

As explained earlier in section 3.5.1.4, the synchrocam device was used to synchronize the DMTA and infrared data. While using it, few difficulties were faced. It was observed in the IR camera integrated software (Altair) that, at the beginning of the recording of the DMTA data and the thermography images, some thermal images were missing (especially the very first ones) and sometimes the acquisition time was slightly different between synchrocam and the actual image acquire (IR camera internal clock). First, to solve the difficulty of the first missing images, a dwell time of ≈10 s was added before starting the loading cycles on the samples in DMTA. Second, the problem of data acquisition at different times was solved during the data processing step by creating two different time vectors, one for the stress and strain coming from synchrocam and one for the IR images coming from the internal clock of the camera. In the end, least square adjustments of the three signals (stress, strain and temperature) allow to replot all of them with the same time vector.

During data processing, an unexpected difficulty appeared during the computation of the phase shift (δ_{th}) between the temperature and the imposed strain. It was observed that, δ_{th} was increasing significantly with the frequency as shown in figure 3.87 for PS.

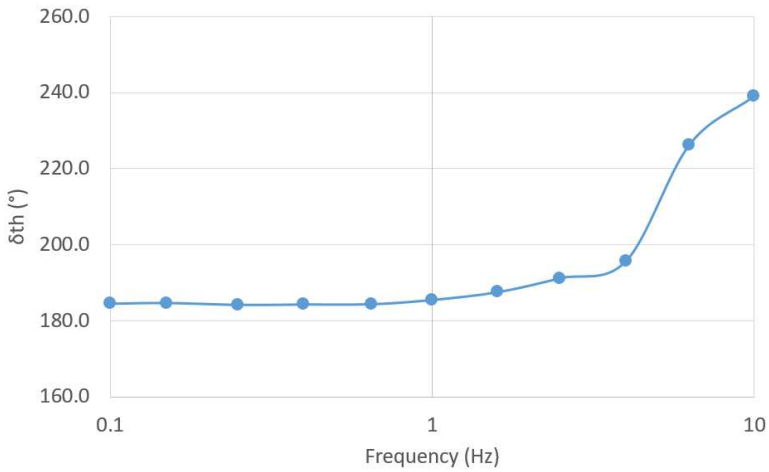

Figure 3.87: Evolution of δ_{th} with frequency for PS at 40° C

This evolution of δ_{th} was observed in every case, i.e., for each temperature and each polymer used for this study. As δ_{th} may mainly come from the heat exchange of the sample with its environment, we measured the time constant for heat losses.

$$\tau_{th} = \frac{\rho C_p}{2h_c} \cdot \frac{el}{e+l} \tag{3.19}$$

where e and l represents the thickness and the width of the specimen used. h_c represents the heat convective coefficient. The simplified 1D heat diffusion equation with only thermoelastic sources can be written as:

$$\dot{\theta} + \frac{\theta}{\tau_{th}} = -K_{th}\varepsilon_0\omega\cos\omega t \tag{3.20}$$

where $K_{th} = \dfrac{E'\alpha T_0}{\rho C_p}$. Solving equation 3.20, we get the solution of the form:

$$\theta = \theta_0 \sin(\omega + \delta_{th}) \tag{3.21}$$

where, $\theta_0 = \dfrac{-K_{th}\varepsilon_0\tau_{th}\omega}{(1+\tau_{th}^2\omega^2)^{1/2}}$. Therefore, τ_{th}, can be linked to δ_{th} through:

$$\tan\delta_{th} = \frac{1}{\tau_{th}\,\omega} \tag{3.22}$$

We measured this time constant experimentally for all the three polymers using thermocouple. The setup is shown in figure 3.88. Samples were drilled to a diameter of 0.1 mm in the middle of the cross-section so that the thermocouple can be put in the center of the sample. Another thermocouple was kept very close to the surface of the specimen under loading to measure the temperature of the furnace close to the sample. The sample was then clamped in the tension mode clamps (to ensure the same heat exchange conditions as during cyclic tests). A temperature increase ramp as fast as possible was imposed by the furnace, one or two times, followed by a strong cooling down (by turning off the furnace and opening its door) as shown in figure 3.89. Finally, using the simplified 1D heat diffusion equation (Eq. (3.25)) and the temperature of the furnace, we adjust a theoretical curve with a least square method that yields an estimation of τ_{th} (table 3.15). These values show that the evolution of δ_{th} seen in figure 3.87 can't be explain by the heat exchange of the sample with its environment.

Finally, we decided to verify the phase shift between the temperature and the strain by using image correlation technique on the thermography images. This technique was performed by Pr. Bertrand Wattrisse and Dr. Jonathan Barès on the thermography images recorded using infrared camera at few frequencies and at room temperature (28°C) only. One of the thermography images that was used is shown in figure 3.90. The outcomes of the image correlation are grouped in form of table 3.16. It was observed from the table 3.16 that, the δ_{th} obtained

Figure 3.88: Setup for the measurement of τ_{th}

Polymers	τ_{th} (s)
PS	48
PA-6.6	34
PMMA	63

Table 3.15: τ_{th} estimation for all three polymers

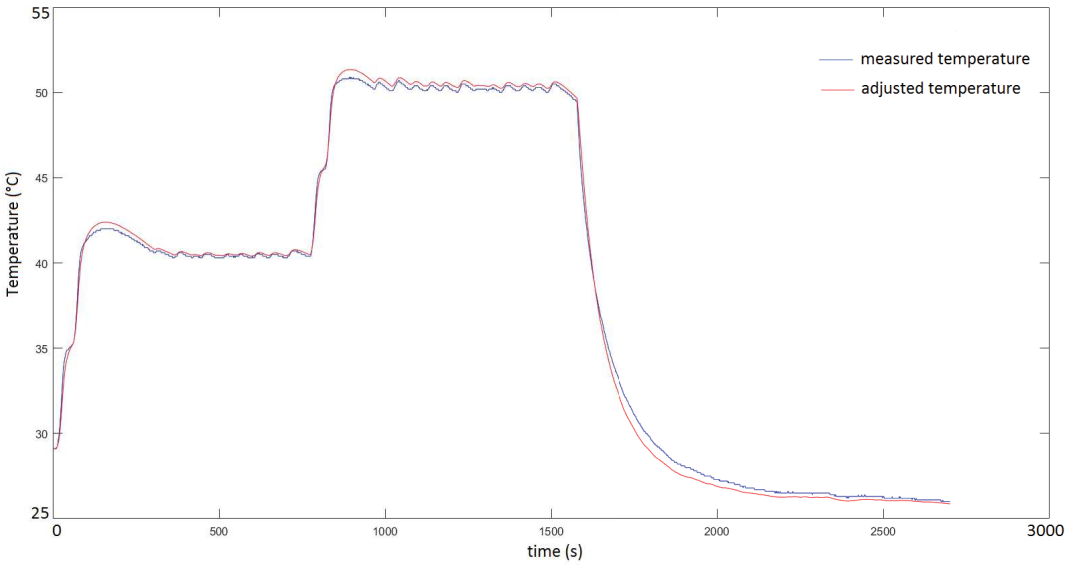

Figure 3.89: Measured and adjusted temperature curves of the sample for the estimation of τ_{th}

using image correlation and equation 3.22 was similar unlike the one obtained using synchrocam.

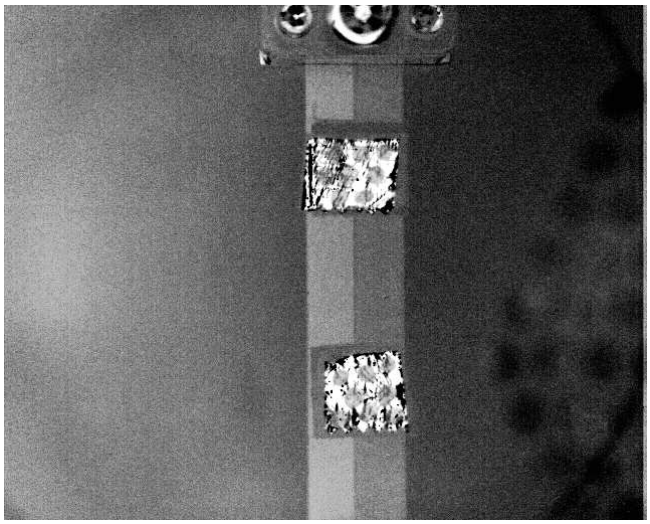

Figure 3.90: Thermography images used for image correlation with specific markers on the sample

Frequency (Hz)	0.1	1	10
δ_{th} (°)-synchrocam	180.3	182.9	221.0
δ_{th} (°) image correlation	179.9	178.8	178.4
δ_{th} (°) theoretical - τ_{th}	181.9	180.2	180.0

Table 3.16: Image correlation results. The last row shows the δ_{th} calculated using equation 3.22

3.5.3 Results

The results of synchronized thermal measurements after passing through image and data processing are shown in this section. First, the storage (E') and loss modulus (E") were determined using the least square fitting method. This determination was performed using the raw DMTA data recorded using synchrocam (in Volts) that were converted (to Newtow and millimeter) and thereafter corrected for electronic phase shift and machine stiffness as previously. Using these values of E' and E'', a master curve was plotted and was compared with the master curve obtained previously. An example (case of PS) of comparison between the two different master curves is shown in figure 3.91 and figure 3.92. It was observed in this comparison that the master curves plotted using the data from least square fitting method and the data obtained directly from DMTA measurements are quite similar and of same order of amplitude. The number of data points per temperature are more in the master curve obtained directly from DMTA measurements as the frequency range used was from 0.01 Hz-10 Hz, whereas, during thermography measurements, it was from 0.1 Hz-10 Hz. The activation energy was also calculated for both the case and was found to be quite close i.e., $E_a = 350$ kJ/molK in case of master curve obtained from least square fitting values and $E_a = 392$ kJ/molK in case of master curve obtained directly from DMTA measurements.

After the comparison of E' and E'' (obtained from DMTA during thermography) with previous E' and E'' (obtained through DMTA measurements), the activation energy (E_a) for the three different materials was calculated using an Arrhenius plot shown in figure 3.93 and reported in table 3.17. The slope of the linear regression showed in figure 3.93 is equal to $-E_a/R_u$, where $R_u = 8.314$ J/(mol.K), represents the universal gas constant.

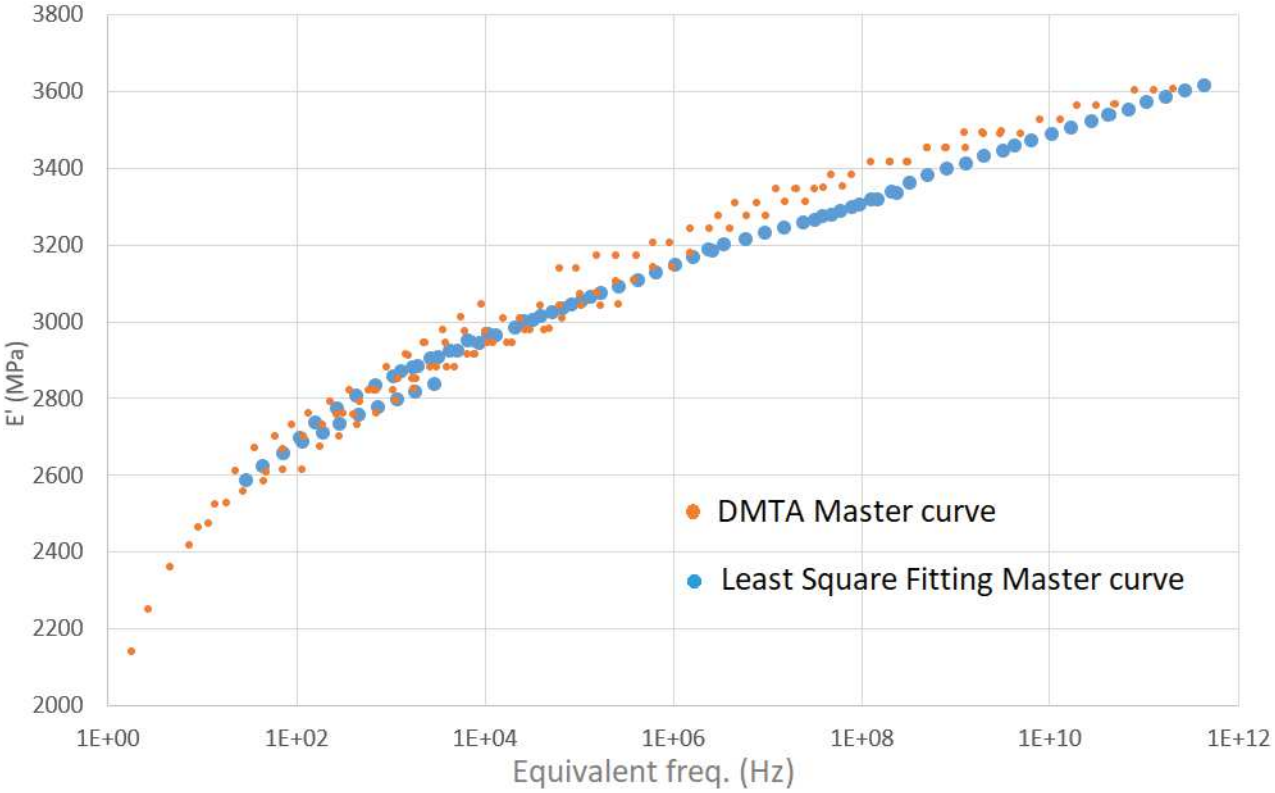

Figure 3.91: Comparison of storage modulus obtained through DMTA during temperature measurements with the previous DMTA results

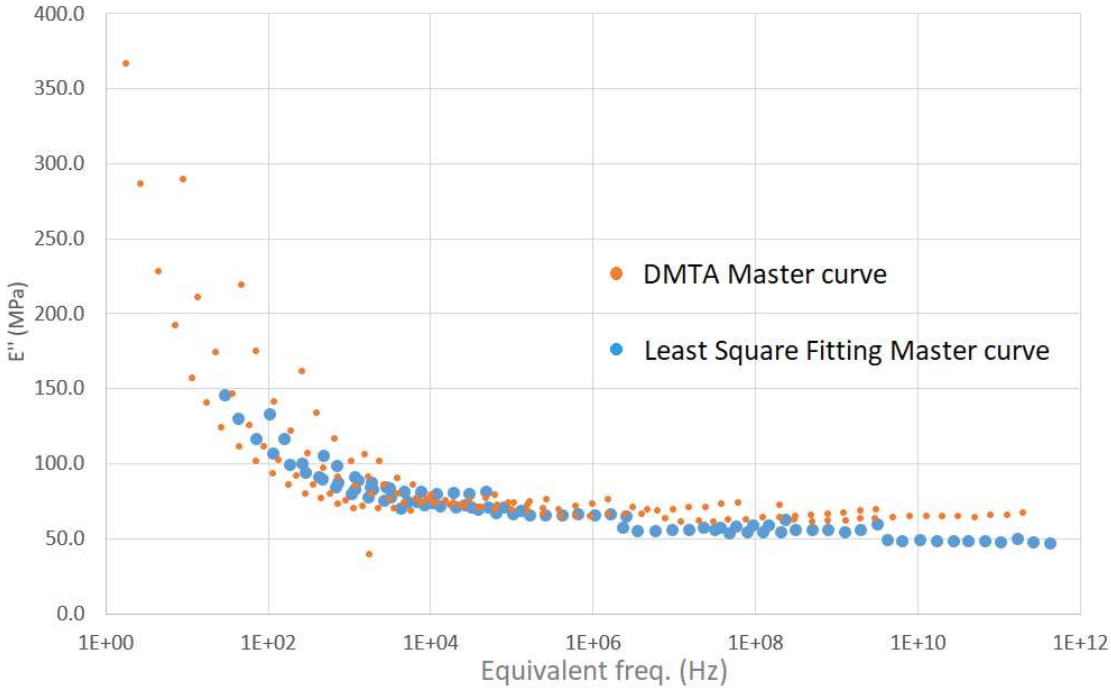

Figure 3.92: Comparison of loss modulus obtained through DMTA during temperature measurements with the previous DMTA results

Thermal image processing results is shown in figures 3.94-3.102 where the mean temperature variation of the sample surface with time is reported. These results are shown for few frequen-

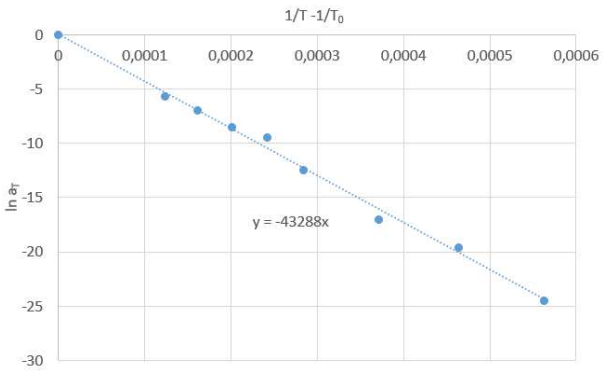

(a) Polystyrene

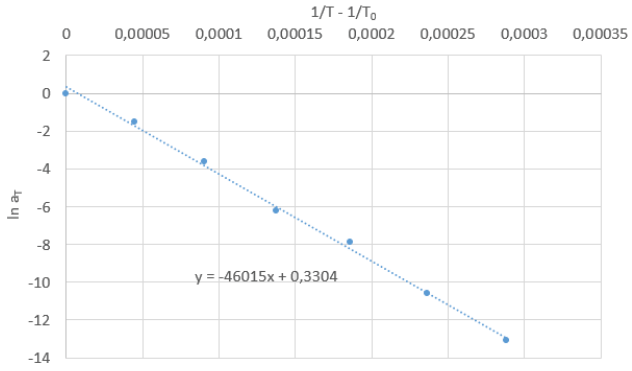

(b) Polyamide-6.6

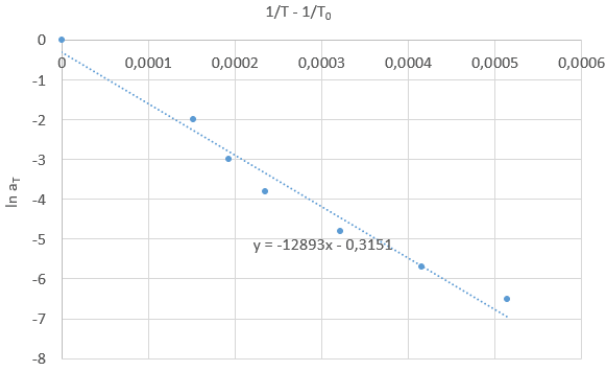

(c) PMMA

Figure 3.93: Arrhenius plot for calculating E_a

Polymers	**PS**	**PA-6.6**	**PMMA**
Activation energy	350	382	107

Table 3.17: Activation energy (kJ/mol) of the three polymers

cies and temperatures for all the three polymers to highlight the effect of increasing frequency and furnace temperature on the cyclic and mean temperature variations of the specimen for all the three polymers used.

In the figures 3.94-3.102, it is reminded that the origin of temperature axis remains arbitrary and that only the oscillation range (thermoelastic effects) and the overall mean variation over a cycle (self-heating) have to be taken into account. The mean temperature of the surface of the reference sample was subtracted to the mean temperature of the loaded sample to minimize the effects of temperature fluctuations of the furnace due to regulation but it doesn't prevent for a slight error on the mean temperature of the sample. In such conditions, the observed temperature variations were considered to be that of the loaded specimen with an arbitrary thermal constant. In this analysis, the monotonous increase of the mean temperature over a cycle can then be associated with the existence of dissipation, while, periodic oscillations correspond to thermoelastic coupling. Using this mechanical and thermal data, it was also possible to compute the hysteresis area associated with mechanical loading, thermo-elastic couplings and estimate the mean dissipation per cycle during the test.

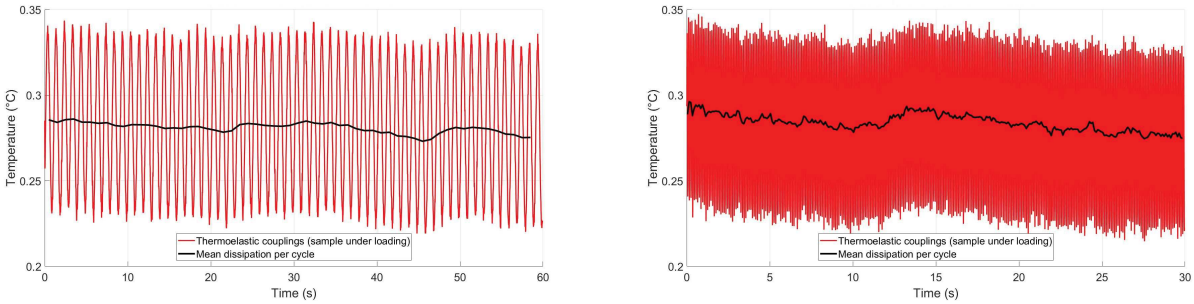

(a) 1 Hz (b) 10 Hz

Figure 3.94: Specimen temperature variation during DMTA measurement in case of PS at 40° C

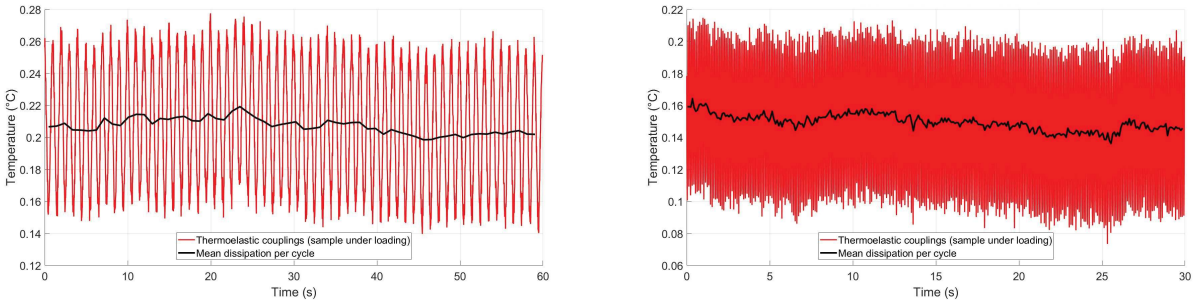

(a) 1 Hz (b) 10 Hz

Figure 3.95: Specimen temperature variation during DMTA measurement in case of PS at 70° C

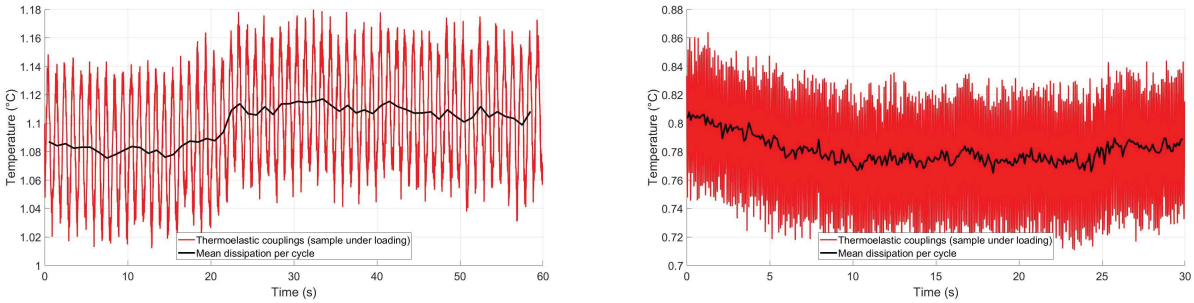

(a) 1 Hz (b) 10 Hz

Figure 3.96: Specimen temperature variation during DMTA measurement in case of PS at 90° C

Despite the narrowness of the temperature variations, figures 3.94-3.96 (PS results) clearly show the presence of the temperature oscillation while any self-heating of the specimen was difficult to observe in case of PS. These results are in accordance to what was found in [78]. This observation of the thermoelastic coupling without significant dissipation at all the loading frequencies questions the viscous origin of loss modulus, which is assumed to be the result of energy dissipation. In the case of PA-6.6 (figures 3.97-3.99) and PMMA (figures 3.100-3.102), the presence of temperature oscillations is clearly observed too and the self-heating of the specimen (i.e., monotonous increase of the mean temperature over a cycle) is observed at high loading frequencies, unlike PS. These different observations lead us to compute the hysteresis

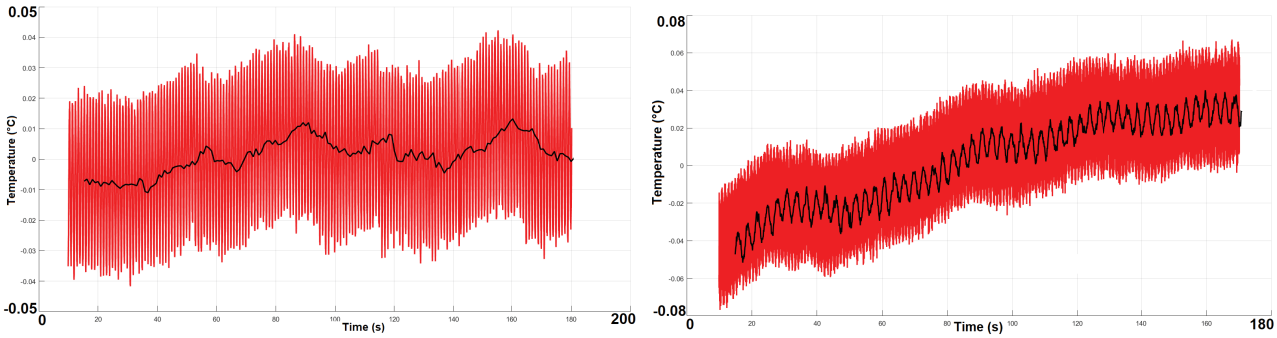

(a) 1 Hz (b) 10 Hz

Figure 3.97: Specimen temperature variation during DMTA measurement in case of PA-6.6 at 40° C

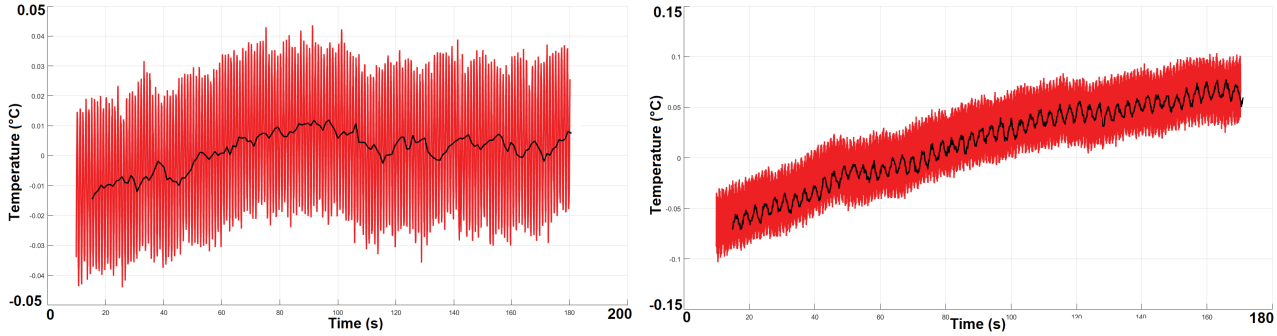

(a) 1 Hz (b) 10 Hz

Figure 3.98: Specimen temperature variation during DMTA measurement in case of PA-6.6 of 50° C

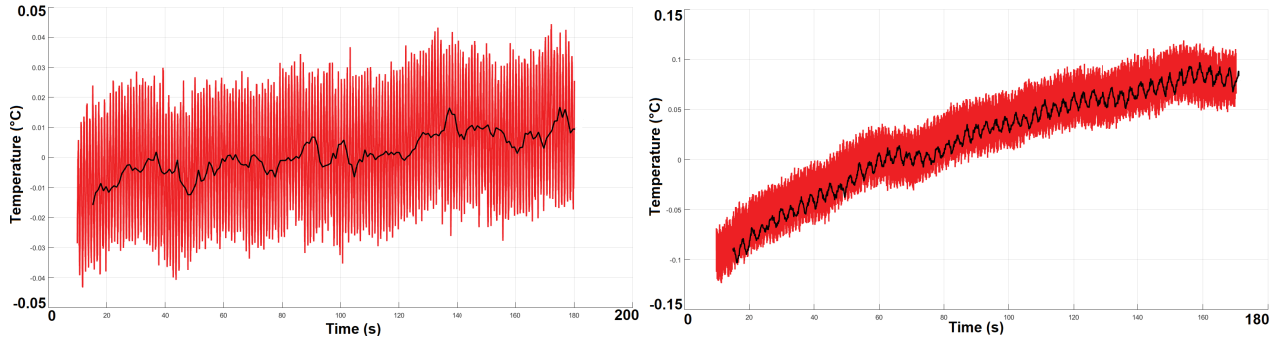

(a) 1 Hz (b) 10 Hz

Figure 3.99: Specimen temperature variation during DMTA measurement in case of PA-6.6 at 60° C

area associated with the dissipation and loss modulus for all the three polymers, for the different frequencies and (furnace) temperatures used during the tests.

Computation of the hysteresis area associated with the mechanical loading A_h was performed and results are reported in table 3.18. The mechanical hysteresis area was calculated using the stress-strain data using:

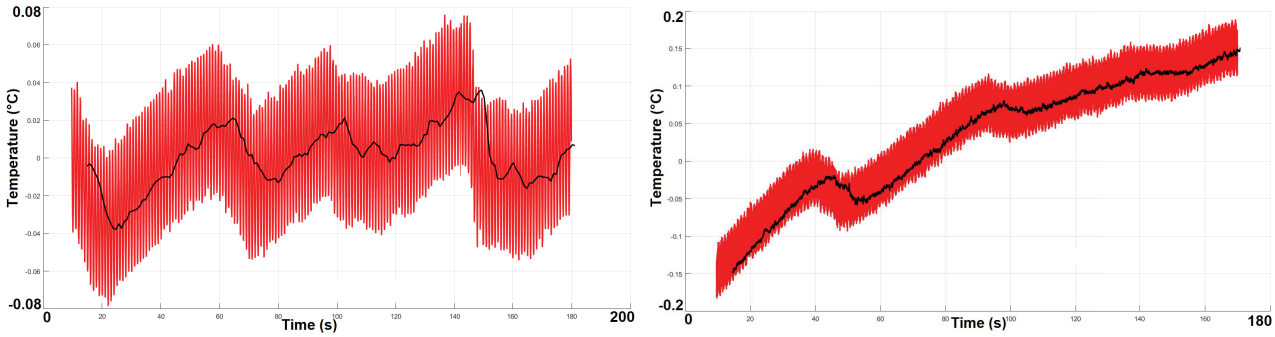

(a) 1 Hz (b) 10 Hz

Figure 3.100: Specimen temperature variation during DMTA measurement in case of PMMA at 40° C

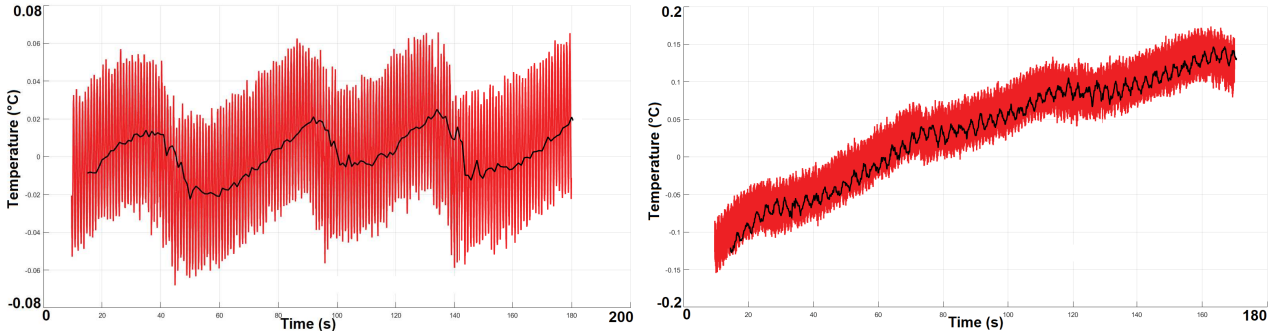

(a) 1 Hz (b) 10 Hz

Figure 3.101: Specimen temperature variation during DMTA measurement in case of PMMA at 60° C

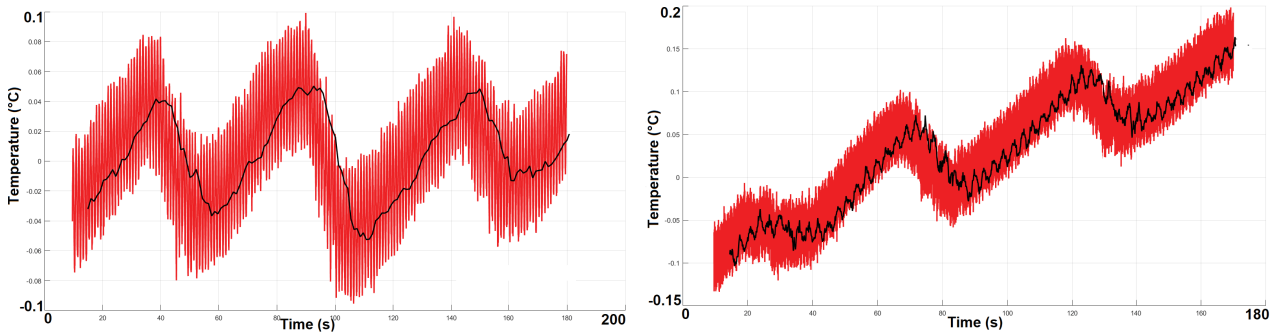

(a) 1 Hz (b) 10 Hz

Figure 3.102: Specimen temperature variation during DMTA measurement in case of PMMA at 70° C

$$A_h = \oint_{cycle} \sigma \cdot \dot{\varepsilon} dt. \tag{3.23}$$

If we consider that this mechanical hysteresis area is solely due to viscous dissipation, one can derive its expression with E'' from Eq. (3.23) and obtain:

$$A_{HL} = \pi E'' \varepsilon_0^2. \tag{3.24}$$

The computed hysteresis area associated with the loss modulus is shown in tables 3.19 and 3.20. The evolution of these hysteresis, for all the three polymers used in this study, is shown in figure 3.103 and 3.104. This evolution of hysteresis area is presented against the frequency for all the temperatures used during the thermography measurements.

It was observed in figure 3.103, that the trend of evolution of A_h is similar for PS and PA-6.6 i.e., decreasing with temperature and frequency as well. Whereas, the trend of evolution of A_h in case of PMMA is different i.e., increasing with the frequency unlike the other two polymers.

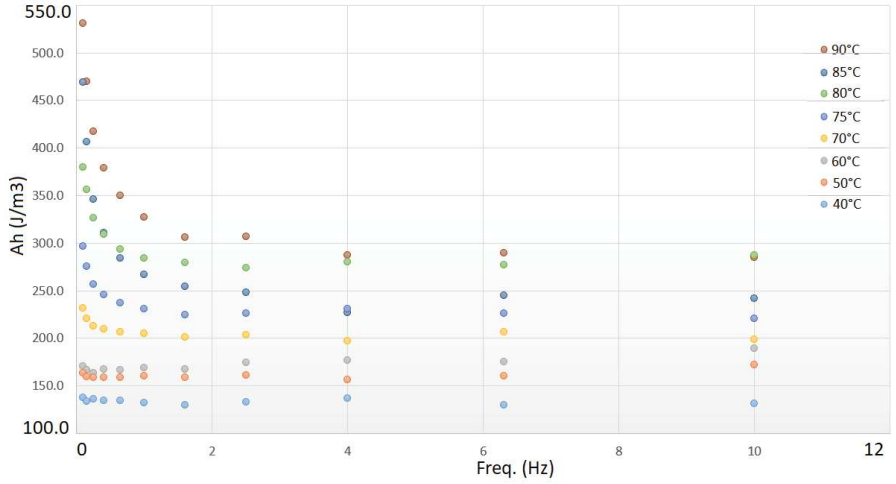

(a) Polystyrene

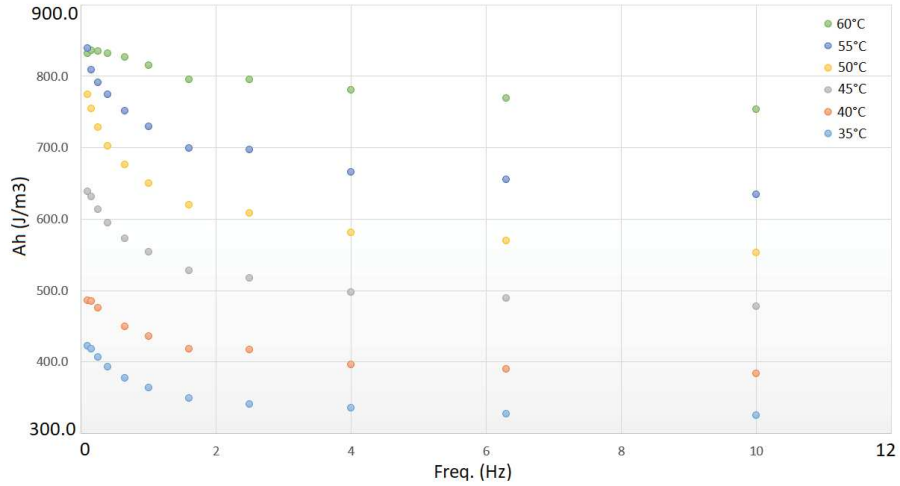

(b) Polyamide-6.6

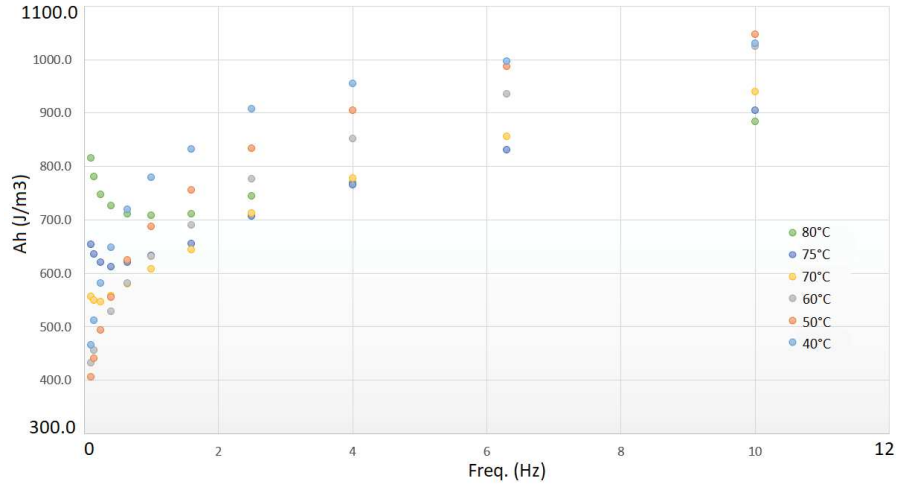

(c) PMMA

Figure 3.103: Evolution of A_h with frequency for different temperatures used

Temp.(°C)	Freq.(Hz) / Polymer	0.1	0.15	0.25	0.4	0.65	1	1.6	2.5	4	6.3	10
35	PS	-	-	-	-	-	-	-	-	-	-	-
	PA-6.6	422.4	418.4	406.3	393.3	377.3	363.7	349.2	340.4	335.1	326.8	325
	PMMA	-	-	-	-	-	-	-	-	-	-	-
40	PS	137.4	133.7	136	134.2	134	131.9	130	133	137.2	129.6	131.1
	PA-6.6	485.7	484.7	475.6	DO	449.7	436.3	417.6	416.8	395.7	389.6	383.2
	PMMA	465.8	512.3	582.1	648.7	719.1	779.1	832.3	907.9	954.8	996.9	1029.9
45	PS	-	-	-	-	-	-	-	-	-	-	-
	PA-6.6	639	631.1	613.4	594.5	573.1	553.9	528	516.9	497.8	489.5	477.4
	PMMA	-	-	-	-	-	-	-	-	-	-	-
50	PS	163.1	159.2	159.1	158.4	158.6	160.1	158.4	160.9	156.7	160.5	172.1
	PA-6.6	774.1	754.8	728.2	702.1	675.9	650.4	619.5	608.1	581.2	569.8	552.7
	PMMA	405.8	441.3	494.1	555.3	624.9	687	755.7	833.7	904.6	986.6	1046.4
55	PS	-	-	-	-	-	-	-	-	-	-	-
	PA-6.6	838.8	808.4	791	774.5	751.1	729	699	696.5	665.9	655	634.6
	PMMA	-	-	-	-	-	-	-	-	-	-	-
60	PS	170.2	166.8	163.3	167.1	166.3	168.8	167.7	174.2	176.8	174.9	189.5
	PA-6.6	831.7	836	834.9	831.8	826.2	814.9	794.8	795.5	780.2	769.4	753.8
	PMMA	431.9	456	DO	528.6	580.8	631.7	690.6	776.9	851.1	935.8	1023.8
70	PS	231.4	220.9	213	209.5	206.5	205.2	201.5	203.4	197.4	206.5	198.9
	PA-6.6	-	-	-	-	-	-	-	-	-	-	-
	PMMA	556.9	549.7	547	557.3	580.1	607.5	644.3	712	777.4	855.9	939.6
75	PS	296.3	275.4	256.4	245.4	237	230.7	224.4	226.4	231	226.1	220.5
	PA-6.6	-	-	-	-	-	-	-	-	-	-	-
	PMMA	653.3	635.6	620.6	612.2	621	632.6	655.7	706.4	764.9	830.8	904.4
80	PS	380.1	356.2	326.3	309.6	293.3	284.2	279.1	274.3	280.2	277	287
	PA-6.6	-	-	-	-	-	-	-	-	-	-	-
	PMMA	815.5	780.9	746.6	726.5	710.5	707.7	710.5	744.5	769.3	DO	883.9
85	PS	469	406.7	345.8	311	283.9	266.6	254	248.1	227.2	244.9	241.7
	PA-6.6	-	-	-	-	-	-	-	-	-	-	-
	PMMA	-	-	-	-	-	-	-	-	-	-	-
90	PS	530.7	470	417.7	378.9	350	327.1	306.4	306.8	287.5	289.4	285.1
	PA-6.6	-	-	-	-	-	-	-	-	-	-	-
	PMMA	-	-	-	-	-	-	-	-	-	-	-

Table 3.18: Computed mechanical hysteresis area (A_h) for all the three polymers in J/m^3

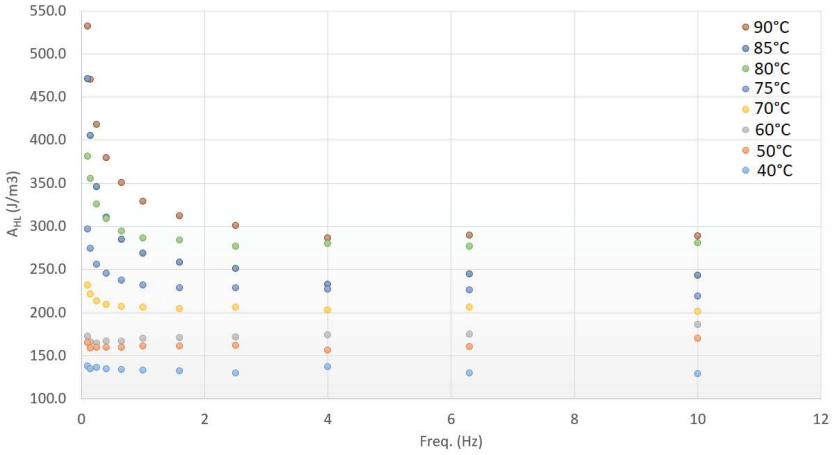

(a) Polystyrene

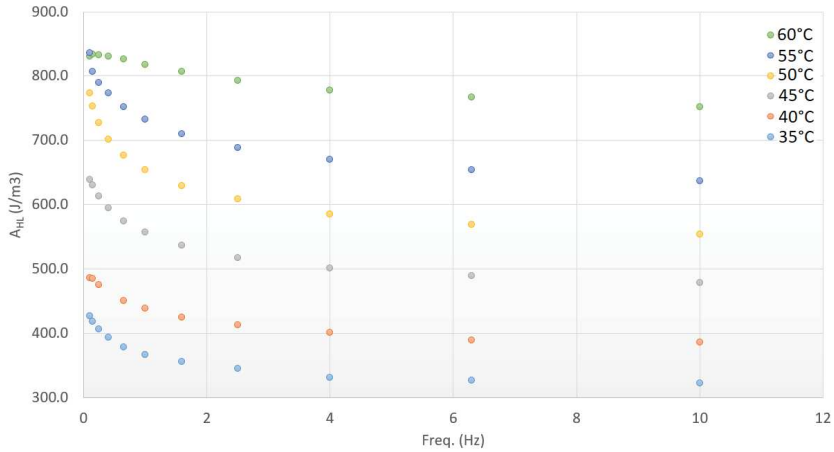

(b) Polyamide-6.6

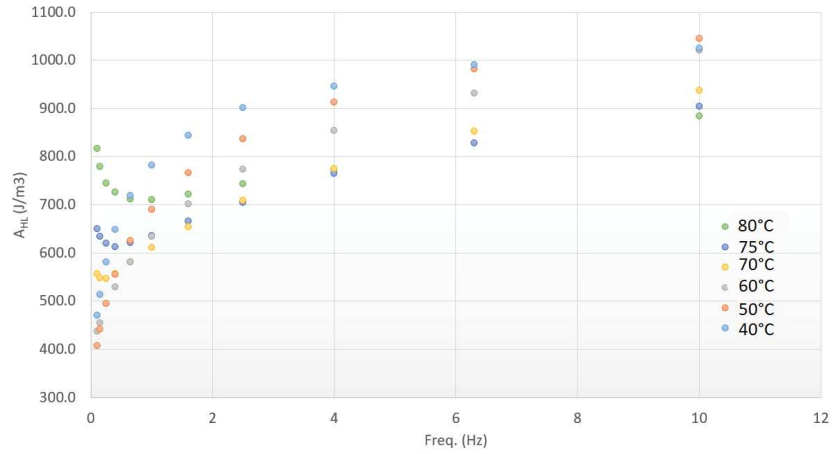

(c) PMMA

Figure 3.104: Evolution of A_{HL} with frequency for different temperatures used

The trend of the evolution of A_{HL} (figure 3.104) was observed to be similar to that of A_h (figure 3.103). This similarity in the evolution trend and the order of magnitude of areas verified that the numerical integration scheme of the hysteresis area is correctly carried out as well as the calculation of the loss modulus using the least square adjustment method.

Temp.(°C)	Freq.(Hz) / Polymer	0.1	0.15	0.25	0.4	0.65	1	1.6	2.5	4	6.3	10
35	PS	-	-	-	-	-	-	-	-	-	-	-
	PA-6.6	427.2	418.5	406	393.7	378.7	366	355.1	345.3	330.8	326.7	321.8
	PMMA	-	-	-	-	-	-	-	-	-	-	-
40	PS	137.7	134.7	136	134.5	134	132.9	133	130	137.3	129.7	128.9
	PA-6.6	486.2	485.2	475.4	DO	450.3	438.9	424.6	412.7	400.8	389.3	385.3
	PMMA	470.5	513	581	647.9	718.8	781.6	843.5	900.7	946	990.8	1025.1
45	PS	-	-	-	-	-	-	-	-	-	-	-
	PA-6.6	639.3	630.4	613	594.3	573.9	556.8	536.7	517.7	501.4	488.9	478
	PMMA	-	-	-	-	-	-	-	-	-	-	-
50	PS	164.8	158.8	159.3	159.8	159.5	161.2	160.9	161.8	156.5	160.3	169.9
	PA-6.6	773.7	752.8	726.7	701.6	676.5	653.5	629.4	609.1	584.7	568.6	554.2
	PMMA	407.4	442	495.3	555.4	624.9	689.9	766.6	836	912	981.2	1044.4
55	PS	-	-	-	-	-	-	-	-	-	-	-
	PA-6.6	836.4	806.6	789.4	773.7	751.7	732.4	709.8	688.2	670	654	636.7
	PMMA	-	-	-	-	-	-	-	-	-	-	-
60	PS	172.6	165.7	164.6	166.5	166.4	170.1	170.5	171.8	173.7	174.9	185.8
	PA-6.6	830.2	833.5	832.7	830.5	826.4	818	806.7	793.4	777.8	767.3	752
	PMMA	437.2	455.2	DO	528.8	581.2	634.7	701	772.9	853.3	931.4	1019.7
70	PS	231.4	221.7	213.3	209.4	206.6	206.5	204.8	205.9	202.9	206.3	201.4
	PA-6.6	-	-	-	-	-	-	-	-	-	-	-
	PMMA	556.9	548.5	546.6	557.1	580.5	610.7	654.4	709.5	775.5	852.6	936.6
75	PS	296.8	274.6	256	245.5	237.3	232.2	228.3	228.6	227.1	226.1	218.9
	PA-6.6	-	-	-	-	-	-	-	-	-	-	-
	PMMA	650.4	634.4	619.5	612.3	621.4	635.6	666	704.1	764.9	828.3	904.4
80	PS	380.9	355.4	326.1	309.2	294.7	286.1	283.8	276.7	279.7	277	280.4
	PA-6.6	-	-	-	-	-	-	-	-	-	-	-
	PMMA	815.8	779.1	745	725.7	711.2	710.7	721.2	743.8	773.4	DO	883.8
85	PS	470.8	405.4	345.5	310.8	285.1	268.4	258.5	251	232.6	244.8	243.2
	PA-6.6	-	-	-	-	-	-	-	-	-	-	-
	PMMA	-	-	-	-	-	-	-	-	-	-	-
90	PS	532.3	469.9	417.6	379.6	350.9	329.3	311.7	301.2	286.6	289.2	288.4
	PA-6.6	-	-	-	-	-	-	-	-	-	-	-
	PMMA	-	-	-	-	-	-	-	-	-	-	-

Table 3.19: Computed hysteresis area (A_{HL}) associated with loss modulus for all the three polymers in J/m^3

Fortunately, the hysteresis area calculated using the stress-strain data given by DMTA and the one computed using its relation with the loss modulus are consistent for all the three polymers. This consistency for these areas shows that the origin of hysteresis area may be attributed to either dissipation and/or stored energy variations induced by microstructural transformation during the loading cycles and in the latter case, the mechanical cycle can no longer be a thermodynamic cycle as explained by equation 2.36 in Chapter-2. Moreover, this helped us to verify, once again, that the numerical integration scheme of the hysteresis area is correctly carried out as well as the calculation of the loss modulus using the least square adjustment method.

Moreover the effect of dissipation on the mean temperature over a cycle variations can be computed using the simplified heat diffusion equation [8]:

$$\dot{\theta} + \frac{\theta}{\tau_{th}} = A_{hd} f / \rho C_p. \tag{3.25}$$

Here, it was assumed that the temperature remains stable. Therefore, using this equation, it was computed that the monotonous temperature drift remained less than 1/100°C in case of PS, which is currently experimentally unreachable via IR techniques and this is why we were not able to measure a significant mean temperature variations.

These image processing results for all the three polymers provided us a whole set of interesting observations, in particular PA-6.6 as this material is strongly dissipative even if the cyclic deformation is accompanied by non-negligible coupling effects [111]. It was also observed from table 3.20 that, in some cases, the hysteresis area associated to dissipation, computed for PS, is not consistent with the hysteresis area associated with loss modulus. This inconsistency of hysteresis areas could be associated because of the noise and/or the thermal regulation of the furnace. An example, at 40 °C and 1 Hz, can be seen in figure 3.105.

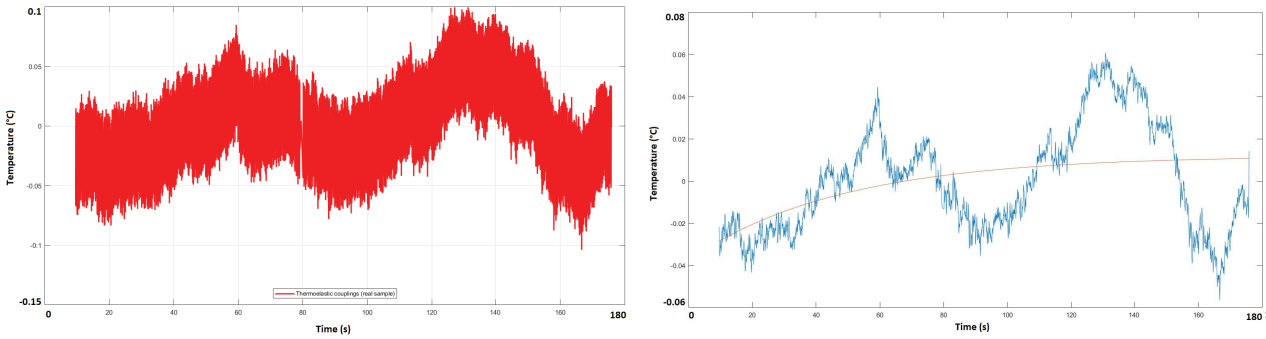

(a) (b)

Figure 3.105: (a) Thermoelastic couplings in the specimen under loading (b) Mean temperature of the specimen over a cycle

Figure 3.105(a) represents the thermoelastic couplings measured using thermography whereas figure 3.105(b) represents the mean temperature calculated over a cycle using the thermography data shown in figure 3.105(a). The dissipation was calculated by fitting an exponential on the mean temperature over a cycle for all the polymers and later used to compute the hysteresis

Temp.(°C)	Freq.(Hz) / Polymer	1	1.6	2.5	4	6.3	10
35	PS	-	-	-	-	-	-
	PA-6.6	283	327	236	187	260	253
	PMMA	-	-	-	-	-	-
40	PS	309	288	54	122	95	103
	PA-6.6	473	361	510	389	267	307
	PMMA	565	518	764	765	901	993
45	PS	-	-	-	-	-	-
	PA-6.6	549	567	348	481	494	404
	PMMA	-	-	-	-	-	-
50	PS	154	184	157	4	181	128
	PA-6.6	503	744	757	578	480	550
	PMMA	650	618	861	682	968	1037
55	PS	-	-	-	-	-	-
	PA-6.6	720	875	638	701	663	522
	PMMA	-	-	-	-	-	-
60	PS	159	218	96	40	138	151
	PA-6.6	795	834	690	742	774	704
	PMMA	349	551	639	756	766	900
70	PS	240	60	197	119	94	150
	PA-6.6	-	-	-	-	-	-
	PMMA	341	629	795	757	592	791
75	PS	262	167	118	151	238	133
	PA-6.6	-	-	-	-	-	-
	PMMA	667	403	570	368	840	671
80	PS	223	111	158	103	292	201
	PA-6.6	-	-	-	-	-	-
	PMMA	592	542	860	183	515	461
85	PS	403	335	285	244	9	217
	PA-6.6	-	-	-	-	-	-
	PMMA	-	-	-	-	-	-
90	PS	116	245	367	136	219	191
	PA-6.6	-	-	-	-	-	-
	PMMA	-	-	-	-	-	-

Table 3.20: Computed hysteresis area (A_{hd}) associated with dissipation for all the three polymers in J/m^3

area associated with this dissipation (table 3.20).

3.6 Conclusion of the chapter

In this chapter, we have presented the experimental framework and the characterization of the physical properties of the three polymers used. Next, we detailed the DMTA experimental devices used in different laboratories with the test parameters used each time. Measurements

made in these laboratories on the PS allowed us to compare the master curves obtained as well as the activation energies according to the Arrhenius law. Subsequently, the experimental setup used at the LMGC, Montpellier, was explained in detail, including all the precautions and corrections that were taken into account to perform the measurements, such as electronic phase shift correction, machine stiffness correction, clamps alignment and verification of the monochromatic response of the polymers. We then presented the results obtained, which were compared with those of the other laboratories, as well as the application of the TTSP hypothesis to predict the linear viscoelastic properties of all the polymers used in constructing the master curves. Finally, these DMTA measurements were complemented by synchronized thermal measurements of the specimen surface temperature during a test. The experimental setup used for these measurements was detailed, as well as the processing of the data and images used to carry out an energy balance.

The realization of DMTA approach and the application of TTSP on the obtained results allowed us to validate the Arrhenius law based on the applied horizontal shift factor (a_T), below the glass transition temperature. The development of method for DMTA measurements in LMGC was validated as well by comparing the results obtained in the different laboratories. Even a unique thermography setup was developed in LMGC during the DMTA measurements which allowed us to validate the hypothesis of standard DMTA i.e., the temperature of the furnace and the temperature of the specimen under cyclic loading remains same during the measurements. It also helped us to show the dominance of thermoelastic couplings over the dissipation during the cyclic measurements. The consistency of mechanical hysteresis area (A_h) and hysteresis area associated with the loss moduli (A_{HL}) validated the E" as the origin of the hysteresis area during the DMTA measurements.

The results obtained in this chapter are used in the following chapter 4 to model and identify polymer behaviour using the thermomechanical framework explained in chapter 2.

Chapter 4

Rheological analysis and thermomechanical modelling

Contents

List of symbols

E – Elastic modulus
η – Viscosity coefficient
τ – Relaxation time
σ_0 – Instantaneous stress
ε_0 – Instantaneous strain
ε – Strain
T_0, T – Initial temperature, Temperature
ψ – Helmholtz free energy potential
ϕ – Dissipation energy potential
σ^r – Reversible stress
σ_{ir} – Irreversible stress
ε_v – Viscous strain
f – Frequency
ω – Pulsation/Angular frequency
D^* – Complex tensile creep compliance
E^* – Complex tensile creep modulus
E' – Storage modulus
E'' – Loss modulus
α_{th} – Coefficient of therma expansion
θ – Temperature variations
s_0 – Volumic entropy
κ – Isotropic conduction coefficient
q – Heat influx vector
ρ – Density
C_p – Specific heat capacity
n_f – Number of loading frequencies
T_{ref} – Reference temperature
E'_{fit} – Identified storage modulus through modeling
E''_{fit} – Identified loss modulus through modeling
E'_{Exp} – Experimental storage modulus
E''_{Exp} – Experimental loss modulus
$\dot{w_{def}}$ – Deformation energy rate
$\dot{w}_d$ – Dissipated energy rate
$\dot{w_{thc}}$ – Thermomechanical coupling sources
$\dot{w_{the}}$ – Thermoelastic sources
d_1 – Dissipative sources

The modelling framework used is based on the phenomenological representation of the linear viscoelastic behaviour of materials. This modelling is also systematically immersed in the framework of generalized standard materials (GSM) presented in Chapter II. Rheological elements are classic tools for representing the viscoelastic behaviour of the materials by using the combination of spring-like and linear dashpot elements. The springs are the elements which are characterized by their rigidity (i.e. E the elastic modulus) and the dashpots by their viscosity (i.e. η the viscosity damping coefficient). The elastic and viscous coefficients are related to the characteristic time or relaxation time by the mathematical formulation shown below by equation 4.1,

$$\tau = \frac{\eta}{E} \tag{4.1}$$

where τ is relaxation time. The first link with thermodependence of the mechanical viscoelastic behavior is often (mainly) introduced using this relaxation time. Temperature occurrence can be related through a thermo-activation law, where, the temperature generally boosts the viscous deformation mechanisms. The relaxation time then becomes a function of the temperature i.e., $\tau(T)$. This means that E and η are both (i.e. not independently) dependant on the temperature.

Chapter IV is dedicated to the introduction and use of the mechanical analog elements along with their combinations so called rheological models. We particularly used the generalized Maxwell model identified using experimental mechanical results that are presented in Chapter III. The structure of this model offers a broad class of linear viscoelastic behaviors. It also allowed us to define a sufficient mathematical condition for this generalized Maxwell model to be compatible with the time-temperature superposition principle (TTSP) or as it is said in France, time-temperature equivalence.

Once mechanically identified, the mechanical and energy predictions deriving from these models were then later discussed and compared with the experimental results obtained during DMTA and thermographic thermal measurements. Naturally, these identified generalized Maxwell models were previously included in the GSM formalism, in order to define and compute the different coupling and dissipation heat sources.

4.1 Rheological elements and elementary models

Currently, there are two rheological elements used to describe isothermal linear viscoelasticity: the spring and the dashpot. If we take into account the thermodilatable nature of the materials, we will add a 3rd element to describe this strong thermomechanical coupling. Naturally, in this case, it will be necessary to remove the isothermal frame of the viscoelasticity. These rheological elements are then assembled, in series, in parallel, in any way,... to build models. The objective is that these models reproduce as accurately as possible the (thermo)mechanical responses of the materials, that we've been able to observe.

4.1.1 Hookean spring

Hookean spring is the simplest mechanical model which is purely elastic with all inertial effects neglected. If a spring is subjected to an instantaneous stress σ_0, it will respond instantaneously with a strain ε_0, which leads us to write:

$$\sigma_0 = E\varepsilon_0 \tag{4.2}$$

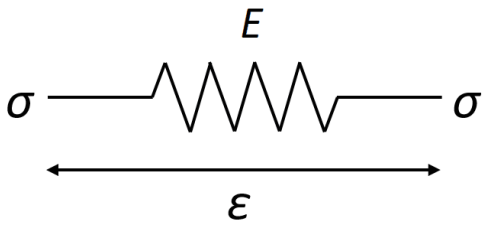

Figure 4.1: Representation of a hookean spring element

The Hookean spring is shown graphically in figure 4.1. The application of instantaneous load will lead to produce no oscillations, but only a constant strain (no inertia).

From an energy standpoint, it signifies the entire deformation energy as the stored energy with zero dissipation. This finding allows us to implement the spring element into GSM framework. The state variables considered are $T = T_0, \varepsilon$. The free energy and dissipation potential can simply be written as,

$$\psi(T = T_0, \varepsilon) = \frac{1}{2}E\varepsilon^2 \tag{4.3}$$

$$\phi(\dot{\varepsilon}) = 0 \tag{4.4}$$

which allows us to write state law and complementary law as:

$$\sigma^r = \frac{\partial \psi}{\partial \varepsilon} = E\varepsilon \tag{4.5}$$

$$\sigma^{ir} = \frac{\partial \phi}{\partial \dot{\varepsilon}} = 0 \tag{4.6}$$

As in the standard framework $\sigma = \sigma^r + \sigma^{ir}$ (cf.Chap.II), we find here naturally $\sigma = \sigma^r = E\varepsilon$. From an energy standpoint, the spring element reversibly stores the mechanical deformation energy provided during loading. It renders this energy in its entirety in mechanical form during the unloading.

4.1.2 Linear dashpot

Linear viscosity introduces a linear relationship between the stress developed by the dash-pot and its strain rate. The corresponding rheological element is symbolically shown in figure 4.2.

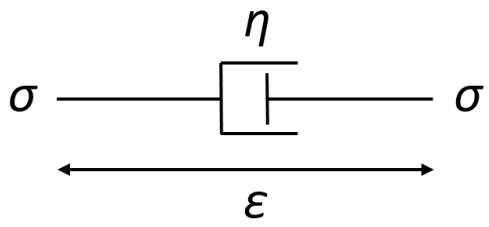

Figure 4.2: Representation of a dash-pot element

The behavioural constitutive equation is simply written as:

$$\sigma = \eta \frac{d\varepsilon}{dt} \tag{4.7}$$

This dashpot element acts as a piston in a cylinder filled with a liquid of viscosity η. Integration of Equation 4.7 for constant stress σ_0, gives

$$\varepsilon(t) = \frac{\sigma_0}{\eta} t \tag{4.8}$$

if naturally $\varepsilon(0) = 0$ in the initial state.

It is the then possible to reproduce the effects of an unlimited creep (fluid type material) with such a simple element. Energetically and contrary to the Hookean spring, the dash-pot dissipates entire deformation energy with zero stored (released) mechanical energy during load (unload). Under the hypothesis of isothermal transformation, these dissipated energy is definitely lost. In the case of anisothermal transformation, the dissipated heat is partly stored and increases the internal energy of the material, this part depending on the values of the mass density, specific heat and diffusivity of the material. For the moment, to implement the dashpot into GSM framework, the state variables taken are $T = T_0, \varepsilon$. The hypothesis of an isothermal transformation is temporarily done for the sake of simplicity. Note however that the temperature has to be introduced as state variable in as much as the free energy potential is the Legendre transform of the internal energy with respect to the couple (entropy, temperature). The selection of state variables leads us to write the free energy and dissipation potential as:

$$\psi(T = T_0, \varepsilon) = 0 \tag{4.9}$$

$$\phi(\dot{\varepsilon}) = \frac{1}{2} \eta \dot{\varepsilon^2} \tag{4.10}$$

and the state law and complementary law can be immediately derived as,

$$\sigma^r = \frac{\partial \psi}{\partial \varepsilon} = 0 \tag{4.11}$$

$$\sigma^{ir} = \frac{\partial \phi}{\partial \dot{\varepsilon}} = \eta \dot{\varepsilon} \tag{4.12}$$

As previously reminded, $\sigma = \sigma^r + \sigma^{ir}$ in the GSM framework, then we find the classical viscous stress-strain rate law: $\sigma = \sigma^{ir} = \eta \dot{\varepsilon}$.

4.1.3 Maxwell model

A single spring or dashpot is, of course, not enough to represent the mechanical behaviour of the polymeric materials. As a result, combination of a spring and a dashpot in series was proposed by J.C. Maxwell [112] for a better approximation of representation of mechanical behaviour of viscoelastic media. It is schematically shown in figure 4.3.

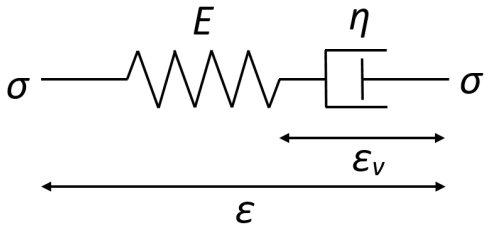

Figure 4.3: Representation of Maxwell model

From a rheological standpoint, the constitutive equation for the Maxwell model is a combination of linear viscous and perfectly elastic behaviour as shown in equation 4.13.

$$\frac{d\varepsilon}{dt} = \frac{1}{E}\frac{d\sigma}{dt} + \frac{\sigma}{\eta} \tag{4.13}$$

This equation simply depicts the fact that the overall strain rate is split into elastic and viscous ones (series model). When a sinusoidal stress is developed by the Maxwell model, the strain response is also sinusoidal but out of phase with the stress by angle δ. Therefore,

$$\sigma(t) = \sigma_0 e^{i\omega t} \tag{4.14}$$

where σ_0 represents the amplitude of the stress and ω represents the angular frequency (also named pulsation). Using equation 4.13, it yields

$$\frac{d\varepsilon(t)}{dt} = \frac{\sigma_0}{E} i\omega e^{i\omega t} + \frac{\sigma_0}{\eta} e^{i\omega t} \tag{4.15}$$

Integrating equation 4.14 and 4.15 between time limits t_1 and t_2 and then dividing the outcome, we get:

$$\frac{\varepsilon(t_2) - \varepsilon(t_1)}{\sigma(t_2) - \sigma(t_1)} = D - i\frac{D}{\tau\omega} = D^* \tag{4.16}$$

where D^* is the complex tensile creep compliance. Since E^* is the reciprocal of D^*, therefore, we can write:

$$E^* = \frac{1}{D - i\dfrac{D}{\tau\omega}} = \frac{\tau\omega E}{\tau\omega - i} \tag{4.17}$$

using complex conjugate, it yields:

$$E^* = \frac{E\tau^2\omega^2}{1 + \tau^2\omega^2} + \frac{iE\tau\omega}{1 + \tau^2\omega^2} = E' + iE" \tag{4.18}$$

We can, then derive that:

$$E' = \frac{E\tau^2\omega^2}{1 + \tau^2\omega^2} \tag{4.19}$$

$$E" = \frac{E\tau\omega}{1 + \tau^2\omega^2} \tag{4.20}$$

Equations 4.19 and 4.20 clearly show that the storage modulus E' and loss modulus $E"$ both depend on the pulsation along with the relaxation time τ and the elastic modulus E. It is worth noting that these famous so-called "dynamic" moduli carry a strong energy content within them via their name. The storage associated with E' evokes the reversible mechanical energy stored in the spring, while the loss associated with $E"$ clearly refers the mechanical energy dissipated by the dashpot.

The Maxwell model can naturally be implemented in the GSM framework. Still under an isothermal approximation, the state variables considered in this case are $T = T_0, \varepsilon, \varepsilon_v$. Using

the definition of the free energy and dissipation potential for each element, the free energy and dissipation potential associated with the Maxwell model can then be written as:

$$\psi(T = T_0, \varepsilon, \varepsilon_v) = \frac{1}{2}E(\varepsilon - \varepsilon_v)^2 \tag{4.21}$$

$$\phi(\dot{\varepsilon}, \dot{\varepsilon_v}) = \frac{1}{2}\eta\dot{\varepsilon}_v^2 \tag{4.22}$$

These energy and dissipation potentials allow us to derive the state laws (equation 4.23) and complementary laws (equation 4.24) as:

$$\sigma^r = E(\varepsilon - \varepsilon_v) \tag{4.23a}$$

$$A_v = \frac{\partial\psi}{\partial\varepsilon_v} = -\sigma^r \tag{4.23b}$$

$$\sigma^{ir} = 0 \tag{4.24a}$$

$$X_v = \frac{\partial\phi}{\partial\dot{\varepsilon_v}} = \eta\dot{\varepsilon_v} \tag{4.24b}$$

Taking into account the standard equations $\sigma = \sigma^r + \sigma^{ir}$ and $A_v = -X_v$, we naturally find the classical rheological equations associated with a series model: $\sigma = E(\varepsilon - \varepsilon_v) = \eta\dot{\varepsilon_v}$ from which we can derive the overall differential equation shown in equation 4.13.

4.1.4 Kelvin-Voigt model

Another basic model, named Kelvin-Voigt, consists of a spring and a dashpot in parallel unlike Maxwell model. This model is also frequently used for predicting some viscoelastic behaviours. The arrangement of spring and dashpot in this model is shown in figure 4.4.

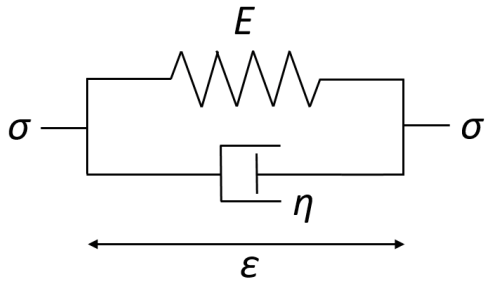

Figure 4.4: Representation of Kelvin-Voigt model

This model is designed in a way that strain must be the same in both elements which leads us to the fact that the stress then must be the sum of the individual stress developed by each

element. Therefore, the fundamental rheological equation for Kelvin-Voigt model is given by:

$$\sigma(t) = E\varepsilon(t) + \eta\frac{d\varepsilon(t)}{dt} \tag{4.25}$$

When a monochromatic cyclic strain is applied,

$$\varepsilon(t) = \varepsilon_0 e^{i\omega t}, \tag{4.26}$$

where, ε_0 represents the strain amplitude, we get, using equation 4.26, a stress response in the following form:

$$\sigma(t) = E\varepsilon_0 e^{i\omega t} + i\omega\eta\varepsilon_0 e^{i\omega t} \tag{4.27}$$

The complex modulus can be the written as:

$$E^* = E + i\omega\eta \tag{4.28}$$

Since, $E^* = E' + iE''$, we can write the storage and loss moduli respectively as follows:

$$E' = E \tag{4.29}$$

$$E'' = \eta\omega \tag{4.30}$$

which shows the independence of E' from loading frequency contrary to the loss modulus E". Moreover this model gives an illustration of what can be a simple stress decomposition into reversible and irreversible parts. Indeed, the combination of the mechanical analogues in parallel can be implemented in GSM framework as well. The state variables considered in this case are $T = T_0, \varepsilon$ and the helmholtz free energy and dissipation potential are written as:

$$\psi(T = T_0, \varepsilon) = \frac{1}{2}E\varepsilon^2 \tag{4.31}$$

$$\phi(\dot{\varepsilon}) = \frac{1}{2}\eta\dot{\varepsilon}^2 \tag{4.32}$$

The state laws and the complementary laws can be then written as,

$$\sigma^r = E\varepsilon \tag{4.33}$$

$$\sigma^{ir} = \eta\dot{\varepsilon} \tag{4.34}$$

The stress decomposition in reversible and irreversible parts is here equivalent to the stress decomposition of this simplest series model. We naturally get the overall differential rheological equation: $\sigma = E\varepsilon + \eta\dot{\varepsilon}$ as initially introduced in equation 4.25.

4.1.5 Zener Model

More complex associations of rheological elements can be proposed. For instance, the Zener model is the viscoelastic rheological system (figure 4.5), which is the combination of two Hookean springs and a dashpot. A spring is placed in parallel with a Maxwell branch.

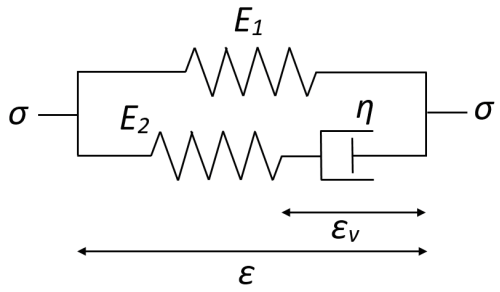

Figure 4.5: Representation of Zener model

This viscoelastic rheological system realizes two following physical relations:

$$\sigma = \sigma_1 + \sigma_2 \tag{4.35a}$$

$$\varepsilon = \varepsilon_1 = \varepsilon_2 \tag{4.35b}$$

where index '1' and '2' corresponds to the two branches of the Zener model.

In the two following sub-sections, the viscoelastic behaviour of Zener model will be derived without and with considering the temperature variations in the modeling. In the case of anisothermal processes, the thermoelastic coupling will also be considered by introducing a new rheological component.

4.1.5.1 Isothermal Zener Model

As the Zener model follows the physical relation given by equation 4.35a, using the relation $\sigma_1 = E_1\varepsilon$ and $\sigma_2 = \eta(\dot{\varepsilon} - \dot{\varepsilon_e})$, σ can be written as follows:

$$\sigma = E_1\varepsilon + \eta(\dot{\varepsilon} - \dot{\varepsilon_e}) \tag{4.36}$$

$$\sigma = E_1\varepsilon + \eta(\dot{\varepsilon} - \frac{\sigma_2}{E_2}) \tag{4.37}$$

where, σ_2 represents the stress developed in branch 2. We also can write:

$$\sigma = E_1\varepsilon + \eta(\dot{\varepsilon} - \frac{(\dot{\sigma} - \dot{\sigma_1})}{E_2}) \tag{4.38}$$

where, σ_1 refers to the stress in branch 1.

$$\sigma = E_1\varepsilon + \eta\dot{\varepsilon} - \frac{\eta\dot{\sigma}}{E_2} + \frac{\eta E_1\dot{\varepsilon}}{E_2} \tag{4.39}$$

Equation 4.39 can be rearranged by using $\tau = \frac{\eta}{E_2}$ as,

$$\sigma + \tau\dot{\sigma} = E_1\varepsilon + \eta\dot{\varepsilon} + \tau E_1\dot{\varepsilon} \tag{4.40}$$

This last differential equation is the overall behavioral equation linking stress and stress rate to stain and strain rate, eliminating the presence of the internal state variables. As we know that, for linear viscoelastic system, the general cyclic loading response can be expressed in terms of E' and E" as follows:

$$\sigma = E'\varepsilon_0 sin\omega t + E"\varepsilon_0 cos\omega t, \tag{4.41}$$

on substituting equation 4.41 in 4.40, we can get,

$$E'sin\omega t + E"cos\omega t + \tau E'\omega cos\omega t - \tau E"\omega sin\omega t = Esin\omega t + \omega cos\omega t(\eta + \tau E). \tag{4.42}$$

On comparing left and right hand side of equation 4.42, we can write,

$$E' - \tau E"\omega = E \tag{4.43a}$$

$$E" + \tau E'\omega = (\eta + \tau E)\omega \tag{4.43b}$$

multiplying equation 4.43b with $\tau\omega$ and adding with equation 4.43a, we get

$$E' = E_1 + \frac{E_2\omega^2\tau^2}{1+\omega^2\tau^2} \tag{4.44a}$$

$$E" = \frac{E_2\omega\tau}{1+\omega^2\tau^2} \tag{4.44b}$$

We can see that both storage and loss modules are depending on the loading frequency. For such a model, the state variables are ε, ε_v, and the free energy and the dissipation potential can be written as:

$$\psi = \frac{E_1}{2}\varepsilon^2 + \frac{E_2}{2}(\varepsilon - \varepsilon_v)^2 \tag{4.45a}$$

$$\phi = \frac{\eta}{2}\dot{\varepsilon_v}^2 \tag{4.45b}$$

The constitutive equations can be written as:

$$\sigma^r = \frac{\partial\psi}{\partial\varepsilon} = E_2(\varepsilon - \varepsilon_v) + E_1\varepsilon \tag{4.46a}$$

$$\sigma^{ir} = \frac{\partial\phi}{\partial\dot{\varepsilon}} = 0 \tag{4.46b}$$

$$A_v = \frac{\partial\psi}{\partial\varepsilon_v} = -E_2(\varepsilon - \varepsilon_v) \tag{4.46c}$$

$$X_v = \frac{\partial\phi}{\partial\dot{\varepsilon_v}} = \eta\dot{\varepsilon_v} \tag{4.46d}$$

The Zener model (like Maxwell's model previously) therefore provides a minimal framework where the E' and E" modules are loading frequency (time) dependent. To get to a behavioural framework, where the time-temperature equivalence can be analyzed, the temperature and its effects on the mechanical behaviour must now be gradually introduced.

4.1.5.2 Anisothermal Zener model

From the energy standpoint, it is important to take into account the temperature as an internal state variable for presenting the behavioural difference of Zener model considering thermal effects. Besides, the elastic spring was replaced by the thermoelastic branch to add in the model the important thermo-dilatation effects of polymeric materials inducing a strong thermomechanical coupling. The models basic sketch is plotted in figure 4.6.

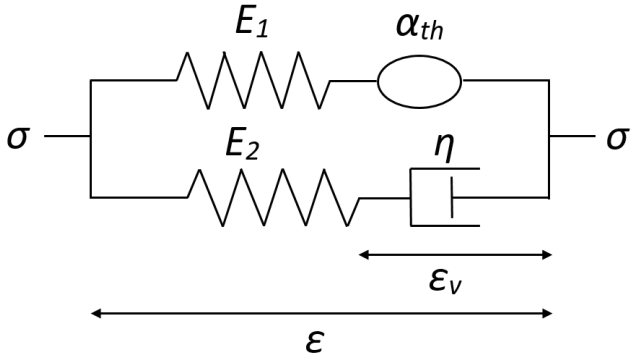

Figure 4.6: Representation of Thermo-visco-elastic Zener model

The rheological equation of branches 1 and 2 respectively becomes: $\sigma_1 = E_1\varepsilon - \alpha_{th}\theta$ and $\sigma_2 = \eta\dot{\varepsilon_v} = E_2(\varepsilon - \varepsilon_v)$. Therefore, equation 4.38 can be rewritten as:

$$\sigma = E_1\varepsilon - \alpha_{th}\theta + \eta\dot{\varepsilon_v} \tag{4.47}$$

Since, the stress will be the same in both the components of branch 2, Equation 4.47 becomes:

$$\sigma = E_1\varepsilon - \alpha_{th}\theta + \eta\dot{\varepsilon} - \eta\frac{\dot{\sigma_2}}{E_2} \tag{4.48}$$

or in an equivalent way,

$$\sigma = E_1\varepsilon - \alpha_{th}\theta + \eta\dot{\varepsilon} - \frac{\eta}{E_2}(\dot{\sigma} - \dot{\sigma_1}) \tag{4.49}$$

Introducing $\tau = \dfrac{\eta}{E_2}$, we can get:

$$\sigma + \tau\dot{\sigma} = E_1\varepsilon + (\eta + \tau E_1)\dot{\varepsilon} - \alpha_{th}\theta - (\tau\alpha_{th}\dot{\theta}) \tag{4.50}$$

The equation 4.50 shows the overall rheological behaviour of the visco-thermo-elastic Zener model and it can be observed on comparing with equation 4.40 that the introduction of the thermo-dilatation notably changes the behavior.

For such models, the state variables chosen are θ the temperature variation, ε the strain and ε_v the viscous part of the strain. The volume free energy and the dissipation potential associated with this model can be written as :

$$\psi = \frac{E_1}{2}(\varepsilon - \alpha_{th}\theta)^2 - (\frac{E_1\alpha_{th}^2}{2} + \frac{\rho C_p}{2T_0})\theta^2 - s_0\theta + \frac{E_2}{2}(\varepsilon - \varepsilon_v)^2 \tag{4.51}$$

$$\phi = \frac{q \cdot q}{2\kappa} + \frac{\eta}{2}\dot{\varepsilon_v}^2 \tag{4.52}$$

where s_0 represents the volume entropy associated with the initial state (θ, ε, ε_v) = (0, 0, 0), κ is the isotropic conduction coefficient and q is the heat influx vector respectively.

The state and complementary laws are:

$$s = -\frac{\partial\psi}{\partial T} = (E_1\alpha_{th}^2 + \frac{\rho C_p}{T_0})\theta + s_0 - \frac{E_1}{2}\alpha_{th}(\varepsilon - \alpha_{th}\theta) \tag{4.53a}$$

$$X_q = \frac{\partial\phi}{\partial q} = -\frac{gradT}{T} \tag{4.53b}$$

$$\sigma^r = \frac{\partial\psi}{\partial\varepsilon} = E_1(\varepsilon - \alpha_{th}\theta) + E_2(\varepsilon - \varepsilon_v) \tag{4.53c}$$

$$\sigma^{ir} = \frac{\partial\phi}{\partial\dot{\varepsilon}} = 0 \tag{4.53d}$$

$$A_v = \frac{\partial\psi}{\partial\varepsilon_v} = -E_2(\varepsilon - \varepsilon_v) \tag{4.53e}$$

$$X_v = \frac{\partial\phi}{\partial\dot{\varepsilon_v}} = \eta\dot{\varepsilon} \tag{4.53f}$$

Following the subsection 2.2. of Chapter 2, the heat diffusion equation for this visco-thermo-elastic Zener model can be written as:

$$\rho C_p(\dot{\theta} + \frac{\theta}{\tau_{th}}) = -E_1\alpha_{th}T_0(\dot{\varepsilon} - \dot{\varepsilon_v}) + \eta\dot{\varepsilon_v}^2 \tag{4.54}$$

The right hand side member of equation 4.54 shows the heat sources related to the viscous dissipation and thermoelastic couplings. Let us remember that the dissipation source is always positive while the thermoelastic source changes sign at each loading inversion.

It must finally be noted that the possible thermo-dependence of the elastic and viscous parameters of the model has not yet been introduced. This will be done in the next subsection, where the generalized Maxwell model will also be used in a anisothermal context. However, we want to be able to use in what follows, as is done in the literature, the highest degree of generality of such a model. The mechanical equivalence of all viscoelastic models whose thermodynamic and dissipation potentials are symmetric positive definite bilinear functions of the state variables and their flux respectively, deserves to be reminded (Biot's models [62]). That's the reason why, the thermo-dilatation effect will be conversely no longer considered when using the generalized Maxwell model even if temperature variations can be considered. Indeed, it has been already observed [78] that the introduction of such a strong coupling make the thermomechanical equivalence between series (i.e. Poynting-Thomson model) and parallel models (i.e. Zener model) invalid.

4.2 Generalized Maxwell model

4.2.1 Introduction

Generalized Maxwell model is one of the most general form of rheological models which is generally used in the literature for modeling the linear viscoelastic behaviour of the polymers [113, 114, 115, 116, 117, 118]. The thermo-dependence is introduced considering the temperature as a controlled parameter. The material temperature is then approximated by the environmental temperature (testing room, furnace, ...). Neither self-heating induced by dissipation nor temperature variations induced by strong thermomechanical couplings are considered. This model consists of several (theoretically, an infinity of...) viscoelastic Maxwell branches connected in parallel. This generalized form of Maxwell model considers that the relaxation occurs in certain set of times instead of occurring at a single characteristic time. This set defines the so-called relaxation time spectrum. This time distribution represents the less contribution of the shorter molecular segments than the longer molecular segments. A schematic representation of the generalized Maxwell model is shown in figure 4.7.

As usual for parallel models, the stress of a $n_b + 2$ branches model ($n_b \in \mathbf{N}$) is decomposed in the following additive form:

$$\sigma = \sigma_0 + \sigma_1 + \cdots + \sigma_i + \cdots + \sigma_{n_b} + \sigma_{n_b+1} \tag{4.55}$$

where, $\sigma_i = \eta_i \dot{\varepsilon}_{vi}$, for each viscoelastic branch ($0 < i < n_b + 1$). For such a branch, we define the viscous strain ε_{vi} and the relaxation time $\tau_i = \frac{\eta_i}{E_i}$. Note that the model includes the possibility of a "pure" elastic branch (modulus E_0) and a "pure" viscous branch (viscosity η_{n_b+1}).

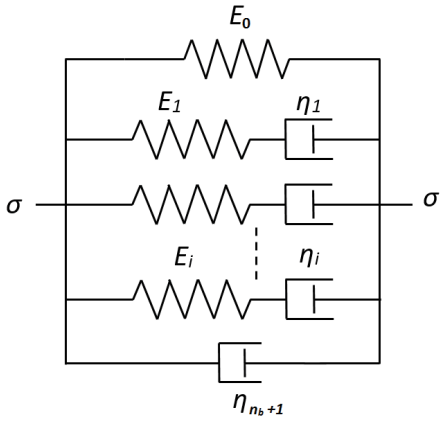

Figure 4.7: Representation of Generalized Maxwell model

We will come back later to the introduction of these 2 particular branches in the generalized Maxwell model. For now we will simply point out that these branches can be interpreted as classic viscoelastic branches for which the viscosity η_0 would tend towards infinity (i.e. $\tau_0 \to \infty$) as well as E_{n_b+1} for the viscous branch (i.e. $\tau_{n_b+1} \to 0$).

The linear viscoelastic behaviour of this model could be presented in terms of dynamic moduli i.e., storage and loss modulus, by the following equations:

$$E'(T,\omega) = E_0(T) + \sum_{i=1}^{n_b} \frac{E_i(T)\tau_i^2(T)\omega^2}{1+\tau_i^2(T)\omega^2} \tag{4.56a}$$

$$E"(T,\omega) = \sum_{i=1}^{n_b} \frac{E_i(T)\tau_i(T)\omega}{1+\tau_i^2(T)\omega^2} + \eta_{n_b+1}(T)\omega \tag{4.56b}$$

By analyzing the contributions to $E'(T,\omega)$ and $E"(T,\omega)$ of each viscoelastic branch, we can verify that the previous interpretations, made in terms of relaxation time on the "pure" elastic and viscous branches, are consistent.

In the GSM framework, the generalized Maxwell model could be represented by the following volume free energy and dissipation potentials:

$$\psi(T,\varepsilon,\varepsilon_{vi}) = \frac{1}{2}E_0(T)\varepsilon^2 + \frac{1}{2}\sum_{i=1}^{n_b} E_i(T)(\varepsilon-\varepsilon_{vi})^2 - \frac{\rho C_p}{2T_0}\theta^2 \tag{4.57}$$

$$\phi(\dot{\varepsilon},\dot{\varepsilon}_{vi},q;T) = \frac{1}{2}\sum_{i=1}^{n_b}\eta_i(T)\dot{\varepsilon}_{vi}^2 + \frac{1}{2}\eta_{n_b+1}(T)\dot{\varepsilon}^2 + \frac{q.q}{2\kappa T} \tag{4.58}$$

The state and complementary laws read:

$$s = -\frac{\partial\psi}{\partial T} = -\frac{1}{2}\frac{dE_0(T)}{dT}\varepsilon^2 - \frac{1}{2}\sum_{i=1}^{n_b}\frac{dE_i(T)}{dT}(\varepsilon-\varepsilon_{vi})^2 + \frac{\rho C_p}{T_0}\theta \tag{4.59a}$$

$$X_q = \frac{\partial \phi}{\partial q} = -\frac{grad(T)}{T} \tag{4.59b}$$

$$\sigma^r = \frac{\partial \psi}{\partial \varepsilon} = E_0(T)\varepsilon + \sum_{i=1}^{n_b} E_i(T)(\varepsilon - \varepsilon_{vi}) \tag{4.59c}$$

$$\sigma^{ir} = \frac{\partial \phi}{\partial \dot{\varepsilon}} = \eta_{n_b+1}\dot{\varepsilon} + \sum_{i=1}^{n_b} \eta_i \dot{\varepsilon}_{vi} \tag{4.59d}$$

$$A_{v_i} = \frac{\partial \psi}{\partial \varepsilon_{v_i}} = -E_i(T)(\varepsilon - \varepsilon_{v_i}) \text{ for } i = 1, .., n_b \tag{4.59e}$$

$$X_{v_i} = \frac{\partial \phi}{\partial \dot{\varepsilon}_{v_i}} = \eta_i \dot{\varepsilon}_{v_i} \text{ for } i = 1, .., n_b \tag{4.59f}$$

Following subsection 2.2 of Chapter 2, the simplified (i.e. differential) heat diffusion equation can be written in the following compact form:

$$\rho C_p(\dot{\theta} + \frac{\theta}{\tau_{th}}) = d_1 + \dot{w_{the}} \tag{4.60}$$

where, $\theta = T - T_0$ is the temperature variation with respect to a reference temperature (room, furnace) supposed to be constant throughout the test. The terms d_1 and $\dot{w_{the}}$ represent in turn, the intrinsic dissipation source and the thermomechanical coupling sources. These sources can be written as:

$$d_1 = \eta_{n_b+1}(T)\dot{\varepsilon}^2 + \sum_{i=1}^{n_b} \eta_i(T)\dot{\varepsilon}_{v_i}^2 \tag{4.61a}$$

$$\dot{w_{thc}} = T\frac{dE_0(T)}{dT}\varepsilon\dot{\varepsilon} + \sum_{i=1}^{n_b} T\frac{dE_i(T)}{dT}(\varepsilon - \varepsilon_{v_i})(\dot{\varepsilon} - \dot{\varepsilon}_{vi}) \tag{4.61b}$$

where, $\varepsilon = \varepsilon_0 \sin \omega t$ and $\dot{\varepsilon} = \varepsilon_0 \omega \cos \omega t$ in the case of a monochromatic strain-controlled symmetric cyclic test.

4.2.2 Discussion about the TTSP

With the modelling framework now defined, it is then possible to analyze, what could be the consequences of applying the time-temperature superposition principle. For monochromatic cyclic test, this principle claims that, for a given mechanical behaviour, defined by two dynamic moduli at"low" temperature and "low" loading frequency, there exists an equivalent mechanical behaviour, defined by the same couple of dynamic moduli at "high" temperature and "high" loading frequency. In other words, this behavioural equivalence from a mechanical

standpoint can be mathematically defined by:

$$E'(T_0, \omega_0) = E'(T, \omega) \tag{4.62a}$$

$$E''(T_0, \omega_0) = E"(T, \omega) \tag{4.62b}$$

where (T_0, ω_0) represents the couple at, for instance,"low" temperature and pulsation and (T, ω) the couple at "high" temperature and pulsation.

Now, consider the mathematical expressions of dynamic moduli E' and E'' in equation 4.56a and 4.56b and particularly the contributions of each viscoelastic branch "i". For such a branch, if we apply TTSP consequences (equations 4.62), we get the following relations:

$$E_i(T_0, \omega_0)\frac{\tau_i^2(T_0)\omega_0^2}{1+\tau_i^2(T_0)\omega_0^2} = E_i(T, \omega)\frac{\tau_i^2(T)\omega^2}{1+\tau_i^2(T)\omega^2} \tag{4.63}$$

$$E_i(T_0, \omega_0)\frac{\tau_i(T_0)\omega_0}{1+\tau_i^2(T_0)\omega_0^2} = E_i(T, \omega)\frac{\tau_i(T)\omega}{1+\tau_i^2(T)\omega^2} \tag{4.64}$$

Multiplying now equation 4.64 by $\tau_i(T_0)\omega_0$, we obtain:

$$E_i(T_0, \omega_0)\frac{\tau_i^2(T_0)\omega_0^2}{1+\tau_i^2(T_0)\omega_0^2} = E_i(T, \omega)\frac{\tau_i(T)\omega\tau_i(T_0)\omega_0}{1+\tau_i^2(T)\omega^2} \tag{4.65}$$

Finally, if $E_i(T, \omega) > 0$, equation 4.65 and equation 4.63 lead to $\tau_i(T)\omega = \tau_i(T_0)\omega_0$, whatever the relaxation time spectrum and its temperature evolution. In order to get the correspondence between (T, ω) and (T_0, ω_0) satisfying equation 4.62, it is sufficient to introduce a unique function of the temperature, the famous shift factor $a_T(T)$ with respect to the reference temperature T_0, so that:

$$\tau_i(T) = \frac{\tau_i(T_0)}{a_T(T)} \tag{4.66}$$

and then,

$$\omega = a_T(T)\omega_0 \tag{4.67}$$

In equation 4.66, we recognize the characteristics of so called *thermo-rheologically simple* materials already evoked in Chapter 1. We stress on the fact that we have highlighted here a sufficient condition to achieve a time-temperature equivalence of the mechanical behaviour. In this approach, we did not consider the two extreme cases of pure viscous and pure elastic branches. In the identification work that follows, we will come back to how we identified the

parameters corresponding to these two particular branches. We can already point out that equation 4.66 could be qualitatively "verified" (from a numerical standpoint) when τ tends towards zero or infinity.

4.2.3 Identification procedure

Maxwell's generalized model therefore provides a broad and flexible modeling framework. Its wide application field comes from its structure which makes it equivalent to any other structure of linear viscoelastic model and its flexibility or adaptability comes from the very many degrees of freedom it offers by multiplying the number of viscoelastic branches on demand.

To be compatible with the TTSP, we have just seen that a sufficient condition is that the relaxation times are linked by the same temperature-dependent law (the shift factor $a_T(t)$ of thermo-rheologically simple materials). This condition reduces drastically the number of degrees of freedom of the model since the evolution of the elastic moduli and viscosity coefficients with temperature are no longer arbitrary.

On the other hand, a re-assuring point about the possibility of identifying a Maxwell model for the three polymers studied in Chapter III, is that the existence of a slip factor according to an Arrhenius law was considered as reasonable, and even good, particularly for the PS and PA-6.6. For each material we experimentally identified an activation energy for a given reference temperature below the glass transition temperature of the material.

Our objective is now to implement a procedure to identify the parameters of Maxwell's generalized model using the E' and E'' measurements made in Chapter 3 on PS, PA 6.6 and PMMA specimens, during cycles at different loading frequencies and furnace temperatures.

For this attempt of identification, it is important to highlight an important hypothesis. To make this identification, we assumed that the temperature of the material remained close to the environmental temperature (furnace temperature). The experimentally observed small temperature variations induced by dissipation and thermomechanical couplings, allowed us to do this.

Equations 4.56a and 4.56b give the shape of the linear system to be solved. The parameters of the model to be identified are E_i, $i = 0, ..., n_b$ and η_{n_b+1}. The set of relaxation times $\tau_i, i = 1, ..., n_b$ will be given *a priority* as well as the number of branches $n_b + 2$ of the model. These last degrees of freedom will be considered as fitting parameters during the comparison of numerical predictions with experimental results. They will be updated at each new testing temperature.

The linear system to be solved for each temperature $T_k, k = 1, .., n_T$ is therefore of the form:

$$\begin{bmatrix} 1 & \frac{\tau_1^2\omega_1^2}{1+\tau_1^2\omega_1^2} & \cdots & \frac{\tau_{n_b}^2\omega_1^2}{1+\tau_1^2\omega_1^2} & 0 \\ \vdots & \vdots & \cdots & \vdots & \vdots \\ 1 & \frac{\tau_1^2\omega_{n_f}^2}{1+\tau_1^2\omega_{n_f}^2} & \cdots & \frac{\tau_{n_b}^2\omega_{n_f}^2}{1+\tau_{n_b}^2\omega_{n_f}^2} & 0 \\ 0 & \frac{\tau_1\omega_1}{1+\tau_1^2\omega_1^2} & \cdots & \frac{\tau_{n_b}\omega_1}{1+\tau_1^2\omega_1^2} & \omega_1 \\ \vdots & \vdots & \cdots & \vdots & \vdots \\ 0 & \frac{\tau_1\omega_{n_f}}{1+\tau_1^2\omega_{n_f}^2} & \cdots & \frac{\tau_{n_b}\omega_{n_f}}{1+\tau_{n_b}^2\omega_{n_f}^2} & \omega_{n_f} \end{bmatrix} \begin{bmatrix} E_0(T_k) \\ \vdots \\ E_i(T_k) \\ E_{i+1}(T_k) \\ \vdots \\ E_{n_b}(T_k) \\ \eta_{n_b+1}(T_k) \end{bmatrix} = \begin{bmatrix} E'(\omega_1, T_k) \\ \vdots \\ \vdots \\ E'(\omega_{n_f}, T_k) \\ E''(\omega_1, T_k) \\ \vdots \\ \vdots \\ E''(\omega_{n_f}, T_k) \end{bmatrix} \tag{4.68}$$

where n_f denotes the number of loading frequencies used during the test campaigns. If the set of relaxation times is given, the identification of the model parameters passes through a linear problem that can be solved, for example, by using a least square method. Given a data vector D_E (i.e. the $2n_f$ dynamic moduli assessments for a given temperature T_k), possibly containing measurement noise, and a matrix A of size $2n_f \times (n_b + 2)$ completely determined since the relaxation time set is given and providing the $n_b + 2$ data (i.e the $n_b + 2$ model parameters), we look for the parameter set $H_{opt} \in \mathbf{R}^{n_b+2}$ such that:

$$H_{opt} = \arg\min \|(AH - D_E)\|^2 \text{ for all } H \in \mathbf{R}^{n_b+2} \tag{4.69}$$

Often, for solution H_{opt} to be satisfactory, additional constraints must be taken into account. For example here, the elements of H_{opt} are physical quantities known to be positive, then a problem of non-negative least squares (NNLS) [119, 120, 121, 122] has to be addressed.

$$H_{opt} = \arg\min \|(AH - D_E)\|^2 \text{ for all } H \in \mathbf{R}^{n_b+2} \text{ where } H_p \geq 0, p = 0, n_b + 2 \tag{4.70}$$

Without going into details, we used to solve this minimization problem under constraint a so-called activation method that do step by step elimination of the branches that would have a negative parameter (modulus in general or viscosity for the last branch). Matlab's "optimization" toolbox offers the most well-known method proposed by Lawson and Hanson (LH) in 1974 [123], under the function name *lsqnonneg*.

After several resolution attempts, we realized that the quality of solutions obtained by solving the system written in Equation 4.68, was not satisfactory enough with regard to the prediction of loss moduli (which remain small compared to the storage moduli). We attributed this poor performance of the LH method to the fact that the introduction of pulsation into the

matrix A associated with the pure viscous branch introduces a large imbalance in the matrix coefficients. All are dimensionless and comprised between 0 and 1 and only the last 1/2 column has coefficients that can go up to $\omega_{n_f} = 62.8 rad/s$. We therefore decided to solve the system by directly estimating the contribution to E'' of the pure viscous branch that we naturally noted E_{n_b+1}. It is important to stress that this choice implies that the contribution of the pure viscous branch to the loss modulus is a constant, probably dependent on temperature, but necessarily independent of the loading frequency. Equation 4.68 then became for each temperature T_k:

$$\begin{bmatrix} 1 & \frac{\tau_1^2\omega_1^2}{1+\tau_1^2\omega_1^2} & \cdots & \frac{\tau_{n_b}^2\omega_1^2}{1+\tau_1^2\omega_1^2} & 0 \\ \vdots & \vdots & \cdots & \vdots & \vdots \\ 1 & \frac{\tau_1^2\omega_{n_f}^2}{1+\tau_1^2\omega_{n_f}^2} & \cdots & \frac{\tau_{n_b}^2\omega_{n_f}^2}{1+\tau_{n_b}^2\omega_{n_f}^2} & 0 \\ 0 & \frac{\tau_1\omega_1}{1+\tau_1^2\omega_1^2} & \cdots & \frac{\tau_{n_b}\omega_1}{1+\tau_1^2\omega_1^2} & 1 \\ \vdots & \vdots & \cdots & \vdots & \vdots \\ 0 & \frac{\tau_1\omega_{n_f}}{1+\tau_1^2\omega_{n_f}^2} & \cdots & \frac{\tau_{n_b}\omega_{n_f}}{1+\tau_{n_b}^2\omega_{n_f}^2} & 1 \end{bmatrix} \begin{bmatrix} E_0(T_k) \\ \vdots \\ E_i(T_k) \\ E_{i+1}(T_k) \\ \vdots \\ E_{n_b}(T_k) \\ E_{n_b+1}(T_k) \end{bmatrix} = \begin{bmatrix} E'(\omega_1, T_k) \\ \vdots \\ \vdots \\ E'(\omega_{n_f}, T_k) \\ E''(\omega_1, T_k) \\ \vdots \\ \vdots \\ E''(\omega_{n_f}, T_k) \end{bmatrix} \tag{4.71}$$

The last point that deserves to be mentioned regarding the numerical strategy developed to identified the model paramaters concerns the final choice of active viscoelastic branches. In fact, we proceeded by iteration, initially taking an extended relaxation time spectrum for a number of branches not exceeding a few dozen (typically $n_b = 60$). Then, we reduced both the number of branches and the width of the spectrum by selecting only the active branches (i.e. those for which the modulus is at least once non-zero over all the tests performed at different temperatures).

4.3 Identified generalized Maxwell models and predictions

In a systematic way, we present hereafter the numerical results obtained via the identification procedure. The resolution of equation 4.71 by the LH method first indicates the active branches of the model, as well as the evolution of parameters E_i with temperature. It is then interesting to verify the quality of the results by reconstructing the storage moduli E'_{fit} and loss moduli E''_{fit} and comparing them with the ones that were experimentally assessed. A series of stress-strain responses at different temperatures and different loading frequencies also give an overview of the quality of the identification procedure. We finally come back to the parameter η_{n_b+1} and its evolution with the temperature but also with the loading frequency, which led us to wonder about the model integration within the GSM framework.

4.3.1 Polystyrene (PS)

For this material, we considered the following activation energy E_a and reference temperature T_{ref} both present in the Arrhenius law : $E_a = 350kJ.mol^{-1}$ and $T_{ref} = 381K$. It is important to stress that the choice of these values is not insignificant. It has a crucial influence on the determination of model parameters. Indeed, these values determine the evolution of the relaxation time of each branch with temperature. They, therefore fix the values of the components of the A matrix, those of the moduli and consequently those of the viscosity coefficients. The identification was performed using the furnace temperatures and the loading frequencies indicated in table 4.1.

Temperature Number	Temperature (K)	Frequency (Hz)
1	313	0.1 - 10
2	323	0.1 - 10
3	333	0.1 - 10
4	343	0.1 - 10
5	348	0.1 - 10
6	353	0.1 - 10
7	358	0.1 - 10
8	363	0.1 - 10

Table 4.1: Temperature and frequency used for the model identification in case of PS

Figure 4.8 allows to rapidly detect the active branches of the model. Here the cyclic loading frequency range is over two decades (from 0.1 Hz up to 10 Hz). The low number of the active branches is probably not surprising.

The top bar chart depicts the overall results obtained for the 60 branches. It can be seen that a very large number of branches remain inactive regardless of the test temperature. Only active branches appear at the ends of branch distribution. The two diagrams at the bottom shows more details about what is happening for the few first and last branches. Only the two first branches and the last one are active. The model structure is finally simple and involves a pure elastic branch, a single viscoelastic branch and a pure viscous branch.

Figure 4.9 shows the evolution of the elastic moduli of branches 0 and 1 with respect to the temperature. We also plotted the evolution of the sum $E_0 + E_1$ which approximately represents the tangent modulus of the model for high strain rates. We observe that this modulus gradually decreases with respect to the temperature.

Apart from the points obtained for the highest temperature, it can also be seen that this overall stiffness is fully supported, from one temperature to another, by branch 0 or branch 1. Let us remember that these branches, individually, have no physical reality. Only the predictions of the global model are to be compared with experimental observations. This is the reason why we have reconstructed the moduli E' and E'' using the identified coefficients of the model. Figure 4.10 and figure 4.11 gives the first overview of the quality of the identification procedure. The comparison between the E_{Exp} modules measured experimentally and the E_{Fit} modules recalculated following the identification of the parameters seems qualitatively satisfactory, for the conservation and loss moduli.

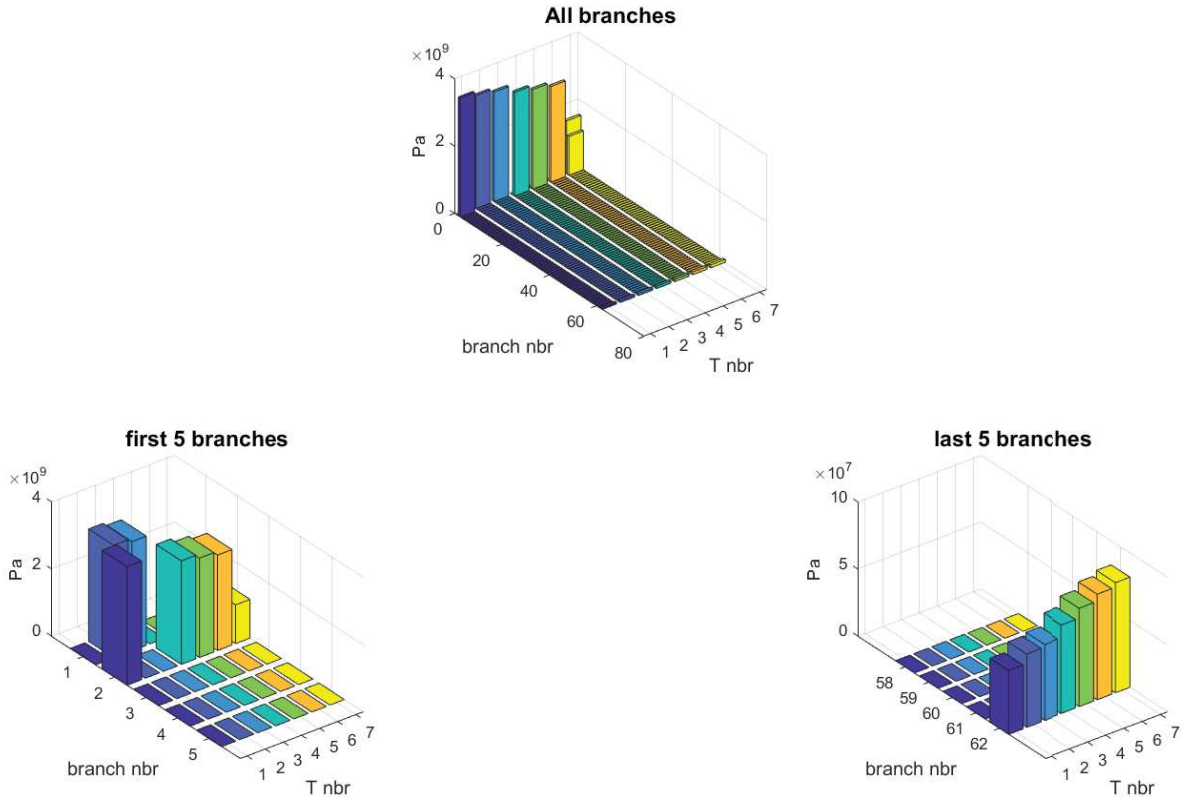

Figure 4.8: Selection of branches in case of PS

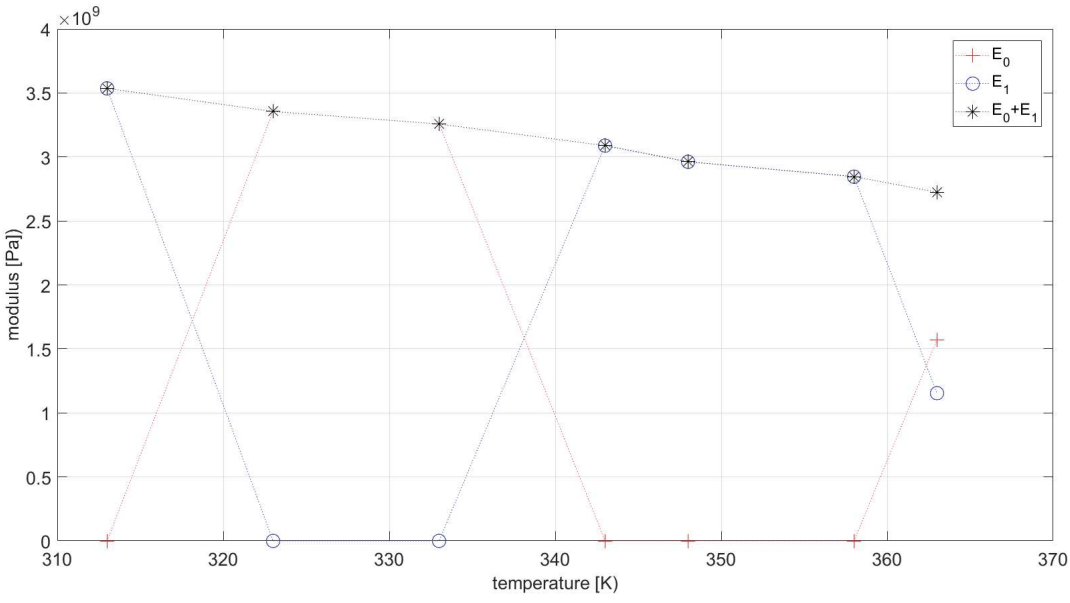

Figure 4.9: Evolution of moduli for elastic and viscoelastic branches for PS

In order to give a more quantitative picture of the relevance of the selected model and the quality of its identification, 9 stress-strain response curves were plotted in figure 4.12. The selection of the curves was made in such a way as to scan the ranges of loading frequency and testing temperature. It can then be seen that the comparison between predictions and

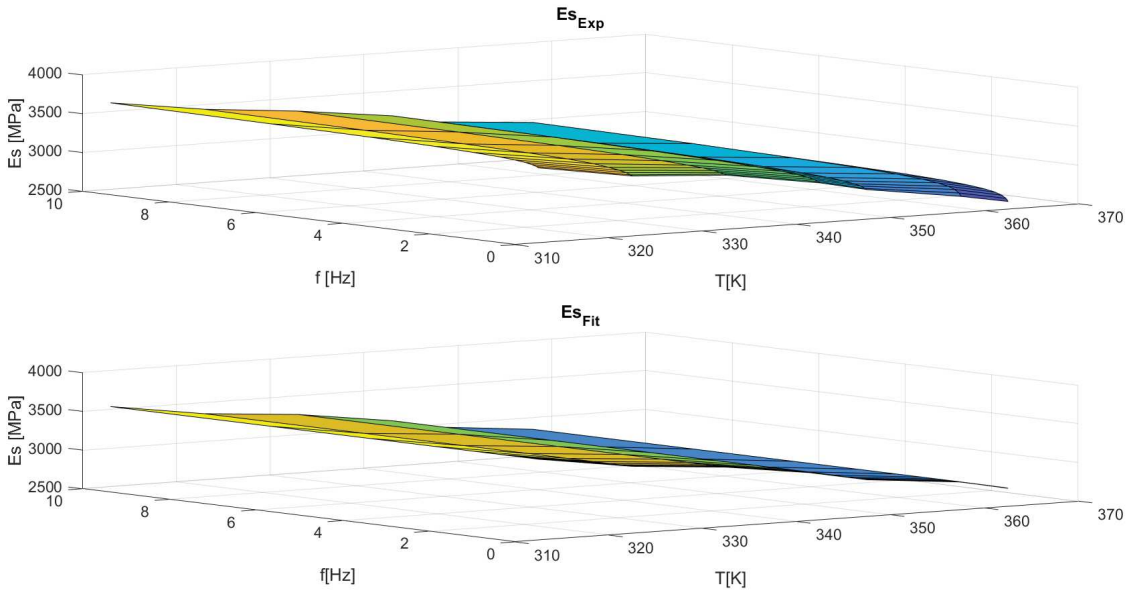

Figure 4.10: Comparison of experimental and identified storage modulus for PS

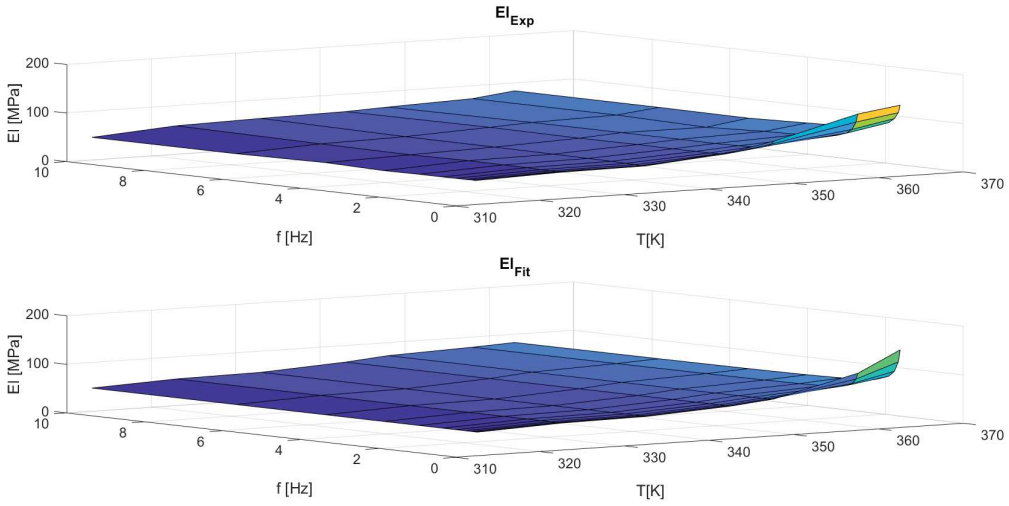

Figure 4.11: Comparison of experimental and identified loss modulus for PS

measurements is quantitatively good for this material. The slopes and the hysteresis area of each stabilized cycle were well reproduced.

The quality of the model predictions having been discussed, and being reassured by the quality of such predictions, it seems important to come back to the choice made to identify the model, solving the system defined in equation 4.71. In formulating the system in this way, we assumed that the pure viscous branch contributed in a constant way, i.e. regardless of the loading frequency, to the construction of the loss moduli. This choice was naturally inspired by the experimental distribution of loss moduli as a function of temperature and frequency. However, a constant contribution $E_{n_b+1}(T) = C_0(T)$ to the loss moduli of the viscous branch must mathematically be translated into the following relation:

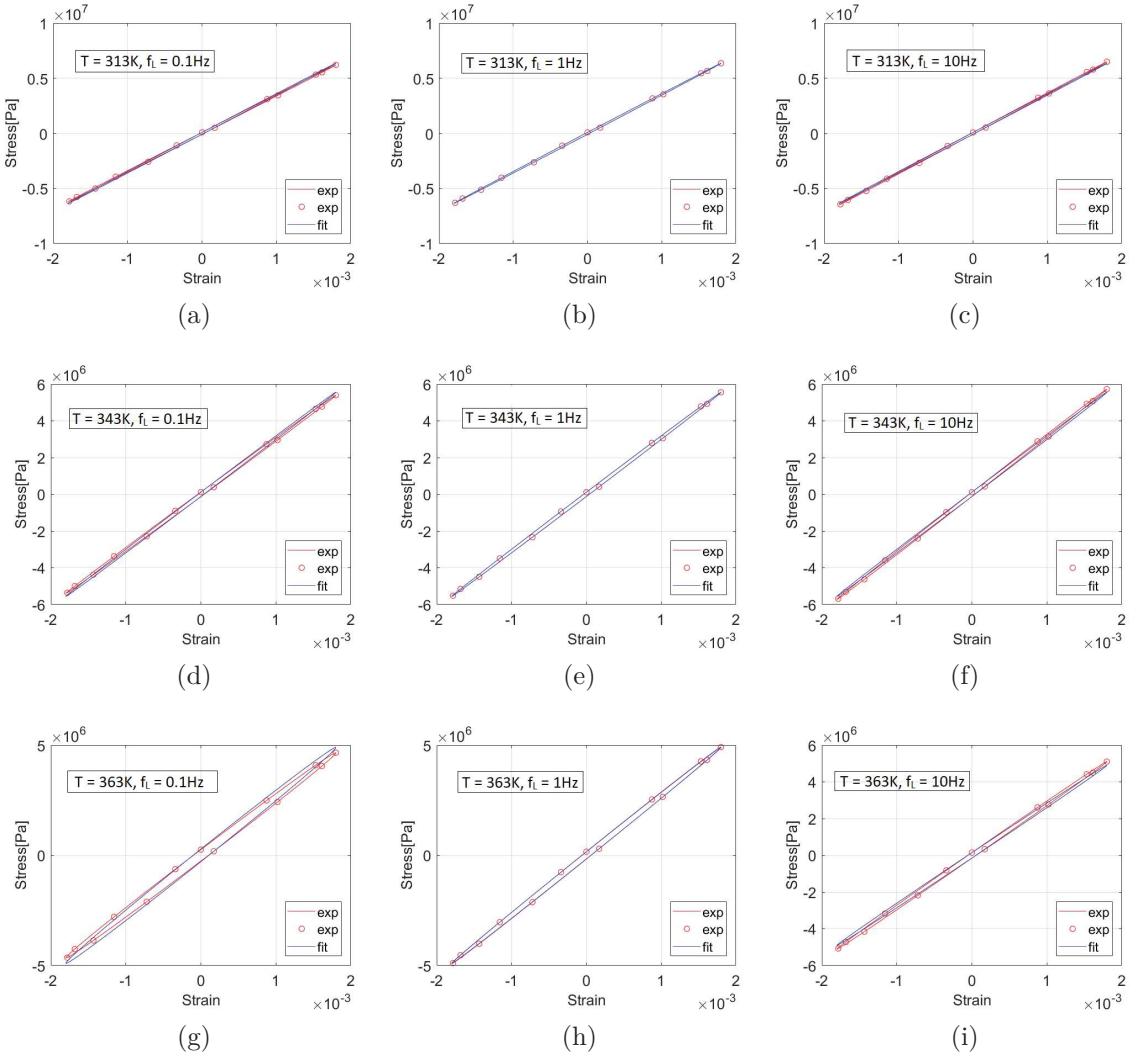

Figure 4.12: Comparison of experimental and predicted mechanical responses for PS

$$\eta_{n_b+1}\omega = E_{n_b+1}(T) = C_0(T) \tag{4.72}$$

For this relationship to be assured, the viscosity coefficient of the branch n_b+1 must evolve in ω^{-1}. However, the loading frequency was, until now, not considered as a state variable. Moreover, if the other parameters of the model (i.e. $E_i, i = 1, .., n_b$) were dependent on ω, equation 4.71 would become a non-linear system and the LH resolution method used would no longer be valid. We should consider non-linear least-squares (NLLS) methods under constraint, which would greatly complicate the resolution of the system and probably the choice of the optimal solution. That's the reason why we imposed only temperature dependent elastic moduli. The last question from a theoretical standpoint has been, how to introduce the pulsation (or the loading frequency) as a state variable in the model. This parameter has a sense here because we considered only monochromatic cyclic loading. But how to extend this variable for polychromatic or, more simply, for monotonous loading (e.g. creep or relaxation tests)?

To try to answer this tricky question, we propose to temporarily define the variable :

$$\tilde{\omega}(t) = \frac{\pi {\varepsilon_0}^2}{\int_{t-\frac{2\pi}{\omega}}^{t} \dot{\varepsilon}^2(\tau) d\tau} \tag{4.73}$$

This definition, compatible with the causality principle, was proposed in order to restore the pulsation ω in the case of a monochromatic cyclic loading. This "state variable" linked to the history (here over a cycle) of the strain rates undergone by the material. However, it should be noted that this variable is likely to have an effect only on the viscosity coefficient of the branch $n_b + 1$ and therefore will have no effect on free energy (i.e., no conjugate state variable A_ω) and will therefore only appear in the dissipation potential as a parameter, given the absence of thermodynamic force X_ω by construction. Moreover, the generalization of this type of variable to a broader situation than monochromatic cyclic loading remains an open question.

Figure 4.13 shows the evolution of the viscosity coefficient as a function of the temperature and the frequency. We observe a slight increase of the viscosity coefficient with the temperature and, as expected, a sharp decrease with the loading frequency. Despite this decrease, it should be kept in mind that the contribution of the viscous branch to the construction of loss moduli is far from negligible. It even represents the main contribution for high frequencies and temperatures.

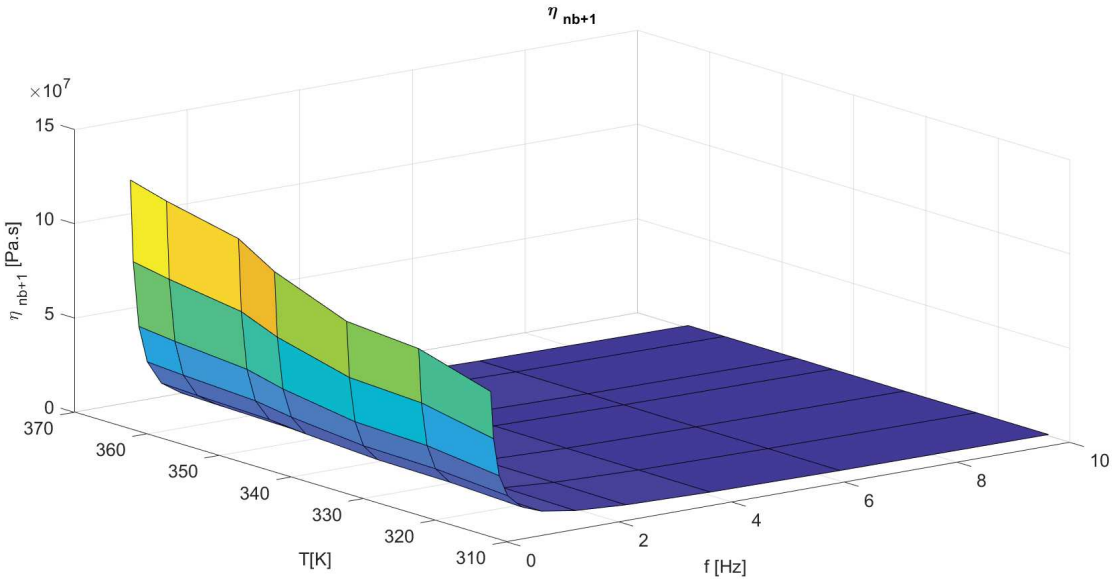

Figure 4.13: Evolution of the viscosity coefficient of the pure viscous branch for PS

4.3.2 Polyamide-6.6 (PA-6.6)

For this material we considered the following activation energy $E_a = 380000 J.mol^{-1}$ and reference temperature $T_{ref} = 353K$. The identification was performed using the furnace temperatures and the loading frequencies indicated in Table 4.2.

The samples were provided by Solvay Engineering Plastics that we wish to warmly thank. The Polyamide 6-6 is an hygrophil material and its water content leads to significant changes in its mechanical behaviour. Indeed, the water generates a so-called plastization of molecular network inducing a decrease of the glass transition temperature. These samples were not conditioned and were left at ambient moisture for several weeks. We therefore do not know the exact water content but we assumed that it was uniform within a sample at the time of testing and constant from one sample to another. In order to avoid to reach the glass transition temperature we limited the furnace temperature to $60°C$.

Temperature number	Temperature (K)	Frequency (Hz)
1	308	0.1 - 10
2	313	0.1 - 10
3	318	0.1 - 10
4	323	0.1 - 10
5	328	0.1 - 10
6	333	0.1 - 10

Table 4.2: Temperature and frequency used for modelling in case of PA-6.6

Figure 4.14 allows to detect the active branches of the model. Once again, the active branches are the pure elastic branch, the first viscoelastic branch and the pure viscous branch.

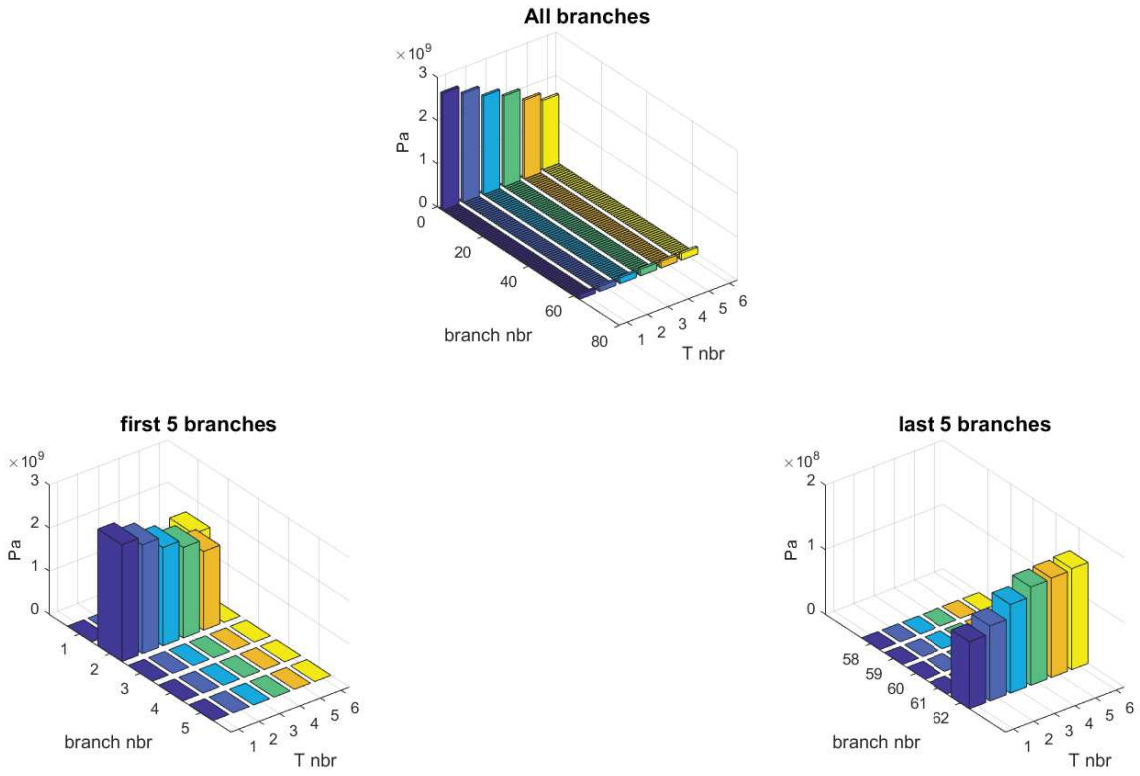

Figure 4.14: Selection of branches in case of PA-6.6

Figure 4.15 shows the evolution with respect to the temperature of the elastic moduli of branches 0 and 1. As previously, we also plotted the evolution of the sum $E_0 + E_1$. We observe

that this modulus gradually decreases with respect to the temperature. Apart from the points obtained at highest temperature, the overall stiffness, for dynamic test, is fully supported by the viscoelastic branch. The pure elastic branch is then really useful for the highest considered temperature ($333K$).

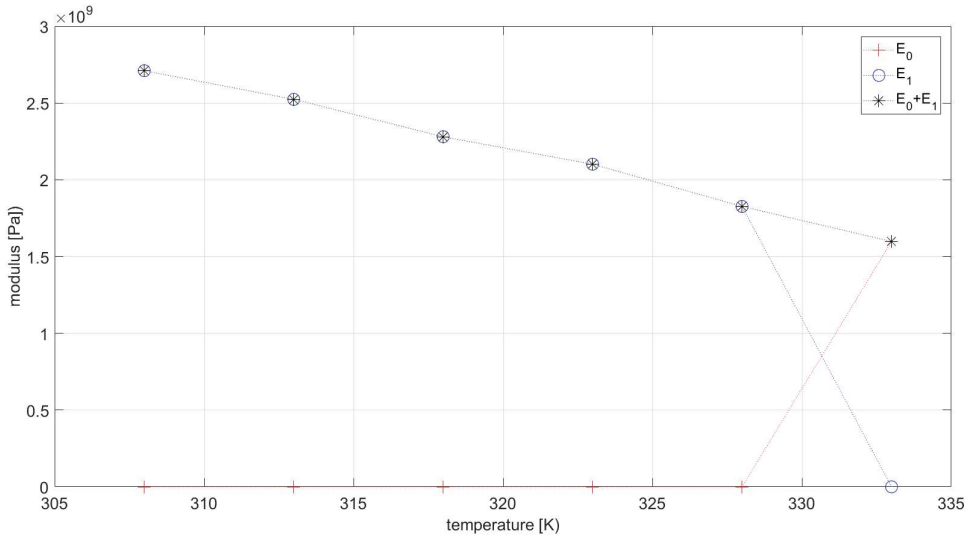

Figure 4.15: Evolution of elastic and viscoelastic branches for PA-6.6

Figure 4.16 and figure 4.17 gives an overview of the quality of the identification procedure. The comparison between the E_{Exp} modules measured experimentally and the E_{Fit} modules recalculated following the identification of the parameters seems, once more time, qualitatively satisfactory.

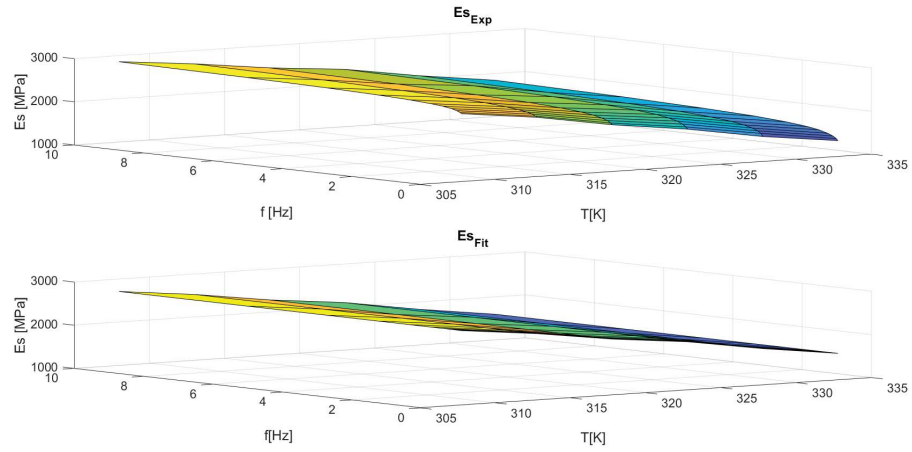

Figure 4.16: Comparison of experimental and identified storage modulus for PA-6.6

We also plotted in figure 4.18 several stress-strain diagrams for different temperatures and frequencies. The confrontations between experimental results and numerical predictions are generally good regarding the size of the hysteresis loops whatever the loading conditions (furnace temperature, loading frequency). We nevertheless observe small differences in the mean

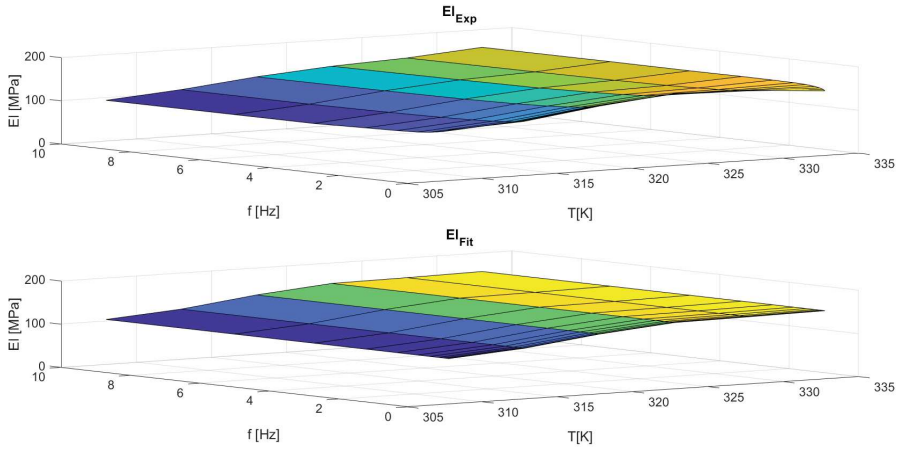

Figure 4.17: Comparison of experimental and identified loss modulus for PA-6.6

slope of the stress-strain curve for some loading conditions.

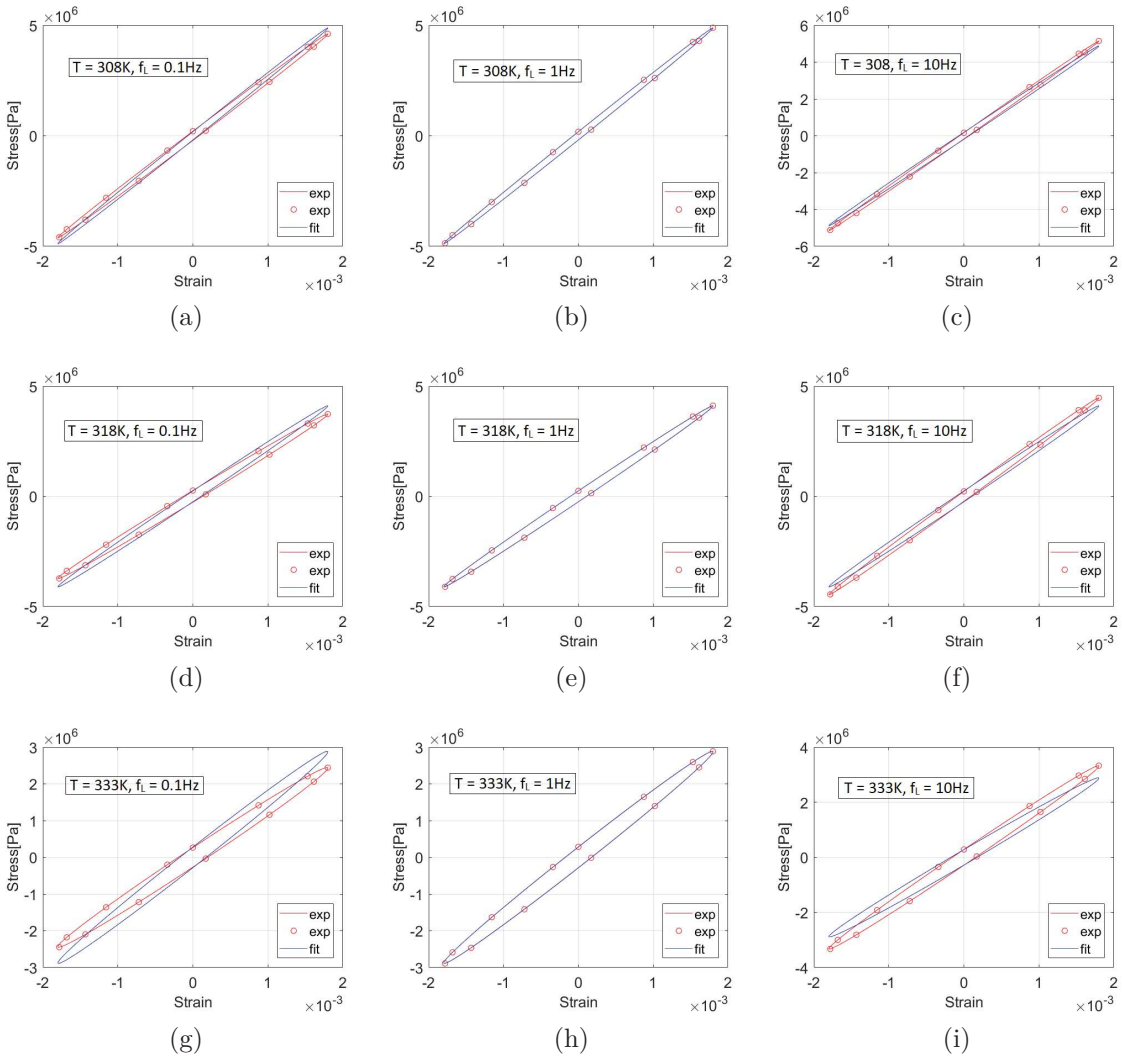

Figure 4.18: Comparison of experimental and predicted mechanical response for PA-6.6

Figure 4.19 shows the evolution of the viscosity coefficient as a function of the temperature and the frequency. Again, we observe a sharp decrease of the viscosity coefficient with the loading frequency.

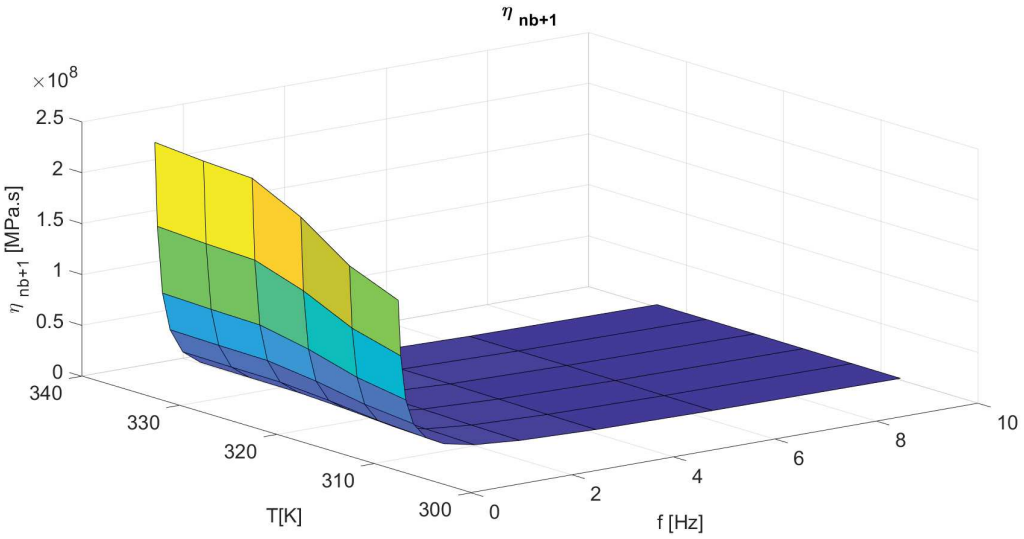

Figure 4.19: Evolution of the viscosity coefficient of the pure viscous branch for PA-6.6

4.3.3 Poly(methyl methacrylate) (PMMA)

For this 3rd tested material, the activation energy taken into consideration was $E_a = 30000 J.mol^{-1}$ and the reference temperature $T_{ref} = 293K$. The identification was performed using the furnace temperatures and the loading frequencies indicated in Table 4.3.

Temperature number	Temperature (K)	Frequency (Hz)
1	313	0.1 - 10
2	323	0.1 - 10
3	333	0.1 - 10
4	343	0.1 - 10
5	348	0.1 - 10
6	353	0.1 - 10

Table 4.3: Temperature and frequency used for modelling in case of PMMA

The selection of active branches is made in figure 4.20. Only the pure elastic branch, the first viscoelastic branch and the pure viscous branch are selected by the optimization algorithm and the evolution of the moduli of branches 0 and 1 are plotted with respect to the temperature in figure 4.21. We observe a regular decrease of the modulus of the pure elastic branch while the one of the viscoelastic branch remains approximately constant.

Figure 4.22 and figure 4.23 gives an overview of the quality of the identification procedure. For PMMA, if the comparison between experimental and predicted storage moduli E' remains

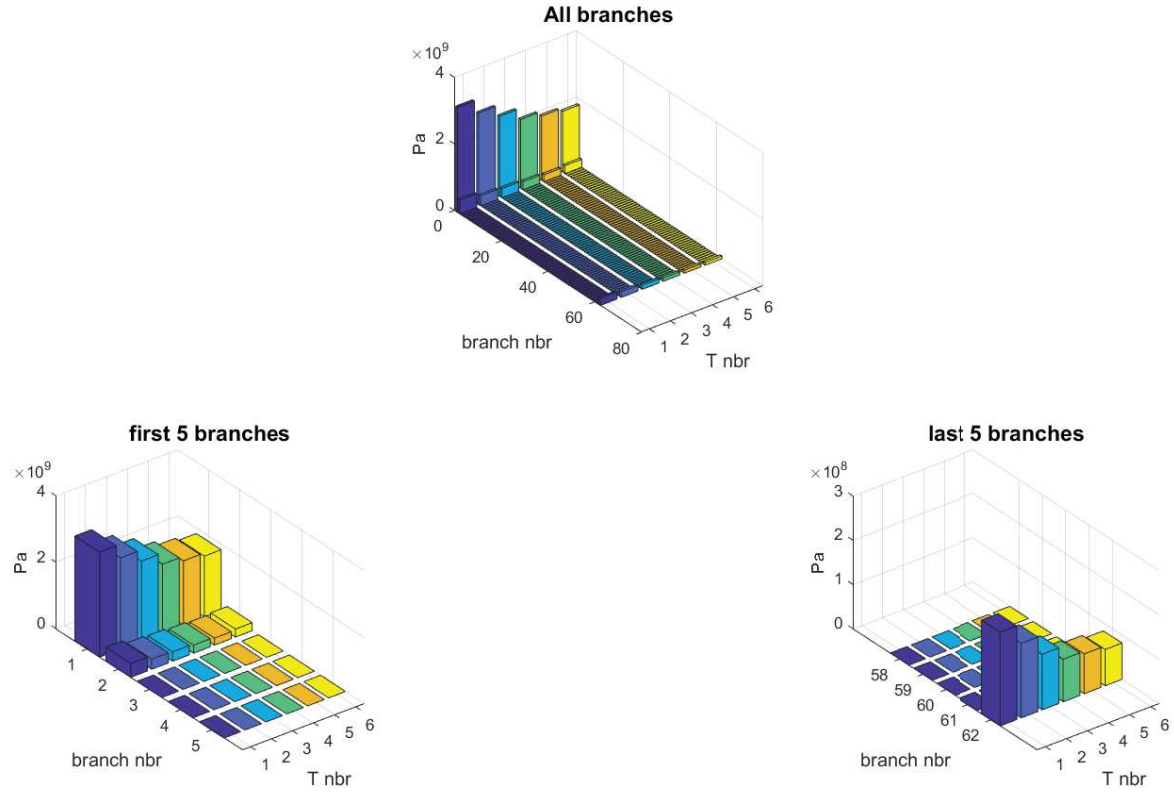

Figure 4.20: Selection of branches in case of PMMA

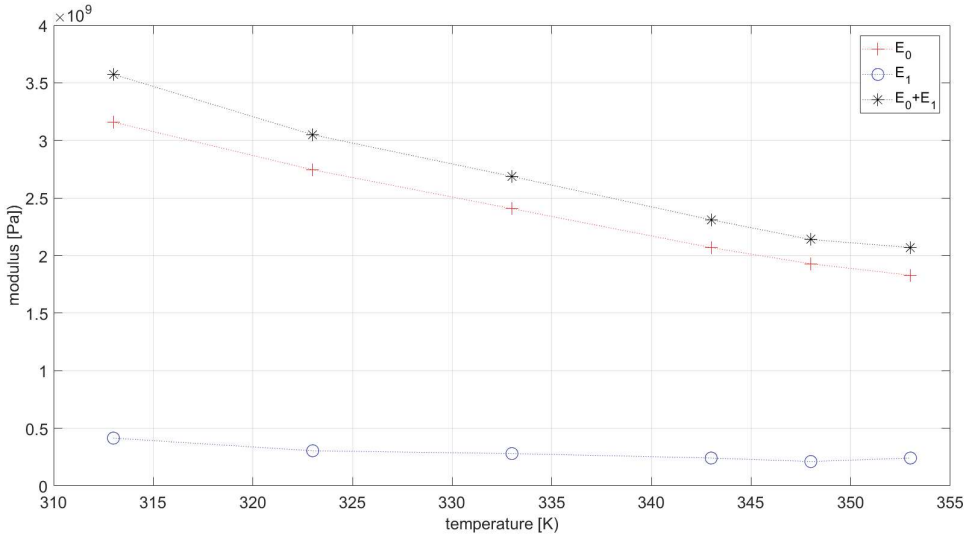

Figure 4.21: Evolution of elastic and viscoelastic branches for PMMA

qualitatively good, the comparison of loss moduli E'' is significantly poorer, particularly at high frequency where the experimental loss moduli are greater than the predicted ones.

This finding is in accordance with the mechanical response curves shown in figure 4.24, where we observe in general that the mean hysteresis slope is respected while the size of the hysteresis loop is underestimated by the model at high frequency. It should be reminded that

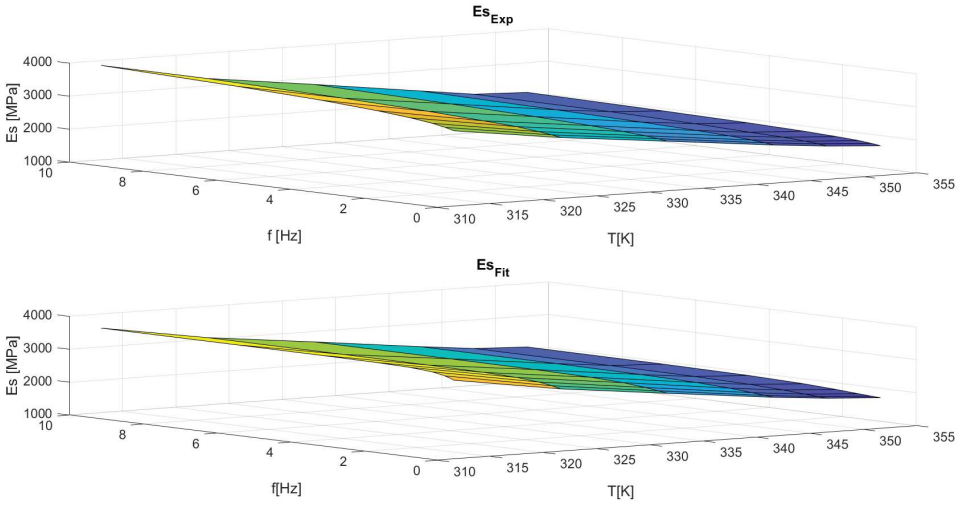

Figure 4.22: Comparison of experimental and identified storage modulus for PMMA

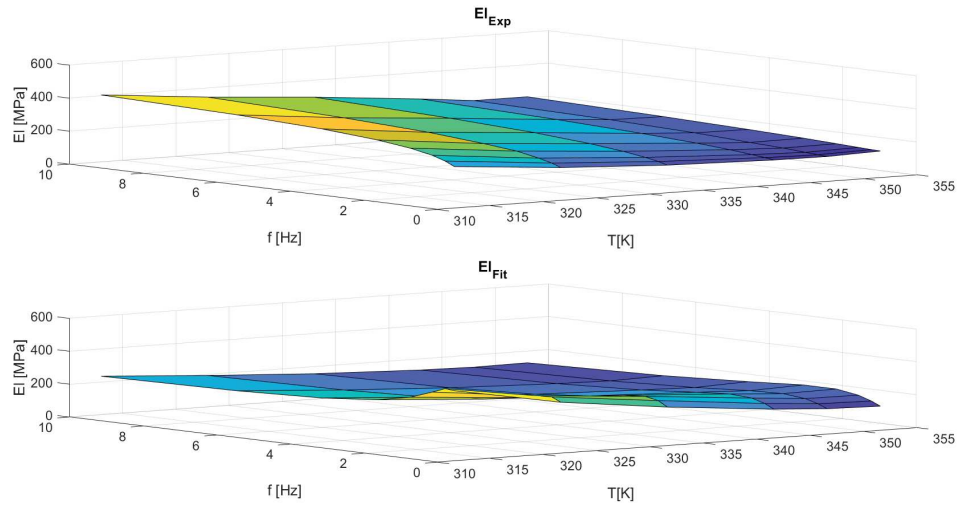

Figure 4.23: Comparison of experimental and identified loss modulus for PMMA

experimentally, it has been observed an evolution of the loss tangent (or loss moduli) with a positive curvature with respect to the frequency, what cannot be predicted by the Generalized Maxwell model in its present form. The generalized Maxwell model rather gives an evolution of the loss modulus with the frequency showing a negative curvature. This is the reason why the moduli assessments obtained for loading frequency less than 0.4Hz were not taken into account during the model identification. This is also probably why the experimental construction of the master curve appeared to be difficult. All these findings led us to question the relevance of the hypothesis of "thermorheologically simple material" for the PMMA.

Figure 4.19 shows the evolution of the viscosity coefficient as a function of the temperature and the frequency. For the third time, we observe a sharp decrease of the viscosity coefficient with the loading frequency.

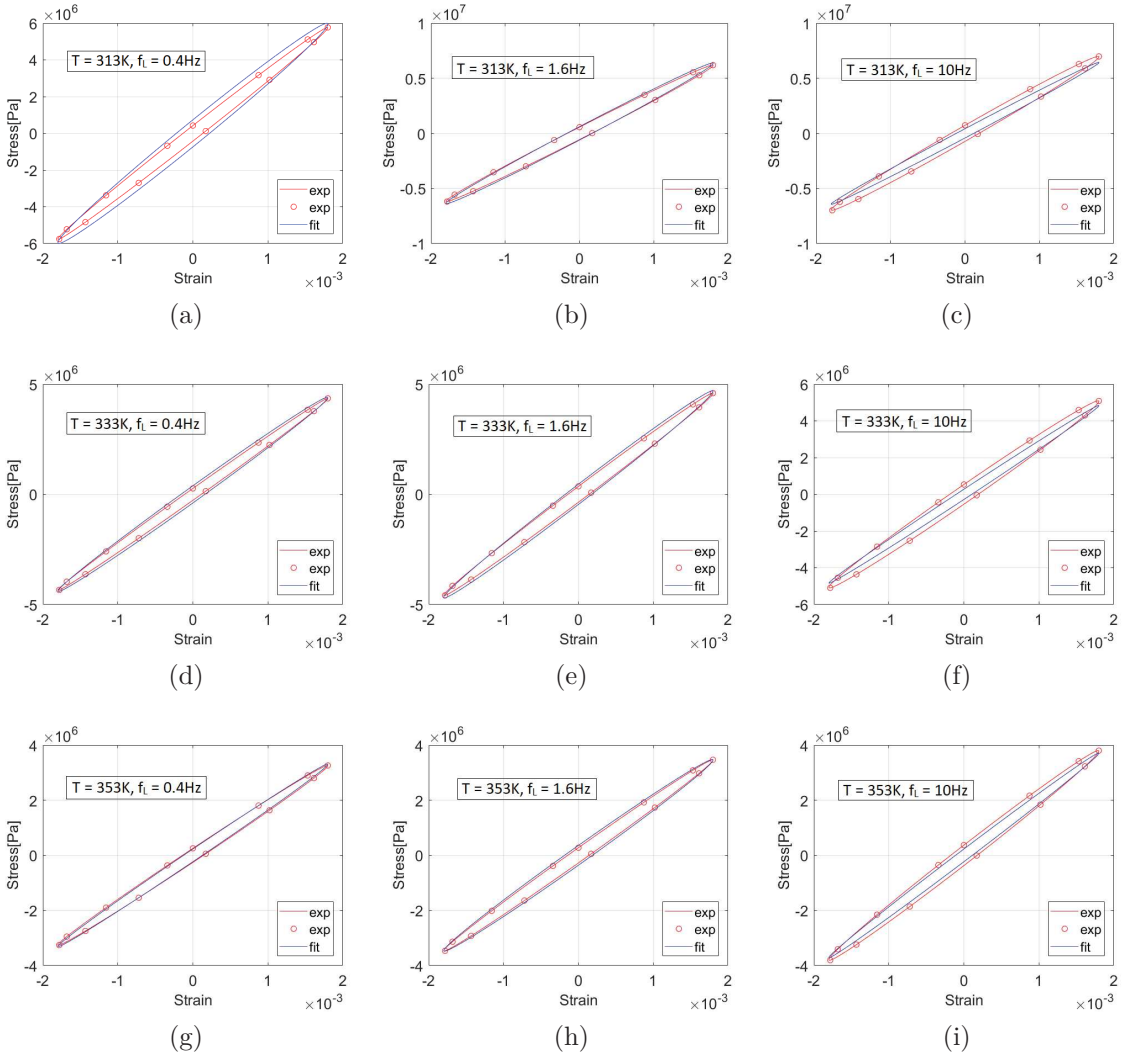

Figure 4.24: Comparison of experimental and modelling response for PMMA

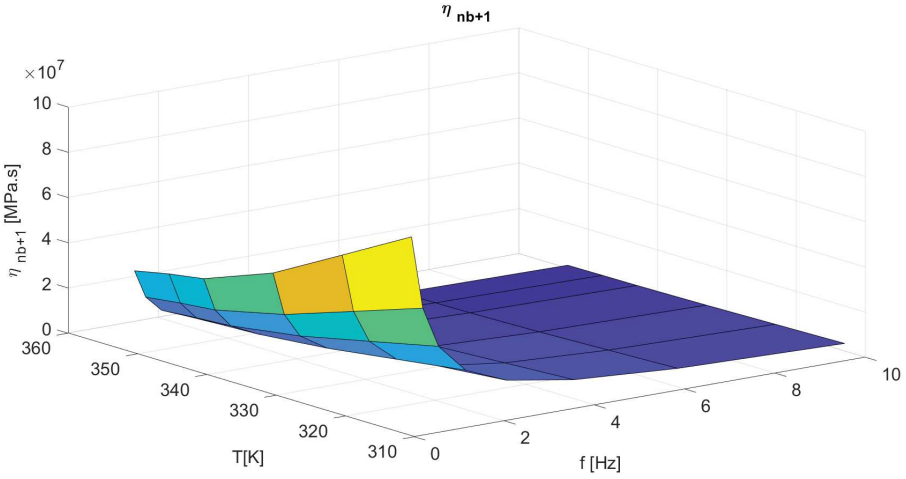

Figure 4.25: Evolution of the viscosity coefficient for the pure viscous branch for PMMA

4.3.4 TTSP and energy effects

In the preceding paragraphs, we have just try to highlight the quality of mechanical results offered by generalized Maxwell type models using the strong hypothesis of thermorheologically simple material. It is now time to discuss the energy predictions of these models. We will mainly discuss the dissipative aspects together with coupling energy. It should be reminded that in the visco-thermo-elastic framework, the hysteresis area of the mechanical curves represents a deformation energy lost mechanically by the material during each loading cycle. This energy, lost mechanically, can be partially dissipated via the irreversibility of the transformation (viscosity), stored by the material in the form of internal energy variation (here due to elasticity) and finally can be exchanged with the external environment via strong coupling mechanisms in non-adiabatic situations (thermal dissipation).

In the framework of linear viscoelasticity, no stored energy variation can be observed over a complete stabilized cycle, the mechanical cycle becoming a thermodynamic cycle. So in this situation the hysteresis area may come from dissipative and/or coupling effects. In order to see the relative importance of the different energy rate, the deformation rate, the elastic energy rate, the dissipation and the thermomechanical energy rate are considered.

For a monochromatic cyclic loading, where ε_0, ω_0, T_0 are respectively the strain amplitude, the loading pulsation, and the environmental temperature, the deformation energy rate $\dot{w_{def}}$ can be written as:

$$\dot{w_{def}}(t) = \sigma(t)\dot{\varepsilon}(t) = (E'(T_0,\omega_0)sin(\omega_0 t) + E''(T_0,\omega_0)\omega cos(\omega_0 t))\varepsilon_0\omega cos(\omega_0 t) \tag{4.74}$$

The deformation energy rate is made of elastic energy rate and dissipated energy rate $\dot{w_d}$, the later being non negative. They can be respectively written as:

$$\dot{w_e}(t) = E'(T_0,\omega_0)\varepsilon_0\omega_0 sin(\omega_0 t)cos(\omega_0 t) \tag{4.75}$$

$$\dot{w_d}(t) = E''(T_0,\omega_0)\varepsilon_0\omega_0 cos^2(\omega_0 t) \tag{4.76}$$

The thermomechanical coupling source $\dot{w_{thc}}$ was already defined in Equation (4.61b). In the case of the identified models for the three polymers, the elasticity was dispatched over the two first branches. It can be written as:

$$\begin{aligned}\dot{w_{thc}} =& T_0\varepsilon_0^2\frac{dE_0}{dT}\sin(\omega_0 t)\cos(\omega_0 t) + \\ & T_0\varepsilon_0^2\frac{dE_1}{dT}\left(\frac{\tau_1^2\omega_0^2}{1+\tau_1^2\omega_0^2}\sin(\omega_0 t) + \frac{\tau_1\omega_0}{1+\tau_1^2\omega_0^2}\cos(\omega_0 t)\right)\left(\frac{\tau_1^2\omega_0^3}{1+\tau_1^2\omega_1^2}\cos(\omega_0 t) - \frac{\tau_1\omega_0^2}{1+\tau_1^2\omega_0^2}\sin(\omega_0 t)\right)\end{aligned} \tag{4.77}$$

Although we did not take the thermodilatation mechanisms in the modelling and identification work into account, we can however determine the thermoelastic coupling source that would have been obtained for the 3 polymers with the expansion coefficients as identified in Chapter III. It should be recalled that we did not consider thermoelasticity in order for Maxwell's model to maintain its degree of generality, but on an experimental level, the temperature variations that were observed as being the most significant are those of thermoelasticity. The standard thermoelastic source $\dot{w_{the}}$ can be written as:

$$\dot{w_{the}}(t) = -E'(T_0, \omega_0)\alpha T_0 \varepsilon_0 \omega_0 cos(\omega_0 t) \tag{4.78}$$

The energy rate balance for the three polymers are successively plotted in figures 4.26,4.27, and 4.28. The writing dW was used on the graph to represent the derivative with respect to time of these energies, i.e. a power density per unit volume (W/m^3). Note that the intensity of the thermoelastic source was divided by 10 before being plotted.

The power balances for these 3 materials are very similar. The main finding to be noted is related to the orders of magnitude of these different energy rates. The dissipation has an intensity that remains much lower than those associated with coupling sources (several dozen times) and even more so with thermoelastic sources (several hundred times).

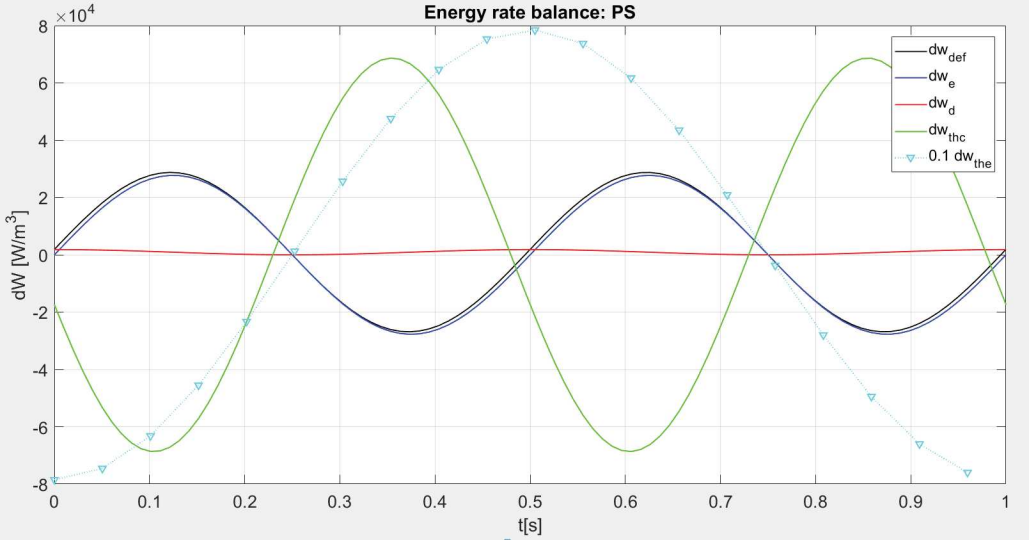

Figure 4.26: Energy rate balance for PS. $T_0 = 343K$, $\omega_0 = 6.28rad/s$

The deformation energy rate has even lower intensities than those of the couplings. When we know that these strong coupling mechanisms, combined with the effects of heat diffusion, can induce an effect of time on the mechanical behaviour of the material, it was therefore legitimate to question the importance of these mechanisms when considering the principle of time-temperature equivalence. It turns out that for the 3 materials studied here, and for the loading frequency selected, a loading cycle can be assimilated to both: - an isothermal loading: given the little temperature variations due to the power in play in relation to the heat volume of

the material. - but also an adiabatic loading: given the very poor diffusivity of these materials and the cycle periods used.

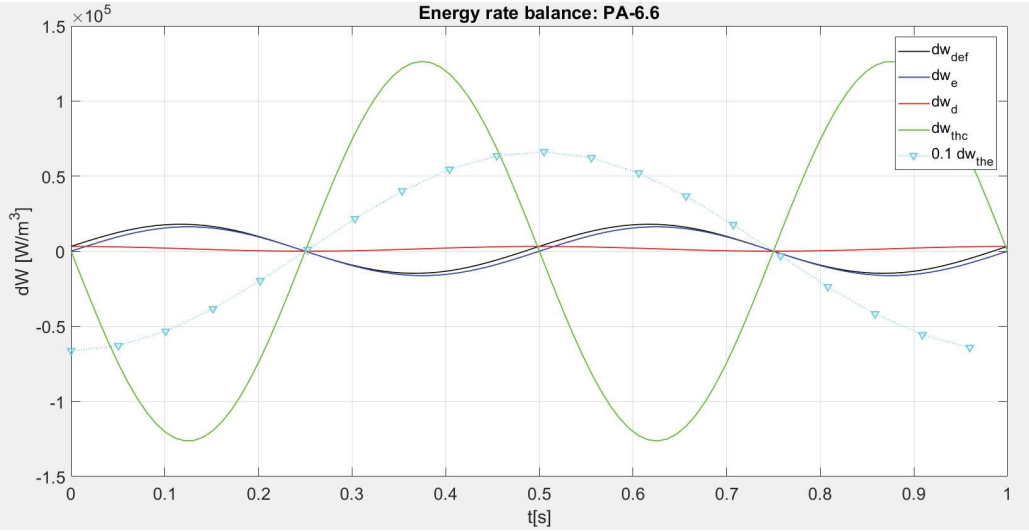

Figure 4.27: Energy rate balance for PA-6.6. $T_0 = 318K$, $\omega_0 = 6.28rad/s$

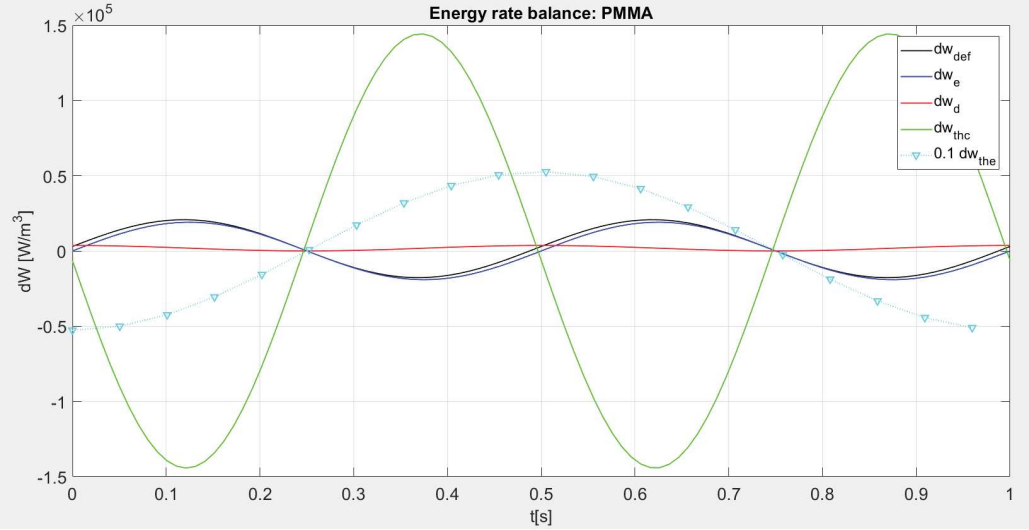

Figure 4.28: Energy rate balance for PMMA. $T_0 = 333K$, $\omega_0 = 6.28rad/s$

The last point to be noted concerns the two coupling mechanisms. The thermoelastic source (linear expansion), whose thermal effects have experimentally been monitored, beats in phase opposition to the strain signal (with a slight phase shift due to the non-adiabatic nature of the transformation). The thermomechanical coupling sources, (induced by temperature dependent relaxation time spectrum), beat at a two time the loading frequency. These sources, giving theoretically temperature ranges less than $10^{-2}K$, were not experimentally observed.

4.4 Conclusion

In this chapter, we have gradually taken up the basic rheological elements and models in order to integrate them into the GSM framework. In order to work with a fairly universal viscoelastic

model form, we focused on the generalized Maxwell model. In order to preserve its degree of generality, we did not take into account the effects of thermodilation, whereas its thermal effects have been certainly small but measurable.

With this general modelling framework in place, we revisited the impact of the TTSP. We have reached the following sufficient condition: if the material is thermorheologically simple in the sense that all relaxation times are bound by the same temperature law, Maxwell's model is compatible with the TTSP.

The cases of pure elastic and pure viscous branches appeared as extreme cases where relaxation times are respectively infinite and zero, regardless of temperature.

We have to mention that this conclusion seems to be widely shared in the literature, although, to our knowledge, it has never been so explicitly introduced using mathematical arguments linked to the structure of the generalized Maxwell model.

Once the numerical tools were in place to identify the model from the test results of Chapter III, we showed the potentialities of this type of modeling by first comparing the mechanical responses experimentally observed and reproduced via the model. This confrontation was judged, on the whole, satisfactory.

Integrating the models into the GSM framework has enabled us to numerically compile a complete energy balance. The main result that we would like to underline is the predominance, in terms of energy rate intensity, of the coupling mechanisms compared to the dissipative ones. Fortunately, because of the low diffusivity of the studied polymers, this predominance did not have any detrimental effect on the TTSP. Indeed, the strong couplings induce time (rate) effects on the mechanical behaviour. In such a case, the loss moduli can no longer be simply attributed to the viscous effects. In chapter 3, we nevertheless verified that the thermoelastic contribution to the hysteresis area remained low. From a modeling standpoint, we can then conclude that a generalized Maxwell model, whose temperature variations remain negligible over a loading cycle, and whose relaxation times are linked by the same temperature law, is TTSP compatible.

General conclusions and future work

General conclusions

This thesis work was focused on re-visiting the concept of so called "time-temperature superposition principle (TTSP)" on the base of viscous analysis of polymers. This re-visit was performed in order to establish the exact role of coupling effects, which could also induce an effect of time. Using the traditional experimental technique i.e., Dynamic mechanical and thermal analysis (DMTA) and via an energy analysis of the behaviour, the work was performed to try to restate the TTSP under the framework of Thermodynamics of Irreversible Processes, taking into account the dissipative effects and thermo-mechanical couplings induced during the deformation.

Chapter-1: A brief introduction about polymers was proposed including the polymer structure, their mechanical properties and the linear viscoelastic properties of the amorphous polymers. Later, a brief explanation about different relaxation transitions of amorphous polymers and their dependency on temperature was presented. At this stage, effect of different parameters like frequency, temperature, molecular weight distribution etc. was discussed. Following the discussion about different relaxation transitions, DMTA techniques were presented along with their application in the field of polymers. Introduction of DMTA techniques leads us to present an empirical formulation (TTSP) used to predict the viscoelastic behaviour on a very large time scale. Different aspects of utilization of TTSP was discussed along with the some literature work performed earlier using the time-temperature superposition principle. Lastly, thermomechanical interpretation of DMTA measurements was discussed.

Chapter-2: Theoretical framework for thermomechanical analysis was developed in this part of thesis. The two principles of thermodynamics were discussed followed by the introduction of thermodynamic potentials i.e., free energy and dissipation potentials along with the state variables used and their complementary laws. Using the principles of thermodynamics, the general heat equation was presented using the state variables and hence, the way to perform the energy balance was introduced. The energy analysis of the mechanical hysteresis area was also introduced in this part of thesis. Later, the application of this theoretical framework for thermomechanical analysis in case of rheology was presented. This entire theoretical framework was presented in this chapter was used for rheological modelling, followed by the energy analysis (Chapter-4) of the linear viscoelastic behaviour of amorphous polymers, that was obtained from DMTA measurements (Chapter-3).

Chapter-3: An experimental setup was developed to study the linear viscoelastic behaviour

of thermo-rheologically simple materials, using the DMTA measurements considering into account the importance of several calibration and correction procedures like machine stiffness correction, electronic phase shift correction etc. It was found that, having the different molecular weight distribution could vary the linear viscoelastic properties of the material. This could result in the change of the activation energy of the material as well. The DMTA measurements were performed at several places on different machines, so that, the entire performed procedure of calibration and correction can be validated. The results obtained from the measurements performed on different machines are then compared. It was observed that the bending measurements gives the highest magnitude of storage modulus because of the fact that, the maximum tensile stresses are concentrated in a small region on the top surface above the neutral axis. Accordingly, for similar sized test specimens, the tensile mode tests sees the maximum stresses throughout its entire gauge length i.e., over a much larger volume than the bending specimen. Using these calibrated and corrected DMTA results, the application of TTSP was found to be valid in the region well below the glass transition region. This also validated the theory of Arrhenius law below the glass transition region. Using the Arrhenius law, the activation energy was also computed using the slope of $\ln a_T$ vs $1/T - 1/T_0$ plot. The activation energy was found to be different for the results obtained from different machines.

The cyclic measurements induces the self-heating phenomenon and hence the temperature of the sample under loading. Considering this self-heating phenomenon of materials during cyclic loading, a precise thermography experimental setup was developed to measure the small scale self-heating of the material during the DMTA measurements. This self-heating of the sample under cyclic loading was observed during the DMTA measurements on all the three different polymers despite the fact that the magnitude of self-heating was of $\approx$0.1°C for PS and $\approx$0.2-0.3°C for PMMA and PA-6.6 at higher frequencies. This experimentally observed self-heating phenomenon in case of PS was associated with the thermo-elastic couplings whereas, in case of PMMA and PA-6.6, it was associated with the thermo-elastic couplings accompanied by the monotonous drift i.e., dissipation during the cyclic measurements at higher frequencies. The narrowness of the temperature variation of the specimen during the DMTA measurements legitimates the assumption that the temperature imposed by the furnace can be considered as the temperature of the sample (very small self-heating), which is in agreement with the DMTA protocol. Following the observation of self-heating of the material, the different hysteresis areas associated with the mechanical loading, loss modulus and dissipation, were computed. The consistency between the first two hysteresis areas validated the numerical scheme integration used for the computation of the loss modulus using the least square fitting method. The hysteresis area associated with loss modulus was compared with the hysteresis area associated with the dissipation to verify the viscous origin of the loss modulus. It was observed that the two hysteresis areas weren't consistent but was of the same order of magnitude. This inconsistency was associated with the noise and/or thermal regulation of the furnace.

Chapter-4: In this chapter, the mechanical analogues were presented in the GSM framework by presenting the free energy and dissipation potential of the mechanical analogues respectively. Later, the possible combinations of these mechanical analogues were presented with and without considering the temperature effects as an internal state variables. At this stage, Generalized Maxwell Model (GMM) was introduced along with the associated free energy and dissipation potentials. The heat equation associated to this model was also discussed along with the possible heat sources in the GSM framework. Following the introduction of Generalized Maxwell Model, a derivation was carried out to associate the so-called time-temperature superposition principle

(TTSP) with GMM. It was validated by this mathematical derivation that the TTSP is valid in the framework of thermo-mechanics for the thermorheologically simple materials. Later, using the experimental results obtained from DMTA during thermography measurements, the identification of a rheological model was performed using a non-negative least squares method (NNLS). Using this NNLS method, the generalized rheological model with one pure elastic, one viscoelastic and one pure viscous branch was identified. The need of pure viscous branch was identified as this identification was performed without any degree of freedom. This pure viscous branch helped in the improving the identification of the model. The role of this pure viscous branch was found to be frequency dependent. Following the identification of the rheological model, the validation was carried out by comparison with the experimental results obtained in Chapter-3 and was found to be a good identification. The validation of identification of rheological model allowed us to compute the different heat sources in the GSM framework. It was finally observed that the thermo-mechanical coupling sources are predominant in the energy rate balance form.

Future work

The applicability of TTSP was found validated for the three different amorphous polymers, using the Arrhenius law below the glass transition temperature. The specific way, that was used to apply TTSP on the raw DMTA results was, to apply a horizontal shift on storage modulus and loss tangent. Where, this horizontal shift was not satisfactorily enough to plot a master curve in the case of loss tangent. Therefore, a small vertical shift was also added to get the master curve but only in case of loss tangent. In the future work, an another way of applying the TTSP proposed by [99] is supposed to be used for validating the existence of TTSP for a specific amorphous polymer. In this method of Rouleau et al., the horizontal shift should be applied to the raw DMTA results such that the loss tangent master curve is smooth. Then a small vertical shift should be applied, if needed, to the storage modulus to get a smooth master curve. It would be interesting to see if the method proposed by Rouleau et al is still valid for the temperatures above glass transition.

The Identified model, based on the experimental results, consisted of a pure elastic, a viscoelastic and a pure viscous branch. The introduction of this pure viscous branch was inspired by the experimental distribution of loss modulus as a function of loading frequency and temperature. It was assumed that the pure viscous branch is contributing only to the loss modulus (E'') of the material. During the consideration of loading frequency as an internal state variable, the monochromatic cyclic loading was considered. It would be interesting to see how to implement the loading frequency as an internal state variable in case of monotonous loading.

This identified model was found to be a good identification for the three different materials, below the glass transition temperature. It would be interesting to see if this model will still be working for other materials. It would also be interesting to see if this identified model would still work for these three (PS, PA-6.6 and PMMA) and other materials above the glass transition temperature.

In the framework of small strains, a predominance of the coupling mechanisms compared to the dissipative ones was observed. The intensity of dissipation energy rates were found to be several dozen times lower than the coupling sources and several hundred times than the thermoelastic sources. It would be interesting to verify the dominance of different energy rates by increasing the strain amplitude.

Bibliography

[1] P. ARIVALAGAN, G. CHANDRAMOHAN, B. SURESHA, and N. PALANIAPPAN. Dynamic mechanical analysis and dry sliding wear behaviour of carbon fabric reinforced epoxy composite with fly ash cenosphere. *International Journal of Applied Engineering Research*, 10(61):2015.

[2] M. PATEL. Viscoelastic properties of polystyrene using dynamic rheometry. *Polymer testing*, 23(1):107–112, 2004.

[3] NETZSCH. Product User Manual. `https://www.netzsch-thermal-analysis.com/en/products-solutions/dynamic-mechanical-analysis/dma-242-e-artemis/`, 2019. [Online; accessed 25-September-2017].

[4] S.B. SANE and W.G. KNAUSS. The time-dependent bulk response of poly (methyl methacrylate). *Mechanics of Time-Dependent Materials*, 5(4):293–324, 2001.

[5] P.A. O'CONNELL and G.B. MCKENNA. Arrhenius-type temperature dependence of the segmental relaxation below t g. *The Journal of chemical physics*, 110(22):11054–11060, 1999.

[6] P. GERMAIN. Cours de mécanique des milieux continus. 1975.

[7] B. HALPHEN and Q.S. NGUYEN. Sur les matériaux standard généralisés. *Journal de mécanique*, 14:39–63, 1975.

[8] A. CHRYSOCHOOS and H. LOUCHE. An infrared image processing to analyse the calorific effects accompanying strain localisation. *International journal of engineering science*, 38(16):1759–1788, 2000.

[9] R.O. EBEWELE. *Polymer science and technology*. CRC press, 2000.

[10] Chem Tube 3D. Chemical structures. `http://www.chemtube3d.com/_polystyrenef`, 2019. [Online; accessed 25-Apr-2019].

[11] Wikipedia. Crystallization of polymers. `https://en.wikipedia.org/wiki/Crystallization_of_polymers`, 2019. [Online; accessed 25-Apr-2019].

[12] D. FRANÇOIS, A. PINEAU, and A. ZAOUI. *Mechanical behaviour of materials. Vol 1: Micro and macroscopic consitutive behaviour*. Springer, 2012.

[13] S.S. KELLEY, T.G. RIALS, and W.G. GLASSER. Relaxation behaviour of the amorphous components of wood. *Journal of materials science*, 22(2):617–624, 1987.

[14] J. DLOUHA. *Comportement viscoélastique longitudinal du bois vert: diversité et prédiction à long terme*. Thesis, Université Montpellier II, July 2009.

[15] J. HEIJBOER. Secondary loss peaks in glassy amorphous polymers. *International Journal of Polymeric Materials*, 6(1-2):11–37, 1977.

[16] TA Instruments. Interpreting DSC data. `https://slideplayer.com/slide/4583037/2004TrainingseminarsDSCbyTAInstruments`, 2019. [Online; accessed 26-Apr-2019].

[17] S. HAVRILIAK and N. ROMAN. The infra-red absorption characteristics of syndiotactic poly (methyl methacrylate) from 1050 cm^{-1} to 1300 cm^{-1}. *Polymer*, 7(8):387–400, 1966.

[18] E.A.W. HOFF, D.W. ROBINSON, and A.H. WILLBOURN. Relation between the structure of polymers and their dynamic mechanical and electrical properties. part ii. glassy state mechanical dispersions in acrylic polymers. *Journal of Polymer Science Part A: Polymer Chemistry*, 18(88):161–176, 1955.

[19] N.G. MCCRUM, B.E. READ, and G. WILLIAMS. Anelastic and dielectric effects in polymeric solids. 1967.

[20] F. KRUM and F.H. MÜLLER. Vorbehandlung und dielektrisches verhalten hochpolymerer. *Kolloid-Zeitschrift*, 164(2):81–107, 1959.

[21] S. MATSUOKA and Y. ISHIDA. Multiple transitions in polycarbonate. In *Journal of Polymer Science: Polymer Symposia*, volume 14, pages 247–259. Wiley Online Library, 1966.

[22] E. CHARRAULT, C. GAUTHIER, P. MARIE, and R. SCHIRRER. Structural recovery (physical ageing) of the friction coefficient of polymers. *Journal of Polymer Science Part B: Polymer Physics*, 46(13):1337–1347, 2008.

[23] D.J. PLAZEK. Temperature dependence of the viscoelastic behavior of polystyrene. *The Journal of Physical Chemistry*, 69(10):3480–3487, 1965.

[24] J.D. FERRY. *Viscoelastic properties of polymers*. John Wiley & Sons, 1980.

[25] M.L. WILLIAMS, R.F. LANDEL, and J.D. FERRY. The temperature dependence of relaxation mechanisms in amorphous polymers and other glass-forming liquids. *Journal of the American Chemical society*, 77(14):3701–3707, 1955.

[26] R.S. LAKES. *Viscoelastic materials*. Cambridge University Press, 2009.

[27] K.P. MENARD. *Dynamic mechanical analysis: a practical introduction*. CRC press, 2008.

[28] G.W. EHRENSTEIN, G. RIEDEL, and P. TRAWIEL. *Thermal analysis of plastics: theory and practice*. Carl Hanser Verlag GmbH Co KG, 2012.

[29] J. ZOU, F. YOU, L. SU, Z. YANG, G. CHEN, and S. GUO. Failure mechanism of time-temperature superposition for poly (vinyl chloride)/dioctylphthalate (100/70) system. *Journal of Applied Polymer Science*, 124(1):452–458, 2012.

[30] H. LEADERMAN. Textile materials and the time factor: I. mechanical behavior of textile fibers and plastics. *Textile Research*, 11(4):171–193, 1941.

[31] J. CAPODAGLI and R. LAKES. Isothermal viscoelastic properties of PMMA and LDPE over 11 decades of frequency and time: a test of time–temperature superposition. *Rheologica Acta*, 47(7):777–786, 2008.

[32] J.Y. CAVAILLE, C. JOURDAN, J. PEREZ, L. MONNERIE, and G.P. JOHARI. Time-temperature superposition and dynamic mechanical behavior of atactic polystyrene. *Journal of Polymer Science Part B: Polymer Physics*, 25(6):1235–1251, 1987.

[33] N.W. TSCHOEGL. Time dependence in material properties: An overview. *Mechanics of Time-Dependent Materials*, 1(1):3–31, March 1997.

[34] D.S. MATSUMOTO. Time-temperature superposition and physical aging in amorphous polymers. *Polymer Engineering & Science*, 28(20):1313–1317, 1988.

[35] I.M. WARD and J. SWEENEY. *Mechanical properties of solid polymers*. John Wiley & Sons, 2012.

[36] M.V. GURP and J. PALMEN. Time-temperature superposition for polymeric blends. *Rheology Bulletin*, 67(1):5–8, 1998.

[37] M. TAJVIDI, R.H. FALK, and J.C. HERMANSON. Time–temperature superposition principle applied to a kenaf-fiber/high-density polyethylene composite. *Journal of Applied Polymer Science*, 97(5):1995–2004, 2005.

[38] A.P. SOKOLOV and Y. HAYASHI. Breakdown of time–temperature superposition: From experiment to the coupling model and beyond. *Journal of Non-Crystalline Solids*, 353(41):3838–3844, 2007.

[39] Y. DING and A.P. SOKOLOV. Breakdown of time−temperature superposition principle and universality of chain dynamics in polymers. *Macromolecules*, 39(9):3322–3326, 2006.

[40] ALEXEI S. and VLADIMIR N. Dynamic crossover in complex systems: From a "simple" liquid to a protein. *AIP Conference Proceedings*, 708(1):533–540, 2004.

[41] J.J. AKLONIS and W.J. MACKNIGHT. Introduction to polymer viscoelasticity. 1983. *A Wiley-Interscience Publication: New York*.

[42] F.R. SCHWARZL and F. ZAHRADNIK. The time temperature position of the glass-rubber transition of amorphous polymers and the free volume. *Rheologica Acta*, 19(2):137–152, 1980.

[43] A.K. DOOLITTLE. Studies in newtonian flow. ii. the dependence of the viscosity of liquids on free-space. *Journal of Applied Physics*, 22(12):1471–1475, 1951.

[44] T. ALFREY, G. GOLDFINGER, and H. MARK. The apparent second-order transition point of polystyrene. *Journal of Applied Physics*, 14(12):700–705, 1943.

[45] S. ONOGI, T. MASUDA, and K. KITAGAWA. Rheological properties of anionic polystyrenes. I. dynamic viscoelasticity of narrow-distribution polystyrenes. *Macromolecules*, 3(2):109–116, 1970.

[46] P. LOMELLINI. Viscosity-temperature relationships of a polycarbonate melt: Williams-landel-ferry versus arrhenius behaviour. *Macromolecular Chemistry and Physics*, 193(1):69–79, 1992.

[47] J.R. MCLOUGHLIN and A.V. TOBOLSKY. The viscoelastic behavior of polymethyl methacrylate. *Journal of Colloid Science*, 7(6):555–568, 1952.

[48] C. ZENER. Internal friction in solids II. general theory of thermoelastic internal friction. *Physical Review*, 53(1):90, 1938.

[49] C. ZENER. Internal friction in solids. I. theory of internal friction in reeds. *Physical review*, 52(3):230, 1937.

[50] H.B. CALLEN. Thermodynamics: An introduction to the physical theories of equilibrium thermodynamics. 1985.

[51] S.Q. NGUYEN and N. TRIANTAFYLLIDIS. Plastic bifurcation and postbifurcation analysis for generalized standard continua. *Journal of the Mechanics and Physics of Solids*, 37(5):545–566, 1989.

[52] A. BENAARBIA. *Analyse énergétique du comportement thermomécanique du PA6. 6 renforcé de fibres de verre*. PhD thesis, Université Montpellier 2, 2014.

[53] J. LEMAITRE, J.L. CHABOCHE, A. BENALLAL, and R. DESMORAT. *Mécanique des matériaux solides-3eme édition*. Dunod, 2009.

[54] M. GRMELA and G. LEBON. Hamiltonian extended thermodynamics. *Journal of Physics A: Mathematical and General*, 23(14):3341, 1990.

[55] C. CUNAT. Thermodynamic treatment of relaxation in frozen-in systems.“universality” of the distribution law for relaxation times. *Zeitschrift für Physikalische Chemie*, 157(1):419–423, 1988.

[56] D. RITTEL. On the conversion of plastic work to heat during high strain rate deformation of glassy polymers. *Mechanics of Materials*, 31(2):131–139, 1999.

[57] M.A.H. QUINNEY. The latent energy remaining in a metal after cold working. In *Proceedings of Royal Society London A*, volume 143, pages 307–326. The Royal Society, 1934.

[58] D. RITTEL, L.H. ZHANG, and S. OSOVSKI. The dependence of the taylor–quinney coefficient on the dynamic loading mode. *Journal of the Mechanics and Physics of Solids*, 107:96–114, 2017.

[59] A. CHRYSOCHOOS, V. HUON, F. JOURDAN, J.M. MURACCIOLE, R. PEYROUX, and B. WATTRISSE. Use of full-field digital image correlation and infrared thermography measurements for the thermomechanical analysis of material behaviour. *Strain*, 46(1):117–130, 2010.

[60] A. CHRYSOCHOOS, B. WATTRISSE, J.M. MURACCIOLE, and Y. EL KAÏM. Fields of stored energy associated with localized necking of steel. *Journal of Mechanics of Materials and Structures*, 4(2):245–262, 2009.

[61] R.L. ANTHONY, R.H. CASTON, and E. GUTH. Equations of state for natural and synthetic rubber-like materials. I. unaccelerated natural soft rubber. *The Journal of Physical Chemistry*, 46(8):826–840, 1942.

[62] M.A. BIOT. Theory of stress-strain relations in anisotropic viscoelasticity and relaxation phenomena. *Journal of Applied Physics*, 25(11):1385–1391, 1954.

[63] T. ALFREY. Mechanical behavior of high polymers. 1948.

[64] H. LEADERMAN and R. SIMHA. Mechanical behavior of high polymers. *Journal of Polymer Science*, 3(5):796–797, 1948.

[65] W. WEBER. Ueber die specifische wärme fester körper, insbesondere der metalle. *Annalen der Physik*, 96(10):177–213, 1830.

[66] K.T. COMPTON and D.B. WEBSTER. Temperature changes accompanying the adiabatic compression of steel. *Physical Review*, 5(2):159, 1915.

[67] R. ROCCA and M.B. BEVER. The thermoelastic effect in iron and nickel as a function of temperature. *The Journal of The Minerals*, 2(2):327–333, 1950.

[68] M.A. BIOT. Variational principles in irreversible thermodynamics with application to viscoelasticity. *Physical Review*, 97(6):1463, 1955.

[69] M.A. BIOT. Theory of elasticity and consolidation for a porous anisotropic solid. *Journal of applied physics*, 26(2):182–185, 1955.

[70] M.A. BIOT. Thermoelasticity and irreversible thermodynamics. *Journal of Applied Physics*, 27(3):240–253, 1956.

[71] D.S. MOUNTAIN and J.M.B. WEBBER. Stress pattern analysis by thermal emission (spate). In *4th European Electro-Optics Conf*, volume 164, pages 189–197. International Society for Optics and Photonics, 1979.

[72] N.F. ENKE. Thermographic stress analysis of isotropic materials. 1990.

[73] W.M. CUMMINGS and N. HARWOOD. Thermoelastic stress analysis under broad-band random loading. In *1985 SEM Spring Conference on Experimental Mechanics, Las Vegas, Nevada*, pages 844–850, 1985.

[74] R.T. POTTER and L.J. GREAVES. The application of thermoelastic stress analysis techniques to fibre composites. In *Optomechanical systems engineering*, volume 817, pages 134–147. International Society for Optics and Photonics, 1987.

[75] A.S. MACHIN, J.G. SPARROW, and M.G. STIMSON. Mean stress dependence of the thermoelastic constant. *Strain*, 23(1):27–30, 1987.

[76] A.K. WONG, R. JONES, and J.G. SPARROW. Thermoelastic constant or thermoelastic parameter? *Journal of Physics and chemistry of solids*, 48(8):749–753, 1987.

[77] S. QUINN, J.M. DULIEU-BARTON, and J.M. LANGLANDS. Progress in thermoelastic residual stress measurement. *Strain*, 40(3):127–133, 2004.

[78] S. MOREAU, A. CHRYSOCHOOS, J.M. MURACCIOLE, and B. WATTRISSE. Analysis of thermoelastic effects accompanying the deformation of PMMA and PC polymers. *Comptes Rendus Mécanique*, 333:648–653, 2005.

[79] M. MOONEY. A theory of large elastic deformation. *Journal of applied physics*, 11(9):582–592, 1940.

[80] L.R.G. TRELOAR. Stress-strain data for vulcanised rubber under various types of deformation. *Transactions of the Faraday Society*, 40:59–70, 1944.

[81] L.R.G. TRELOAR. *The physics of rubber elasticity*. Oxford University Press, USA, 1975.

[82] E.M. ARRUDA and M.C. BOYCE. A three-dimensional constitutive model for the large stretch behavior of rubber elastic materials. *Journal of the Mechanics and Physics of Solids*, 41(2):389–412, 1993.

[83] R.S. RIVLIN. Large elastic deformations of isotropic materials IV. further developments of the general theory. *Philosophical Transactions of the Royal Society London A*, 241(835):379–397, 1948.

[84] J.L. DIANI and C. REY. New phenomenological behavior laws for rubbers and thermoplastic elastomers. *European Journal of Mechanics-A/Solids*, 18(6):1027–1043, 1999.

[85] R. CABORGAN. *Contribution à l'analyse expérimentale du comportement thermomécanique du caoutchouc naturel*. PhD thesis, Université Montpellier II, 2011.

[86] GOODFELLOW. Technical Catalogue. `http://www.goodfellow.com/catalogue/GFCat2C.php?ewd_token=Ff4fNucLNlw1ZLlD94Eq8tPE6Hg8Di&n=mFaalmJwjWV5jqoMoNqKBrTRIt7JXV&ewd_urlNo=GFCat26&type=30&prop=2`, 2019. [Online; accessed 15-June-2017].

[87] J.E. MARK. *Polymer data handbook*. Oxford university press, 2009.

[88] B. ELLIS and R. SMITH. *Polymers: a property database*. CRC Press, 2008.

[89] Thomas G. Fox J. and P.J. Flory. Viscosity—molecular weight and viscosity—temperature relationships for polystyrene and polyisobutylene1, 2. *Journal of the American Chemical Society*, 70(7):2384–2395, 1948.

[90] HICHROM expert in chromatography. SEC. `https://www.hichrom.com/technical/Techniques/SEC/index.htm`, 1978. [Online; accessed 15-June-2019].

[91] C.S. WU. *Handbook of size exclusion chromatography and related techniques: revised and expanded*, volume 91. CRC Press, 2003.

[92] Polymer Science Learning Centre. Molecular Weight. `https://pslc.ws/macrog/weight.htm`, 2019. [Online; accessed 15-June-2018].

[93] T. TADANO, R. ZHU, Y. MUROGA, T. HOSHI, D. SASAKI, S. YANO, and T. SAWAGUCHI. A new mechanism for the silica nanoparticle dispersion–agglomeration transition in a poly (methyl methacrylate)/silica hybrid suspension. *Polymer Journal*, 46(6):342, 2014.

[94] J. BRANDRUP, E.H. IMMERGUT, E.A. GRULKE, A. ABE, and D.R. BLOCH. *Polymer handbook*, volume 89. Wiley New York, 1999.

[95] J.G. ROCHA, V. CORREIA, M. MARTINS, and J.M. CABRAL. Dilatometer for characterization of thermal expansion of ceramic samples. In *2009 35th Annual Conference of IEEE Industrial Electronics*, pages 1853–1858. IEEE, 2009.

[96] NETZSCH. Product User Manual. `https://www.netzsch-thermal-analysis.com/en/products-solutions/dilatometer/dil-402-expedis-classic/`, 2019. [Online; accessed 10-July-2019].

[97] J. MCHUGH, P. FIDEU, A. HERRMANN, and W. STARK. Determination and review of specific heat capacity measurements during isothermal cure of an epoxy using tm-dsc and standard dsc techniques. *Polymer Testing*, 29(6):759–765, 2010.

[98] TA Instruments. Product User Manual. `http://www.tainstruments.com/wp-content/uploads/dma.pdf`, 2019. [Online; accessed 10-April-2019].

[99] L. ROULEAU, J.F. DEÜ, A. LEGAY, and F. LE LAY. Application of kramers–kronig relations to time–temperature superposition for viscoelastic materials. *Mechanics of Materials*, 65:66–75, 2013.

[100] METRAVIB. Product User Manual. `http://metravib.acoemgroup.com/dma/catalog/METRAVIB-DMA-25-DMA50-desktop-series`, 2019. [Online; accessed 25-November-2019].

[101] METRAVIB. Product User Manual. `http://metravib.acoemgroup.com/dma/catalog/METRAVIB-DMA300-DMA1000-DMA2000-series`, 2019. [Online; accessed 15-November-2019].

[102] TA Instruments. Product User Manual. `https://www.tainstruments.com/dma-3200/`, 2019. [Online; accessed 15-November-2018].

[103] A. OLUSANYA. A comparison of techniques for monitoring the cure of adhesives. *National Physical Laboratory Report CMMT (B)*, 104, 1996.

[104] PICO Technology. Product User Manual. `https://sg.element14.com/pico-technology/picoscope-2204/oscilloscope-2-ch-10mhz-100msps/dp/1471476`, 2019. [Online; accessed 15-March-2018].

[105] M.F. ARIF. *Damage mechanisms in short glass fiber reinforced polyamide-66 under monotic and fatigue loading : Effect of relative humidity and injection molding induced microstructure*. Thesis, Ecole nationale supérieure d'arts et métiers - ENSAM, March 2014.

[106] A. CHRYSOCHOOS. Infrared thermography applied to the analysis of material behavior: a brief overview. *Quantitative InfraRed Thermography Journal*, 9(2):193–208, 2012.

[107] A. CHRYSOCHOOS. Thermomechanical analysis of the cyclic behavior of materials. *Procedia Iutam*, 4:15–26, 2012.

[108] V. HONORAT, S. MOREAU, J.M. MURACCIOLE, B. WATTRISSE, and A. CHRYSOCHOOS. Calorimetric analysis of polymer behaviour using a pixel calibration of an irfpa camera. *Quantitative InfraRed Thermography Journal*, 2(2):153–171, 2005.

[109] FLIR. Product Manuel. `http://www.flirmedia.com/MMC/THG/Brochures/RND_017/RND_017_US.pdf`, 2000. [Online; accessed 22-January-2019].

[110] A. BENAARBIA, A. CHRYSOCHOOS, and G. ROBERT. Influence of relative humidity and loading frequency on the PA6. 6 cyclic thermomechanical behavior: Part I. mechanical and thermal aspects. *Polymer Testing*, 40:290–298, 2014.

[111] A. BENAARBIA, A. CHRYSOCHOOS, and G. ROBERT. Thermomechanical analysis of the onset of strain concentration zones in wet polyamide 6.6 subjected to cyclic loading. *Mechanics of Materials*, 99:9–25, 2016.

[112] J.C. MAXWELL. *The Scientific Papers of James Clerk Maxwell...*, volume 2. University Press, 1890.

[113] N. MAKRIS, G.F. DARGUSH, and M.C. CONSTANTINOU. Dynamic analysis of generalized viscoelastic fluids. *Journal of Engineering Mechanics*, 119(8):1663–1679, 1993.

[114] J.A. HERNÁNDEZ, S.J. HERNÁNDEZ, G.A. MACIAS, and G.J. SÁNCHEZ. Relaxation modulus in PMMA and PTFE fitting by fractional maxwell model. *Polymer Testing*, 21(3):325–331, 2002.

[115] L. ROGERS. Operators and fractional derivatives for viscoelastic constitutive equations. *Journal of Rheology*, 27(4):351–372, 1983.

[116] F. RENAUD, J.L. DION, G. CHEVALLIER, I. TAWFIQ, and R. LEMAIRE. A new identification method of viscoelastic behavior: Application to the generalized maxwell model. *Mechanical Systems and Signal Processing*, 25(3):991–1010, 2011.

[117] P. HAUPT, A. LION, and E. BACKHAUS. On the dynamic behaviour of polymers under finite strains: constitutive modelling and identification of parameters. *International Journal of Solids and Structures*, 37(26):3633–3646, 2000.

[118] H. SCHIESSEL, R. METZLER, A. BLUMEN, and T.F. NONNENMACHER. Generalized viscoelastic models: their fractional equations with solutions. *Journal of physics A: Mathematical and General*, 28(23):6567, 1995.

[119] B. BABAEI, A. DAVARIAN, K.M. PRYSE, E.L. ELSON, and G.M. GENIN. Efficient and optimized identification of generalized maxwell viscoelastic relaxation spectra. *Journal of the mechanical behavior of biomedical materials*, 55:32–41, 2016.

[120] R. LEWANDOWSKI and B. CHORAŻYCZEWSKI. Identification of the parameters of the kelvin–voigt and the maxwell fractional models, used to modeling of viscoelastic dampers. *Computers & structures*, 88(1-2):1–17, 2010.

[121] J. CHEN, C. RICHARD, J.C.M. BERMUDEZ, and P. HONEINE. Nonnegative least-mean-square algorithm. *IEEE Transactions on Signal Processing*, 59(11):5225–5235, 2011.

[122] S. GERLACH and A. MATZENMILLER. Comparison of numerical methods for identification of viscoelastic line spectra from static test data. *International journal for numerical methods in engineering*, 63(3):428–454, 2005.

[123] C.L. LAWSON and R.J. HANSON. *Solving least squares problems*, volume 15. Siam, 1995.